VARIABLE-PROPERTY FLOW AND HEAT TRANSFER TO SINGLE SPHERES

VARIABLE-PROPERTY FLOW AND HEAT TRANSFER TO SINGLE SPHERES IN HIGH TEMPERATURE SURROUNDINGS

VARIABLE PROPERTY FLOW AND HEAT TRANSFER TO SINGLE SPHERES IN HIGH TEMPERATURE SURROUNDINGS

A

THESIS

by

NAMIR NAJIB SAYEGH, B.Sc., M.Sc.

Department of Chemical Engineering - McGill University

Under the Supervision of Dr. W.H. Gauvin

Submitted to the Faculty of Graduate Studies and Research of McGill University in partial fulfilment of the requirements for the degree of Doctor of Philosophy

McGill University
MONTREAL, Canada

March 1977

ABSTRACT

Experimental and theoretical studies have been conducted to investigate the effect of large temperature differences on the rate of heat transfer from a very hot gas to stationary spheres.

In the numerical analysis, the momentum and energy equations for variable-property flow past a sphere were solved simultaneously, using finite-difference techniques. Results were obtained in the low and intermediate ranges of the Reynolds number with surface temperature to gas temperature ratios varying between 0.25 and unity. The flow behaviour, drag coefficients and Nusselt number were calculated for each case. A heat transfer correlation was derived which included the effect of large variations in the physical properties of the fluid.

Heat transfer rates from a plasma jet to single stationary spheres were also determined experimentally, in similar ranges of the Reynolds number and temperature ratios. The experimental results were correlated fairly accurately by the equation derived in the numerical analysis.

RÉSUMÉ

On a étudié expérimentalement et théoriquement l'effet de larges écarts de température sur le taux d'échanges thermiques entre un gaz chaud et des sphères immobiles. L'utilisation de méthodes aux différences finies a permis de résoudre simultanément les équations décrivant l'énergie et la quantité de mouvement relatives à un écoulement de caractéristiques variables autour d'une sphère. On a obtenu des résultats pour des nombres de Reynolds de valeurs faibles et intermédiaires avec un rapport de la température de surface de la sphère à la température des gaz variant de 0.25 à l'unité. Les caractéristiques de l'écoulement, coefficient de trainée et nombre de Nusselt, ont été calculés dans chaque cas. On en a déduit une corrélation qui tient compte de variations importantes dans les propriétés physiques du fluide.

On a également déterminé expérimentalement le taux d'échanges thermiques entre un jet de plasma et des sphères isolées immobiles, pour un domaine du nombre de Reynolds et un rapport de températures similaires. Ces résultats expérimentaux étaient en parfait accord avec les valeurs déduites de la corrélation obtenue précédemment.

To my parents

ACKNOWLEDGEMENTS

The author wishes to express his gratitude to all those who, in various ways, contributed to this work.

To the members of the Plasma Technology Group and, in particular, Professors J.R. Grace, R.J. Munz, M.I. Boulos and Dr. D. Bhattacharyya for many interesting and fruitful discussions, and fellow graduate students Mr. O. Biceroglu and Mr. T. Mehmetoglu for their help in the experimental work and in the final preparation of the thesis.

To Professor A.E. Hemielec, of McMaster University, for his assistance in the numerical analysis and computer programming.

To Mr. F. Kitzinger for his help with the thermocouple measurements.

To Mr. A. Krish and the staff of the Chemical Engineering Workshop and Mr. R. Malboeuf of Noranda Research Centre for the prompt construction of the essential items of the equipment.

The National Research Council of Canada for their financial support in the form of a special grant to the Plasma Technology

Group and post-graduate scholarships to the author for a period of two years.

To Mrs. B. Toivanen for her patience and excellent typing of the Manuscript, and to Mr. I. Sabadin for careful preparation of the drawings.

To the rest of my family for their continued moral support.

TABLE OF CONTENTS

NUMERICAL ANALYSIS OF VARIABLE-PROPERTY FLOW PAST A SINGLE SPHERE

EXPERIMENTAL MEASUREMENT OF HEAT TRANSFER TO A STATIONARY SPHERE IN A PLASMA JET

APPENDICES

LIST OF FIGURES

EXPERIMENTAL MEASUREMENTS

LIST OF TABLES

GENERAL INTRODUCTION

The present study forms part of a continuing programme of investigation carried out in this laboratory by the Plasma Technology Group towards the application of plasmas to chemical and metallurgical processes of industrial interest. Solids-gas reactions involving the contacting of fine particles with an entraining plasma gas appear to be particularly promising, as for example in the production of such refractory metals like molybdenum, zirconium and titanium from their respective ores. Owing to the very short contacting times available between the high-temperature plasma and the entrained particles (of the order of a few milliseconds), an accurate knowledge of the rate of heat transfer to the particles is a prime requirement for the reliable design of plasma reactors, particularly when a high degree of conversion is required. The purpose of the present study was to provide this fundamental information.

Although a good deal of work has been published on heat transfer to particles under conditions of moderate temperature difference, little information is available on the situation where this difference is so large that the assumption of constant-property flow is no longer permissible. In addition, the Reynolds number of a

particle exposed to a plasma flame is characteristically small, typically less than 50.

The thesis is divided into three parts: a literature review, a theoretical section where an original analysis is presented, based on the numerical solution of the equations of motion and energy for pure steady-state heat transfer and variable-property flow at low Reynolds numbers, and an experimental section where the measurements of heat transfer rates to small stationary spheres in a confined argon plasma jet are reported. The latter two sections are complete in themselves, in that they each have a separate Introduction, Conclusion, Nomenclature and Bibliography.

LITERATURE REVIEW

INTRODUCTION

The review presented in this chapter is intended to provide background information on the problem of heat transfer to spheres in high-temperature environments and some insight into the practical aspects of plasmas. As a plasma was used solely as a high-temperature heat source in the experimental part of this study, discussion of plasma phenomena will be very brief.

The review is divided into two parts, plasma phenomena and diagnostics, and transport phenomena from spheres. The first part will describe plasmas in general, methods of plasma generation, and some aspects of plasma radiation. Plasma diagnostic techniques, (mainly temperature and velocity measurements) will be discussed also in somewhat greater detail. Finally, a short review of recent studies of heat transfer phenomena in plasmas will be given.

The second part of this review will be concerned with the problems of flow around and heat transfer to spheres at low Reynolds numbers. A stronger emphasis will be placed on the theoretical approach to these problems. A brief review of experimental studies on heat transfer to cylinders in laminar flows will be presented also.

PLASMA PHENOMENA AND DIAGNOSTICS

GENERAL

A plasma is a partially ionized gas composed of free electrons, positive ions, neutral atom and molecules. These species are in continuous interaction and their composition and respective concentration are a function of the temperature. A plasma, on a macrosopic scale, is approximately neutral, since the number of positively - and negatively - charged particles present at any instant in time is almost equal.

A plasma is initiated whenever sufficient energy is imparted to a gas. This energy causes acceleration of randomly-occurring free electrons up to the point where they can cause ionization of the neutral gas molecules. The additional electrons formed by this ionization are in turn accelerated, resulting in further ionization. This cascading effect will lead to an extensive breakdown of the gas. In all electrical discharges the electrons act as the main agent for transferring energy from the electric field to the gas. This transfer is a result of either elastic collision where only the kinetic energy of the molecule is increased or inelastic collision leading to excitation, fragmentation or ionization of the molecule. Steady state is reached where there is equilibrium between the rate of formation of ions and the rate of their recombination. In order to maintain the

plasma, energy must be supplied continuously to make up for conductive and radiative losses and to prevent immediate reattachment and recombination.

The presence of charged species causes the plasma gas to behave differently from an ordinary hot gas. The electrical conductivity, which is almost negligible for a gas at relatively low temperatures, becomes quite significant at higher temperature levels and is a function of the latter. While a heated gas loses energy to the surroundings by atomic conduction (atom-atom collision) only, a plasma loses additional energy by heat conduction of other plasma constituents (electron-ion collisions) and also by diffusion of chemical energy (dissociation and ionization energy) to the surroundings. Moreover, energy is also lost by self-emitted radiation from the plasma at high temperatures to the surroundings.

PLASMA GENERATION

Plasma can be generated by three different methods, either by electrical means, by combustion processes or by shock waves. Shock waves produce only quasi-steady plasmas. Shock tubes of different designs are used to generate high-temperature, high-density plasmas which are used mainly in basic studies. The generation of plasmas by combustion is particularly interesting for magnetohydrodynamics applications. Such plasmas have relatively low temperatures and are frequently seeded with alkali metals or their compounds. These compounds have low ionization potential and, thus, the plasma can be sustained in spite of the relatively low temperatures.

The generation of steady, high-temperature (thermal) plasmas is limited to electrical methods which can be either arc discharges or electrodeless discharges. Arc discharges can be produced in either a stationary or in a transferred arc configuration. In a stationary (non-transferred) arc, the plasma gas is heated and ionized by passing it through or around the electric discharge, in the gap between the two electrodes. In a transferred arc, the arc is struck between the cathode and an external workpiece which acts as the anode. Based on the modes of stabilization, non-transferred arcs can be further divided into five categories: vortex-stabilized, gas-sheath stabilized, wall-stabilized, magnetically-stabilized and water-stabilized. This is discussed in detail by Baddour and Timmins (1967) and by Gerdeman and Hecht (1972).

In electrodeless discharges, the presence of electrodes inside the plasma chamber is eliminated. The energy is transferred from the high-frequency source (radio-frequency or microwave) to the gas by either inductive or capacitive coupling. As in the case of arc discharges, the electrons gain energy from the field, resulting in an increase in their kinetic energy. Ionization is effected by the collision of these electrons with the neutral atoms. Baddour and Timmins (1967) give an extensive description of radio-frequency devices.

A review of apparatus for generating laboratory-scale plasmas and of techniques used in plasma chemistry is presented by McTaggart (1967) and more recently by Hollahan and Bell (1974). In both of

these works, the authors are concerned with low-temperature non-equilibrium plasmas, where species generated by ionization take part in the reaction; applications of high-temperature plasmas have been excluded, as these require the plasma only as a source of high temperature.

PLASMA DIAGNOSTIC METHODS

The subject of plasma diagnostics is well covered in the literature [see Huddlestone (1965), Lochte-Holtgreven (1968), Baddour (1967) and Kettani (1973)]. However, these works deal with fundamental parameters of the plasma, such as electron density, electron temperature, degree of ionization, etc. The work presented in this thesis, on the other hand, was carried out in the lower region of a plasma tail flame where the temperatures are lower and the ionization of the gas used (argon) is almost negligible. Therefore, the techniques discussed in these references are largely inapplicable, as they rely mainly on the presence of ionized species in the gas for sensing purposes. The review presented here is thus limited to the determination of the two major characteristic parameters of the gas after leaving the generating device, namely the gas velocity and gas temperature. Generally speaking, it can be stated that the transport properties of a plasma are characterized by very high viscosities and very low Reynolds numbers, even at high velocities.

Gas Velocity Measurement

The velocity of a plasma stream can be measured either

directly by the insertion of an impact probe into the plasma, or indirectly by following the trajectories of tracers introduced in the plasma at points higher upstream. When probes are used, there is always an irreducible, but in many cases small disturbance of the local plasma conditions. The simplicity and good resolution of this method, however, outweigh the inaccuracies caused by the disturbance of the flow. Tracer methods, on the other hand, pose difficulties in obtaining local measurements and in interpreting the results. Moreover, the method of introduction and the presence of the tracer may also cause disturbance of the flow.

Several excellent reviews have appeared in the literature on the use of pressure probes for velocity measurements [Dean (1953), Folsom (1956), Daily (1964), Chue (1975), Becker (1974, 1975)]. As the bulk of the work on pitot tubes has been carried out in the field of aerodynamics, experience with this sensing method is largely limited to isothermal flows. The effect of the compressibility of the fluid has been studied extensively, but variation of fluid properties due only to Mach number effects was considered. The effect of viscous forces on pitot tube calibrations is discussed also in these reviews. However, no definite conclusions are given. Finally, none of the studies reported in these reviews was concerned with velocity measurements in high-temperature flows, where the presence of a cooler probe disturbs not only the velocity field, but also the temperature field.

Pressure probes have been used by several researchers to

measure the velocity of plasma flows. Grey et al. (1962, 1964) studied the mixing of coolant streams with both laminar and turbulent plasma jets. Impact pressures were measured by a water-cooled probe, 3.75 mm in diameter. Velocities were calculated by using Bernoulli's equation for incompressible and inviscid fluids. Katta et al. (1973) and Gol'dfarb et al. (1967) also used this method to determine axial and radial velocity profiles in a plasma jet. In a study on heat and mass transfer between a plasma jet and a gaseous coolant, Smith (1965) used a water-cooled probe to measure the gas velocity. However, in interpreting his results he modified the Bernoulli equation to include the effect of varying fluid density between the free stream and probe tip conditions, thus,

$$u_2^2 - u_1^2 = -2 \int_1^2 1/P \, dP \qquad (1)$$

Carleton (1970) and Carleton and Kadlec (1972) presented an approximate analysis of the flow around the tip of a pressure probe. In this analysis, the stagnation streamline is divided into two regions. The flow region near the free stream is considered to be isentropic, inviscid and compressible, and the region next to the probe surface to be laminar, viscous and incompressible. The probe tip is assumed hemispherical. The expression arrived at consisted of three terms, as shown in Equation (2). The first term is that obtained when no viscous or temperature effects are present, the second accounts for Mach number effects, and the last represents a correction for the effect of viscous forces near the probe. This last term, however, does not reflect the influence of variable fluid properties directly,

but is affected by the latter only through the evaluation of average fluid properties. Carleton's expression can be written as:

$$P_o - P_\infty = \rho_\infty U^2/2 + \rho_\infty^2 U^2/8\gamma P_\infty + 2\bar{\mu} U/R \qquad (2)$$
$$(1 + 0.5576/\sqrt{Re})$$

where $Re = UR\bar{\rho}/\bar{\mu}$

Hare (1972) reported a study on the effect of impact tube tip temperature on velocity measurements in flames at temperatures higher than 1 500C. It was found that the impact pressure measured by a pitot tube was strongly affected by the heat flux between the gas and the tube for temperatures in excess of 1 000C. When the temperature difference was over 1 000C between the gas and the probe tip, there was a significant change in the measured impact pressure, and when this difference increased to 1 500C the error was too large to be ignored. For their probe geometry the error in the velocity measurements caused by using Bernoulli's equation was about 16 and 30 m/s for temperature differences of 1 500 and 2 000C, respectively. The actual velocity of the flow was in the range 20-50 m/s. No quantitative description was, however, given for this phenomenon.

Kimura and Kanzawa (1963) studied plasma streaming in an arc, caused by Lorentz forces generated by self-magnetic fields. The streaming velocity was evaluated by measuring the drag on a small plate swept across the arc. The temperature of the gas was determined both spectroscopically and by means of thermocouples. The plate and its holder were made of molybdenum. The holder was

attached to the diaphragm of a capacitance-type pressure sensor. The sum of the drag force acting on the plate and part of the holder was recorded on an oscillograph via the pressure sensor. This method of measurement was applicable only to conditions where the direction of the flow is perpendicular to the plate surface. The overall uncertainty in the velocity measurement was estimated to be less than 17.5%.

The velocity of a plasma jet can be measured by injecting tracer particles in the flow and following their trajectories by optical means. Desai et al. (1968) measured the velocity distribution in an argon plasma jet in laminar flow, using boron nitride particles of diameters between 40 and 80 microns. The radial position of the particles in the jet was determined accurately by getting the front and the side views of the jet on the same frame by the use of split mirror techniques. Chase (1971) obtained flow visualization and gas velocities in the core of an RF induction plasma, by injecting particles and following their trajectory with a movie camera. Waldie (1975) studied the flow patterns of powders and plasma gas in and around the coil region of an induction plasma, by using cine photography. The trajectories of spherical particles with diameters of the order of 100 microns were measured in three dimensions by simultaneous recording of two views at right angles to each other (similar to Desai's technique). Frame by frame measurements of particle coordinates then allowed the calculation of particle velocity vector and particle acceleration or deceleration as function of time

and space. When deducing plasma gas velocities from the particle velocities, the flow around the particle was assumed to be Stokesian and the physical properties were evaluated at mean film temperatures.

In an investigation of flow patterns in an RF induction plasma, Gold (1975) described an optico-electronic method which is based on the spatially and temporally resolved measurements of plasma luminosity. The velocities of plasma and injected particles were both determined by this method. The optical system formed an image of the plasma on a linear photodiode array. These photodiodes were scanned sequentially and the amount of light falling on them between two scans was determined. Each single scanning-cycle thus provided an instantaneous intensity profile of the plasma. In order to examine the flow pattern of the plasma, sodium chloride particles were injected into the flame and the velocity was then deduced from following the propagation of increased intensity. With this method, it was not possible to determine the exact radial position of the particles and therefore the results obtained were not very accurate.

Gol'dfarb et al. (1967) estimated the flow velocity of an induction plasma from the lengths of the streaks of carbon particles originating from the end of a carbon striking rod. This method was inaccurate in the sense that it was difficult to determine the location of the particles in space.

Bohn et al. (1967) obtained radial temperature and velocity profiles of an argon plasma at very low pressures (1.5 torr). The

velocities of the heavy particles were determined by measuring the Doppler shift with a Fabry-Perot interferometer.

Meubus (1974) injected hydrogen into an argon plasma and was able to determine the concentration profiles spectroscopically. From these profiles and the knowledge of the temperature field (measured also spectroscopically), the argon velocity profiles were calculated by making a simplified material balance.

Meubus and Parent (1969) proposed a flow model of a helium plasma jet. From a knowledge of the luminous profile equation, temperature distribution and gas flow rate, the velocity distribution in the plasma was determined by making an energy balance. This model was later used for experimentally evaluating transfer coefficients for helium. Comparison of these results with theoretical values showed a 40% error, with an estimated error in the velocity measurement of the order of 25%. Gottschlich et al. (1966) described a similar model where the axial velocity of the jet was calculated from the temperature profile by a simple energy balance. The temperature field was obtained by spectroscopy. In this model, the flow was assumed to be axisymmetric and unidirectional. The derivatives of the temperature were estimated numerically from local values of the temperature.

The use of laser-Doppler anemometry in plasmas has been suggested by several researchers. This method determines the instantaneous velocity of a particle suspended in the flow by

measuring the Doppler shift of optical radiation scattered by the moving particle. If small enough particles are used, then their velocities will represent the actual gas velocity. The use of this technique in plasma is somewhat restricted by several factors such as the method of seeding, material of the particles, cooling effect of the particle and most importantly, how accurately the particles can follow the plasma flow. A preliminary study has been carried out in these laboratories and is described in more detail by Ho (1976).

Gas Temperature Measurement

As in the case of velocity measurements, temperature measurements in plasmas can be made either with the aid of insertion probes or by optical methods. Optical methods, in general, are preferable because they do not disturb the flow. Spectroscopic techniques have been widely used to measure plasma temperatures in excess of 9 000 K [Olsen (1959), Smith (1965), Gol'dfarb (1965, 1967), Bott (1966), Rovinskii (1967), Cremers (1968), Meubus (1969), Carleton (1970)]. The spectroscopic techniques are based on measuring one of the following quantities: absorption of radiation of known intensity, spectral line broadening, absolute intensity of a spectral line, relative intensities of different spectral lines or of a single line (Larenz method), or the intensity of continuum radiation [Knopp (1962), Incropera (1967)]. In general, absorption spectroscopy is impractical in plasma diagnostics since the radiation intensities of the plasma are quite high compared with that of the light source.

The single-line (Larenz or Fowler-Milne) method is considered one of the more suitable methods for plasma temperature measurement [Knopp (1962), Gottschlich (1966) and Incropera (1967)] because it does not require a knowledge of the transition probabilities of the plasma gas. This method, however, requires thermal equilibrium within the plasma, radial symmetry of the flow, negligible self-absorption by the gas and that the line under study must exhibit an intensity maximum. To satisfy the last condition, the plasma temperature must be high enough to produce significant reduction in the number of particles of the species under observation. In other words, this condition limits the use of the Larenz method to plasmas where the degree of ionization is appreciable. For argon this temperature is around 9 000 K and when the two-line method is used this lower limit is pushed up to 12 000 K [Incropera (1967)].

Grey (1965) reviewed the thermodynamic methods of high-temperature measurement of gas flows and classified them into three general categories: pneumatic probes, heat-flux gauges, and calorimetric sampling probes. Pneumatic probes consist essentially of two flow restrictions through which the hot gas sample is allowed to flow and between which it is cooled. The temperature of the gas at the stagnation point can be determined from the continuity equation, provided that the pressures at each constriction, the total pressure of the flow, the temperature at the downstream constriction and the area and discharge coefficients of the constrictions are known. When the flow through both constrictions is sonic then the intermediate

pressure between the two nozzles need not be known, and the continuity equation reduces to [Simmons and Glawe (1957)]:

$$T_\infty = (C_1A_1/C_2A_2)^2 \cdot T_2(P_0/P_2)^2 \qquad (3)$$

In practice, the quantity (C_1A_1/C_2A_2) is not constant and some variations are expected due to changes in the actual areas of the nozzles (A_1 and A_2) and because of the dependency of the discharge coefficients (C_1 and C_2) on the Reynolds number and the rate of heat transfer from the gas to the nozzle surface. The value of this term can be found by calibrating the probe at room temperature, where $T_\infty = T_2$.

This method has several drawbacks in that it needs pre-calibration of the nozzles, ideal isentropic flow must take place at each nozzle, a certain degree of suction is required when the total pressure is low, and that the nozzle ratio does not change between calibration and actual operation. Since the nozzle ratio is a function of the fourth power of the nozzles diameters, slight expansion effects in the first nozzle (expected when measuring high-temperatures around 4 000 K) can cause errors of the order of 10% in the stagnation temperature [Grey (1965)].

Heat-flux gauges measure the enthalpy or temperature of the gas by determining heat transfer rates across the calorimeter surface. A prerequisite for this method is calibration or knowledge of the relation between the heat transfer rate and the gas temperature. The main sources of error in this technique are inaccuracies in estimating

heat transfer rates to the insulating jacket and the relatively large size of the probe required for adequate resolution, which reduces the validity of stagnation-point heat transfer assumption (Grey 1965).

Calorimetric methods determine the local enthalpy of the gas by cooling a small amount of sample of the hot gas and measuring the increase in the coolant temperature and the final temperature of the gas. Grey et al. (1962, 1964) developed a water-cooled probe capable of measuring gas temperatures up to 15 000 K. The calorimetric method used to determine the gas temperature relied on a tare measurement to correct for heat transfer to and from the probe. The change in coolant temperature was observed for the case when the valve in the gas sample line was closed and when it was open. The difference in the enthalpy change of the coolant was a measure of the heat lost by the gas sample. The accuracy of this method depends heavily on duplicating the flow conditions near the probe tip in the flow and no-flow cases.

El-Shamy (1975), in his study of heat transfer to spheres in RF induction plasmas, described a 'tare' calorimetric probe similar to that of Grey. The coolant temperatures were measured by thermistors and the exit gas temperature by means of a thermocouple. Petrov and Sepp (1970) developed a similar calorimetric probe for the measurement of temperature and total pressure of high velocity dense air plasma. These authors claim that their design is more suitable than that of Grey for high heat flux environments and is also less sensitive to variations of the suction rate of the gas sample. Temperatures up to

5 000 K on the axis of the flow with velocities up to 900 m/s were measured.

Smith and Churchill (1965) measured plasma jet temperature both spectroscopically and by a calorimetric probe. They concluded that reliable enthalpy data could not be obtained by using a sampling probe. They showed that this method is very dependent on the sampling rate. At too low sampling rates, the sample is drawn only from the cold region near the probe and at too high sampling rates a greater portion of the gas which normally flows past the outside of the probe is drawn through the sampling probe. Both of these effects result in a lower than actual enthalpy value. Under one plasma condition they found that the maximum temperature measured by the probe was 5 000 K, while at that same point, spectrographic measurements gave a temperature value in excess of 9 000 K. This discrepancy was also observed by Chludzinski (1964). Similar results to those of Smith and Churchill were obtained by Hare and co-workers (1972). They mention that their results show the same trend of variation of measured gas enthalpy with the sampling rate. They note that in regions where both thermocouples and enthalpy probes could be used to measure the temperature, the thermocouple always indicated significantly higher temperatures. Also, when using the measured temperature and velocity profiles, it was not possible to conserve the mass of the gas in the jet. This view, however, was not shared by Incropera and Leppert (1967) who measured radial temperature and velocity profiles in a d.c. argon plasma, both by calorimetry and

spectroscopically. They found that, provided the flow conditions are duplicated for actual and tare measurements (they did not say how), calorimetric results agreed within a few percents with those obtained by spectroscopic methods. Spectroscopic methods were found to be more accurate as the temperature increased (over 12 000 K). Below 10 000 K, they agree with Hare's findings that uncertainties with probe measurement rise to excessively high values. They suggest, however, that more reliable results can be obtained by choosing a suitable coolant flow rate.

In a later paper, Grey (1968) describes two other geometries of calorimetric probes. He first points out that the above method can be used only in large heat flux environments. Its principal disadvantage, he maintains, is lack of sensitivity at lower heat flux conditions caused by small difference between two large numbers (tare and actual measurements). For lower heat-flux conditions, the fully-isolated non-tare measurement probe was recommended. Here the calorimetric part of the probe is isolated from the cooling jacket by a gas or vacuum gap. The enthalpy measurement is then obtained directly without the need of a tare measurement. For very low ambient pressures such as encountered in most hypersonic flows, the gas sample energy is so small that the coolant flow rate cannot be reduced sufficiently to produce a measurable temperature difference. Moreover, the stagnation pressure is too low to drive an adequate amount of sample through the probe. Under these conditions, the sharp-inlet shock-swallowing probe was recommended.

Katta et al. (1973) made extensive tests with the improved, double-jacketed non-tare probe, designed by Grey, for axial temperature measurement of argon and helium d.c. plasma jets, in the range of 2 000 - 13 000 K. At high temperature levels (12 000 K) the probe measurements agreed with spectrographic data reported in the literature, while values in the lower temperature range were confirmed by thermocouple measurements. They found that this calorimeter was indeed capable of good accuracy but great care had to be exercised in the adjustment of the coolant flow rates, making its use rather ponderous and time-consuming.

Provided that gas temperatures are not very high (less than 5 000 K), they can be measured by means of a bare thermocouple immersed directly in the flow. The limitions of this method are the restrictions on gas temperature level, fragility of the fine thermocouple wires and the need for temperature corrections to account for the heat losses from the junction by radiation and conduction through the support. Bradley and Matthews (1968) presented a model for obtaining actual gas temperatures from thermocouple readings. This model accounted for heat transfer to and from the thermocouple junction and support. Klyuchnikov (1966) suggested a method for determining the true gas temperature from the readings of two thermocouples slightly different in size. By this method, uncertainties concerning radiation to the junction from the gas or the solid walls were eliminated.

PLASMA HEAT TRANSFER

The problem of plasma heat transfer to solid surfaces is important in various engineering applications, such as in arc technology, MHD generators, re-entry of space vehicles, etc. The most important aspect of plasma heat transfer is the effect of electric and magnetic fields, caused by the presence of charged particles, on the heat transfer process. Emmons (1963) and Eckert and Pfender (1967) reviewed plasma heat transfer to electrically insulating and electrically conducting surfaces, both in the absence of external fields and in the presence of electric and magnetic fields in the boundary layer.

Kimura and Kanzawa (1965) reported values for average heat fluxes to wires immersed in a flowing plasma produced by a high intensity electric arc. Average heat transfer results were obtained by measuring the change in the electrical resistance of a wire swept quickly through the arc. The temperature of the arc was determined spectroscopically. By making certain assumptions concerning the flow conditions, they were able to correlate their results by using empirical heat transfer equation derived for constant-property flows.

In order to determine the effect of ionization on the heat transfer process to a solid surface, Petrie and Pfender (1969) described a method for measuring heat transfer to wires immersed in a rotationally symmetric, high density and high intensity plasma. They used a technique similar to that of Kimura where total heat

transfer rates to wires, swept at a constant speed, were measured by recording the change in the electrical resistance as function of position of the wire in the plasma. Local values of the heat flux were calculated by using Abel inversion on the average heat transfer rates. A slightly different technique was reported by Pfender (1971) where average heat transfer rates to a water-cooled probe were determined calorimetrically, thus yielding more accurate results. For both of the methods (wire or probe) the object was biased electrically at various potentials to allow the study of the effect of electric current on heat transfer. Contrary to the expected, heat transfer rates by thermal conduction to solid surfaces were not strongly affected by the presence of free electrons in the plasma. This was due to thermal insulation provided by the presence of a cool and less ionized layer at the solid wall which separates the latter from the hot plasma.

A similar study was conducted by Kanzawa (1973) to determine heat transfer rates to spherical probes immersed in atmospheric argon plasma. The probe temperature was measured by means of thermocouples. The effect of the electric field was found by applying an external potential on the probe with values ranging from -30 to +5 volts.

Experimental values of the Nusselt number were measured for heat transfer from a confined plasma jet to the entrance region of water-cooled circular tubes [Skrivan (1965), Johnson (1968)]. The maximum entry temperature of the plasma was less than 7 000 K and the maximum Reynolds number was 900. The results were presented as cor-

relations between the Nusselt and the Reynolds numbers. Incropera and Leppert (1967) solved a simplified form of the equations for the laminar flow of a plasma stream in the entrance region of a circular tube. The solution was obtained numerically, using implicit finite-difference techniques. Schmidt and Leppert (1970) determined heat transfer rates from a partially ionized argon plasma to a water-cooled circular tube. Entrance gas temperatures were of the order of 12 000 K and Re between 140 and 527. They found that the numerical solution of Incropera under-predicted the heat transfer rates in the first few tube diameters down from the plasma entrance. They attributed this discrepancy to non-equilibrium effects and inaccuracies in the measured inlet enthalpy profiles.

Abu-Romia and Bhatia (1972) measured stagnation point heat transfer from a plasma jet by means of a heat pipe. Results were obtained for plasma mean temperatures of up to 12 000 K and for different gas flow rates. At low flow rates, the experimental results were in agreement with theoretical laminar flow stagnation point heat transfer predictions. However, as the gas flow rate increased the plasma jet flow was no longer laminar and due to turbulent effects, the heat transfer rates were much higher than those predicted theoretically.

The motion of particles entrained in a hot jet is of a particular interest in powder processing in plasmas. Lewis and Gauvin (1973) followed the trajectories of small glass particles entrained in a free argon plasma jet, by means of high-speed cine streak photo-

graphy. They found this system to be characterized by low Reynolds number of the particles and high deceleration rates. A computer program was proposed which predicted the particle trajectory, velocity and temperature during its flight. Their results indicated the necessity of including the Basset term in the computation of the drag coefficient. Boulos and Gauvin (1974) developed a model to calculate the trajectories of small particles in a plasma jet, in order to predict the effect of various plasma parameters on the reaction rates of molybdenum disulfide particles that are injected into the hot flame. This model was later modified by Bhattacharyya and Gauvin (1975) to include the effect of the swirl component of the flow on the trajectories and reaction rates of these particles. A similar model to that of Boulos was presented by Harvey et al. (1975) which calculated heat and momentum transfer to small particles injected in a high temperature cylindrical reactor. The particular case studied was the spheroidization of magnetite particles, 75 to 125 microns in diameter.

Farnell and Waldie (1975) investigated the technique of fluid dynamic levitation of particles in an induction plasma tail flame flowing vertically upwards. Theoretical predictions were made by solving the transport equations around the particle. Results from experimental work on alumina particles in an argon plasma were in general agreement with the theory.

Heat transfer to single stationary spheres in a plasma jet was first studied by Kubanek, Chevalier and Gauvin (1968). Overall

heat transfer rates to water-cooled spheres, 16 and 25 mm in diameter were measured calorimetrically. The Reynolds numbers encountered were between 600 and 4 300 with temperature differences between the sphere surface and the plasma gas of up to 3 000 K. Local heat transfer rates were reported by Katta and Gauvin (1973, 1973) to stationary sphere in similar Re range (between 860 and 3 100) and temperature differences. El-Shamy (1975) conducted a similar study, but the Reynolds numbers of the sphere were much lower, namely between 200 and 400. The reliability of El-Shamy's results is rather debatable since the sphere supports were very short and of a comparable diameter size to that of the sphere. Also, the theoretical analysis was not very accurate, as it did not take into consideration the effect of the large temperature differences.

Several simplified models describing an inductively-coupled plasma have been reported recently [Armstrong (1968), Freeman (1968), Eckert (1970, 1970), Pridmore-Browne (1970), Eckert and Pridmore-Browne (1971)]. Miller and Ayen (1969) presented a model to predict radial and axial temperature profiles in an induction plasma. This model included temperature-dependence of the physical properties and radiative losses from the gas. The energy and magnetic flux equations were solved numerically by an implicit finite-difference method. The solution was obtained for an assumed velocity field. The velocity field was adjusted to conserve the mass flow rate at any given section in the torch. Yoshida and Akashi (1975) modified this model by using the concept of mixing of two ideal gas streams to obtain the assumed velocity field. They also studied the effect of gas flow rate on

the axial flow pattern and on the temperature field. Boulos (1975) calculated the two-dimensional flow and temperature fields in an inductively coupled plasma. The complete flow, continuity, energy and magnetic and electric field equations were solved simultaneously, by using an iterative finite-difference procedure.

PLASMA RADIATION

When an electron at a high energy level makes a spontaneous transition to a lower level, a photon of light is emitted. This photon has an energy equal to the difference between the two energy levels. This is the principle behind plasma radiation. The number of such transitions is dependent on the concentration of atoms in the high excited levels and on the probability of instantaneous transition. From measurement of absolute intensity of a spectral line, or relative intensities of two or more lines, the plasma temperature can be determined. When the plasma gas comprises molecules, then the spectrum always consists of bands and the temperature is determined from the intensity of these molecular bands rather than from atomic lines.

Total radiation from plasmas has been measured by several methods. Tankin (1964) and Evans (1967) used a thermistor bolometer, while the use of a total radiometer was reported by Emmons (1967) and Barzelay (1966). Results from different researchers vary as much as by a factor of 4. The most reliable data seem to be that reported by Emmons. Total emissivity values for argon were given by Moskvin (1968) for the temperature range of 6 000 to 12 000 K and by Kon'kov and Kulagin (1974) in the range of 12 000 to 16 000 K.

TRANSPORT PHENOMENA

GENERAL

A large number of studies have been published in the literature on the subject of momentum and heat transport to spheres and cylinders. To review them all is almost an impossible task. Clift et al. (1977) give an extensive coverage of transport phenomena around solid and fluid spheres. The review in this section will, therefore, be limited to studies pertinent to the type of flow encountered in plasma jets, mainly in the low and intermediate ranges of the Reynolds number ($0<Re<100$). Also, the emphasis will be more on theoretical analyses of the problems of flow and heat transfer to spheres, than on experimental results on drag coefficients or heat transfer rate.

FLOW AROUND A SINGLE SPHERE

The Navier-Stokes equations for the flow around a sphere are highly non-linear even for the simplfied case of constant physical property fluids. Consequently, no completely exact solution exists for these equations. All reported solutions simplify the equations to suit a particular flow condition. The earliest "exact" solution for the flow around a single sphere was given by Stokes (1850). This solution linearizes the Navier-Stokes equations by assuming the inertia forces to be negligible compared to the viscous and pressure

forces. This assumption limits the validity of the Stokes' solution to very small Reynolds numbers. Because of the absence of the inertia terms, the flow is 'reversible' and possesses a fore-and-aft symmetry. In the Stokes' flow solution, the ratio of the neglected inertia terms to the viscous terms is of the order of Rer/2R. Consequently, even at very small Reynolds numbers the error in the Stokes' assumption is significant at large distances away from the surface of the sphere.

Oseen (1910) modified the Navier-Stokes equation by simplifying the non-linear terms, instead of dropping them out completely. Oseen's equation can be written as:

$$\bar{U} \cdot \nabla \bar{u} = -1/\rho \nabla P + \nu \nabla^2 \bar{u} \qquad (4)$$

The introduction of the free stream velocity vector $\bar{U}$ accounts for the inertia forces which gain importance at large distances away from the sphere.

Proudman and Pearson (1957) obtained higher order approximations for the flow around a sphere by the method of matched asymptotic expansions. These authors used the solutions of Stokes and Oseen as the "inner" and "outer" expansions, respectively. The method of matched asymptotes assumes that the solution possesses asymptotic expansions at the inner and outer boundaries. By matching these expansions, a uniformly valid asymptotic representation of the flow can be found. In other words, the Proudman and Pearson's solution makes use of the fact that the Stokes' solution is valid

near the surface while Oseen's solution satisfies the flow conditions at large distances away from the sphere. These authors carried out their analysis up to the term of the order of $Re^2 \ell nRe$. Chester and Breach (1969), following the same method, extended the analysis as far as the term of the order of $Re^3 \ell nRe$. This solution converged more slowly as the Reynolds number increased and was not accurate above a Reynolds number of 5.

Kawaguti (1955, 1958) obtained separate approximate solutions of the Navier-Stokes equation for the low (0-10) and intermediate (10-80) ranges of the Reynolds number. He used a Galerkin error-distribution method which involves the choice of a trial polynomial for the stream function that is made to satisfy the flow equations and the boundary conditions. This method was extended by Hamielec et al. (1962, 1963) to viscous flow around fluid and solid spheres at Reynolds numbers up to several thousands. Hoffman and Ross (1972) employed the error-distribution method, modified to include a finite radial mass efflux from the surface, to investigate the effect of mass transfer on heat transfer to an evaporating droplet.

Several numerical solutions have appeared in the literature for the problem of incompressible, axially-symmetric, viscous flow past a sphere. In these solutions the partial differential equations of the flow were simplified by finite-difference approximations. Since the non-linearity was retained in the resulting algebraic difference equations, a direct solution was not possible and an iterative method had to be used. The earliest finite-difference solution was

reported by Jenson (1959) for steady state flow at Re of 5, 10, 20 and 40. Since a desk calculator was used for the computation, the grid size used was relatively large and the distance to the outer boundary was only six radii away from the centre of the sphere. Hamielec et al. (1967) obtained more accurate results by using a finer grid and a larger size field. The Reynolds number range of their solution was between 0.1 and 100. LeClair et al. (1970) extended this work up to Re of 400. At low Re their results departed significantly from those of Jenson, while agreeing well with the results of Hamielec and of Rimon and Cheng (1969) at higher Re. A more thorough discussion of the numerical results was presented by Pruppacher, LeClair and Hamielec (1970). Rimon and Cheng (1969) solved the time-dependent Navier-Stokes equations numerically for very long times, to obtain the steady state solution. In this method, only the stream function equation is solved iteratively. The vorticity is computed directly at each time step. By this approach the temporal development of the flow can be followed, and the steady state solution is independent of the initial flow conditions. However, because of the small time steps necessary for the stability of the solution, the process requires relatively large computer times to reach steady state. LeClair and Hamielec (1970) studied the flow behaviour of an accelerating sphere in a viscous fluid in the Reynolds number range of 0.1 to 150. The complete Navier-Stokes equations were solved numerically together with the Basset equation for the sphere.

Dennis and Walker (1971) solved the Navier-Stokes equations for the flow around a sphere for Reynolds numbers between 0.1 and 40. They used a semi-analytical formulation where the flow variables were expanded as series of Legendre functions, hence reducing the equations of motion to ordinary differential equations. The ODE were then solved numerically. As the Reynolds number increased, more terms in the series were necessary to approximate the flow, leading to an increase in the number of equations to be solved simultaneously. Consequently, this limited the analysis to Reynolds numbers of no more than 40. These authors show that at low Reynolds numbers this method is faster than the numerical solution of the complete Navier-Stokes equations, by the finite-difference technique.

All the solutions discussed above were obtained for the case of a constant-property fluid. Very few researchers have studied the problem of variable-property flow. Kassoy et al. (1966) presented solutions of the momentum equation for cases involving significant variations of the physical properties and temperature. The method of matched asymptotic expansions was used, thus restricting the Reynolds number to the order of unity and the dimensionless temperature difference, $\underline{I}$, to the order of the Reynolds number. The viscosity and thermal conductivity were assumed to vary linearly with $\underline{T}$. The coefficients of drag and the Nusselt number were estimated from the velocity and temperature profiles.

Seymour (1971) calculated the aerodynamic drag on a small sphere moving in an ionized gas where the temperature ratios between

the bulk of the gas and the sphere surface were of the order of 40:1. The properties were allowed to vary exponentially with the temperature. The temperature and property profiles were calculated, assuming forced convection to be negligible. Using these profiles, the momentum equation was then solved numerically. With the assumption of low Re (<1.5), the resulting solution possessed a fore-and-aft symmetry similar to that of Stokes flow. The drag force on the sphere was estimated by integrating the viscous dissipation of energy throughout the flow field.

Dumargue et al. (1974) studied the problem of evaporation from a spherical super-refractory particle in a fluid with variable physical properties. The case of zero Reynolds number was solved first. Dufour effects, radiation and forced convection heat transfer were introduced later by the use of perturbation techniques, while assuming the flow to be Stokesian. The results were presented as the ratio of terminal velocity in the variable-property fluid to that calculated by Stokes' equation.

Woo (1971) using relaxation methods, solved the flow and energy equations, numerically, for a variable-density fluid. The viscosity and the thermal conductivity were assumed temperature-independent. Flow patterns were calculated for cases where natural convection was significant.

HEAT TRANSFER TO SPHERES

Quite a large number of studies have been carried out on the problem of heat transfer from single spheres. Because of the difficulties involved in the solution of the momentum and energy equations for flow around a sphere, the results from the published work cannot be compared with an exact theoretical model. Consequently, the heat transfer correlations that are available are solely based on experimental results. Errors and uncertainties in the experimental procedure have prevented these workers from reaching a single valid expression. Rowe et al. (1965) reviewed all the experimental work that had been done in this field up to the early 1960's. They concluded that although the heat transfer results can be expressed as:

$$Nu' = A + B\ Pr^m\ Re^n \qquad (5)$$

there are no single values of A, B, m and n that would correlate all the reviewed experimental results. Also, since most of the data had been obtained for air or water systems, it was not possible to examine the applicability of such expressions to other fluid systems.

Baird and Hamielec (1962) predicted theoretically approximate local and overall Sherwood numbers for forced-convective transfer around solid and fluid spheres for Re up to 100. The diffusion equation was solved analytically for the case of a thin concentration boundary layer (Pe>>1). The velocity field used was that derived by Kawaguti and by Hamielec. The results agreed reasonably with experi-

mental correlations of Griffith (1960) and of Ranz and Marshall (1954). Hoffman and Ross (1972), assuming a similar velocity profile, solved the energy equation to investigate the effect of mass transfer on heat transfer. The solution was based on the integral boundary layer formulation of the energy equation. Solutions were obtained for the case of zero mass efflux in the Prandtl number range of 0.7 to 10 and Reynolds number between 20 and 500. Assuming the following expression for the Nusselt number:

$$Nu = 2 + A\ Pr^{m}\ Re^{n} \qquad (6)$$

m was found to be a function of the Reynolds number, thus,

$$m = 1/3 + 2/3\ \exp(-0.85\ Re^{0.24}) \qquad (7)$$

The upper and lower limits for m, namely 1 and 1/3 respectively, were predicted by "thick" and "thin" boundary layer assumptions.

Series truncation method was used by Dennis, Walker and Hudson (1973) to solve the energy equation around a sphere. The velocity profiles were those calculated by Dennis and Walker (1971). The basis of the method is to approximate the solution, which in theory consists of an infinite series, by a finite number of terms. For the case of low Re, and Pr of the order of unity, only few terms are required to give an adequate representation of the flow conditions, making this approach superior to the finite-difference method.

Acrivos and Taylor (1962) solved the equation of energy for the flow around a sphere by the method of matched asymptotic

expansions. The flow field used was that given by Stokes' solution. The expression derived was accurate for $Pe<1$ and $Re<<1$. The analysis was carried out up to terms of the order of $Pe^3 \ell nPe$. Rimmer (1968) modified this analysis by using the velocity field equations given by Proudman and Pearson (1957). He obtained an expression which was similar to the one given by Acrivos and Taylor, except that it contained one term that was a function of the Prandtl number only. The equations for the Nusselt number given by Acrivos and Taylor and by Rimmer can be written respectively as:

$$Nu = 2 + Pe + Pe^2 + Pe^2 \ell nPe + 0.8293\ Pe^2 + 0.5\ Pe^3 \ell nPe + \ldots \quad (8)$$

$$Nu = 2 + Pe + Pe^2 \ell nPe + f(Pr)\ Pe^2 + \ldots \quad (9)$$

where $1.1 < f(Pr) < 0.79$ for $0.5 < Pr < 1.5$

with a value of $f(Pr) = 0.83$ at $Pr = 1.35$.

Assuming the same flow field as that used by Rimmer, Gupalo and Ryazantsev (1972) obtained a solution for the problem of steady state heat or mass transfer when a first-order chemical reaction on the surface of sphere is also considered. Even though the same method of analysis was employed, their results, reduced for the case when the chemical reaction does not influence the transfer process, were different from those of Rimmer for pure heat transfer. These authors claim that certain mistakes in the matching procedure prevented Rimmer from obtaining the correct results. Gupalo and Ryazantsev gave the following expression for the Nusselt number for the case of pure heat

transfer to the sphere:

$$Nu = 1 + Pe + Pe^2 \ell nPe + 0.5\, Pe^3 \ell nPe + g(Pr)Pe^2 + 2g(Pr)Pe^3 \quad (10)$$

where

$$g(Pr) = 0.25[2Pr^2 - Pr + 4\ell n\gamma - 173/40 + 2(Pr + 1)^2(Pr - 2)\ell n\,(1 + Pr^{-1})] \quad (11)$$

It is worth noting here that the above equation is very similar to that given by Rimmer. However, Gupalo and Ryazantsev defined the Reynolds and the Nusselt numbers in terms of the sphere radius and, consequently, the Peclet number appearing in their equation has half the value of that in Rimmer's equation. Nusselt numbers calculated from Equation (9) are much lower than those obtained from Acrivos and Taylor's or from Rimmer's equations.

Kassoy et al. (1966) studied low Reynolds number flow past a sphere for cases involving variations in the fluid properties. The equations of the flow were solved simultaneously with the energy equation, using the method of matched asymptotic expansions. The viscosity and thermal conductivity were allowed to vary linearly with the dimensionless temperature difference, $\underline{\tau}$. Solutions were obtained of $\underline{Re} \ll 1$ and $\underline{\tau}$ of the order of $\underline{Re}$ and of unity. Expressions were given for the Nusselt number, drag coefficient and the pressure distribution. For $\underline{\tau} = O(1)$:

$$Nu = (\tau + 2)/(\tau + 1)\,[2 + Pe + O(Re^2)] \quad (12)$$

$$C_D = 12/Re\,(16C/3K - K/3) \quad (13)$$

where

$$K = \tau(\tau + 2)$$

and the values of C (K) were calculated numerically for $0.055 < \tau < 1.236$.

The solutions for the case of $\tau = O(Re)$ were given up to terms of the order of $Re^3 \ell nRe$.

Woo (1970, 1971) solved the energy equation numerically in conjunction with the equations of the flow. The steady-state equations were transformed to difference form using Taylor series expansions (finite-difference method). For the case of forced convection alone, the flow equations were solved first and the results were then inserted in the energy equation. When natural convection effects were also considered, the density was temperature-dependent and, therefore, both equations had to be solved simultaneously. Local and average values of the Nusselt number were obtained for Re up to 500. Beard and Pruppacher (1971) in a complementary work investigated the rate of evaporation of small water drops falling at terminal velocities in air. For Re larger than 2, they found that the Sherwood number was proportional to the square root of the Reynolds number, thus:

$$1/2\ Sh = 0.78 + 0.308\ Sc^{1/3}\ Re^{1/2} \qquad (14)$$

At Reynolds numbers lower than 2, the Sherwood number smoothly approached the limiting value of 2 at Re = 0. In this range, the expression can be written as:

$$1/2\ Sh = 1 + 0.108\ (Sc^{1/3}\ Re^{1/2})^2 \qquad (15)$$

Pei et al. (1962, 1965) studied pure and evaporative heat transfer from spheres under combined forced and natural convection.

They found that the two mechanisms of heat transfer were nonadditive and that the transition between the two was a gradual one. They also gave the upper and lower limits of the parameter Gr/Re^2 when the effects of natural or forced convection can be neglected.

HEAT TRANSFER TO CYLINDERS

Heat transfer to cylinders will be discussed briefly in this section, as it will be needed in connection with gas temperature measurements in the experimental section of this thesis. Convective heat transfer to cylinders has been widely studied because of its importance in engineering applications, such as flow around tubes, hot-wire anemometry, etc. Morgan (1975) recently gave a very exhaustive review of this subject. The discussion will therefore be limited to studies carried out at conditions similar to those expected in the plasma jet, namely low Re and large temperature differences.

Collis and Williams (1959) reported a very careful study of heat transfer from hot wires in the Reynolds number range of 0.01 to 140. They were able to correlate their results in the following functional form:

$$Nu\ (T_m/T_\infty)^{-0.17} = A + B\ Re^n \qquad (16)$$

The Nusselt and Reynolds numbers were evaluated at mean film temperatures. Two sets of values for the constants A, B and n were given, depending on whether the Reynolds number was above or below that at

which vortex shedding occurs, namely at Re = 44. This value of Re was found to be independent of the scale or intensity of the turbulence. They also found that free convection effects decrease rapidly with increasing Re and therefore the orientation of the wire with the vertical (for horizontal flow conditions) had little influence at higher Re. An approximate point at which natural convection effects began to assume importance was when $Re<Gr^{1/3}$.

Kassoy (1967) gave an approximate analytic solution for the problem of variable-property flow past a heated cylinder at low Reynolds numbers, using Oseen's approximation. The flow and energy equations were solved by means of matched asymptotic expansions. The effect of velocity and thermal slip at the surface was also considered. Experimental heat transfer results were in good agreement with the theory [Aihara (1967)]. One shortcoming of this study was that the expression given for the Nusselt number was very long and cumbersome, and moreover, its validity was limited to Re<0.1. Also, the temperature differences considered were restricted to values of the order of Re. At Re<0.1, the values of the Nusselt number were almost identical to those of Collis and Williams. Hodnett (1969) extended Kassoy's analysis to larger temperature differences. However, slip effects were not included. Matched asymptotic expansions were used also in this analysis. Although the temperature field was calculated, Hodnett did not give any values for the Nusselt number.

Dennis, Hudson and Smith (1968) obtained the solution of the energy equation based on a velocity field that satisfied the full

Navier-Stokes equations. Both of the temperature and velocity fields were given in series form. The analysis was limited to constant-property flow. Their results at low Re (<40) agree reasonably well with those of Collis and Williams.

Hatton, James and Swire (1970) carried out a similar study to that of Collis and Williams, to investigate the lower range of applicability of hot-wire anemometry. They were able to correlate their results in the same functional form as Equation (16). However, the exponent of the temperature loading factor was -0.154 instead of -0.17. For combined convection they gave the following expression:

$$Nu\ (T_m/T_\infty)^{-0.154} = 0.384 + 0.581\ Re_{eff}^{0.439} \qquad (17)$$

where $$Re_{eff}^2 = Re^2\ (1 + 2.06\ Ra^{0.418}/Re\ .\ \cos\Theta + 1.06\ Ra^{0.836}/Re^2) \qquad (18)$$

and $$Ra = Gr\ .\ Pr$$

It is possible from this equation to find approximately at what point natural convection effects become important.

Woo (1970) solved the complete flow and energy equations for flow past a cylinder numerically, using finite-difference approximations. He calculated local values of the Nusselt number, at several Reynolds numbers. The physical properties of the fluid were kept constant. No correlation for the Nusselt number was, however, given.

Ahmed (1971) investigated the response characteristics of cooled-film probes for the measurement of heat fluxes from high

temperature gas flows. In order to be able to characterize the flow from the probe measurements, Ahmed measured forced convective heat transfer rates to the cooled film from a d.c. arc-heated jet. He proposed a similar correlation to that of Collis and Williams:

$$Nu\ (\nu_m/\nu_\infty)^{-0.15} = 0.2068 + 0.4966\ Re^{0.45} \qquad (19)$$

This equation is applicable for helium or nitrogen flow in the Reynolds number range of 5 to 40 and temperature ratios (T_∞/T_s) between 2 and 4. Ahmed also noted discontinuities in the heat transfer curve at Reynolds numbers of 40 and 55. No physical explanation for these discontinuities was however given, because no flow visualization studies were conducted.

Bradbury and Castro (1972) investigated the accuracy of some heat ransfer correlations. They found that the Collis and Williams' equation represented their experimental results best.

Mucoglu and Chen (1977) gave a theoretical analysis of the problem of combined natural and forced convection across a horizontal cylinder. The transformed boundary layer equations were solved by a finite-difference method. Local values of the Nusselt number were calculated for a wide range of Grashoff and Reynolds number ratios.

NOMENCLATURE

A	-	Constant
A_1, A_2	-	Nozzle cross-sectional areas, Equation (3)
B	-	Constant
C	-	A function of K, Equation (13)
C_1, C_2	-	Nozzle coefficients, Equation (3)
Gr	-	Grashoff number
K	-	Dimensionless temperature, Equation (13)
m	-	Exponent of Prandtl number
n	-	Exponent of Reynolds number
Nu	-	Nusselt number
P	-	Pressure
P_2	-	Pressure at second nozzle exit, Equation (3)
Pe	-	Peclet number
R	-	Radius
Ra	-	Raleigh number
Re	-	Reynolds number
Re_{eff}	-	Effective Reynolds number for combined free and forced convection
Sc	-	Schmidt number
Sh	-	Sherwood number
T	-	Temperature
T_2	-	Temperature at second nozzle exit, Equation (3)
U	-	Free-stream velocity

U	–	Free-stream velocity vector
u	–	Velocity vector
u_1, u_2	–	Velocities

Greek Letters

γ	–	Euler's constant
μ	–	Viscosity
ν	–	Kinematic viscosity
ρ	–	Density
τ	–	Dimensionless temperature difference $(T - T_s) / (T_\infty - T_s)$

Subscripts

∞	–	Free-stream conditions
g	–	Bulk gas conditions
m	–	Mean film conditions
o	–	Surface conditions

REFERENCES

Abu-Romia, M.M. and Bhatia, B., "Heat Pipe Calorimetry for Plasma Stagnation-Point Heat Transfer", AIAA Journal 10 (3), 313 (1972).

Acrivos, A. and Taylor, T.D., "Heat and Mass Transfer from Single Spheres in Stokes' Flow", Phys. Fluids 5 (4), 387 (1962).

Ahmed, A.M., "Application of the Cooled-film to the Study of Premixed Turbulent Flames", Ph.D. Thesis, McGill University, Montreal, 1971.

Aihara, V., Kassoy, D.R. and Libby, P.A., "Heat Transfer from Circular Cylinders at Low Reynolds Numbers", Phys. Fluids 10 (5), 947 (1967).

Armstrong, D.R. and Ranz, W.E., "Design of Inductively Coupled Plasma", I & EC Process Dev. Design 7 (1), 31 (1968).

Baddour, R.F. and Timmins, R.S., The Application of Plasmas to Chemical Processing, MIT Press, 1967.

Baird, M.H. and Hamielec, A.E., "Forced Convection Transfer Around Spheres at Intermediate Reynolds Numbers", Can. J. Chem. Eng. 40 (3), 119 (1962).

Barzelay, M.E., "Continuum Radiation from Partially Ionized Argon", AIAA Journal 4 (5), 815 (1966).

Beard, K.V. and Pruppacher, H.R., "A Wind Tunnel Investigation of the Rate of Evaporation of Small Water Drops Falling at Terminal Velocity in Air", J. Atmosph. Sci. 28, 1455 (1971).

Becker, H.A. and Brown, A.P.G., "Response of Pitot Probes in Turbulent Streams", J. Fluid Mech. 62 (1), 85 (1974).

Becker, H.A., Cho, S.H. and Dhanjal, M.S., "Response of Static Pressure Probes in Turbulent Flames", submitted to J. Fluid Mech. (1975).

Bhattacharyya, D. and Gauvin, W.H., "Modeling of Heterogeneous Systems in a Plasma Jet Reactor", AIChE Journal 21 (5), 879 (1975).

Bohn, W.L., Beth, M.-U. and Nedder, G., "On Spectroscopic Measurements of Velocity Profiles and Non-equilibrium Radial Temperatures in an Argon Plasma Jet", J. Quant. Spectrosc. Radiat. Transfer 7, 661 (1967).

Bott, J.F., "Spectroscopic Measurement of Temperatures in an Argon Plasma Arc", Phys. Fluids 9 (8), 1540 (1966).

Boulos, M.I. and Gauvin, W.H., "Powder Processing in a Plasma Jet : A Proposed Model", Can. J. Chem. Eng. 52, 355 (1974).

Boulos, M.I., "Flow and Temperature Fields in the Fire-ball of an Inductively Coupled Plasma", International Round Table on Study and Applications of Transport Phenomena in Thermal Plasmas, 1975. Lab. Ultra-Refractaires du CNRS, Odeillo-66120, Font Romeau, France. Paper IV-7.

Bradbury, L.J.S. and Castro, I.P., "Some Comments on Heat Transfer Laws for Fine Wires", J. Fluid Mech. 51 (3), 487 (1972).

Bradley, D. and Matthews, K.J., "Measurement of High Gas Temperature with Fine Wire Thermocouples", J. Mech. Eng. Sci. 10 (4), 299 (1968).

Carleton, F.E., "Flow Patterns in a Confined Plasma Jet", Ph.D. Thesis, University of Michigan, Ann Arbor, 1970.

Carleton, F.E. and Kadlec, R.H., "Impact Tube Gas Velocity Measurement at High Temperatures", AIChE Journal 18 (5), 1065 (1972).

Chase, J.D., "Theoretical and Experimental Investigation of Pressure and Flow in Induction Plasmas", J. Appl. Phys. 42 (12), 4870 (1971).

Chester, W. and Breach, D.R., "On the Flow Past a Sphere at Low Reynolds Number", J. Fluid Mech. 37 (4), 751 (1969).

Chludzinski, G.R., "Energy Transfer to Solids in R.F. Generated Plasmas", Ph.D. Thesis, University of Michigan, Ann Arbor, 1964.

Chue, S.H., "Pressure Probes for Fluid Measurement", Prog. Aerospace Sci. 16 (2), 147 (1975).

Clift, R., Grace, J.R. and Weber, M.E., Bubbles, Drops and Particles, Academic Press, 1977.

Collis, D.C. and Williams, M.J., "Two-dimensional Convection from Heated Wires at Low Reynolds Numbers", J. Fluid Mech. 6, 357 (1959).

Cremers, C.J. and Pfender, E., "Temperatures in a Plasma Jet", Int. J Heat Mass Transfer 11 (7), 1203 (1968).

Daily, J.W. and Hardison, R.L., "Rigid Particle Suspensions in Turbulent Shear Flow : Measurement of Total Head, Velocity and Turbulence with Impact Tubes", Hydrodynamics Lab. Rep. no. 67, MIT, 1964.

Dean, R.C., Aerodynamic Measurements, MIT Press, 1953.

Dennis, S.C.R., Hudson, J.D. and Smith, N., "Steady Laminar Forced Convection from a Circular Cylinder at Low Reynolds Numbers", Phys. Fluids 11 (5), 933 (1968).

Dennis, S.C.R. and Walker, J.D.A., "Calculation of the Steady Flow Past a Sphere at Low and Moderate Reynolds Numbers", J. Fluid Mech. 48 (4), 771 (1971).

Dennis, S.C.R., Walker, J.D.A. and Hudson, J.D., "Heat Transfer from a Sphere at Low Reynolds Numbers", J. Fluid Mech. 60 (2), 273 (1973).

Desai, S.V., Daniel, E.S. and Corcoran, W.H., "Use of Particles of Boron Nitride in the Measurement of the Velocity Distribution in Laminar Flow in an Argon Plasma Jet", Rev. Sci. Instrum. 39, 612 (1968).

Dumargue, P., Bonet, C. and Daguenet, M., "Convective Evaporation of a Spherical Super-Refractory Particle Inside a Thermal Plasma : The Stokes' Problem in a Fluid with Variable Properties", Paper CT2.6 presented at the Fifth International Heat Transfer Conference, Sept. 3-7, Tokyo, 1974.

Eckert, E.R.G. and Pfender, E., "Plasma Heat Transfer", in Advances in Heat Transfer, Vol. 4, pp 227-316, Academic Press, 1967.

Eckert, H.U., "Analysis of Thermal Induction Plasma Dominated by Radial Conduction Losses", J. Appl. Phys. 41 (4), 1520 (1970).

Eckert, H.U., "Analytical Treatment of Radiation and Conduction Losses in Thermal Induction Plasmas", J. Appl. Phys. 41 (4), 1529 (1970).

Eckert, H.U. and Pridmore-Browne, D.C., "Temperature Profiles in Argon Induction Plasmas : Theory and Experiment", J. Appl. Phys. 42 (12), 5051 (1971).

El-Shamy, A., "Heat Transfer from a Plasma Torch to Solid Bodies", Int. Round Table Study and Appl. Transport Phenomena Thermal Plasmas, Odeillo, 1975. Paper II-3.

Emmons, H.W., "Recent Developments in Plasma Heat Transfer", in Modern Development in Heat Transfer, W. Ibele (ed.), Academic Press, 1963.

Emmons, H.W., "Arc Measurement of High-Temperature Gas Transport Properties", Phys. Fluids 10 (6), 1125 (1967).

Evans, D.L. and Tankin, R.S., "Measurement of Emission and Absorption of Radiation by an Argon Plasma", Phys. Fluids 10 (6), 1137 (1967).

Farnell, G.A. and Waldie, B., "Transport Processes between Levitated Particles and a Plasma Tail Flame", Int. Round Table Study and Appl. Transport Phenomena Thermal Plasmas, Odeillo, 1975. Paper III-3.

Folsom, R.G., "Review of the Pitot Tube", Trans. ASME 78, 1447 (1956).

Freeman, M.P. and Chase, J.D., "Energy-Transfer Mechanism and Typical Operating Characteristics for the Thermal rf Plasma Generator", J. Appl. Phys. 39 (1), 180 (1968).

Gerdeman, D.A. and Hecht, N.L., Arc Plasma Technology in Material Science, Springer-Verlag, 1972.

Gold, D., "Velocity Measurement in a Radio-Frequency Induction Plasma", Int. Round Table on Plasmas, Odeillo, 1975. Paper IV.8.

Gol'dfarb, V.M. and Drevsin, S.V., "Optical Investigation of the Distribution of Temperature and Electron Density in an Argon Plasma", High Temp. 3, 303 (1965).

Gol'dfarb, V.M., Danskoi, A.V., Drevsin, S.V. and Klubnikin, V.S., "Investigation of Plasma Torch of High-Frequency Argon Burner", High Temp. 5, 495 (1967).

Gottschlich, C.F., Enright, J.A. and Cadek, F.C., "Measurement of the Velocity Distribution in a Plasma Jet", AIAA Journal 4 (6), 1085 (1966).

Grey, J., Jacobs, P.F. and Sherman, M.P., "Calorimetric Probe for the Measurement of Extremely High Temperatures", Rev. Sci. Instrum. 33 (7), 738 (1962).

Grey, J. and Jacobs, P.F., "Experiments on Turbulent Mixing in a Partially Ionized Gas", AIAA Journal 2 (3), 433 (1964).

Grey, J., "Thermodynamic Methods of High-Temperature Measurement", ISA Trans. 4, 102 (1965).

Grey, J., "Proposed Method for Measuring Gas Enthalpy Using Calorimetric Probes", ASTM, Committee E-21 on Space Simulation, 1968.

Griffith, R.M., "Mass Transfer from Drops and Bubbles", Chem. Eng. Sci., 12, 198 (1960).

Gupalo, Y.P. and Ryazantsev, Y.S., "Mass and Heat Transfer from a Sphere in a Laminar Flow", Chem. Eng. Sci. 27, 61 (1972).

Hamielec, A.E. and Johnson, A.I., "Viscous Flow Around Fluid Spheres at Intermediate Reynolds Numbers (I)", Can. J. Chem. Eng. 40, 41 (1962).

Hamielec, A.E., Storey, S.H. and Whitehead, J.M., "Viscous Flow Around Fluid Spheres at Intermediate Reynolds Numbers (II)", Can. J. Chem. Eng. 41, 246 (1963).

Hamielec, A.E., Hoffman, T.W. and Ross, L.L., "Numerical Solution of the Novier-Stokes Equation for Flow Past Spheres", AIChE Journal 13 (2), 212 (1967).

Hare, A.L., "Some Problems Associated with Using Cooled Probes to Characterize Flames at Temperatures in Excess of 1500°C", presented at 21st Aerodynamics Panel Meeting, International Flame Research Foundation, Ijmuiden, Nov. 8, 1972.

Harvey, F.J., Meyer, T.N., Kothmann, R.E. and Fey, M.G., "A Model of Particle Heat Transfer in Arc Heated Gas Streams", Int. Round Table on Plasmas, Odeillo, 1975. Paper II.6.

Hatton, A.P., James, D.D. and Swire, H.W., "Combined Forced and Natural Convection with Low-Speed Air Flow over Horizontal Cylinders", J. Fluid Mech. 42 (1), 17 (1970).

Ho, Thi Hien, "Laser Doppler Anemometry and Its Applications to High Temperature Reactors", M.Eng. Thesis, McGill University, Montreal, 1976.

Hodnett, P.F., "Low Reynolds Number Flow of a Variable Property Gas Past a Heated Circular Cylinder", J. Fluid Mech. 39 (3), 465 (1969).

Hoffman, T.W. and Ross, L.L., "A Theoretical Investigation of the Effect of Mass Transfer on Heat Transfer to an Evaporating Droplet", Int. J. Heat Mass Transfer 15, 559 (1972).

Hollahan, J.R. and Bell, A.T., Techniques and Applications of Plasma Chemistry, J. Wiley, 1974.

Huddlestone, R.H. and Leonard, S.L., (eds.), Plasma Diagnostic Techniques, Academic Press, 1965.

Incropera, F.P. and Leppert, G., "Investigation of Arc Jet Temperature Measurement Techniques", ISA Trans. 6, 35 (1967).

Incropera, F.P. and Leppert, G., "Laminar Flow Heat Transfer from an Argon Plasma in a Circular Tube", Int. J. Heat Mass Transfer 10, 1861 (1967).

Jenson, V.G., "Viscous Flow Round a Sphere at Low Reynolds Numbers (<40)", Proc. Roy. Soc. (London) 249A, 346 (1959).

Johnson, J.R., Choksi, N.M. and Eubank, P.T., "Entrance Heat Transfer from a Plasma Stream in a Circular Tube", I & EC PDD 7 (1), 34 (1968).

Kanzawa, A., "Plasma Heat Transfer Experiments Using a Thermocouple", Heat Transfer Jap. Res. 2 (1), 63 (1973).

Kassoy, D.R., Adamson, T.C. and Messiter, A.F., "Compressible Low Reynolds Number Flow around a Sphere", Phys. Fluids 9 (4), 671 (1966).

Kassoy, D.R., "Heat Transfer from Circular Cylinders at Low Reynolds Numbers", Phys. Fluids 10 (5), 938 (1967).

Katta, S., Lewis, J.A. and Gauvin, W.H., "A Plasma Calorimetric Probe", Rev. Sci. Instrum. 44 (10), 1519 (1973).

Katta, S. and Gauvin, W.H., "The Effect of Local Gas Velocity and Temperature on Local Heat Transfer to a Sphere in a High-Temperature Jet", Can. J. Chem. Eng. 51, 307 (1973).

Katta, S. and Gauvin, W.H., "Local and Overall Heat Transfer to Spheres in a Confined Plasma Jet", AIChE Symp. Ser. 69 (131), 174 (1973).

Kawaguti, M.J., "The Critical Reynolds Number for the Flow Past a Sphere", J. Phys. Soc., Japan 10, 694 (1955).

Kawaguti, M.J., "An Approximate Solution for the Slow Viscous Flow Around a Sphere", J. Phys. Soc., Japan 13, 209 (1958).

Kettani, M.A. and Hoyaux, M.F., Plasma Engineering, J. Wiley, 1973.

Kimura, I. and Kanzawa, A., "Measurement of Stream Velocity in an Arc", AIAA Journal 1 (2), 310 (1963).

Kimura, I. and Kanzawa, A., "Experiments of Heat Transfer to Wires in a Partially Ionized Gas Argon Plasma", AIAA Journal 3 (3), 476 (1965).

Klyuchnikov, A.D., "A Method for Determining the True Gas Flow Temperature from the Readings of Two Thermocouples", Thermal Engineering 13 (12), 111 (1966).

Knopp, C.F., Gottschlich, C.F. and Cambel, A.B., "The Spectroscopic Measurement of Temperature in Transparent Argon Plasmas", J. Quant. Spectrosc. Radiat. Transfer 2, 297 (1962).

Kon'kov, A.A. and Kulagin, S.G., "Radiation of an Argon Plasma at Temperatures of 12 000 - 16 000 K", High Temp. 12 (3), 426 (1974).

Kubanek, G.R., Chevalier, P. and Gauvin, W.H., "Heat Transfer to Spheres in a Confined Plasma Jet", Can. J. Chem. Eng. 46, 101 (1968).

LeClair, B.P., Hamielec, A.E. and Pruppacher, H.R., "A Numerical Study of the Drag on a Sphere at Low and Intermediate Reynolds Numbers", J. Atmos. Sci. 27 (2), 308 (1970).

LeClair, B.P. and Hamielec, A.E., "Flow Behaviour Around a Sphere Accelerating in a Viscous Fluid", Fluid Dynamics Symp., McMaster University, Hamilton, Ontario, Aug. 1970.

Lewis, J.A. and Gauvin, W.H., "Motion of Particles Entrained in a Plasma Jet", AIChE Journal 19 (5), 982 (1973).

Lochte-Holtgrever, W., Plasma Diagnostics, North Holland Pub. Co., Amsterdam, 1968.

McTaggart, F.K., Plasma Chemistry in Electrical Discharges, Elsevier Pub. Co., 1967.

Meubus, P. and Parent, J.R., "Temperature Distributions in a Helium Plasma", Can. J. Chem. Eng. 47, 536 (1969).

Meubus, P. and Parent, J.R., "Velocity Distributions in a Gaseous Plasma : I. Derivation of Flow Types Within a Helium Plasma", Can. J. Chem. Eng. 47, 542 (1969), "II. Application of a Flow Model to a Helium Plasma", Can. J. Chem. Eng. 47, 548 (1969).

Meubus, P., "Hydrogen Concentration Profiles and Velocity Distribution in a Reducing Argon-Hydrogen Plasma", Can. J. Chem. Eng. 52, 616 (1974).

Miller, R.C. and Ayen, R.J., "Temperature Profiles and Energy Balances for an Inductively Coupled Plasma Torch", J. Appl. Phys. 40 (13), 5260 (1969).

Morgan, V.T., "Heat Transfer from Cylinders", in Advances in Heat Transfer, Vol. 11, Academic Press, 1975.

Moskvin, Yu V., "Emissivity of Some Gases at High Temperatures of 6 000 - (2 000) - 12 000 K", High Temp. 6 (1), 1 (1968).

Mucoglu, A. and Chen, T.S., "Analysis of Combined Forced and Free Convection Across a Horizontal Cylinder", to be published in Can. J. Chem. Eng. (1977).

Olsen, H.N., "Thermal and Electrical Properties of an Argon Plasma", Phys. Fluids 2 (6), 614 (1959).

Oseen, C.W., "Ueber die Stokes' sche Formel, und über eine verwandte Aufgabe in der Hydrodynamik", Ark. f. Mat. Astr. och Fys. 6 (29) (1910).

Pei, D.C.T., Narasimhan, C. and Gauvin, W.H., "Evaporation from Drops and Particles in High-Temperature Surroundings", presented at Interaction Between Fluids and Particles Symposium, London, June 1962.

Pei, D.C.T., "Heat Transfer from Spheres Under Combined Forced and Natural Convection", C.E.P. Symp. Ser. 61 (59), 57 (1965).

Petrie, T.W. and Pfender, E., "A Sweeping Wire Probe for the Study of Local Heat Transfer in Plasmas", in Progress in Heat and Mass Transfer, Vol. 2, Pergamon Press, 1969.

Petrov, M.D. and Sepp, V.A., "Use of a Small Probe for Determining the Temperature and Total Pressure Profiles in a Dense Plasma Flow", High Temp. 8 (4), 814 (1970).

Pfender, E., "Recent Results of Plasma-Wall Heat Transfer Studies in Highly Ionized Dense Plasmas", Sonderdruck aus dern Jahrbuch 1971 de DGLR, p. 196.

Pridmore-Brown, D.C., "Numerical Study of the Inductive Electrodless Discharge", J. Appl. Phys. 41 (9), 3621 (1970).

Proudman, I. and Pearson, J.R.A., "Expansions at Small Reynolds Numbers for the Flow Past a Sphere and a Circular Cylinder", J. Fluid Mech. 2, 237 (1957).

Pruppacher, H.R., LeClair, B.P. and Hamielec, A.E., "Some Relations between Drag and Flow Pattern of Viscous Flow Past a Sphere and a Cylinder at Low and Intermediate Reynolds Numbers", J. Fluid Mech. 44 (4), 781 (1970).

Ranz, W.E. and Marshall, W.R., "Evaporation from Drops", Chem. Eng. Prog. 48 (3), 141 (1952).

Rimmer, P.L., "Heat Transfer from a Sphere in a Stream of Small Reynolds Number", J. Fluid Mech. 32 (1), 1 (1968).

Rimon, Y. and Cheng, S.I., "Numerical Solution of a Uniform Flow over a Sphere at Intermediate Reynolds Numbers", Phys. Fluids 12 (5), 949 (1969).

Rovinskii, R.E., Gruzdev, V.A., Gutenmakhler, T.M. and Sovoley, A.P., "Determination of Temperature in a Stationary High-Frequency Induction Discharge", High Temp. 5, 502 (1967).

Rowe, P.N., Claxton, K.T. and Lewis, J.B., "Heat and Mass Transfer from a Single Sphere in an Extensive Flowing Fluid", Trans. Instn. Chem. Engrs. 43, T14 (1965).

Schmidt, P.S. and Leppert, G., "Heat Transfer from Plasma in Tube Flow", Trans. ASME J. Heat Transfer 92C, 483 (1970).

Seymour, E.V., "The Hydrodynamic Drag on a Small Sphere in an Ionized Gas", Trans. ASME J. Appl. Mech. 93, 739 (1971).

Simmons, F.S. and Glawe, G.E., "Theory and Design of a Pneumatic Temperature Probe and Experimental Results Obtained in a High Temperature Gas Stream", NACA TN 3893 (1957).

Skrivan, J.F. and von Jaskowsky, W., "Heat Transfer from Plasma to Water-Cooled Tubes", I & EC PDD 4 (4), 371 (1965).

Smith, D.L. and Churchill, S.W., "Mass and Energy Transfer between a Confined Plasma Jet and a Gaseous Coolant", Technical Report, ORA Project 05607, Dept. of Chem. and Metall. Eng., University of Michigan, Ann Arbor, 1965.

Stokes, C.G., "On the Effect of the Internal Friction of Fluids on the Motion of Pendulums", Trans. Camb. Phil. Soc. 9, 8 (1850).

Tankin, R.S. and Berry, J.M., "Experimental Investigation of Radiation from an Argon Plasma", Phys. Fluids 7 (10), 1620 (1964).

Waldie, B., "Velocity Measurements in and Around the Coil Region of an Induction Plasma", Int. Round Table on Plasmas, Odeillo, 1975. Paper IV-9.

Woo, S.E., Ph.D. Thesis, McMaster University, Hamilton, 1970.

Woo, S.E. and Hamielec, A.E., "A Numerical Method of Determining the Rate of Evaporation of Small Water Drops Falling at Terminal Velocity in Air", J. Atmos. Sci. 28 (8), 1448 (1971).

Yoshida, T. and Akashi, K., "Numerical Study of the Inductively Coupled Plasma Torch", Int. Round Table on Plasmas, Odeillo, 1975. Paper IV-6.

NUMERICAL ANALYSIS OF

VARIABLE-PROPERTY FLOW

PAST A SINGLE SPHERE

INTRODUCTION

In the Literature Review chapter, several numerical solutions for the equations of momentum and heat transfer from spheres were discussed. In all of these solutions, the transport properties of the fluid were assumed to be constant. For isothermal conditions, this assumption is valid and it simplifies the problem significantly by reducing the size of the equations and by uncoupling the flow equations from the energy equation. However, when large temperature gradients exist between the surface of the sphere and the bulk of the fluid, the constant-property assumption can no longer be justified.

The aim of the work described in this chapter was to solve the coupled momentum and energy equations for variable-property flow around a sphere by numerical method. By using finite-difference approximations, the non-linear partial differential equations are reduced to a set of non-linear algebraic equations. The method of solution of these algebraic equations depends on the nature of the original partial differential equations. If steady-state is assumed when formulating the problem, the resulting equations are elliptic and can only be solved by iterative methods. This approach was used by Jenson (1959) and by Hamielec (1967). Convergence with this method is dependent on the relaxation coefficients and on the initial guess for the flow and temperature fields. Another approach is that

reported by Cheng (1970) where the equations are written for the time-dependent flow and then solved for large times to obtain the steady-state solution. The vorticity equation in this case is parabolic and can be solved explicity at each time step. This approach is very useful in giving description of the development of the flow. However, because of the small time increment necessary for a stable solution, this method requires a large number of steps to reach the steady state.

DESCRIPTION OF THE MODEL

In order to reduce the size and duration of the computations required for the solution of the governing equations, a few simplifying assumptions were necessary. To retain the generality of the solution, however, as few assumptions as possible were made. These were:

- The flow past the sphere is laminar and axisymmetric with zero velocity in the angular (ϕ) direction.

- The flow and thermal conditions are invariant with time.

- The flow field is uniform and isothermal, except for the perturbations caused by the presence of the sphere.

- The heat transferred to the sphere by convection is completely dissipated by other means, such as radiation. This balance of heat transfer results in a constant sphere temperature.

- The physical properties of the gas are dependent on the

temperature only. The heat capacity is assumed to be constant.

- The temperature of the sphere is uniform all over the surface.

- Gravity effects are not considered, and the effect of free convection on heat transfer is insignificant.

- The fluid is extensive and an outer boundary was set for computational purposes only.

- Viscous dissipation and compressibility effects are negligible.

THE GOVERNING EQUATIONS

The steady-state continuity, Navier-Stokes and energy equations describing the above model can be written, in spherical coordinates, as [Bird (1960)]:

Continuity

$$1/r^2\ \partial/\partial r(\rho r^2 v_r) + 1/r\ \sin\theta\ \partial/\partial\theta(\rho v_\theta \sin\theta) = 0 \quad . \quad (1)$$

Momentum

r-component

$$\rho(v_r \partial v_r/\partial r + v_\theta/r\ \partial v_r/\partial\theta - v_\theta^2/r) = -\partial p/\partial r - [1/r^2\ \partial/\partial r(r^2\tau_{rr}) + 1/r\ \sin\theta\ \partial/\partial\theta(\tau_{r\theta}\sin\theta) - (\tau_{\theta\theta} + \tau_{\phi\phi})/r] \quad (2)$$

θ-component

$$\rho(v_r \partial v_\theta/\partial r + v_\theta/r\ \partial v_\theta/\partial\theta + v_r v_\theta/r) = -1/r\ \partial p/\partial\theta - [1/r^2\ \partial/\partial r(r^2\tau_{r\theta}) + 1/r\ \sin\theta\ \partial/\partial\theta\ (\tau_{\theta\theta}\sin\theta) + \tau_{r\theta}/r - \cot\theta/r\ \tau_{\phi\phi}] \quad (3)$$

where $\tau_{rr} = -\mu(2\partial v_r/\partial r - 2/3\ \nabla.\bar{v})$ (4)

$\tau_{\theta\theta} = -\mu[2(1/r\ \partial v_\theta/\partial\theta + v_r/r) - 2/3\ \nabla.\bar{v}]$ (5)

$\tau_{\phi\phi} = -\mu[2(v_r/r + v_\theta \cot\theta/r) - 2/3\ \nabla.\bar{v}]$ (6)

$\tau_{r\theta} = -\mu[r\partial/\partial r(v_\theta/r) + 1/r\ \partial v_r/\partial\theta]$ (7)

$\nabla.\bar{v} = 1/r^2\ \partial/\partial r(r^2 v_r) + 1/r\ \sin\theta\ \partial/\partial\theta(v_\theta \sin\theta]$ (8)

Energy

$$c_v(v_r \partial T/\partial r + v_\theta/r\ \partial T/\partial\theta) = -[1/r^2\ \partial/\partial r(r^2 q_r) + 1/r\ \sin\theta\ \partial/\partial\theta(q_\theta\ \sin\theta)] \quad (9)$$

The number of the above equations was reduced by the introduction of the stream function. For three-dimensional flows the concept of the stream function is valid only when the flow is axisymmetric. The stream function, modified for variable-density fluid, was related to the velocity components by the following equations:

$v_r = -1/r^2\rho\sin\theta\ \partial\Psi/\partial\theta$ (10)

$v_\theta = 1/r\rho\sin\theta\ \partial\Psi/\partial r$ (11)

With its units changed from volume/unit time to mass/unit time, the stream function defined in the above equations satisfied the continuity equation for a variable-density fluid.

The vorticity vector is defined as the curl of the velocity vector. The components of vorticity, in spherical coordinates [Yuan (1967)] are:

$$\Omega_r = 1/r^2 \sin\theta [\partial/\partial\theta (r v_\phi \sin\theta) - \partial/\partial\phi (r v_\theta)] \quad (12)$$

$$\Omega_\theta = 1/r\sin\theta [\partial/\partial\phi (v_r) - \partial/\partial r (r v_\phi \sin\theta)] \quad (13)$$

$$\Omega_\phi = 1/r [\partial/\partial r (r v_\theta) - \partial/\partial\theta (v_r)] \quad (14)$$

For axisymmetric flow with $v_\phi = 0$, the vorticity components Ω_r and Ω_θ are both equal to zero. Replacing the velocity terms by the stream function, reduces Equation (14) to:

$$E^2\Psi = \zeta\rho r\sin\theta + 1/\rho(\partial\Psi/\partial r \cdot \partial\rho/\partial r + 1/r^2\, \partial\Psi/\partial\theta \cdot \partial\rho/\partial\theta) \quad (15)$$

where $\zeta = \Omega_\phi$

and $E^2 = \partial^2/\partial r^2 + \sin\theta/r^2\, \partial/\partial\theta(1/\sin\theta\, \partial/\partial\theta)$ (16)

The momentum equations (2) and (3) written in the above form cannot be solved before the boundary condition for the pressure at the surface is defined. For a blunt body, such as a sphere, the surface pressure varies significantly over the surface and can only be determined from a knowledge of the velocity field. To overcome this difficulty, Equations (2) and (3) can be cross-differentiated to eliminate the pressure terms completely. Carrying out these operations and replacing the velocities by the stream function and vorticity, reduces the momentum equations to:

$$Re\,r\sin\theta/2\,[\partial\Psi/\partial z.\partial/\partial\theta(\zeta/r\sin\theta) - \partial\Psi/\partial\theta.\partial/\partial z(\zeta/r\sin\theta)] = E^2\mu\zeta r\sin\theta + \Sigma(\mu)\sin\theta - Re\,r\sin\theta/2\;\Gamma(\rho) \quad (22)$$

where $$E^2 = \partial^2/\partial z^2 - \partial/\partial z + \sin\theta\,\partial/\partial\theta(1/\sin\theta\,\partial/\partial\theta) \quad (23)$$

$$\Sigma(\mu)/2 = \partial\mu/\partial z[\partial^2 v_r/\partial z\partial\theta + v_\theta + \partial v_r/\partial\theta + \partial^2 v_\theta/\partial\theta^2 + \partial(v_\theta\cot\theta)/\partial\theta - \partial v_\theta/\partial z] + \partial\mu/\partial\theta[v_r - \partial^2 v_r/\partial z^2 - \partial^2 v_\theta/\partial z\partial\theta - \cot\theta(\partial v_\theta/\partial z - v_\theta)] + \partial^2\mu/\partial z^2[\partial v_r/\partial\theta - v_\theta] + \partial^2\mu/\partial\theta^2[-\partial v_\theta/\partial z] + \partial^2\mu/\partial z\partial\theta[\partial v_\theta/\partial\theta + v_r - \partial v_r/\partial z] \quad (24)$$

and $$\Gamma(\rho) = \partial\rho/\partial r(v_r\partial v_r/\partial\theta + v_\theta\partial v_\theta/\partial\theta) - \partial\rho/\partial\theta\,(v_r\partial v_r/\partial z + v_\theta\partial v_\theta/\partial z) \quad (25)$$

Defining the dimensionless temperature as:

$$T' = T/T_\infty \qquad k' = k/k_\infty$$

and $$Pe = 2RU_\infty\rho_\infty C_p/k_\infty \quad (26)$$

gives $$(Pe\,r\rho/2)(v_r\partial T/\partial z + v_\theta\partial T/\partial\theta) = k[\partial^2 T/\partial z^2 + \partial T/\partial z + \partial^2 T/\partial\theta^2 + \cot\theta\,\partial T/\partial\theta] + \partial T/\partial z.\partial k/\partial z + \partial T/\partial\theta.\partial k/\partial\theta \quad (27)$$

The superscript on all the dimensionless variable was dropped out for simplicity.

The thermal conductivity, viscosity and density of argon [Amdur (1958), Drellishak (1963)] in the temperature range of 1 500

$$\partial\Psi/\partial\theta \cdot \partial/\partial r(\zeta/r\sin\theta) - \partial\Psi/\partial r \cdot \partial/\partial\theta(\zeta/r\sin\theta) =$$

$$E^2\mu\zeta r\sin\theta/\sin\theta + \Sigma(\mu) + \Gamma(\rho) \qquad (17)$$

where $\Sigma(\mu)/2 = \partial\mu/\partial r[\partial\nabla.\bar{v}/\partial\theta - \partial v_\theta/\partial r] + \partial\mu/\partial\theta[\partial(v_r/r)/\partial r -$

$2/r^2\partial v_\theta/\partial\theta - \partial\nabla.\bar{v}/\partial r] + \partial^2\mu/\partial r^2(\partial v_r/\partial\theta - v_\theta) -$

$\partial^2\mu/\partial\theta^2(1/r\partial v_\theta/\partial r) + \partial^2\mu/\partial r\partial\theta[\partial(v_\theta/r)/\partial\theta -$

$r\partial(v_r/r)/\partial r] \qquad (18)$

$$\Gamma(\rho) = -\partial\rho/\partial\theta \cdot \partial/\partial r(v_r^2 + v_\theta^2)/2 +$$

$$\partial\rho/\partial r \cdot \partial/\partial\theta(v_r^2 + v_\theta^2)/2 \qquad (19)$$

and ζ and $E^{2\theta}$ are defined by Equations (15) and (16), respectively.

The above equations are normalized by introducing new variables, non-dimensionalized in terms of the bulk conditions of the gas, thus:

$$\Psi' = \Psi/\rho_\infty U_\infty R^2 \qquad \zeta' = \zeta R/U_\infty \qquad r' = r/R$$

$$v_r' = v_r/U_\infty \qquad v_\theta' = v_\theta/U_\infty \qquad \rho' = \rho/\rho_\infty$$

$$\mu' = \mu/\mu_\infty \qquad Re = 2RU_\infty\rho_\infty/\mu_\infty$$

also $r' = e^z \qquad (20)$

The dimensionless radial distances, z, allows exponential increase in r for equal increments of z. Also, when z is used, the radial spacing near the surface of the sphere is kept small, while still maintaining a relatively large domain with a reasonable number of mesh points. Substituting Equations (20) into Equations (15) to (19) gives:

$$E^2\Psi = \zeta r^3\rho\sin\theta + 1/\rho(\partial\Psi/\partial z.\partial\rho/\partial z + \partial\Psi/\partial\theta.\partial\rho/\partial\theta) \qquad (21)$$

to 5 000 K, are related to the absolute temperature by the following expressions:

$$\rho = 487/T \qquad (kg\ m^{-3})$$

$$\mu = 2 \times 10^{-7} T^{x} \qquad (Nsm^{-2})$$

$$k = 1.57 \times 10^{-4} T^{x} \qquad (Jm^{-1}\ s^{-1}\ k^{-1}) \qquad (28)$$

where $x = 0.8$

The actual values of these properties are listed in Appendix C. In dimensionless variables:

$$\rho = 1/T \qquad (29)$$

$$\mu = k = T^{x} \qquad (30)$$

With C_p for argon independent of the temperature, Equation (30) agrees with the fact that the Prandtl number for argon is constant, and is equal to 0.672.

With the physical properties varying only with the temperature, the independent variables that characterized the flow around a sphere are the Reynolds number, Peclet number and the dimensionless temperature. The actual level of the temperature affects the flow only by changing the value of the exponent x.

Equations (29) and (30) couple the energy equation to the vorticity and the stream function. Substituting Equations (29) and (30) into the governing equations results in three equations with

three variables only, namely, Ψ, ζ and T.

THE BOUNDARY CONDITIONS

The three main variables in the momentum and energy equations are the stream function, vorticity and temperature. In the numerical solution, a few other variables were also introduced, to reduce the number of calculations and the size and complexity of the difference equations. The functions F and G were defined as:

$$F = \zeta/r \sin\theta \tag{31}$$

$$G = \mu\zeta r \sin\theta \tag{32}$$

Furthermore, when the functions Σ and Γ were evaluated, v_r and v_θ were used and not the stream function.

The boundary conditions at the sphere surface, ($z = 0$) were:

$$\Psi = 0$$

$$T = T_o$$

$$v_r = \partial\Psi/\partial\theta = 0$$

$$v_\theta = \partial\Psi/\partial z = 0$$

The condition for the vorticity at the surface was derived as follows:

[from Equation (14)]

$$\zeta = + (\partial v_\theta/\partial z + v_\theta - \partial v_r/\partial\theta)/r$$

At the surface, this reduced to:

$$\zeta = \partial v_\theta/\partial z = \partial/\partial z\ (1/\rho r^2 \sin\theta . \partial\Psi/\partial z)$$

Carrying out the differentiation and dropping out all terms containing $\partial\Psi/\partial z$ gave:

$$\zeta_o = 1/\rho_o \sin\theta . \partial^2\Psi/\partial z^2 = T_o/\sin\theta . \partial^2\Psi/\partial z^2$$

Also $F = \zeta_o/\sin\theta$

$$G = \mu_o \zeta_o \sin\theta = T_o^x\ \zeta_o \sin\theta$$

At the outer boundary ($z = z_\infty$):

$$\Psi = 1/2\ r^2 \sin^2\theta$$

$$\zeta = F = G = 0$$

$$T = 1$$

$$v_r = -\cos\theta$$

$$v_\theta = \sin\theta$$

To reduce the size of the computation domain, only the upper half of the flow field was considered. The other half was exactly the same since the flow was symmetric around the axis. Consequently, conditions along the axis of symmetry also had to be defined.

At $\theta = 0^\circ$:

$$\Psi = 0$$

$$\zeta = G = 0$$

$$\partial T/\partial\theta = 0$$

$$v_\Theta = 0$$

$$v_r = -1/\rho r^2 \sin\Theta \cdot \partial\Psi/\partial\Theta$$

$$F = \zeta/r\sin\Theta$$

Since $\sin\Theta = 0$ at $\Theta = 0°$, v_r and F had to be found by taking the limits as Θ approached zero, thus:

$$v_r = -1/\rho r^2 \cdot \partial^2\Psi/\partial\Theta^2$$

$$F = 1/r \cdot \partial\zeta/\partial\Theta$$

At $\Theta = 180°$:

$$\Psi = 0$$

$$\zeta = G = 0$$

$$\partial T/\partial\Theta = 0$$

$$v_\Theta = 0$$

$$v_r = 1/\rho r^2 \partial^2\Psi/\partial\Theta^2$$

$$F = -1/r \; \partial\zeta/\partial\Theta$$

THE DIFFERENCE EQUATIONS

The stream function, vorticity and temperature equations were transformed from their original partial differential form to a set of algebraic equations, thus, making them amenable to a computer solution. To do this, the flow field was first divided into a large number of mesh points. The variables, at each of these points, were approximated by Taylor series and the derivatives determined in terms of adjacent points. The solution, then, consisted of satisfying the difference equations at every lattice point. The central-difference

method was used for all of the internal points. With this method, the derivative is approximated by the difference between points on both sides of the point under consideration. Forward-difference and backward-difference approximations evaluate the derivatives in terms of two or more consecutive points in the same direction, either in front or behind the lattice point. These were used to approximate the Neumann-type boundary conditions. The general finite-difference equations, accurate up to the order of h^2 are listed in Appendix A.

Figure 1 illustrates the circular mesh used. It can be seen that the divisions are smallest near the surface of the sphere. This was necessary for obtaining accurate description of the flow where the gradients are steepest. The governing equations, written in the difference form accurate to $O(h^2)$, together with the boundary conditions are listed below.

Stream Function

$$[\Psi(I,J+1)(2-A) + \Psi(I,J-1)(2+A)]/2A^2 + [\Psi(I+1,J)(2-B\cot\theta) + \Psi(I-1,J)(2+B\cot\theta)]/2B^2 - \Psi(I,J)(2/A^2+2/B^2) - \zeta(I,J)r^3\sin\theta/T(I,J) + 1/T(I,J)\ [\partial\Psi/\partial z.\partial T/\partial z + \partial\Psi/\partial\theta.\partial T/\partial\theta] = 0 \qquad (33)$$

Vorticity

$$[G(I,J+1)(2-A) + G(I,J-1)(2+A)]/2A^2 + [G(I+1,J)(2-B\cot\theta) + G(I-1,J)(2+B\cot\theta)]/2B^2 - G(I,J)(2/A^2+2/B^2) + \Sigma(\mu)\sin\theta - Re r\sin\theta/2\Gamma(\rho) + Re r\sin\theta/4\{\partial\Psi/\partial\theta[F(I,J+1) - F(I,J-1)/A - \partial\Psi/\partial z[F(I+1,J) - F(I-1,J)]/B\} = 0 \qquad (34)$$

FIGURE 1

CIRCULAR MESH SYSTEM

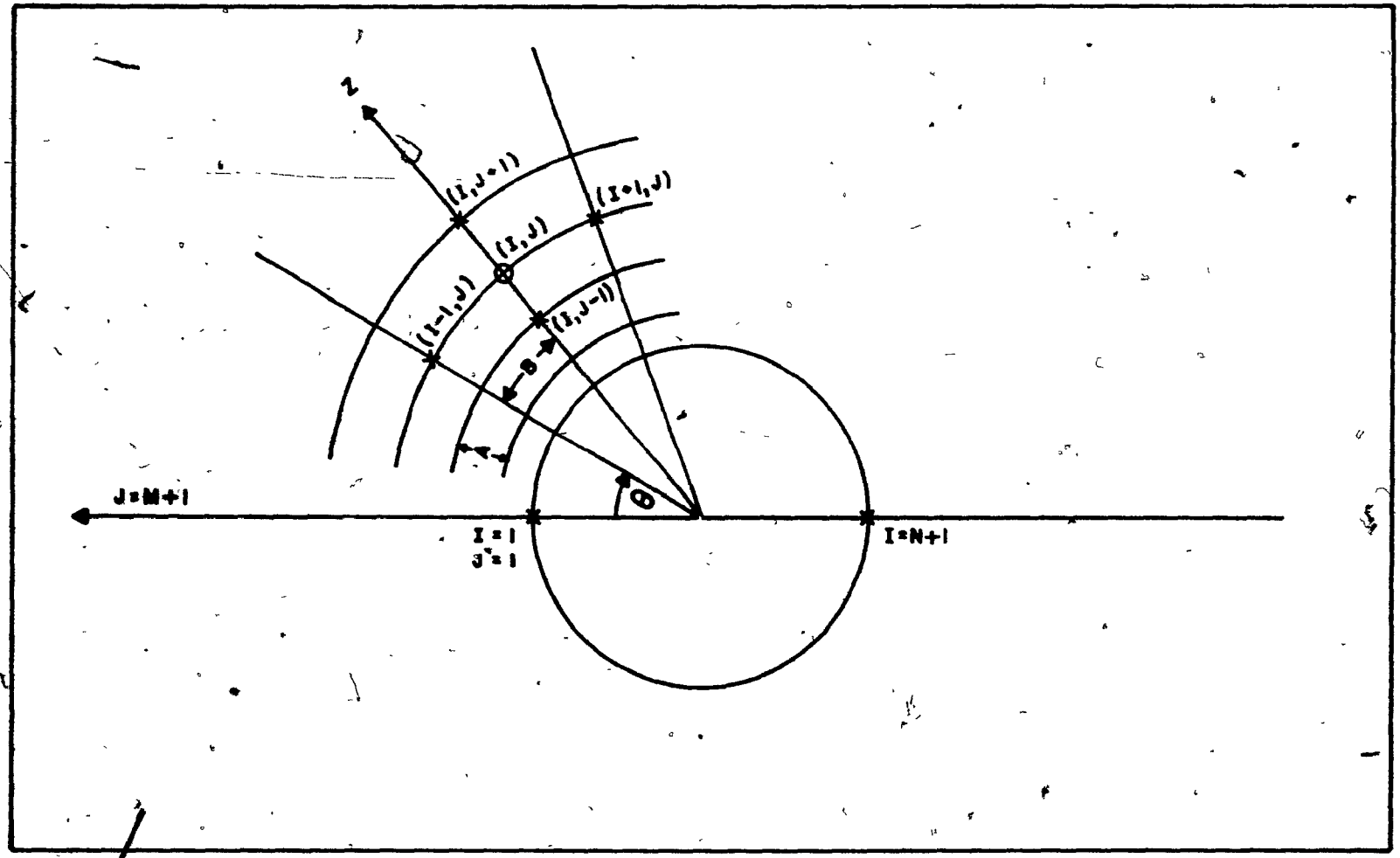

CIRCULAR MESH, Z vs. θ

The functions $\underline{\Sigma}$ and $\underline{\Gamma}$, in difference form are given in Appendix A. For simplicity, some of the derivatives in the difference equations are written in their differential form. The difference equivalent of these derivatives can be obtained by direct substitution into the finite-difference equations listed in Appendix A.

Energy

$$[T(I,J+1)(2+A) + T(I,J-1)(2-A)]/2A^2 + [T(I+1,J)(2+B\cot\Theta) + T(I-1,J)(2-B\cot\Theta)]/2B^2 - T(I,J)(2/A^2 + 2/B^2) + Pe/[2r\sin\Theta T(I,J)^X](\partial\Psi/\partial\Theta.\partial T/\partial z - \partial\Psi/\partial z.\partial T/\partial\Theta) + x/T(I,J)\ [(\partial T/\partial z)^2 + (\partial T/\partial\Theta)^2] = 0 \qquad (35)$$

Boundary Conditions

At $z = 0$:

$$\Psi(I,1) = 0$$

$$v_\Theta(I,1) = 0$$

$$v_r(I,1) = 0$$

$$T(I,1) = T_o$$

$$\zeta(I,1) = T_o.[8\Psi(I,2) - \Psi(I,3)]/2A^2\sin\Theta$$

$$G(I,J) = -T_o^X\zeta(I,1)\sin\Theta$$

$$F(I,1) = \zeta(I,1)/\sin\Theta$$

At $z = z_\infty$:

$$\Psi(I,M+1) = 1/2\ r_\infty^2 \sin^2\theta$$

$$\zeta(I,M+1) = 0$$

$$F(I,M+1) = G(I,M+1) = 0$$

$$T(I,M+1) = 1$$

$$v_\theta(I,M+1) = \sin\theta$$

$$v_r(I,M+1) = -\cos\theta$$

At $\theta = 0$:

$$\Psi(1,J) = 0$$

$$\zeta(1,J) = 0$$

$$T(1,J) = [4T(2,J) - T(3,J)]/3$$

$$v_\theta(1,J) = 0$$

$$v_r(1,J) = -2T(1,J)\ \Psi(2,J)\ /B^2r^2$$

$$F(1,J) = \zeta(2,J)/Br$$

$$G(1,J) = 0$$

At $\theta = \pi$:

$$\Psi(N+1,J) = 0$$

$$\zeta(N+1,J) = 0$$

$$T(N+1,J) = [4T(N,J) - T(N-1,J)]/3$$

$$v_\theta(N+1,J) = 0$$

$$v_r(N+1,J) = 2T(N+1,J)\ \Psi(N,J)/B^2r^2$$

$$F(N+1,J) = -\zeta(N,J)/Br$$

$$G(N+1,J) = 0$$

The derivation of the Neumann-type boundary conditions is given in Appendix A.

The above algebraic equations cannot be solved directly because of their non-linearity. Hence, an iterative procedure was used. The most appropriate iteration method is the Successive Over Relaxation (SOR) method, where a relaxation factor is used to control the speed of convergence of the process and to maintain its stability.

THE RELAXATION PROCEDURE

Equations (33) to (35) can be written in a general form as:

$$\Phi(I,J) = f[\Phi(I+1,J),\ \Phi(I-1,J),\ \Phi(I,J+1),\ \Phi(I,J-1)] \qquad (36)$$

Hence, to find the value of the function Φ at the point (I,J), the values of this function must be defined for the four adjacent points. In other words, to start the process, initial values for all the functions at every mesh point in the grid must be assigned. To satisfy the governing equations, new values of the variable are then calculated with the aid of Equation (36). If the initial guess was very far from the required solution, then direct substitution of the

new values in the grid can cause instabilities which may lead to divergence. To avoid this, the new value of the function that is placed in the grid is chosen somewhere between the old and the calculated values, thus:

$$\Phi_{new} = \Phi_{old} + W(\Phi_{calc} - \Phi_{old}) \qquad (37)$$

W is known as the relaxation coefficient. Equation (36) can be re-written as:

$$Res = f[\Phi(I+1,J), \Phi(I-1,J), \Phi(I,J+1), \Phi(I,J-1)] + \Phi(I,J) \qquad (38)$$

This simplifies Equation (37) to:

$$\Phi_{new} = \Phi_{old} + W.Res \qquad (39)$$

Equation (39) was easier to program than Equation (37). Either of two methods can be used to evaluate Equation (38): (a) Richardson's method where the old values for all of the variables are used to evaluate Res, or (b) Liebmann's method where the new values are used as they are calculated. Liebmann's method converges much faster than Richardson's and requires about one half the storage space, and therefore it was the method used in this study.

The optimum value of the relaxation coefficient that will give the fastest convergence depends on the mesh, the shape of the domain, the type of boundary conditions and on the nature of the equations [Roache (1972)]. Roache (1972) and Lapidus (1962) gave

methods for calculating the optimum relaxation coefficients for linear elliptic equations. No such methods are available when the equations are non-linear. Moreover, because of the large times required for solving a set of non-linear equations, it is not practical to conduct a systematic study of the effect of different relaxation coefficients on the rate of convergence. In such instances, the relaxation coefficients are chosen by trial and error, and their value is specific to the system under consideration. Usually, the selection of the relaxation coefficient is based on the highest value that does not cause instabilities.

For non-linear problems, there is no reason for assuming that the optimum relaxation coefficient has the same value over the entire flow field. In the logarithmic grid of the present study, the mesh size increased exponentially with radial distance away from the surface resulting in an increased instability near the outer boundary. Therefore, small values of the relaxation coefficient near the outer boundary were necessary to reduce error propagation and to dampen oscillations.

The general form of a second-order elliptic equation is:

$$\nabla^2_{xy}\phi = P\partial\Phi/\partial x + Q\,\partial\Phi/\partial y \qquad (40)$$

Woo (1970) derived the following expression for the relaxation coefficients to be used in the solution of the above equation:

$$W_{\Phi i,j} = 2/[1 + \sqrt{0.5(P^2 + Q^2)}] \qquad (41)$$

and for the linear Poisson's equation:

$$W_\psi = 2/[1 + \pi\sqrt{0.5(N^{-2} + M^{-2})}] \qquad (42)$$

Woo found that for linear equations, such as constant-property heat transfer to a sphere, convergence with these relaxation coefficients was much faster than when constant factors were used. No such comparison was possible for the non-linear problem, where the relaxation coefficients had to be evaluated at every step since P and Q were continuously changed during the computation. Fortunately, Woo found that these coefficients (P and Q) did not vary much from one iteration to the other and, thus, had to be re-calculated only once in every K iterations. K was of the order of 20.

To speed up the rate of convergence, Woo also described a "convergence promotion technique", where the process was given a periodical pulse change every K iterations, by multiplying the relaxation coefficients by a large factor (of the order of 30). This pulse change caused temporary instability that, in general, 'shot' the solution towards convergence. To prevent such instability from propagating across the field, a new sequence of calculations was devised. In this sequence, each complete iteration cycle was divided into two alternating half-cycles: one used direct substitution and the other variable coefficients with convergence promotion. It was found that this method was more stable and two to three times faster than direct SOR.

The values of P and Q were found from Equations (22) and (27):

$$P_\zeta = Re/2r\sin\theta \; \partial\Psi/\partial z \qquad (43)$$

$$Q_\zeta = -Re/2r\sin\theta \; \partial\Psi/\partial\theta \qquad (44)$$

$$P_T = Pe/2r\sin\theta \cdot \partial\Psi/\partial \qquad (45)$$

$$Q_T = -Pe/2r\sin\theta \; \partial\Psi/\partial\theta \qquad (46)$$

A computer programme was written for the simultaneous solution of the governing equations by the above iteration method. Direct substitution and varying relaxation coefficients were applied alternately on the mesh points, to calculate the new values of the vorticity, stream function and temperature. The programme listing is given in Appendix D. The independent variables of the programme were the Reynolds number, Peclet number, dimensionless surface temperature and the property exponent x. The programme, however, did not give the constant-property solution when x was set to zero, because the variation of the density with temperature was still included in the equations. This less general set of equations was found to require less computations, as compared to that where the properties were evaluated individually at every point. To obtain the constant-property solution a separate programme was written. Since the simpler constant-property equations were used in this programme, the energy equation was no longer coupled to the momentum equations, and thus, the former was solved after the flow field had been calculated. This programme is also listed in Appendix D.

COMPUTATION SEQUENCE

The number of iterations required to reach convergence depended on the nature of the problem, the relaxation coefficients used and on the initial guess. Starting with a guess that was far from the condition under study caused instabilities and required the use of very low relaxation coefficients which in turn led to an increase in the number of iterations. To overcome this problem, the solutions were obtained in small faster steps, through which the Reynolds number and the surface temperature, T_o were changed gradually.

To allow the use of one solution as an initial guess for a successive one, the lattice spacing and the domain size must be the same, otherwise a complicated interpolation scheme would be required. The mesh size and spacing thus chosen should be suitable over a reasonable range of the Reynolds number. At low Reynolds numbers wall effects are important and consequently the flow field must be fairly large. As the Reynolds number increases, the effect of the proximity of the outer boundary on the flow decreases. Lattice spacing starts to gain importance with increasing Re because the gradients become steeper near the surface of the sphere. From a computation point of view, the direct effect of increasing field size and reducing lattice spacing is an increase in the computer memory and in the time required per iteration. Decreasing the number of points by increasing lattice spacing or reducing the field size may cause inaccuracies and instabilities in the solution,

especially at the rear part of the sphere.

The complexity of the equations under study prevented a systematic investigation of the exact effects of lattice spacing and field size on the accuracy of the solutions, in order to permit the selection of an optimum mesh. Woo (1971) studied the constant-property problem extensively and made some recommendations on the optimum mesh and field sizes. These guidelines were used in this study, where two different mesh sizes were used for the low and the intermediate Reynolds number ranges, thus:

Re	Δz	M	r_∞	$\Delta\theta$	N
0.1 - 1	0.1	40	54.6	6°	30
10 - 50	0.05	40	7.39	6°	30

In the present work, the constant-property solutions were obtained first for all Reynolds numbers under consideration. The simpler computer programme was used. It was found that, per iteration, this programme was four times faster than the variable-property one. For the constant-property flow, all the temperature profiles were calculated with T_∞ set equal to 0.5.

For low Reynolds numbers (Re = 0.1, 1) the initial guesses were the creeping flow and the heat conduction solutions around a sphere. These solutions, and not the solution for Re = 1, were also used as first approximation for Re = 10, since the solution at Re = 1 was obtained with a different grid.

The convergence criterion in this study was based on maximum absolute error in the temperature and vorticity. When the change in these variables between successive iterations was less than the tolerance, at every lattice point, the computation process was stopped and the Nusselt number and the drag coefficients calculated. These were also calculated once every K iterations. The tolerance was 10^{-5} for low Re and went up to 10^{-3} at Reynolds number of 50. As the computation times became excessive, the calculations were stopped when the variations in the Nusselt number and the drag coefficients from one iteration to the other were small. It was felt that very accurate solutions were not quite necessary since, in practice, the flow variables in high temperature environments are not known to such an accuracy as to justify the increase in the computation work.

The constant-property flow and temperature fields were calculated for Re = 0.1, 1, 10, 20, 30 and 50. The surface temperature was set at a value of 0.50. Since the constant-property energy equation is linear in temperature, the temperature field is not affected by the actual value of the surface temperature. The variable-property flow conditions studied are listed in Table I. The variable-property solution for the limiting case of $T_o = 1$ was the same as the constant-property solution.

The constant-property solutions were used as the initial guess for the variable-property calculations. In cases when T_o of the initial guess was different from that of the required solution,

TABLE I

VARIABLE-PROPERTY FLOW CONDITIONS

	VALUE OF SURFACE REYNOLDS NUMBER, Re_o		
Re_∞	$T_o = 0.75$	$T_o = 0.50$	$T_o = 0.25$
0.1	0.17	0.35	1.2
1	1.68	3.48	12.1
10	16.8	34.8	121
20	33.6	69.6	242
30	50.4	104	364
50	83.9	174	606

the temperature field was multiplied by a scaling factor. This step was necessary to avoid divergence and to accelerate the solution. The following equation was used to change the temperature field from $T_{o,1}<T(I,J)_1<1$ to $T_{o,2}<T(I,J)_2<1$:

$$T(I,J)_2 = (1 - T_{o,2})/(1 - T_{o,1}) \cdot [T(I,J)_1 - T_{o,1}] + T_{o,2} \qquad (47)$$

A one-step jump from constant-property to variable-property flow, at $T_o = 0.5$, was found to diverge at $Re<10$. This reflects the large effect of the variation of properties on the flow and temperature patterns. To stabilize the process the following sequence was used:

Constant-property ($T_o = 0.5$) → Variable-property:

$T_o = 0.75 \rightarrow T_o = 0.50 \rightarrow T_o = 0.25$

At each step the temperature profile was adjusted by Equation (47).

Even with the above stepwise procedure, the computation process still tended to diverge as the Reynolds number increased or T_o decreased. A further dampening factor was introduced in the vorticity calculation to check these instabilities; the residue of the vorticity equation was multiplied by a factor α at every lattice point. α had a value between zero and unity. Table II lists the values of α used at different Reynolds numbers and temperature.

As T_o decreased, the solution took longer to converge and, therefore, it was not possible to go below $T_o = 0.25$. It is worth

TABLE II

VALUES OF DAMPENING FACTOR, α

Re_∞	$T_o = 1.00$*	$T_o = 0.75$	$T_o = 0.50$	$T_o = 0.25$
0.1	1.0	1.0	0.7	0.7
1	1.0	1.0	0.7	0.7
10	1.0	1.0	0.5	0.4
20	1.0	0.7	0.5	0.4
30	1.0	0.7	0.5	0.4
50	1.0	0.7	0.4	0.4

*$T_o = 1$ refers to constant-property solution.

noting here that the surface Reynolds number at $T_o = 0.25$ was twelve times larger than that evaluated at bulk flow conditions. This may explain the difficulties incurred in reaching convergence. It is quite possible that the process might have been more stable had the initial guess been at a higher Reynolds number than that of the required solution.

As the Reynolds number increased and T_o decreased the process became more susceptible to instabilities caused by the convergence promotion technique. The number of iterations between the promotion steps, K, had to be increased from 20 to 30, and the acceleration factor reduced from 30 to 20, for the constant property solution. For the variable-property situation it was found that convergence was slowed by this technique due to increased instabilities and therefore the promotion factor was set at a value of unity.

It should be emphasized again, at this point, that all the methods used above to accelerate or reach convergence were very arbitrary. By no means are they the fastest or the 'optimum' ones. Because of the lengthy nature of the problem, it was not possible to investigate the methods of solution systematically and come up with definite recommendations on the best method that should be used.

CALCULATION OF THE DRAG COEFFICIENTS

The drag acting on a sphere can be divided into two components: skin drag which is due to viscous forces at the surface of the sphere, and pressure drag which is caused by differences in the

pressure between the front and rear of the sphere.

The force acting on a sphere is the sum of the pressure and friction forces minus the static forces [Bird (1960)], thus:

$$F_k = (F_n - F_s) + F_t \tag{48}$$

where $$F_n = \int_0^{2\pi}\int_0^{\pi} [p|_{r=R} \cos\theta]\, R^2 \sin\theta\, \partial\theta\, \partial\phi \tag{49}$$

$$F_s = \int_0^{2\pi}\int_0^{\pi} [p_\infty|_{r=R} \cos\theta]\, R^2 \sin\theta\, \partial\theta\, \partial\phi \tag{50}$$

$$F_t = \int_0^{2\pi}\int_0^{\pi} \{\mu[r\, \partial/\partial r(v_\theta/r) + 1/r\, \partial v_r/\partial\theta]|_{r=R} \sin\theta\}R^2 \sin\theta\, \partial\theta\partial\phi \tag{51}$$

The friction factor (drag coefficient) is defined as:

$$C_D = F_k/AE_k \tag{52}$$

where $\underline{A}$ is a characteristic area and $\underline{E_k}$ a characteristic kinetic energy per unit volume. For a sphere the characteristic area is the projected area, πR^2, and the kinetic energy is $\rho_\infty U^2_\infty/2$. The choice of $\underline{\rho}$ is arbitrary and can be taken as any density in the flow field. Since all the variables were non-dimensionalized in terms of the bulk gas condition, the density used in the kinetic energy term was evaluated at bulk gas temperature. The components of the drag are then:

$$C_{DP} = (F_n - F_s)/[\pi R^2 \rho_\infty U^2_\infty/2] \tag{53}$$

$$C_{DF} = F_t/[\pi R^2 \rho_\infty U^2_\infty/2] \tag{54}$$

Assuming axisymmetric flow and defining the surface pressure, $p(\theta)$, as:

$$p(\theta) = (p - p_\infty)/[\rho_\infty U^2_\infty/2] \tag{55}$$

reduce the drag equations to the following dimensionless form:

$$C_{DP} = \int_0^\pi p(\theta) \sin 2\theta \, \partial\theta \tag{56}$$

$$C_{DF} = 8\mu_o/Re \int_0^\pi \zeta_o \sin^2\theta \, \partial\theta \tag{57}$$

Details of the derivation can be found in Appendix B.

To evaluate the surface pressure from the velocity field, a similar method to that of Jenson (1959) was used, except the physical properties were allowed to vary with the radial and angular positions. With this method the stagnation pressure, p_o, (at $\theta=0°$) was evaluated first by integrating the r-component of the Navier-Stokes equation along the forward axis of symmetry. The surface pressure distribution was then found by integrating the θ-component of the flow equation along the surface of the sphere between $\theta=0°$ and $\theta=\theta$. This is briefly described below with further details to be found in Appendix B.

r-component:

$$\partial p/\partial r\big|_{\theta=0} = f(v_r, v_\theta, \rho, \mu) \tag{58}$$

$$p_o = \int_1^{r^\infty} \partial p/\partial r\big|_{\theta=0} \, dr = \int_0^{z^\infty} \partial p/\partial z\big|_{\theta=0} \, dz \tag{59}$$

Substitution of Equation (58) into (59) gave, in dimensionless variables:

$$p_\theta = \int_0^{z_\infty} \{8/Re.T^x \partial\zeta/\partial\Theta - 2/3\ \partial\nabla.\bar{v}/\partial z + x/T\ \partial T/\partial z(\nabla.\bar{v}/3 - \partial v_r/\partial z/3)] - 2/T\ v_r \partial v_r/\partial z\}\ dz \quad (60)$$

In a similar manner, the dimensionless surface pressure can be expressed as:

$$p(\Theta) = p_o + 4T_o^x/Re \int_0^{\Theta} (\partial\zeta/\partial z + \zeta + \zeta x/T.\partial T/\partial z)\ d\Theta \quad (61)$$

Equation (60) was integrated numerically along the axis. The derivatives were evaluated by central- and forward-difference methods. Simpson's rule was used for approximating the integrals. The pressures at the surface mesh points were found by successive integration of Equation (61), using the Trapezoidal rule.

EVALUATION OF THE NUSSELT NUMBER

The local Nusselt number can be found by estimating the rate of heat transfer to a point at the surface of the sphere, thus:

$$q_r = -k\ \partial T/\partial r \quad (62)$$

$$q_r = h\ \Delta T \quad (63)$$

$$h(\Theta) = (k/\Delta T\ \partial T/\partial r)\big|_{r=R} \quad (64)$$

The Nusselt number was based on bulk gas conditions. Therefore,

$$Nu(\Theta) = h(\Theta)\ D/k_\infty \tag{65}$$

From Equation (64):

$$Nu(\Theta) = k_g/k_\infty \cdot 1/(T_\infty - T_g)\ D\ \partial T/\partial r \tag{66}$$

In dimensionless variables:

$$Nu(\Theta) = 2k_0'/(1 - T_0) \cdot \partial T'/\partial z \tag{67}$$

To calculate the overall Nusselt number, $\underline{Nu(\Theta)}$ is averaged over the entire surface,

$$Nu = \{\int_0^\pi Nu(\Theta)\ 2\pi R \sin\Theta\ R\ d\Theta\}/\{\int_0^\pi 2\pi R^2 \sin\Theta\ d\Theta\} \tag{68}$$

or

$$Nu = 1/2 \int_0^\pi Nu(\Theta) \sin\Theta\ d\Theta \tag{69}$$

$\underline{\partial T/\partial z}$ was evaluated numerically at every mesh point at the surface. The overall Nusselt number was obtained by numerical integration of Equation (69), using Simpson's rule.

RESULTS AND DISCUSSION

It is perhaps useful to keep in mind at this point that the objective of this analysis was to obtain predictions of the heat transfer rate, as expressed by the Nusselt number, under conditions of variable properties of the flow. These predictions are presented in the next section. In the course of the numerical computations, however, a number of intermediate results were obtained concerning certain parameters of the flow around the sphere which will be

presented first. These results are extremely interesting, since they provide an insight as to the complex phenomena occurring during the particular situation studied in this investigation. A detailed quantitative discussion of these phenomena is, however, beyond the scope of this thesis. The discussion will therefore be limited to a qualitative consideration of the major aspects of the numerical results.

In the discussion that follows, results obtained under isothermal conditions (constant-property flow) will be presented and comparison will be made with the results obtained under conditions of increasing departure from isothermal conditions, as the temperature difference between the free stream and the sphere surface increases. In this comparison, it will be useful to visualize that the free stream conditions remain constant for a given Reynolds number, and the increasing temperature difference as expressed by the value of T_o is brought upon by a decreasing sphere surface temperature. In other words, while T_o decreases, the free stream temperature, kinematic viscosity and velocity remain constant, thus facilitating the interpretation of the observed trends.

Flow Field

The surface vorticity distributions for $0.1<Re_\infty<50$ and $0.25<T_o<1.0$ are shown in Figures 2 to 7. At low Reynolds numbers the surface vorticity distribution exhibits a fore-and-aft symmetry with a maximum value at the equator, ($\theta=90^\circ$). As the Reynolds number

FIGURE 2

EFFECT OF SURFACE TEMPERATURE ON

SURFACE VORTICITY DISTRIBUTION

RE = 0.1

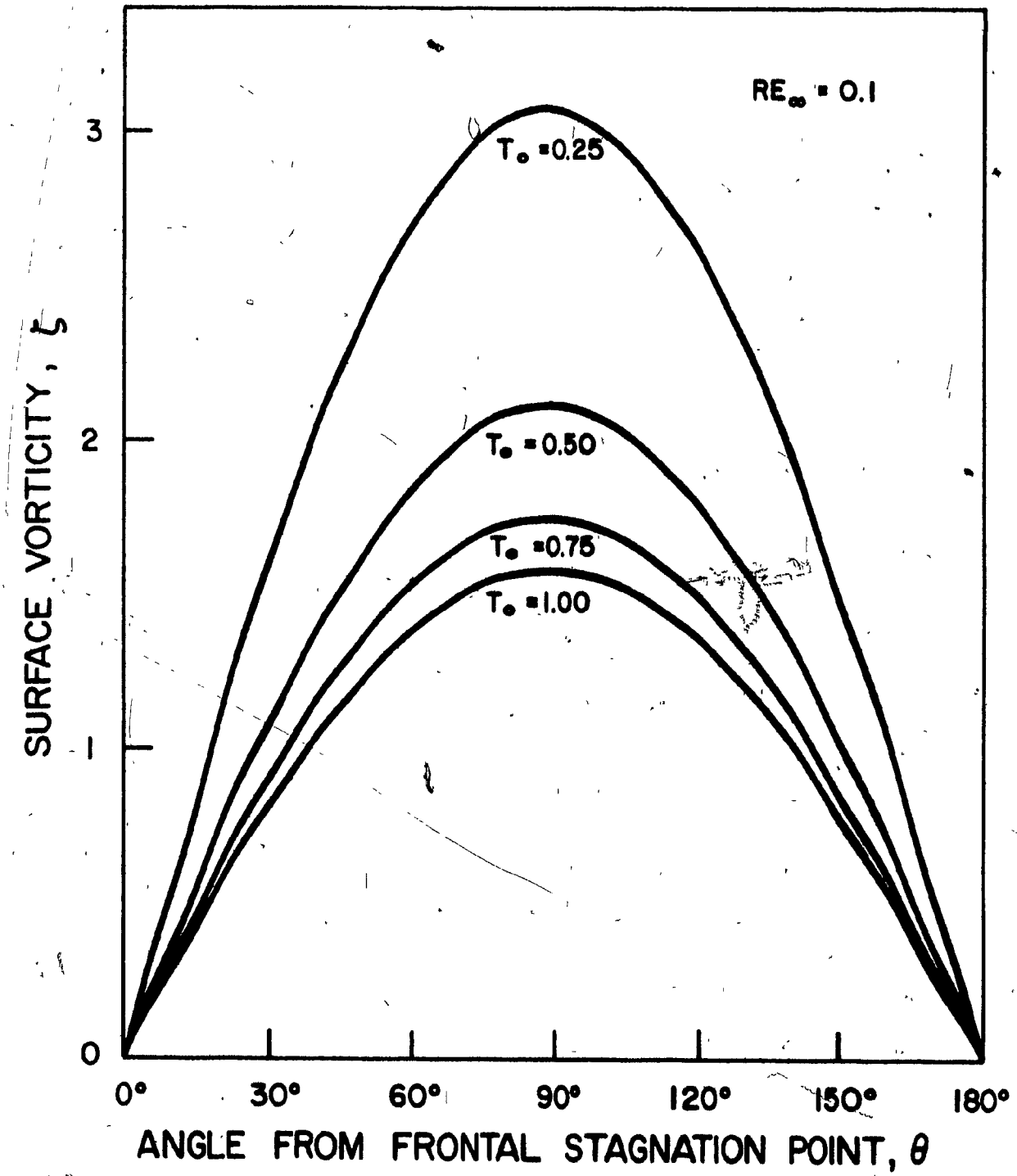
RE∞ = 0.1
T∘ =0.25
T∘ =0.50
T∘ =0.75
T∘ =1.00
SURFACE VORTICITY, ζ
0
1
2
3
0°
30°
60°
90°
120°
150°
180°
ANGLE FROM FRONTAL STAGNATION POINT, θ

FIGURE 3

EFFECT OF SURFACE TEMPERATURE ON

SURFACE VORTICITY DISTRIBUTION

RE = 1.0

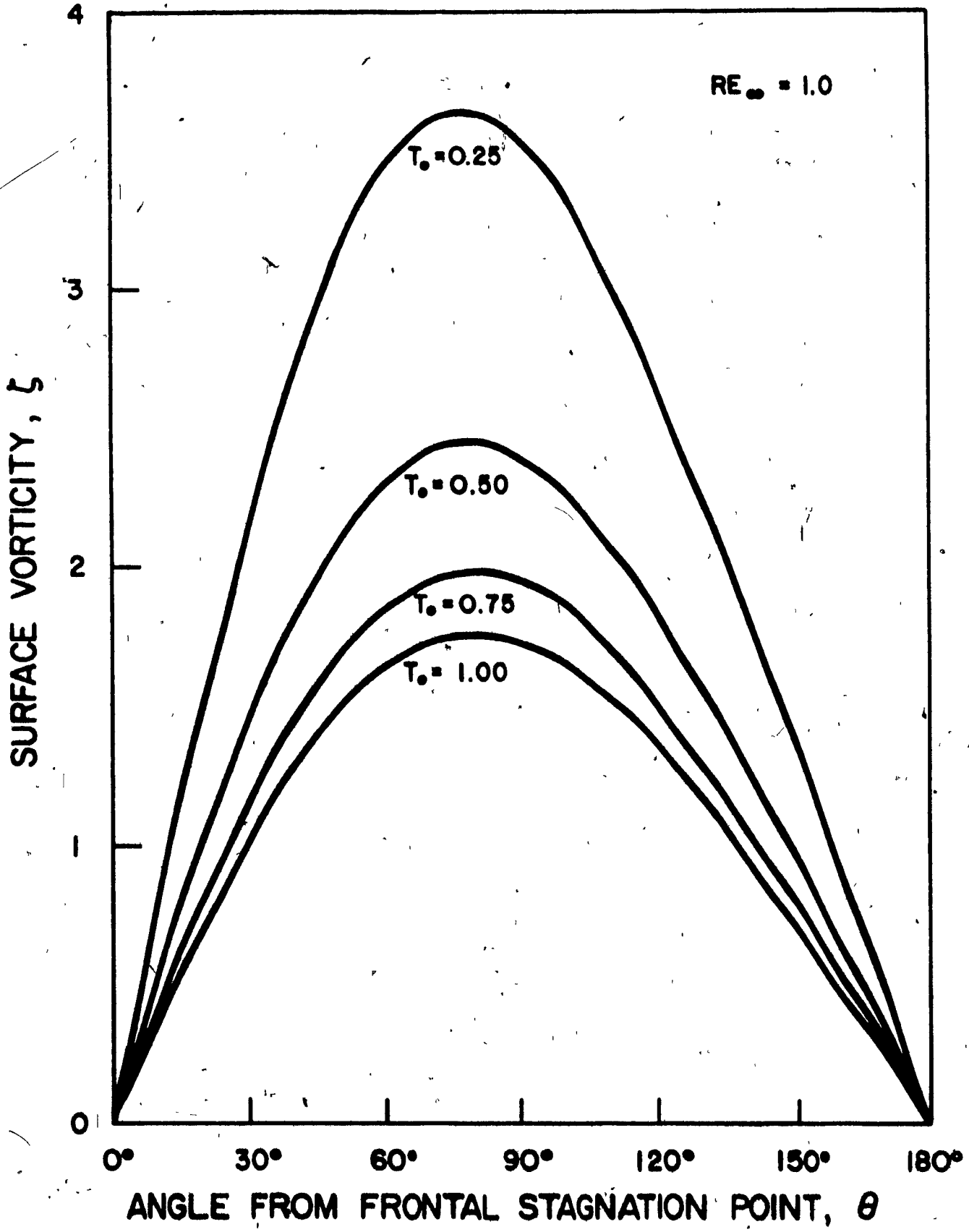
RE∞ = 1.0
T∞ = 0.25
T∞ = 0.50
T∞ = 0.75
T∞ = 1.00
SURFACE VORTICITY, ζ
0
1
2
3
4
0°
30°
60°
90°
120°
150°
180°
ANGLE FROM FRONTAL STAGNATION POINT, θ

FIGURE 4

EFFECT OF SURFACE TEMPERATURE ON

SURFACE VORTICITY DISTRIBUTION

RE = 10

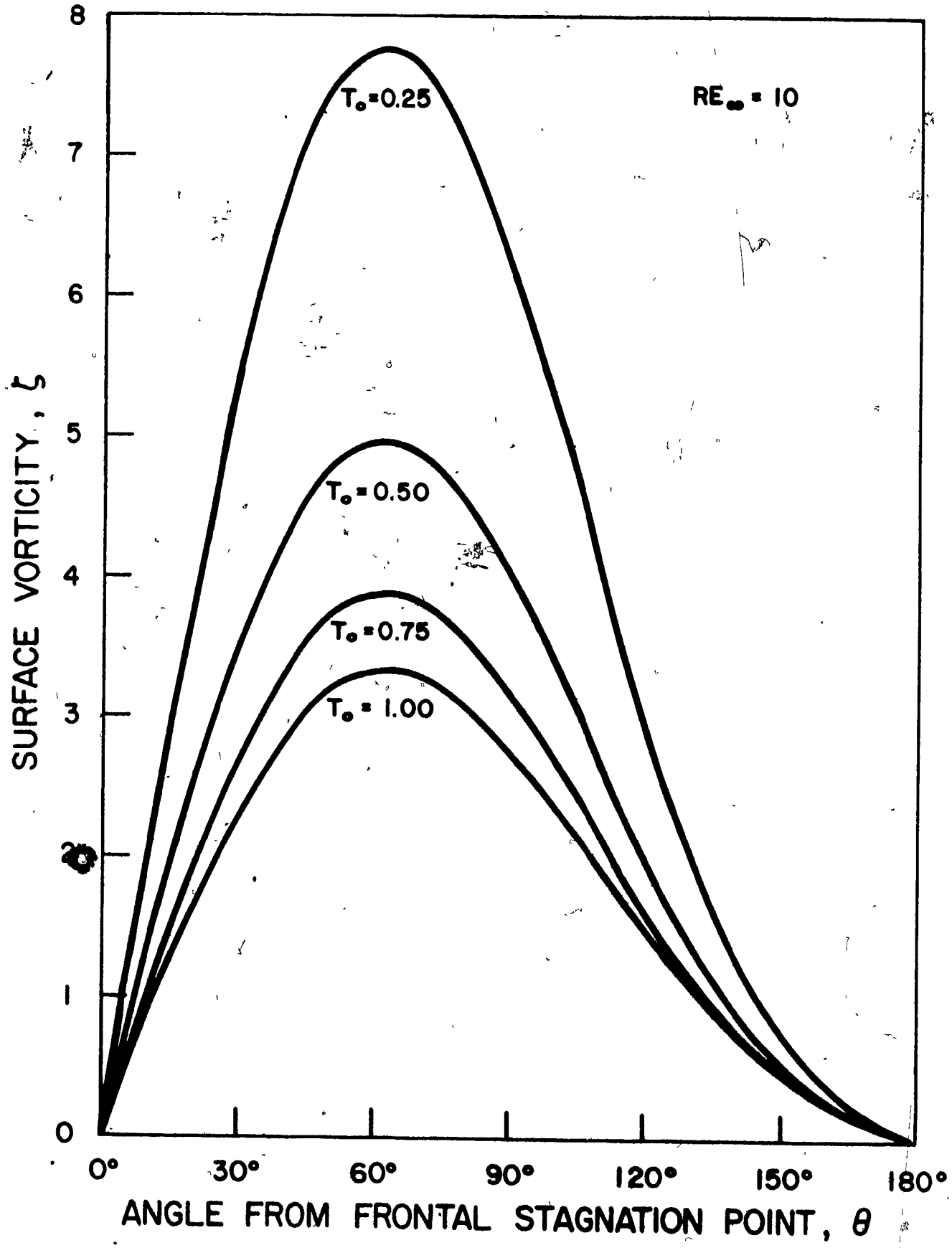
8
7
6
5
4
3
2
1
0
SURFACE VORTICITY, ζ
T_o=0.25
RE_∞ = 10
T_o = 0.50
T_o = 0.75
T_o = 1.00
0°
30°
60°
90°
120°
150°
180°
ANGLE FROM FRONTAL STAGNATION POINT, θ

FIGURE 5

EFFECT OF SURFACE TEMPERATURE ON

SURFACE VORTICITY DISTRIBUTION

RE = 20

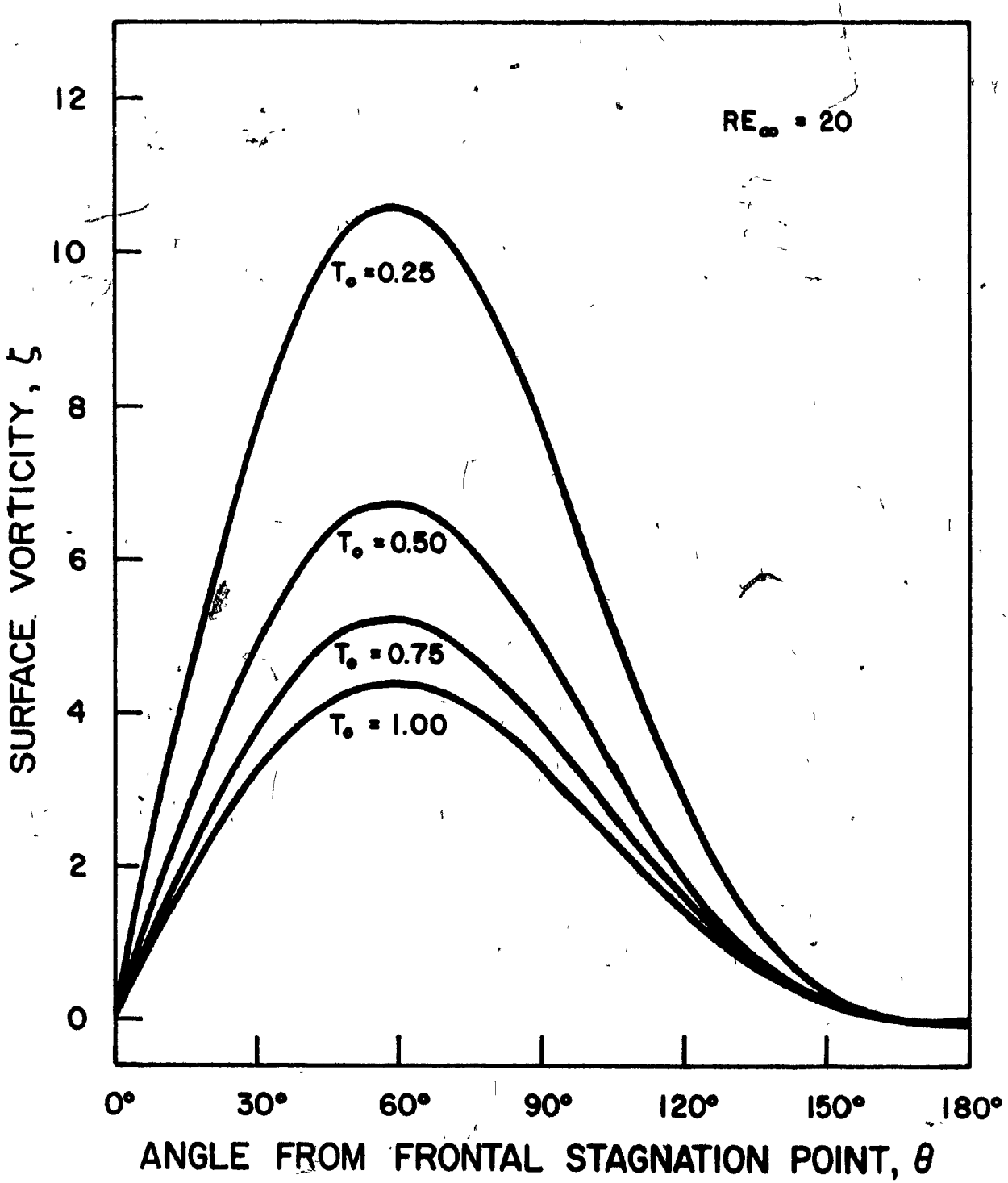
RE∞ = 20
T₀ = 0.25
T₀ = 0.50
T₀ = 0.75
T₀ = 1.00
SURFACE VORTICITY, ζ
0
2
4
6
8
10
12
0°
30°
60°
90°
120°
150°
180°
ANGLE FROM FRONTAL STAGNATION POINT, θ

FIGURE 6

EFFECT OF SURFACE TEMPERATURE ON

SURFACE VORTICITY DISTRIBUTION

RE = 30

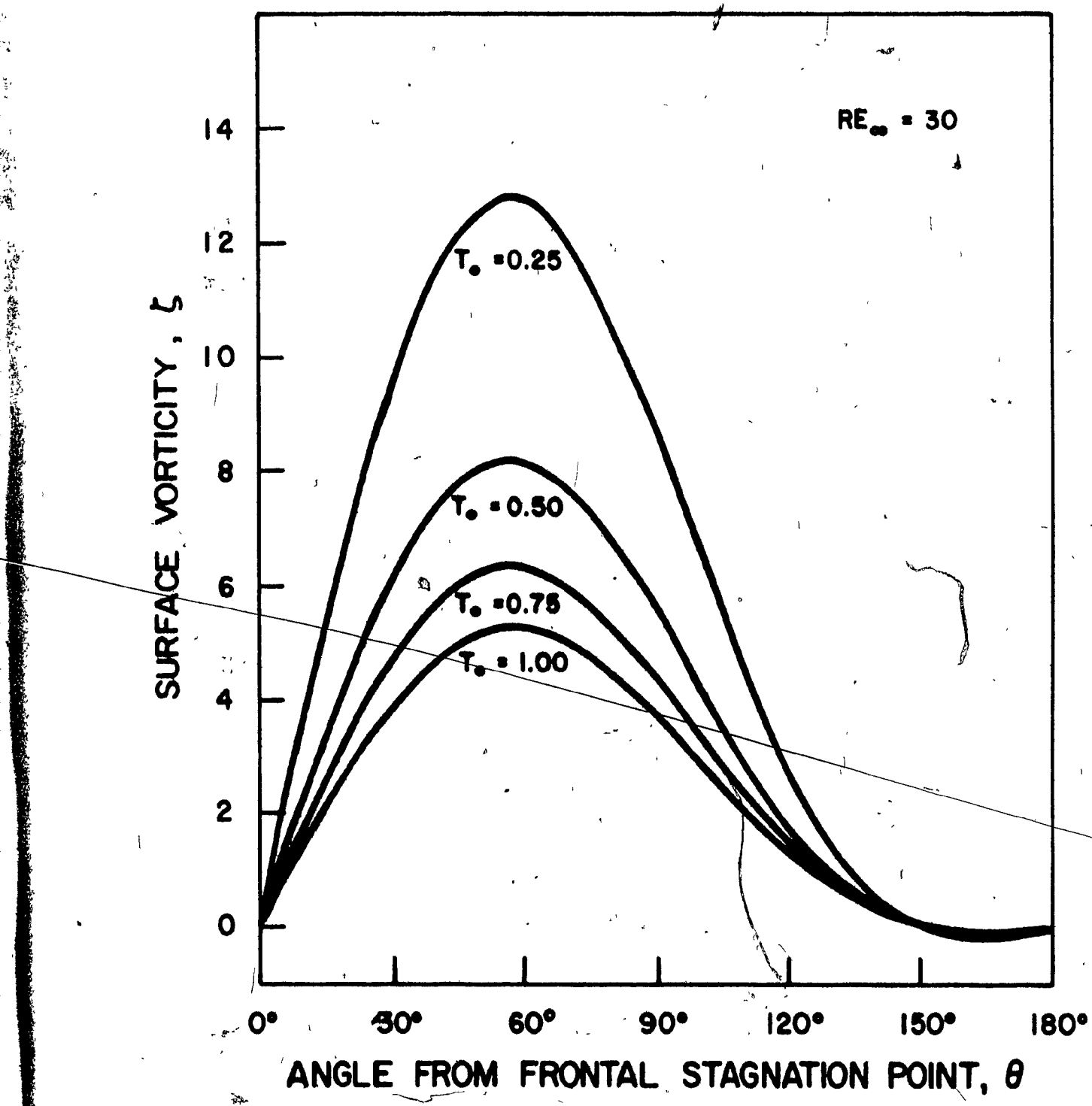
RE∞ = 30
T∞ =0.25
T∞ =0.50
T∞ =0.75
T∞ = 1.00
SURFACE VORTICITY, ζ
0
2
4
6
8
10
12
14
0°
30°
60°
90°
120°
150°
180°
ANGLE FROM FRONTAL STAGNATION POINT, θ

FIGURE 7

EFFECT OF SURFACE TEMPERATURE ON

SURFACE VORTICITY DISTRIBUTION

RE = 50

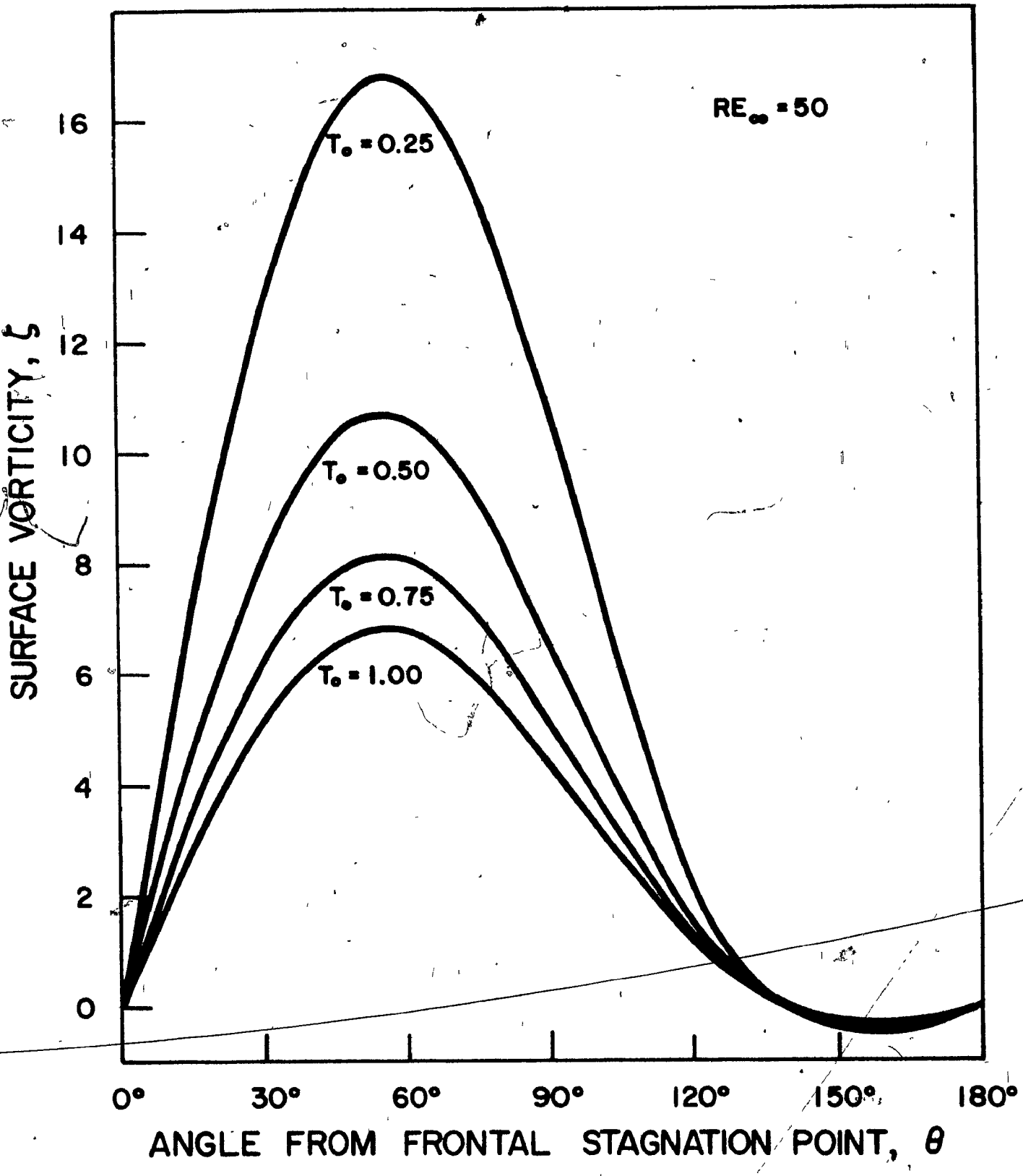
RE∞ = 50
T₀ = 0.25
T₀ = 0.50
T₀ = 0.75
T₀ = 1.00
SURFACE VORTICITY, ζ
0
2
4
6
8
10
12
14
16
0°
30°
60°
90°
120°
150°
180°
ANGLE FROM FRONTAL STAGNATION POINT, θ

increases, the velocity gradients near the surface become steeper, leading to an increase in the vorticity of the flow in this region. Moreover, the fore-and-aft symmetry is lost and the point of maximum vorticity moves up closer to the front stagnation point. This is caused by the increase in the inertia forces in the boundary layer so that at high enough Reynolds numbers the flow can no longer follow the contour of the body and separation occurs. Flow separation leaves a region of recirculating flow behind the sphere. The velocity gradients near the surface in this wake region are negative since the flow is in the direction opposite to the main flow. Consequently, the surface vorticity in the recirculating vortex is also negative. Separation thus takes place at the point where the surface vorticity is equal to zero. Separation points at different Reynolds numbers were determined from Figures 5 to 7 and are listed in Table III. The boundary of the vortex is defined by the streamline $\Psi=0$. The length of the vortex is then the distance at which this streamline intersects the axis of symmetry. The variations of the vortex length, expressed as the ratio L/D, with the Reynolds number and $\underline{T_o}$ are listed in Table IV.

It can be observed from Figures 2 to 7 and Tables III and IV that the decrease in the sphere surface temperature had little effect on the overall trends of the flow. At a specific Reynolds number, the maximum value of the surface vorticity occurred at the same angle, at all $\underline{T_o}$ values. Flow separation point and vortex size were also only marginally affected by the decrease in the surface temperature.

TABLE III

SEPARATION ANGLE, θ_s

Re	$T_o = 1.0$	$T_o = 0.75$	$T_o = 0.50$	$T_o = 0.25$
20	-	11.0°	13.5°	12.5°
30	26.5°	28.5°	30.5°	28.5°
50	40.0°	41.0°	42.0°	42.5°

TABLE IV

VORTEX LENGTH, L/D

Re	T_o = 1.0	T_o = 0.75	T_o = 0.50	T_o = 0.25
20	-	0.02	0.03	0.03
30	0.22	0.20	0.21	0.22
50	0.48	0.54	0.55	0.52

The actual vorticity values, however, became very much higher as T_o decreased, actually increasing exponentially with a decrease in T_o. This is attributed to higher velocities and hence steeper velocity gradients near the surface caused by a decrease in the fluid viscosity. It is certainly the most striking feature of the vorticity calculations.

Figures 8 and 9 compare the separation angle and vortex lengths obtained in this study for constant-property flow with experimental and theoretical results reported in the literature. Very good agreement is indicated. It was not possible to present a similar comparison for the variable-property case, due to the unavailability of pertinent data.

Figures 10 to 15 show the streamlines and vorticity contours for constant-property flow and the variable-property case at T_o = 0.25 for Re = 0.1, 10 and 50. Here again, the general shape of the flow field did not change significantly with departure from isothermal conditions. The streamlines, however, moved closer as the surface temperature was reduced. This was partly caused by an increase in the fluid density accompanied with little change in the velocity, and partly due to lower viscosity which was the main reason for higher velocities near the surface. For the same reasons, the recirculation in the wake was much faster for colder sphere surfaces while the actual size of the vortex was approximately the same as for the constant-property case. The presence of low viscosity, higher density and velocity near the surface, as that experienced in the variable-

FIGURE 8

EFFECT OF REYNOLDS NUMBER ON SEPARATION ANGLE, Θ_s,

FOR CONSTANT-PROPERTY FLOW

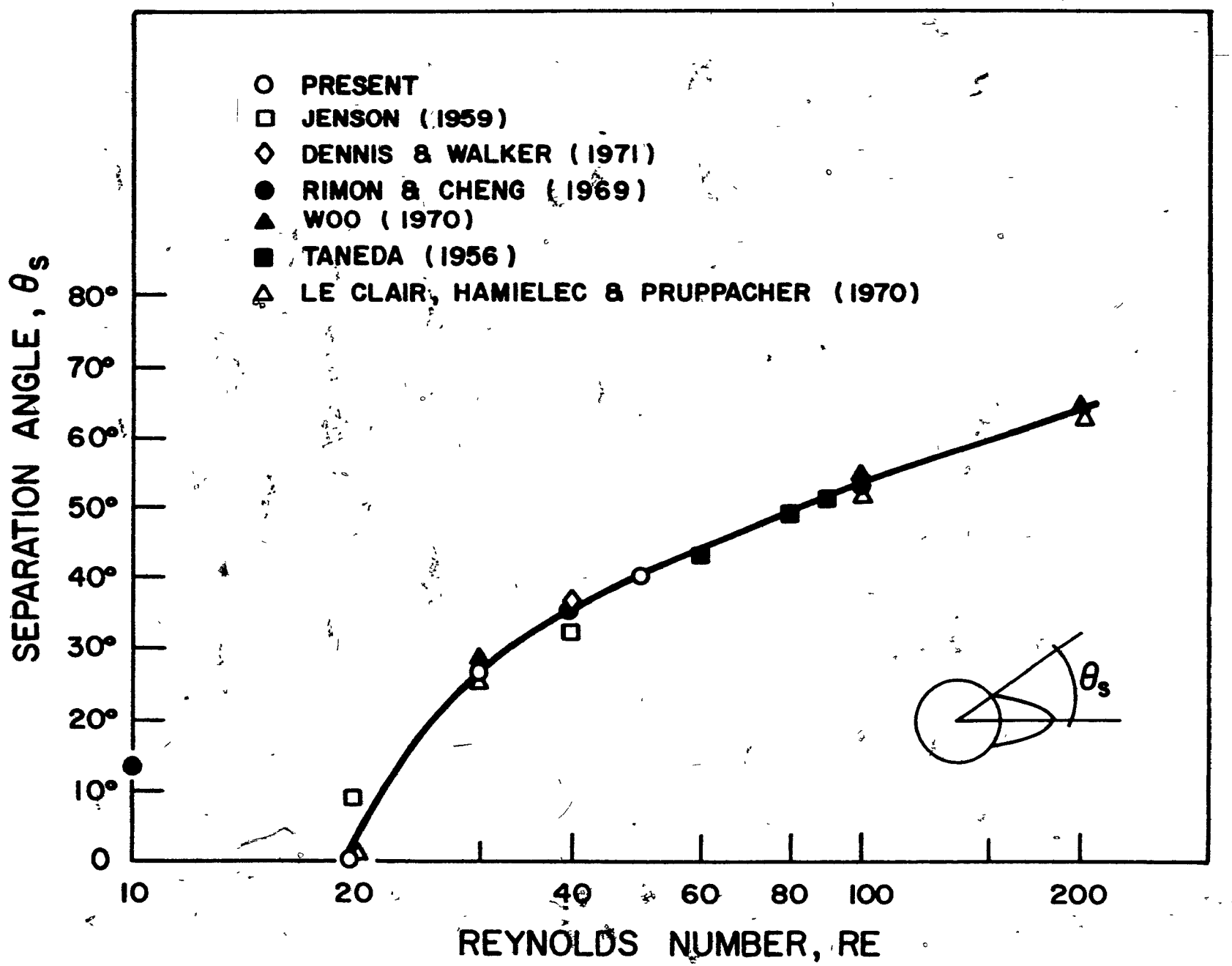
PRESENT
JENSON (1959)
DENNIS & WALKER (1971)
RIMON & CHENG (1969)
WOO (1970)
TANEDA (1956)
LE CLAIR, HAMIELEC & PRUPPACHER (1970)
SEPARATION ANGLE, θ_s
80°
70°
60°
50°
40°
30°
20°
10°
0
10
20
40
60
80
100
200
REYNOLDS NUMBER, RE
θ_s

FIGURE 9

EFFECT OF REYNOLDS NUMBER ON VORTEX LENGTH, L/D,
FOR CONSTANT-PROPERTY FLOW

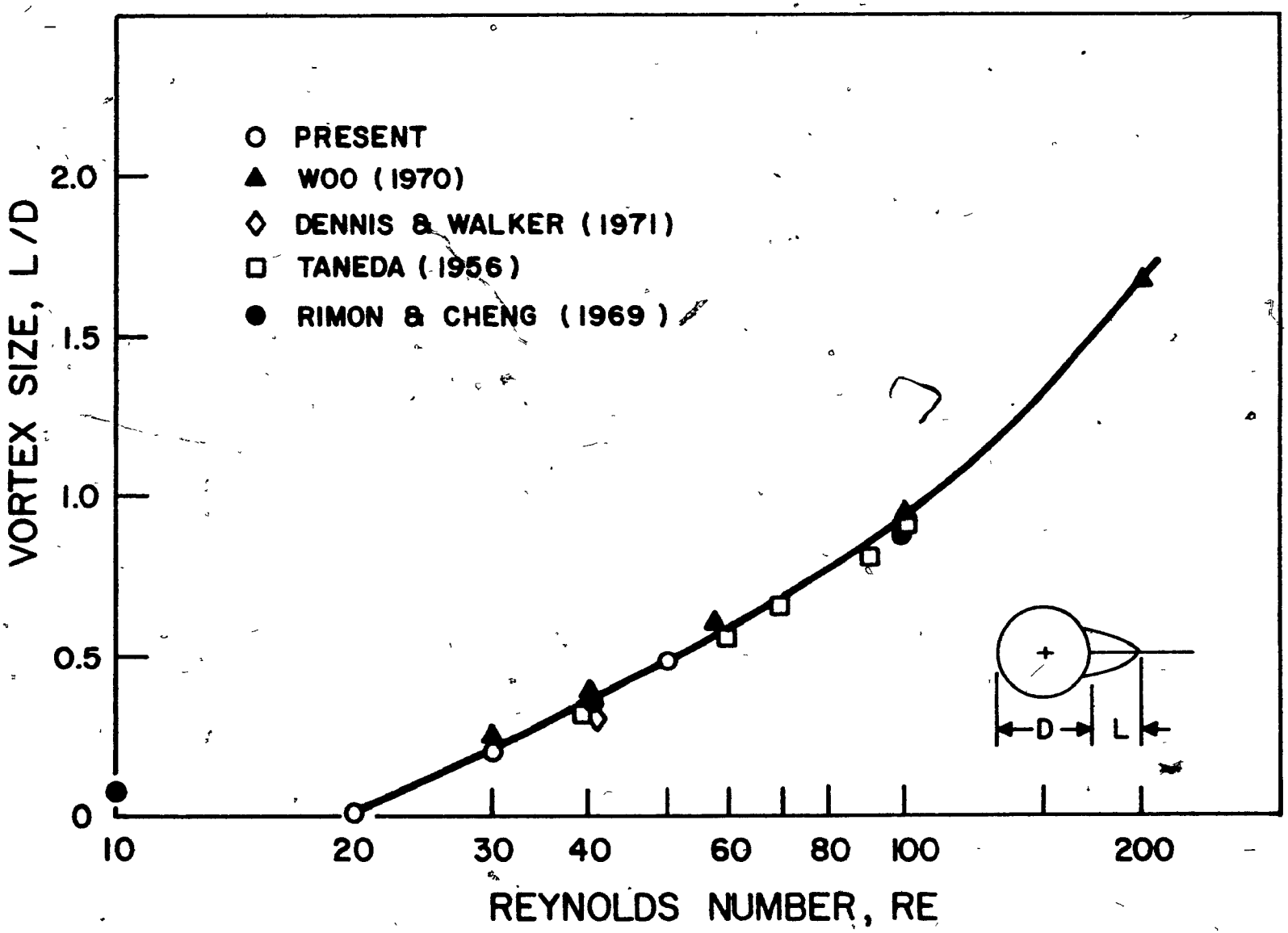
PRESENT
WOO (1970)
DENNIS & WALKER (1971)
TANEDA (1956)
RIMON & CHENG (1969)
VORTEX SIZE, L/D
2.0
1.5
1.0
0.5
0
10
20
30
40
60
80
100
200
REYNOLDS NUMBER, RE
D
L

FIGURE 10

STREAMLINES FOR

CONSTANT- AND VARIABLE-PROPERTY FLOWS

AT $T_o = 0.25$

RE = 0.1

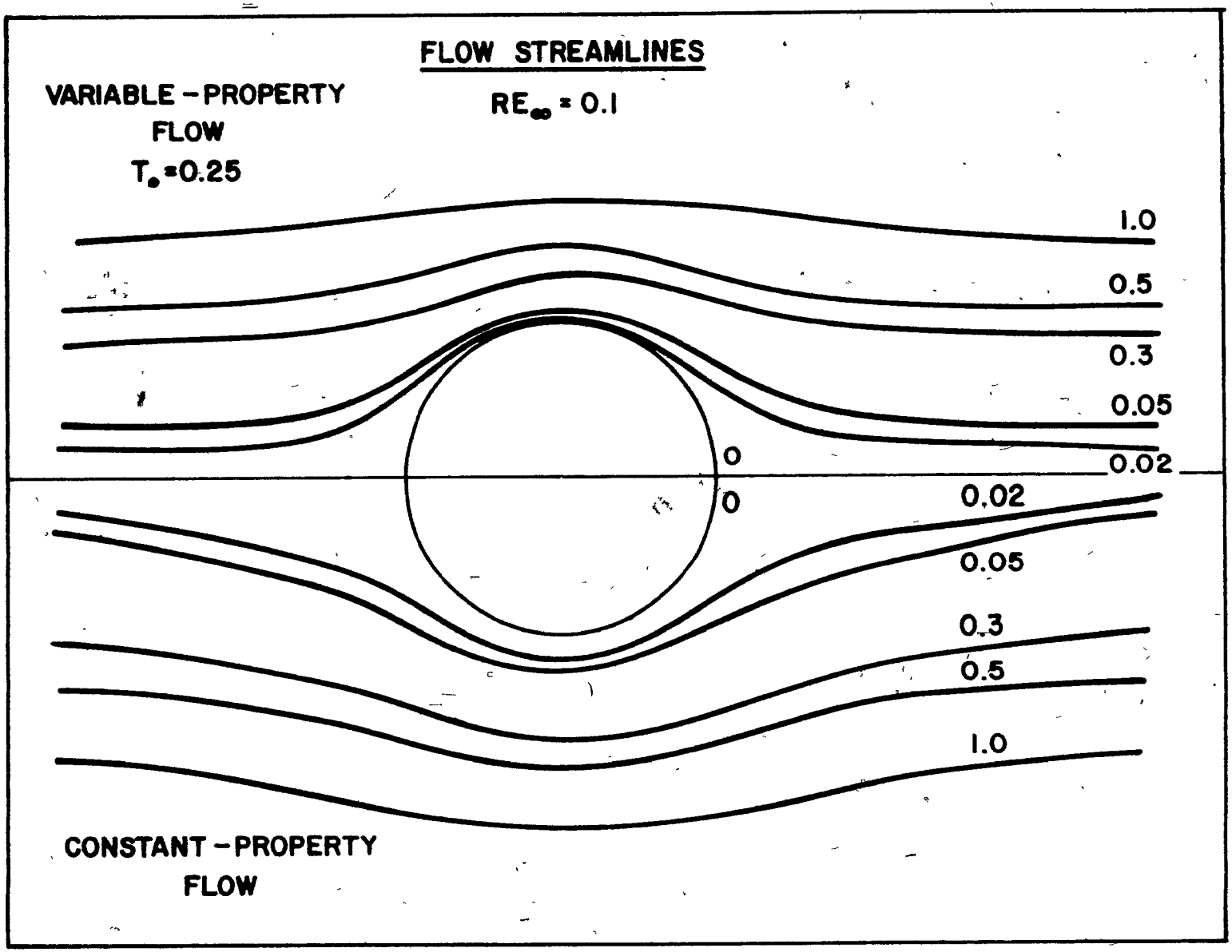
FLOW STREAMLINES
VARIABLE - PROPERTY FLOW
T_∞ = 0.25
RE_∞ = 0.1
1.0
0.5
0.3
0.05
0.02
0
0
0.02
0.05
0.3
0.5
1.0
CONSTANT - PROPERTY FLOW

FIGURE 11

STREAMLINES FOR

CONSTANT- AND VARIABLE-PROPERTY FLOWS

AT $T_o = 0.25$

$RE = 10^5$

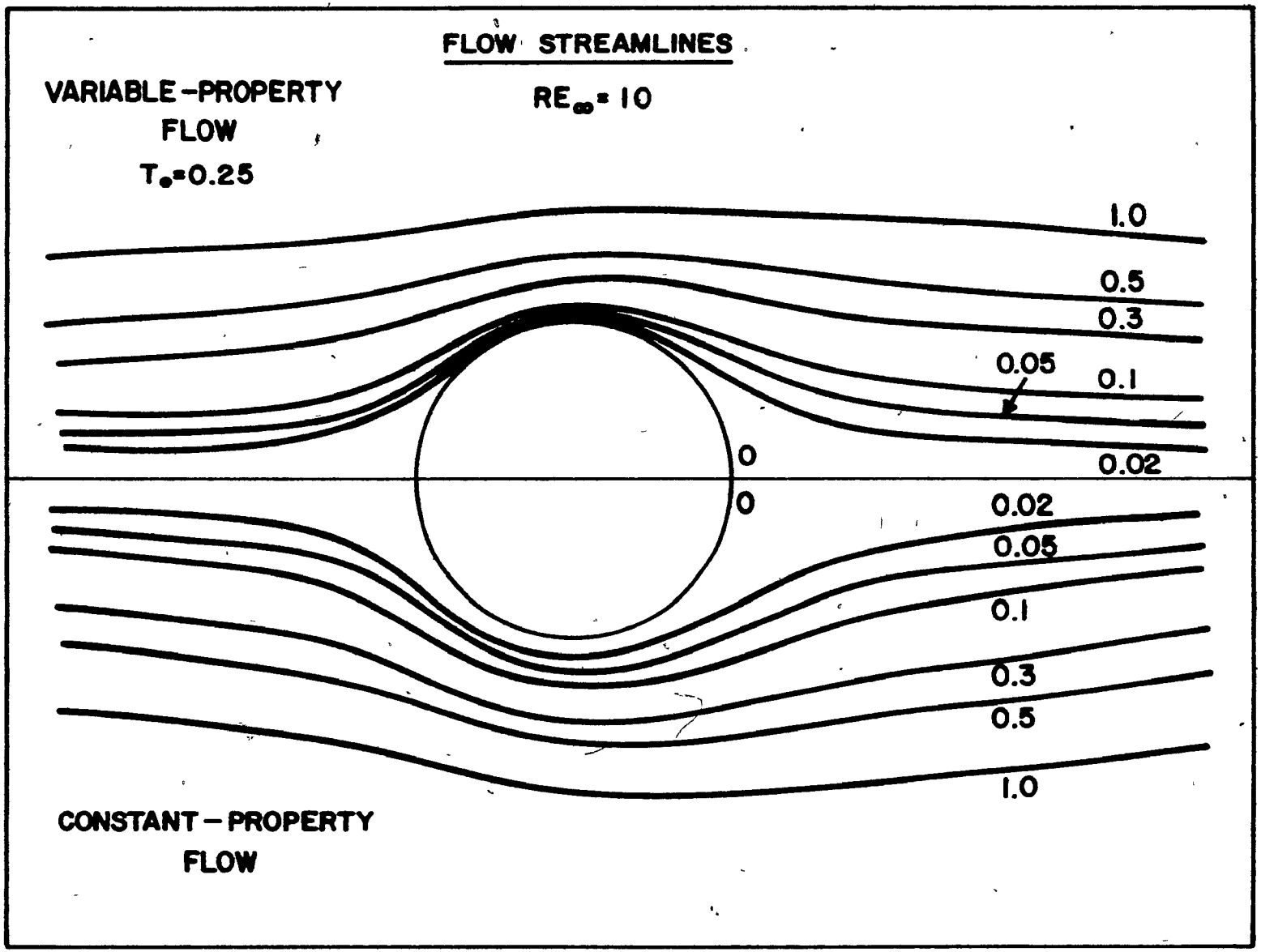
FLOW STREAMLINES
VARIABLE-PROPERTY FLOW
T_∞=0.25
RE_∞= 10
1.0
0.5
0.3
0.05
0.1
0.02
0
0
0.02
0.05
0.1
0.3
0.5
1.0
CONSTANT-PROPERTY FLOW

FIGURE 12

STREAMLINES FOR

CONSTANT- AND VARIABLE PROPERTY-FLOWS

AT $T_o = 0.25$

RE = 50

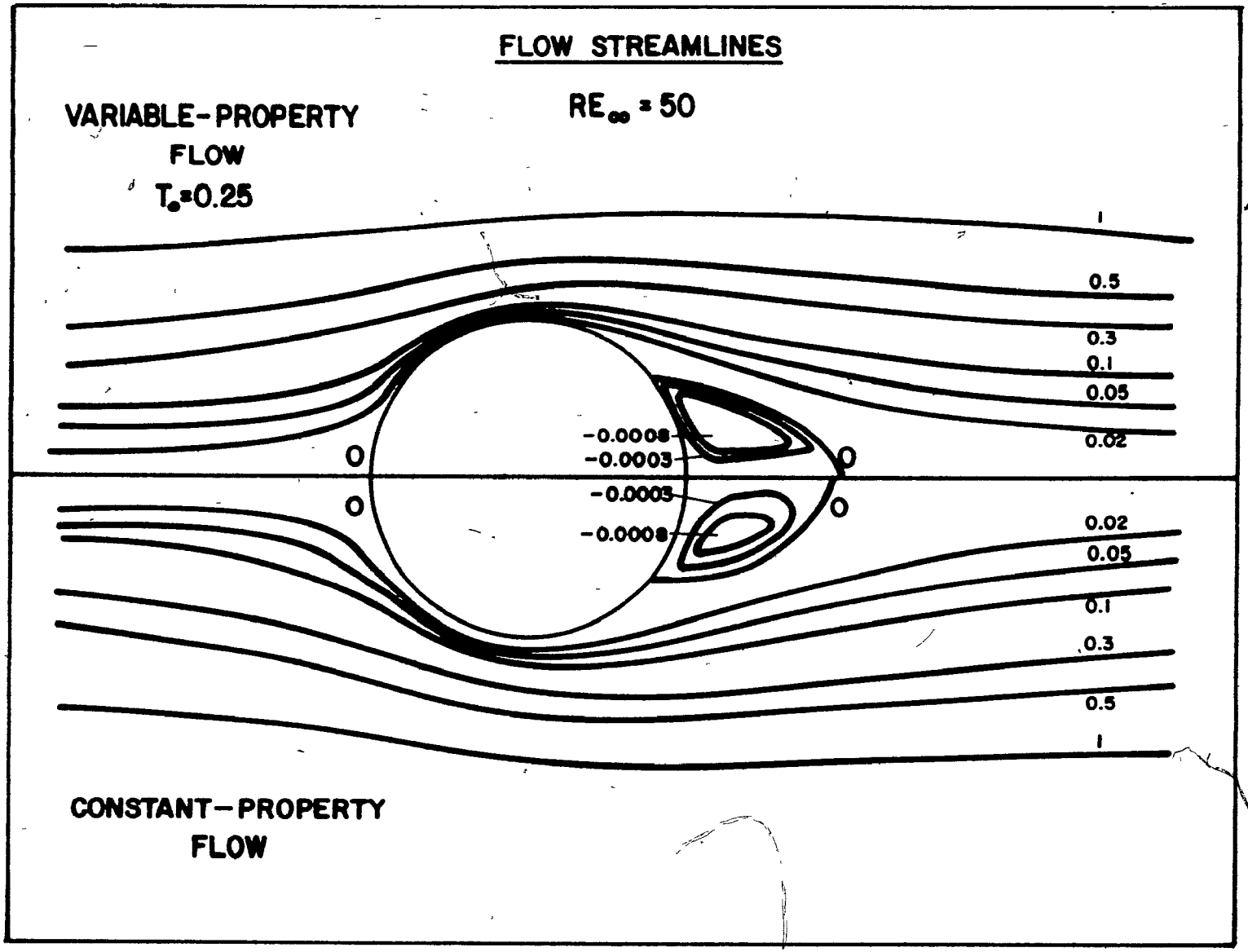
FLOW STREAMLINES
VARIABLE-PROPERTY FLOW
T_o=0.25
RE_∞ = 50
1
0.5
0.3
0.1
0.05
0.02
-0.0008
-0.0003
-0.0003
-0.0008
0.02
0.05
0.1
0.3
0.5
1
CONSTANT-PROPERTY FLOW

FIGURE 13

VORTICITY CONTOURS FOR

CONSTANT- AND VARIABLE-PROPERTY FLOWS

AT $T_o = 0.25$

RE = 0.1

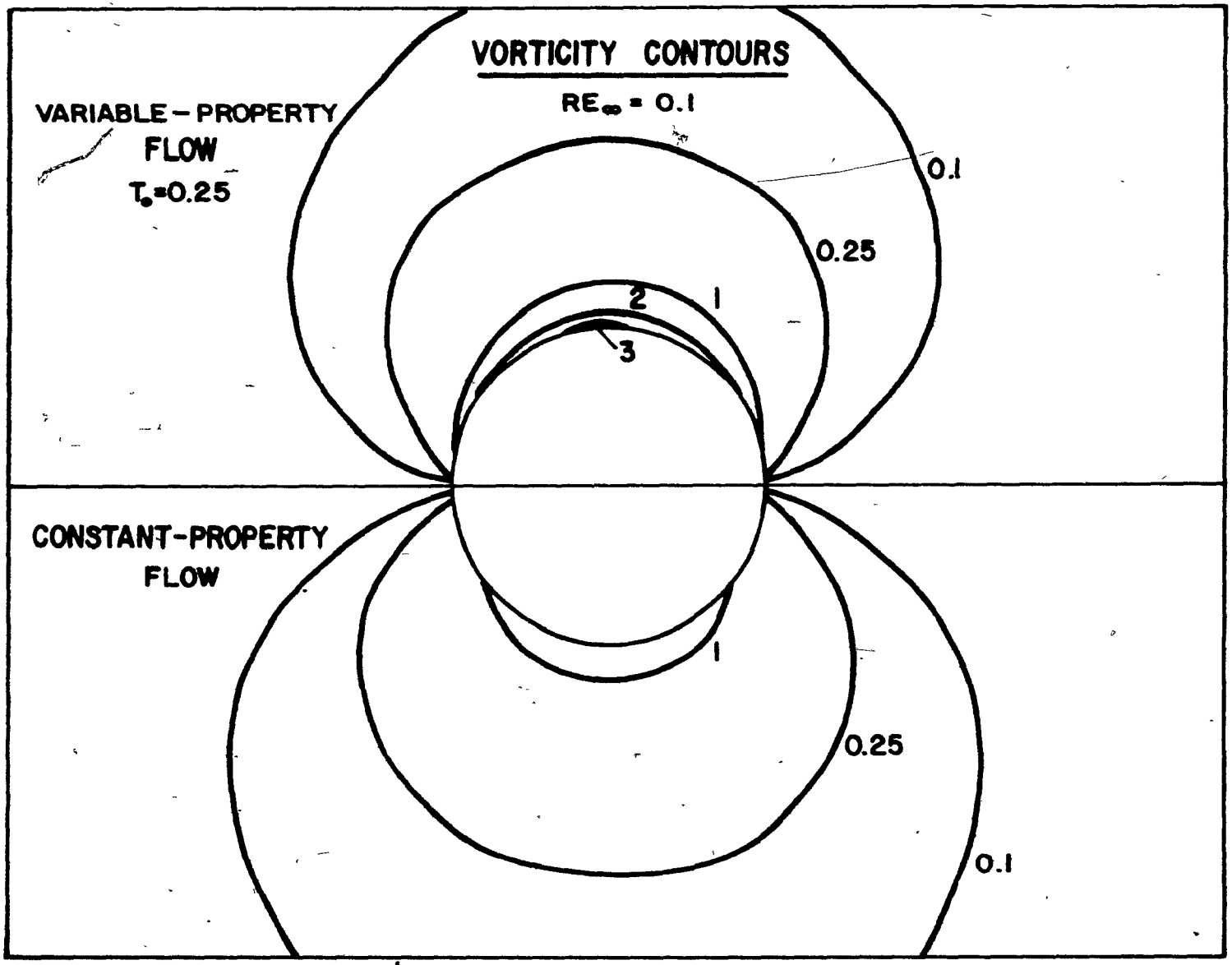
VORTICITY CONTOURS
RE∞ = 0.1
VARIABLE – PROPERTY FLOW
T∞=0.25
0.1
0.25
2
1
3
CONSTANT-PROPERTY FLOW
1
0.25
0.1

FIGURE 14

VORTICITY CONTOURS FOR

CONSTANT- AND VARIABLE-PROPERTY FLOWS

AT $T_o = 0.25$

RE = 10

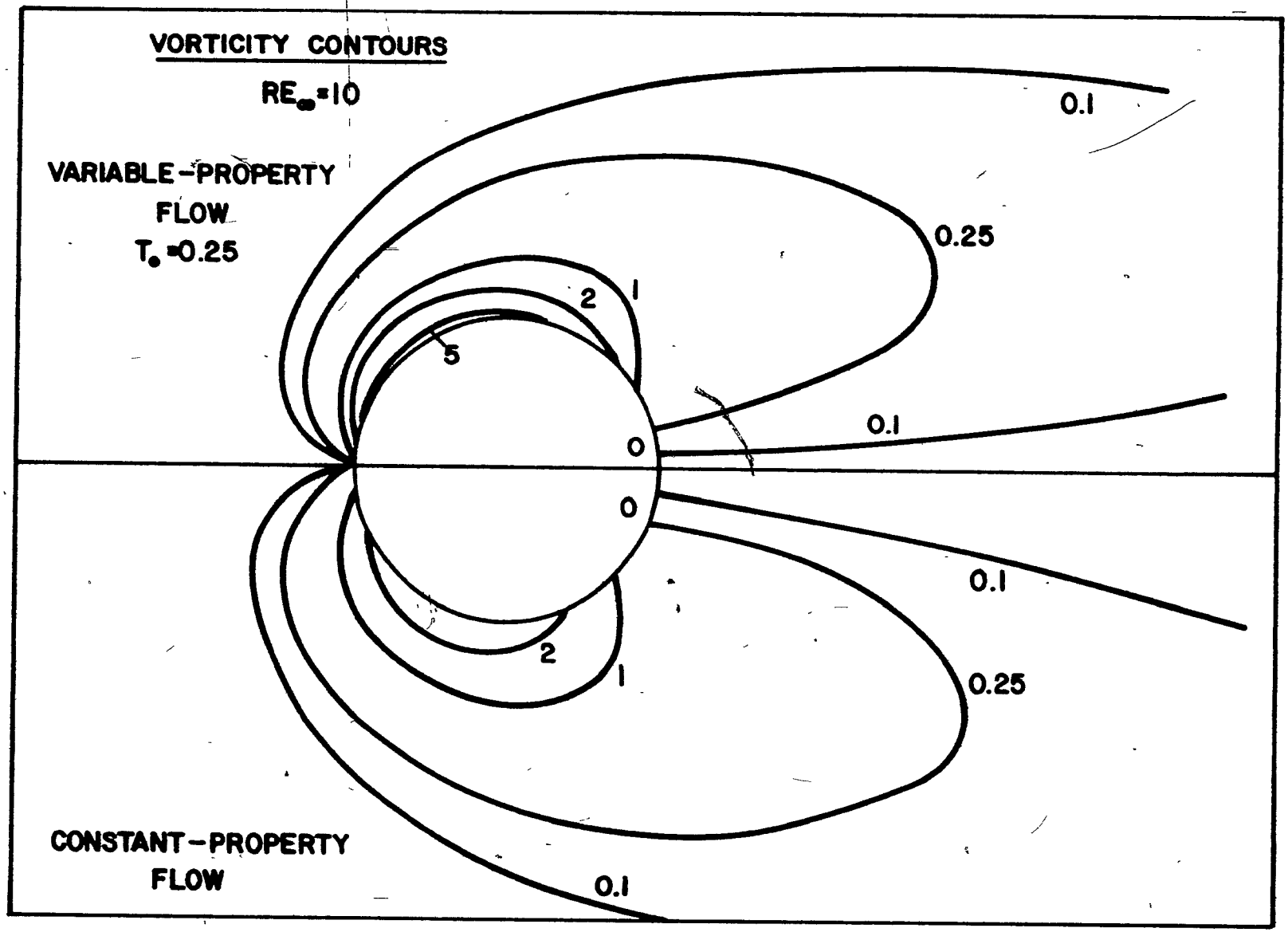
VORTICITY CONTOURS
RE∞=10
VARIABLE-PROPERTY FLOW
T∞=0.25
CONSTANT-PROPERTY FLOW
0.1
0.25
0.1
2
1
5
0
0
0.1
0.25
0.1
2
1

FIGURE 15

VORTICITY CONTOURS FOR

CONSTANT- AND VARIABLE-PROPERTY FLOWS

AT $T_o = 0.25$

RE = 50

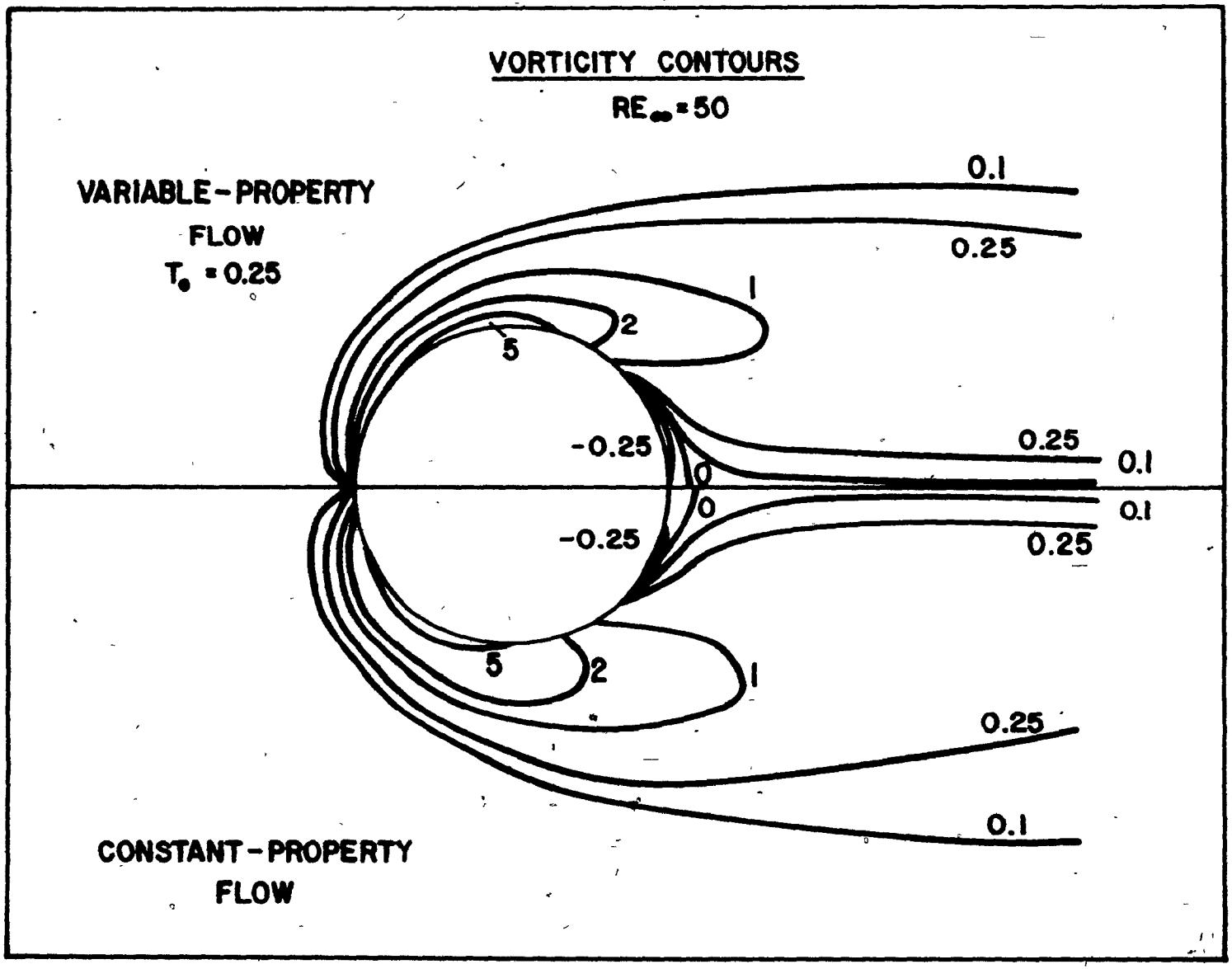
VORTICITY CONTOURS
RE∞ = 50
VARIABLE-PROPERTY
FLOW
T∞ = 0.25
0.1
0.25
1
2
5
-0.25
0.25
0.1
0
0
0.1
-0.25
0.25
5
2
1
0.25
0.1
CONSTANT-PROPERTY
FLOW

property case, should effect a much earlier separation. This, however, was not the case due to the complex interaction between the steep velocity, temperature and property gradients near the surface. A detailed discussion of these phenomena is beyond the scope of this thesis.

Temperature Field and Local Nusselt Numbers

The temperature fields for constant-property flows and variable-property flows at $T_o = 0.25$ are shown in Figures 16 to 18, for Re = 0.1, 10 and 50. Figures 19 to 24 are plots of the local Nusselt number distributions along the sphere surface for all the cases studied. All of the Nusselt numbers were evaluated at free-stream conditions (same k_∞) to allow comparison between different surface temperature conditions.

Once again, the change in the surface temperature affected the level of the temperature only and not the general pattern of the temperature field. The variable-property flow isotherms moved closer to each other as the surface temperature was decreased, resulting in higher temperature gradients at the surface than in the constant-property case. This increase in the temperature gradient, however, did not result in higher heat transfer rates, or Nusselt numbers (see Figures 19 to 24) since the decrease of the surface temperature was accompanied by a similar reduction in the thermal conductivity of the gas near the surface.

FIGURE 16

TEMPERATURE FIELDS FOR

CONSTANT- AND VARIABLE-PROPERTY FLOWS

AT $T_o = 0.25$

RE = 0.1

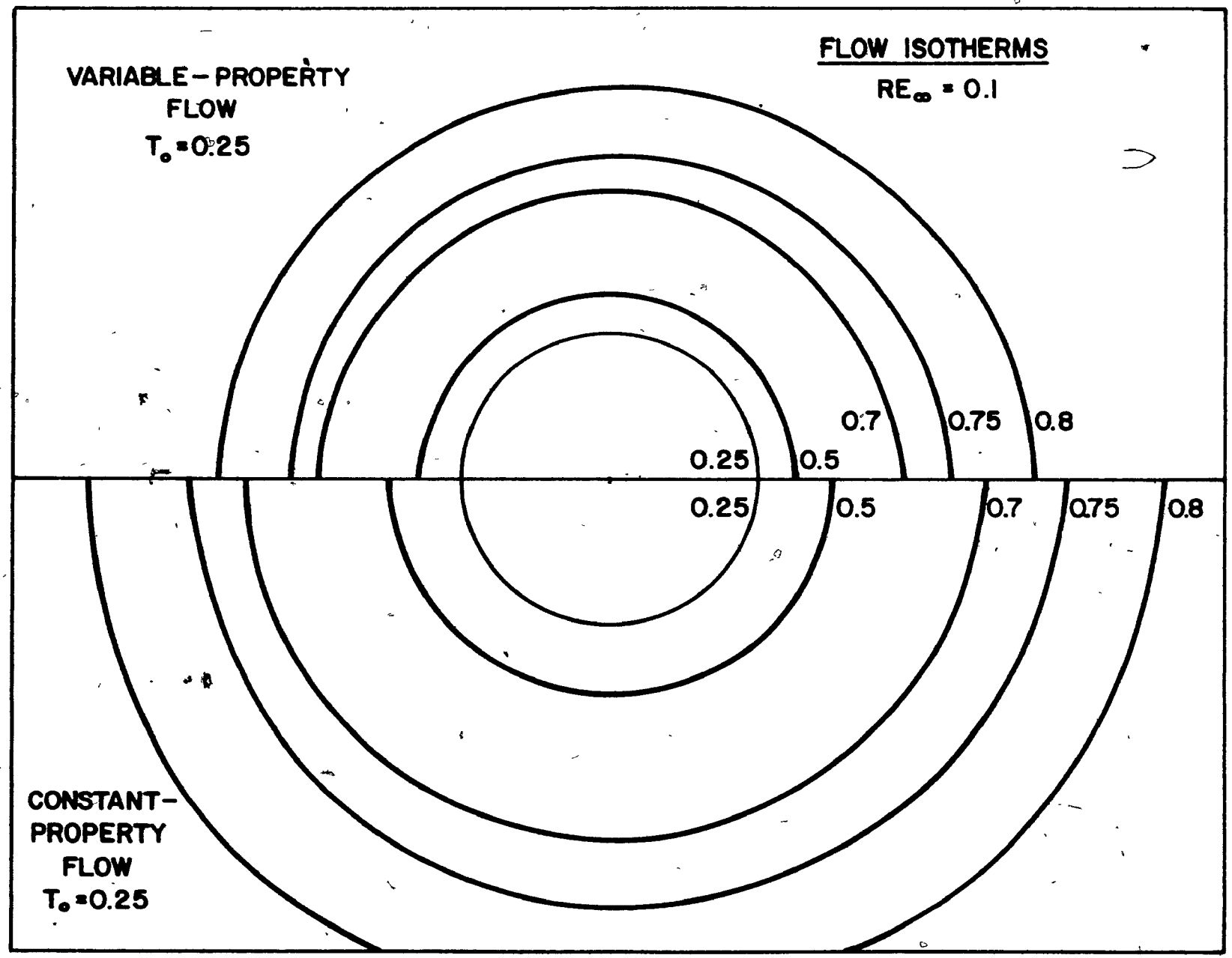
FLOW ISOTHERMS
$RE_\infty = 0.1$
VARIABLE – PROPERTY FLOW
$T_o = 0.25$
0.25
0.5
0.7
0.75
0.8
0.25
0.5
0.7
0.75
0.8
CONSTANT – PROPERTY FLOW
$T_o = 0.25$

FIGURE 17

TEMPERATURE FIELDS FOR

CONSTANT- AND VARIABLE-PROPERTY FLOWS

AT $T_o = 0.25$

RE = 10

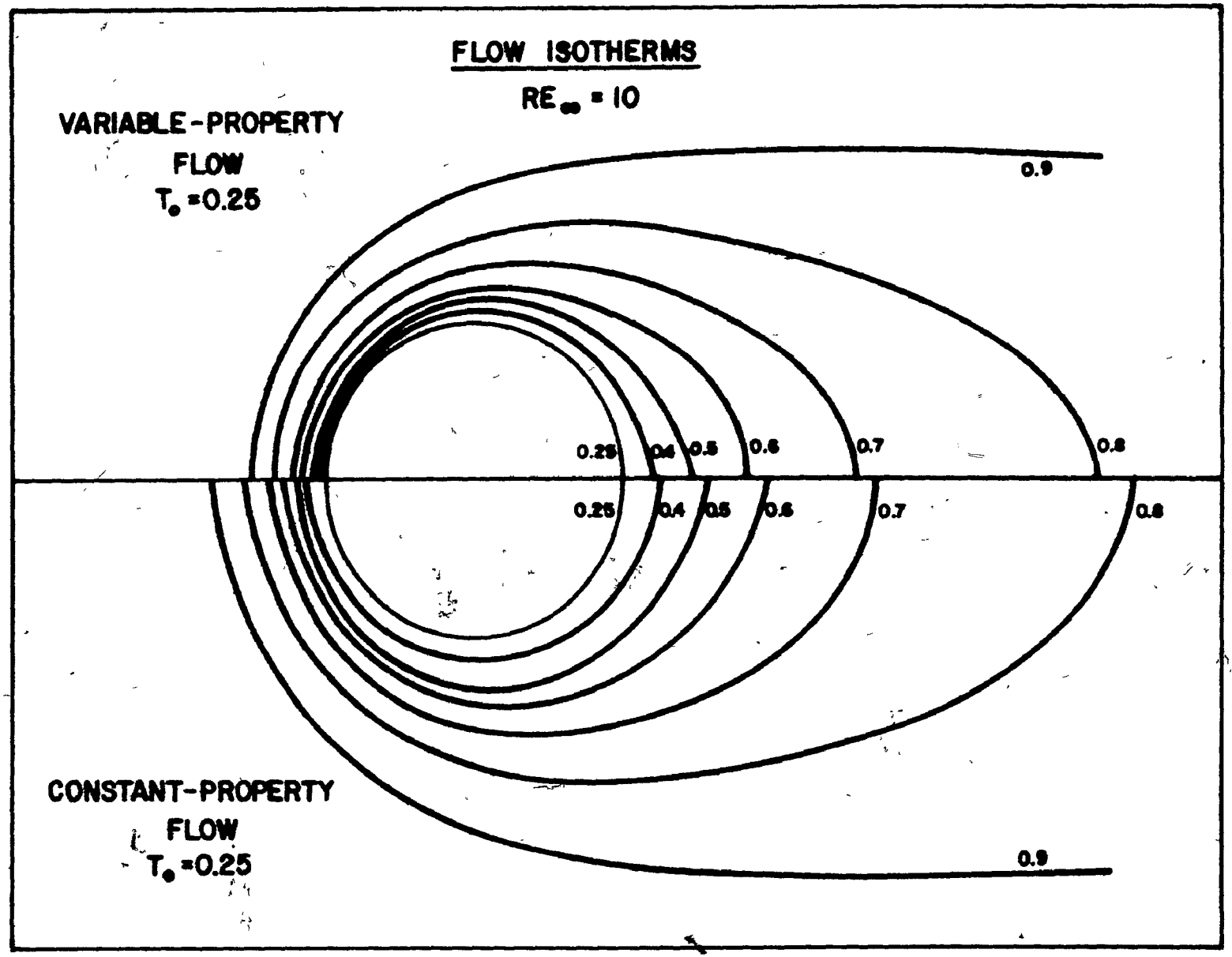
FLOW ISOTHERMS
RE∞ = 10
VARIABLE-PROPERTY
FLOW
T₀ =0.25
0.9
0.25
0.4
0.5
0.6
0.7
0.8
0.25
0.4
0.5
0.6
0.7
0.8
CONSTANT-PROPERTY
FLOW
T₀ =0.25
0.9

FIGURE 18

TEMPERATURE FIELDS FOR

CONSTANT- AND VARIABLE-PROPERTY FLOWS

AT $T_o = 0.25$

RE = 50

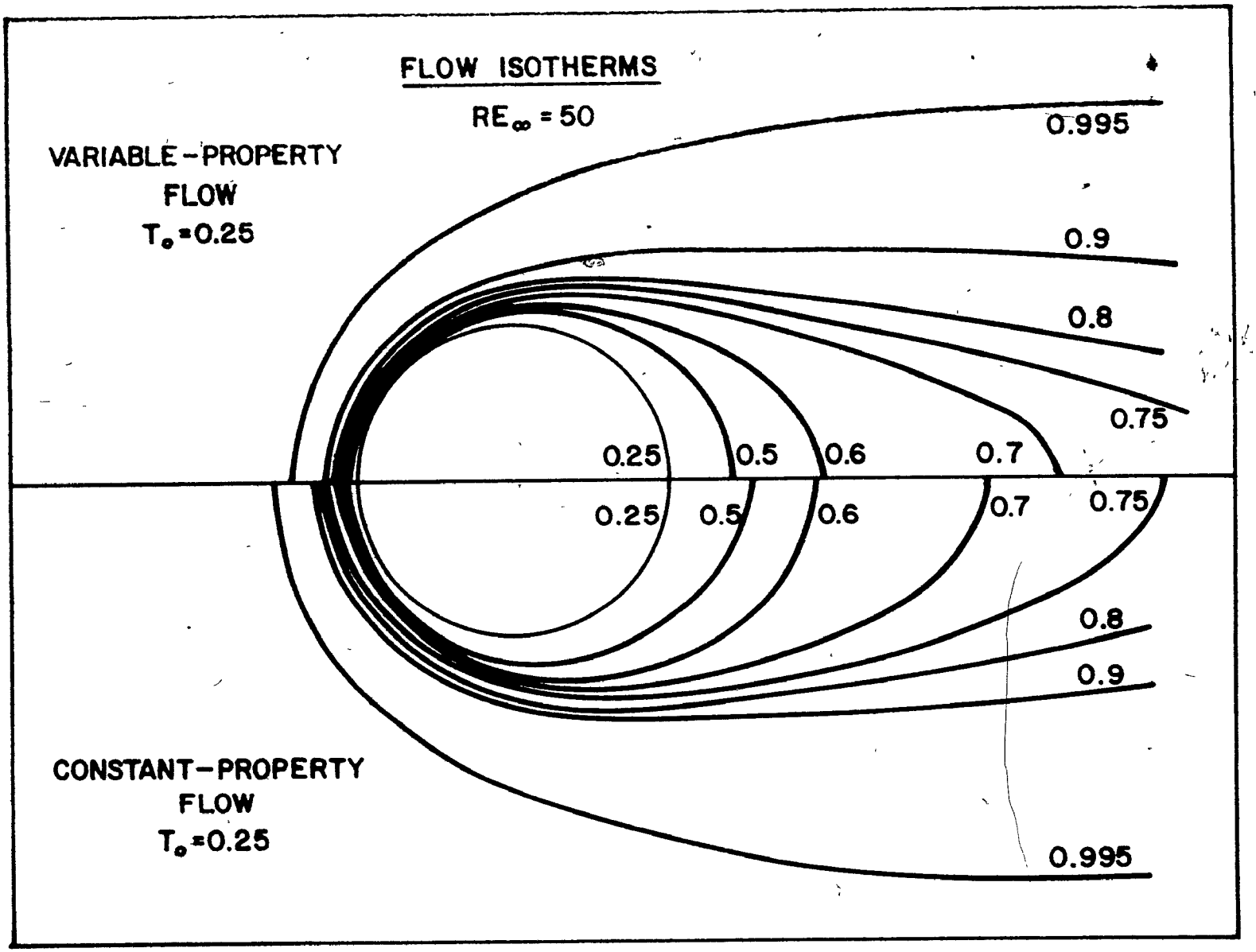
FLOW ISOTHERMS
$RE_\infty = 50$
VARIABLE-PROPERTY FLOW
$T_o = 0.25$
0.995
0.9
0.8
0.75
0.25
0.5
0.6
0.7
0.25
0.5
0.6
0.7
0.75
0.8
0.9
CONSTANT-PROPERTY FLOW
$T_o = 0.25$
0.995

FIGURE 19

EFFECT OF SURFACE TEMPERATURE

ON LOCAL NUSSELT NUMBER DISTRIBUTION

RE = 0.1

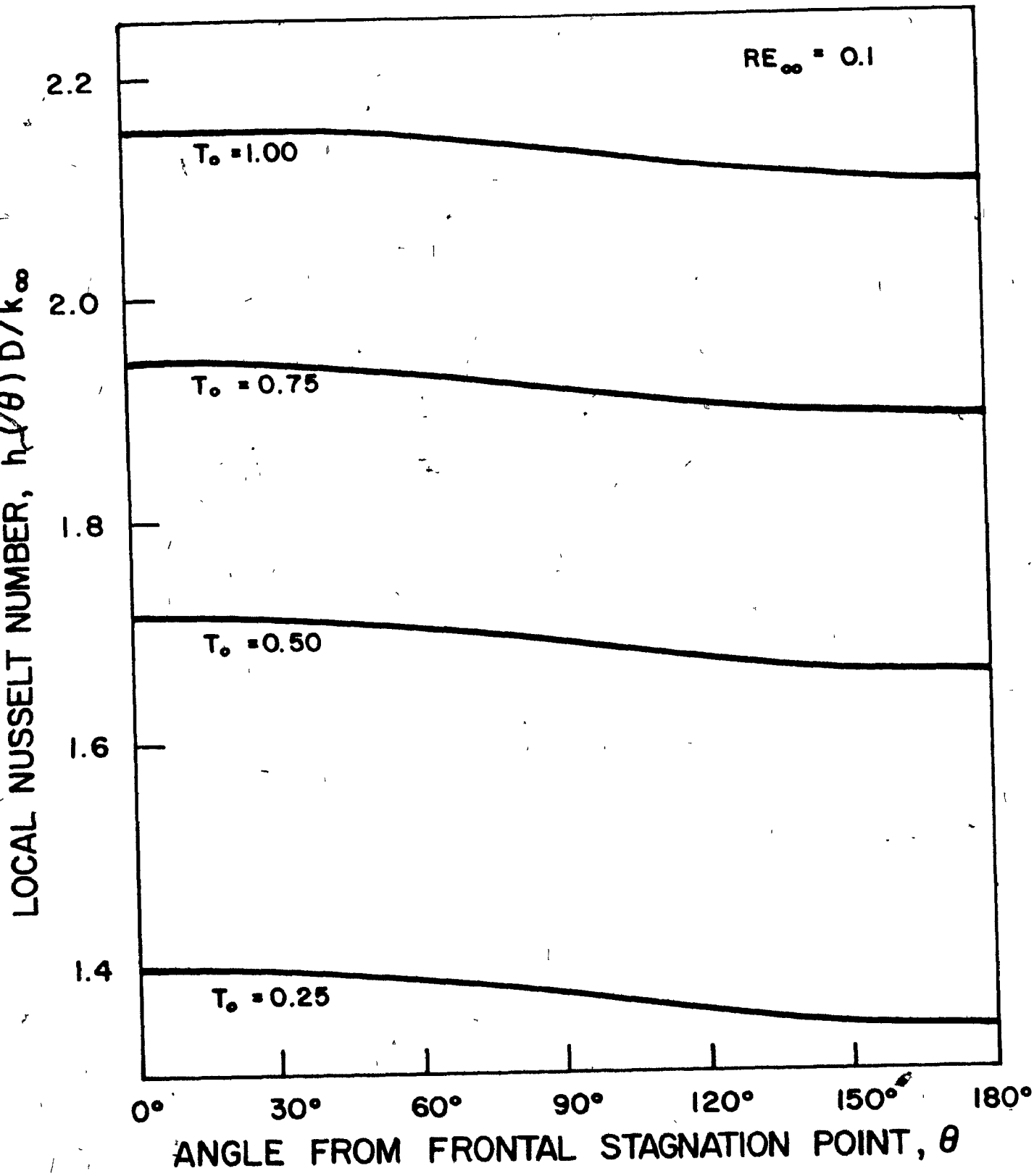
RE∞ = 0.1
T₀ = 1.00
T₀ = 0.75
T₀ = 0.50
T₀ = 0.25
2.2
2.0
1.8
1.6
1.4
LOCAL NUSSELT NUMBER, h(θ) D/k∞
0°
30°
60°
90°
120°
150°
180°
ANGLE FROM FRONTAL STAGNATION POINT, θ

FIGURE 20

EFFECT OF SURFACE TEMPERATURE

ON LOCAL NUSSELT NUMBER DISTRIBUTION

RE = 1.0

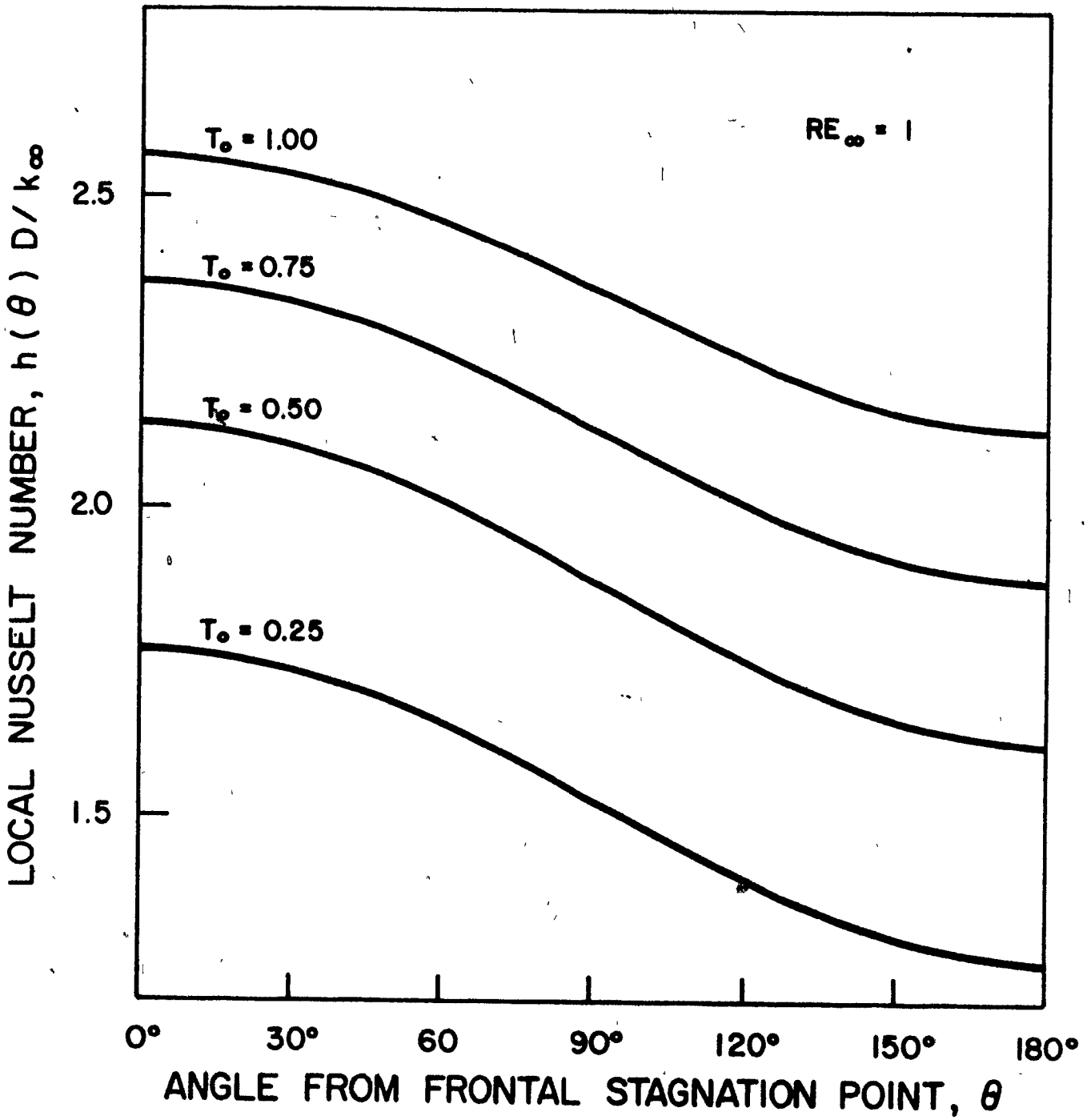
$RE_\infty = 1$
$T_o = 1.00$
$T_o = 0.75$
$T_o = 0.50$
$T_o = 0.25$
LOCAL NUSSELT NUMBER, $h(\theta) D / k_\infty$
2.5
2.0
1.5
0°
30°
60
90°
120°
150°
180°
ANGLE FROM FRONTAL STAGNATION POINT, θ

FIGURE 21

EFFECT OF SURFACE TEMPERATURE

ON LOCAL NUSSELT NUMBER DISTRIBUTION

RE = 10

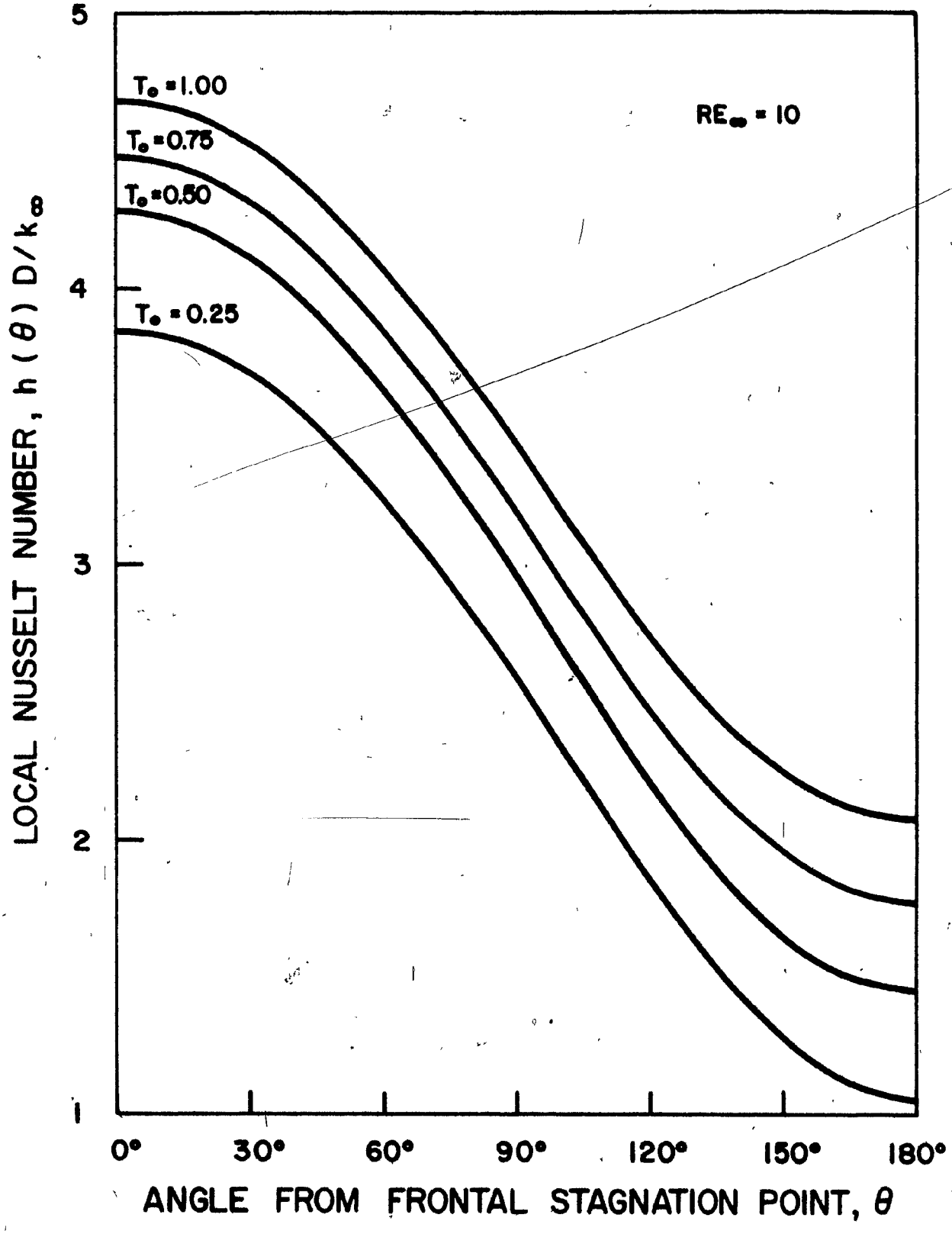
5
4
3
2
1
T_o = 1.00
T_o = 0.75
T_o = 0.50
T_o = 0.25
RE_∞ = 10
LOCAL NUSSELT NUMBER, $h(\theta) D/k_\infty$
0°
30°
60°
90°
120°
150°
180°
ANGLE FROM FRONTAL STAGNATION POINT, θ

FIGURE 22

EFFECT OF SURFACE TEMPERATURE

ON LOCAL NUSSELT NUMBER DISTRIBUTION

RE = 20

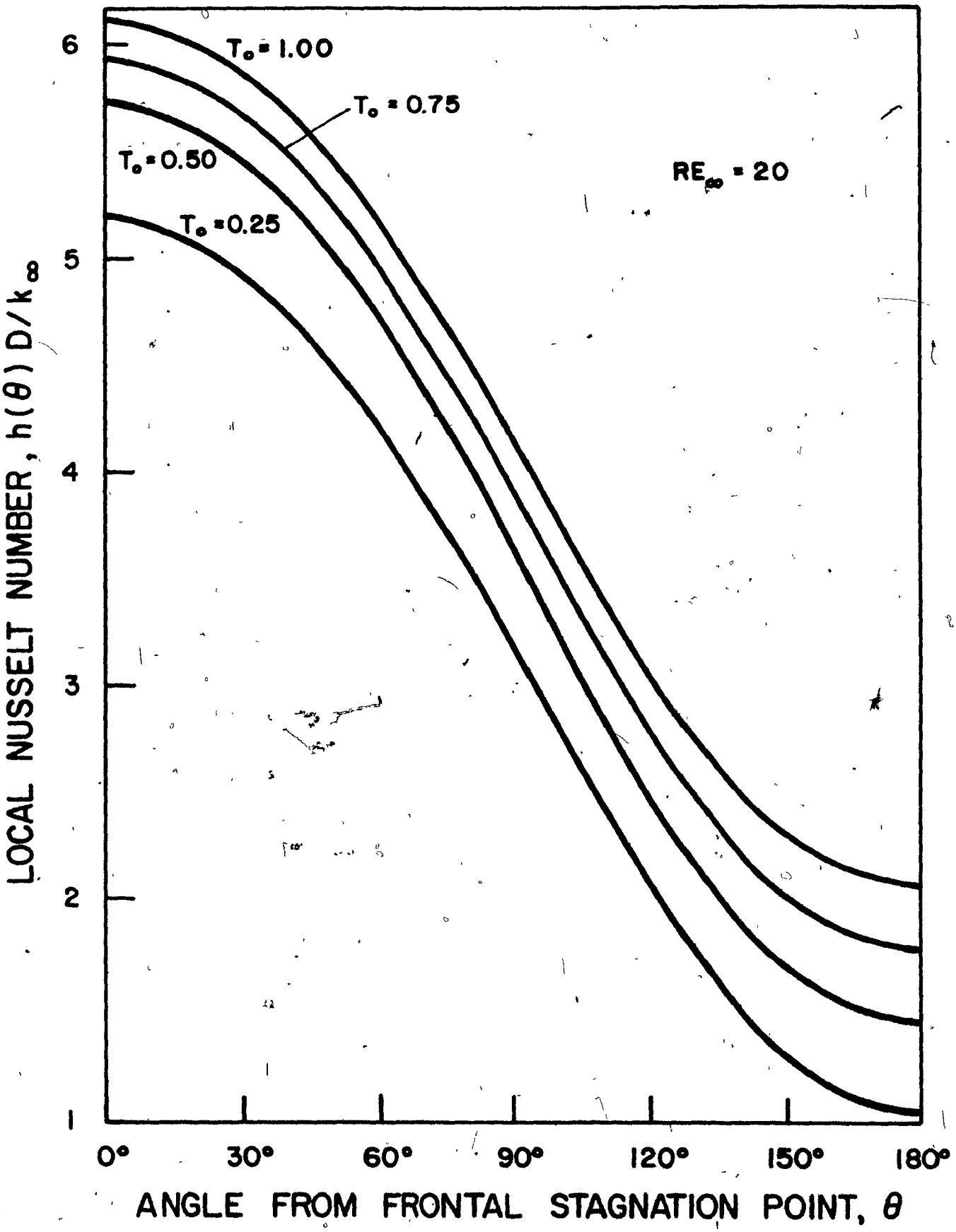
$T_o = 1.00$
$T_o = 0.75$
$T_o = 0.50$
$T_o = 0.25$
$RE_\infty = 20$
LOCAL NUSSELT NUMBER, $h(\theta) D/k_\infty$
6
5
4
3
2
1
0°
30°
60°
90°
120°
150°
180°
ANGLE FROM FRONTAL STAGNATION POINT, θ

FIGURE 23

EFFECT OF SURFACE TEMPERATURE

ON LOCAL NUSSELT NUMBER DISTRIBUTION

RE = 30

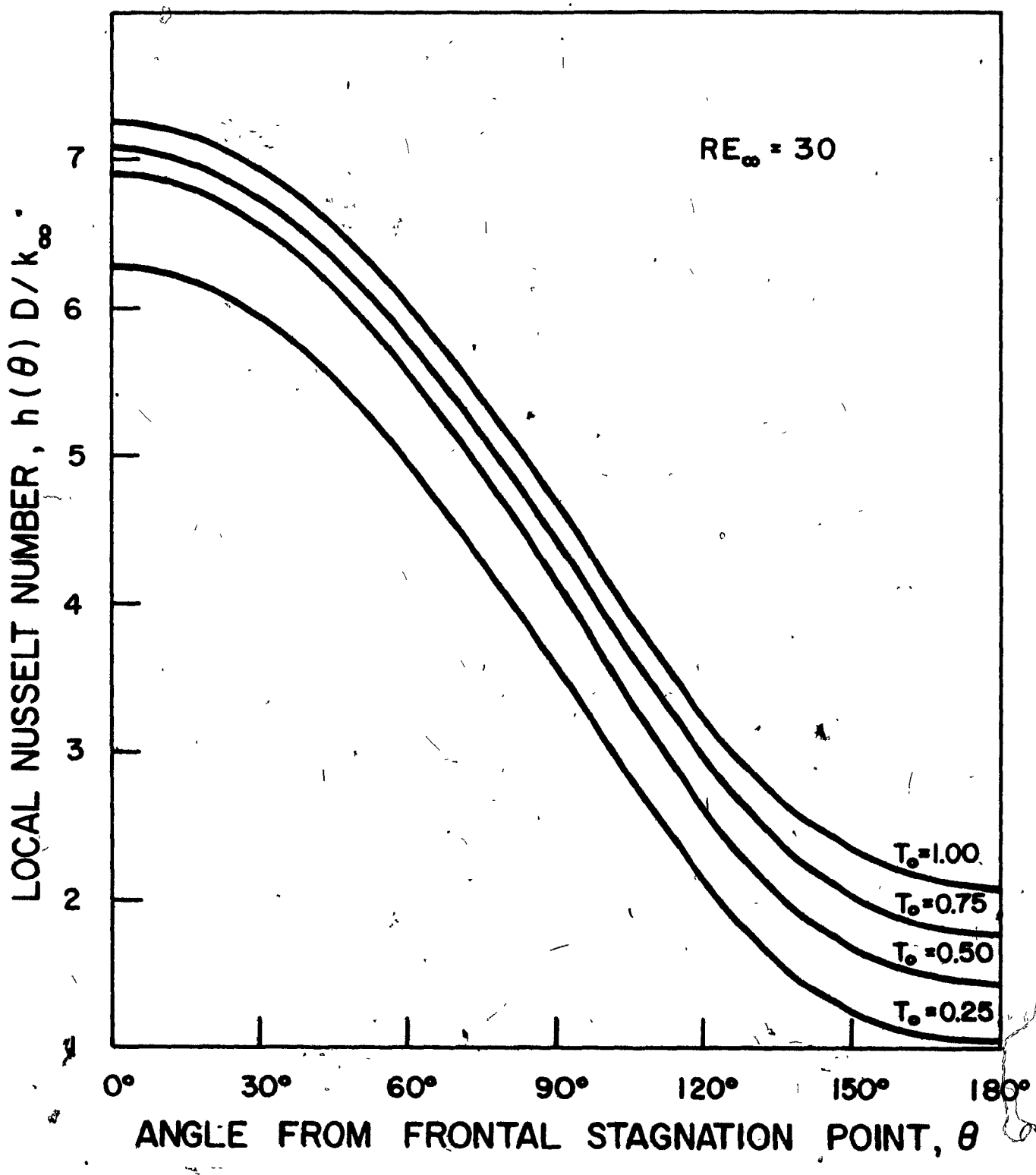
RE∞ = 30
LOCAL NUSSELT NUMBER, h(θ) D/k∞
7
6
5
4
3
2
1
T∞=1.00
T∞=0.75
T∞=0.50
T∞=0.25
0°
30°
60°
90°
120°
150°
180°
ANGLE FROM FRONTAL STAGNATION POINT, θ

FIGURE 24

EFFECT OF SURFACE TEMPERATURE

ON LOCAL NUSSELT NUMBER DISTRIBUTION

RE = 50

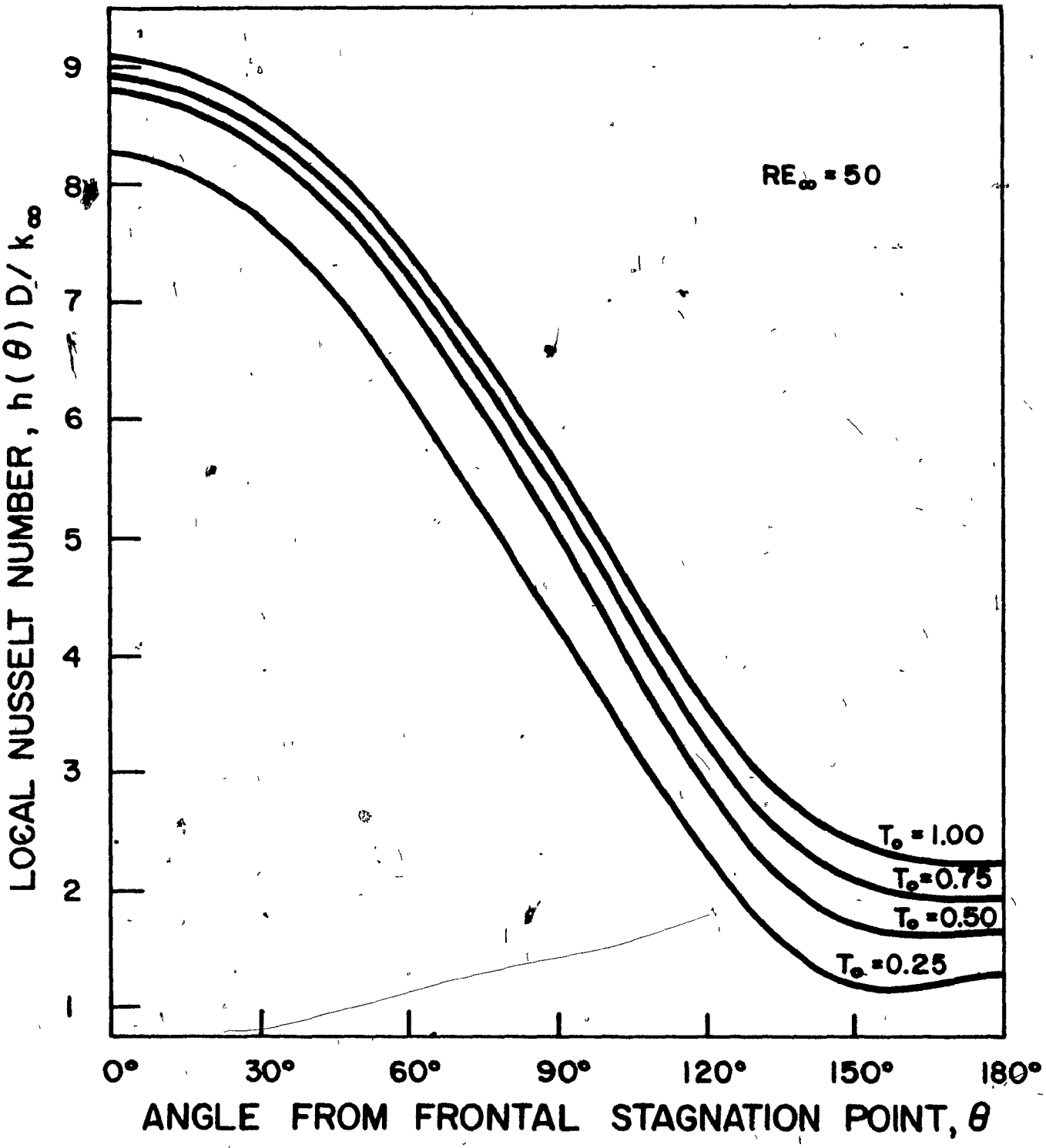
LOCAL NUSSELT NUMBER, $h(\theta) D / k_\infty$
9
8
7
6
5
4
3
2
1
$RE_\infty = 50$
$T_o = 1.00$
$T_o = 0.75$
$T_o = 0.50$
$T_o = 0.25$
0°
30°
60°
90°
120°
150°
180°
ANGLE FROM FRONTAL STAGNATION POINT, θ

Surface Pressure Distribution

Figures 25 to 30 show the surface pressure distributions for all of the cases studied. It can be observed that at low Reynolds numbers (Re<1) the effect of decreasing the surface temperature was a lowering in the value of the front stagnation pressure, p_o. On the other hand, for intermediate values of the Reynolds number this influence was reversed and p_o attained higher values at lower surface temperatures. Equation (60) can be re-written in the following simplified form:

$$p_o = \text{inertia term} + 8/Re \quad [\text{viscous term}]$$

As the surface temperature is lowered, the density of the fluid increases, resulting in higher inertia forces. On the other hand, lower surface temperature reduces viscous forces by reducing fluid viscosity near the sphere. At low Reynolds number the viscous forces are predominating and by reducing them the front stagnation pressure is also reduced. However, at higher Reynolds numbers, the inertia forces gain importance, leading to higher p_o values at lower temperatures.

In Figure 31 the values of the front stagnation pressure for constant-property flow were plotted versus the Reynolds number. A very good agreement between the present results and the results of others can be observed-

Figures 25 to 30 indicate that for all the Reynolds numbers

FIGURE 25

EFFECT OF SURFACE TEMPERATURE

ON SURFACE PRESSURE DISTRIBUTION

RE = 0.1

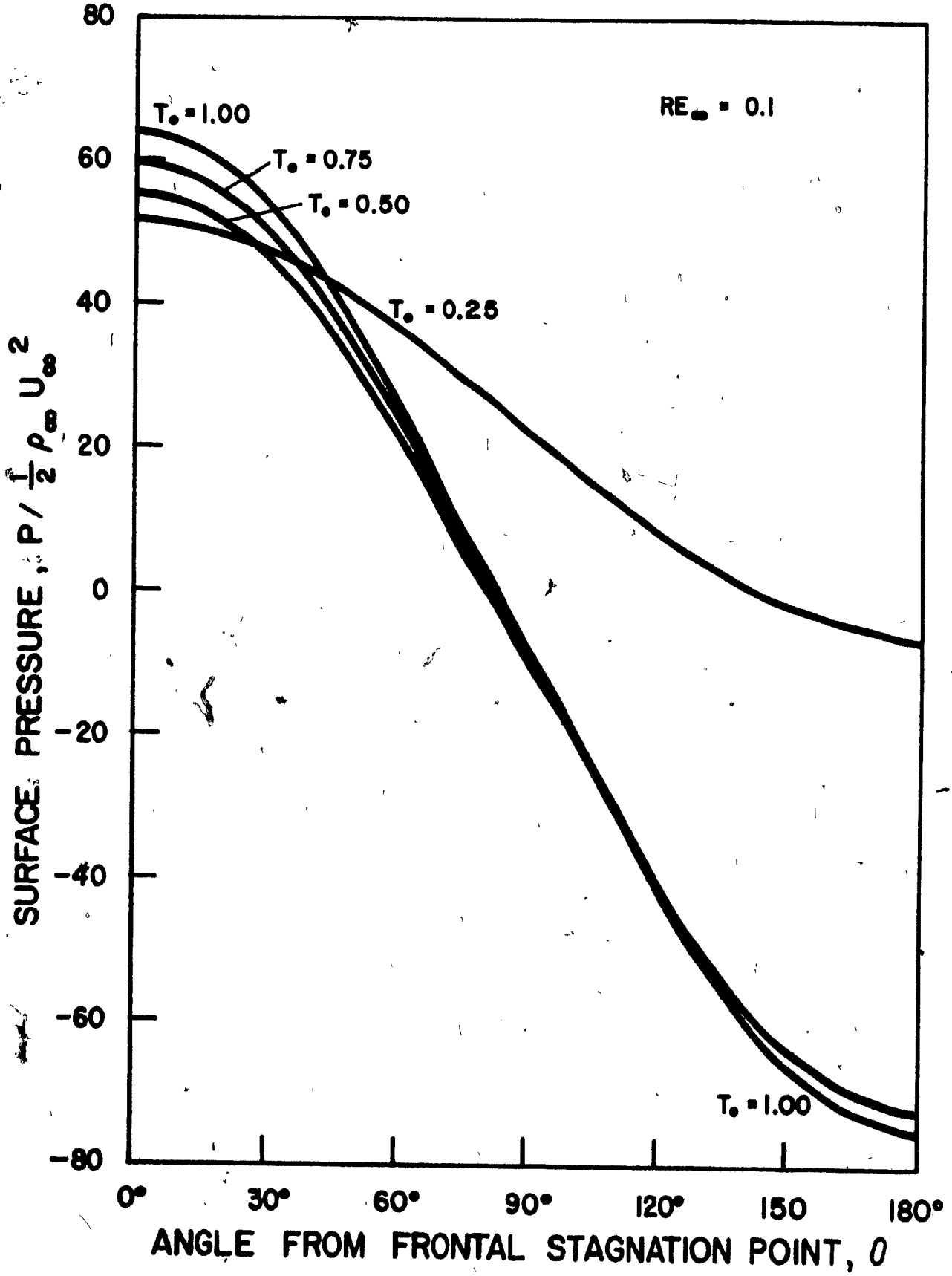
80
60
40
20
0
-20
-40
-60
-80
T_o = 1.00
RE_∞ = 0.1
T_o = 0.75
T_o = 0.50
T_o = 0.25
T_o = 1.00
SURFACE PRESSURE, $P / \frac{1}{2} \rho_\infty U_\infty^2$
0°
30°
60°
90°
120°
150
180°
ANGLE FROM FRONTAL STAGNATION POINT, θ

FIGURE 26

EFFECT OF SURFACE TEMPERATURE

ON SURFACE PRESSURE DISTRIBUTION

RE = 1.0

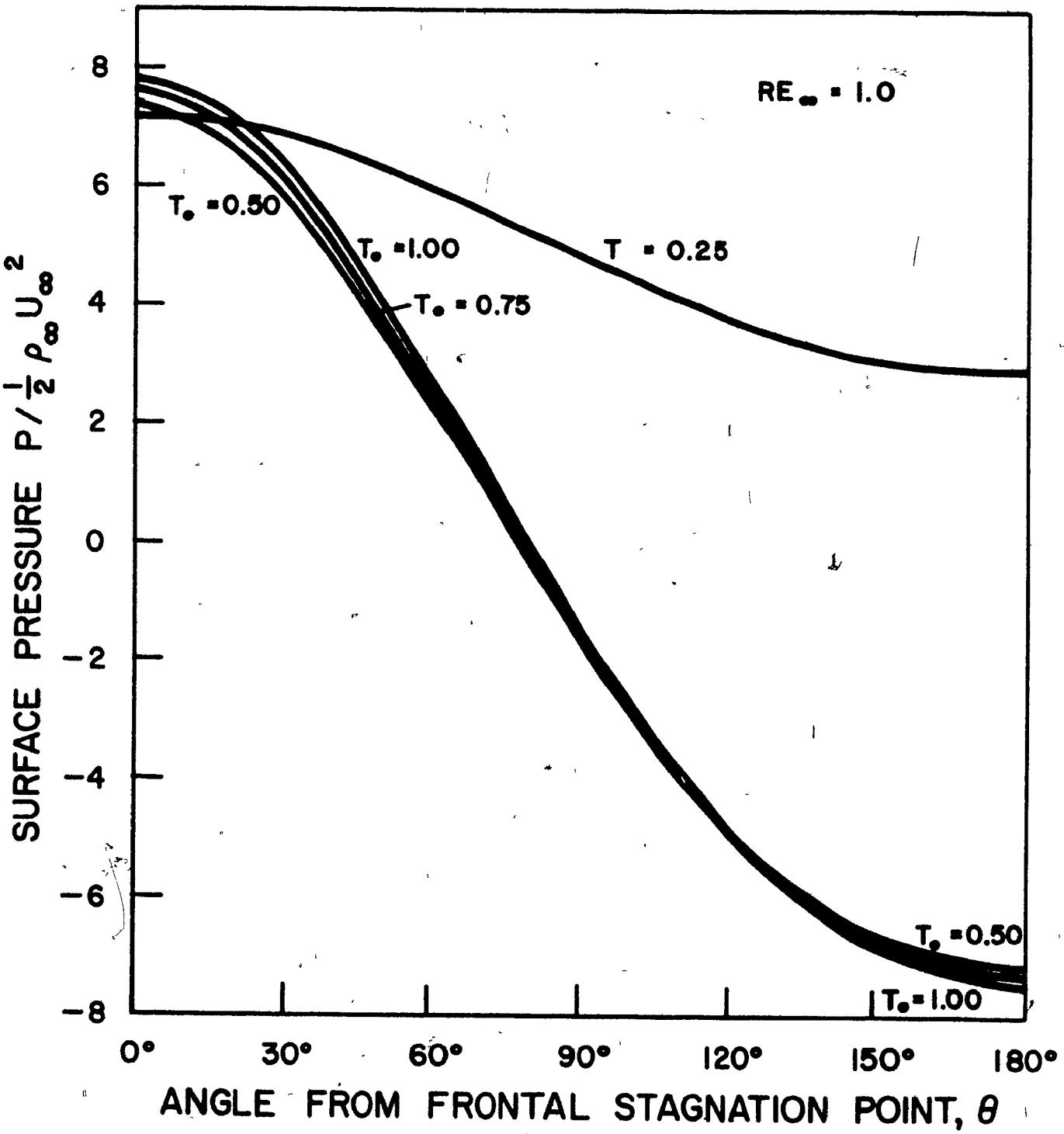
RE∞ = 1.0
T∘ =0.50
T∘ =1.00
T = 0.25
T∘ = 0.75
T∘ =0.50
T∘ =1.00
8
6
4
2
0
−2
−4
−6
−8
0°
30°
60°
90°
120°
150°
180°
SURFACE PRESSURE P/½ ρ∞ U∞²
ANGLE FROM FRONTAL STAGNATION POINT, θ

FIGURE 27

EFFECT OF SURFACE TEMPERATURE

ON SURFACE PRESSURE DISTRIBUTION

RE = 10

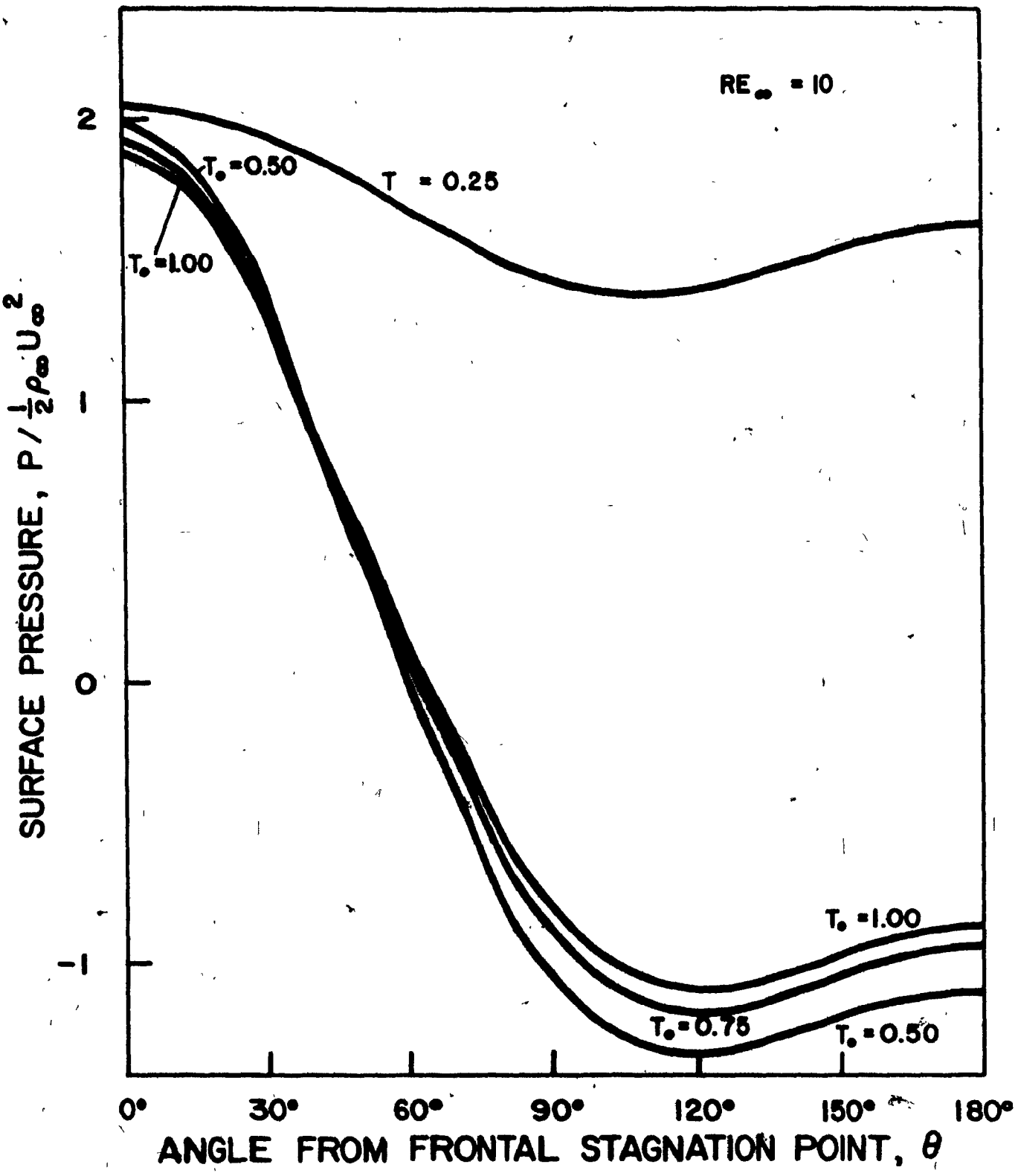
RE∞ = 10
T = 0.25
T∞ = 0.50
T∞ = 1.00
T∞ = 1.00
T∞ = 0.75
T∞ = 0.50
2
1
0
-1
SURFACE PRESSURE, P / ½ρ∞U∞²
0°
30°
60°
90°
120°
150°
180°
ANGLE FROM FRONTAL STAGNATION POINT, θ

FIGURE 28

EFFECT OF SURFACE TEMPERATURE

ON SURFACE PRESSURE DISTRIBUTION

RE = 20

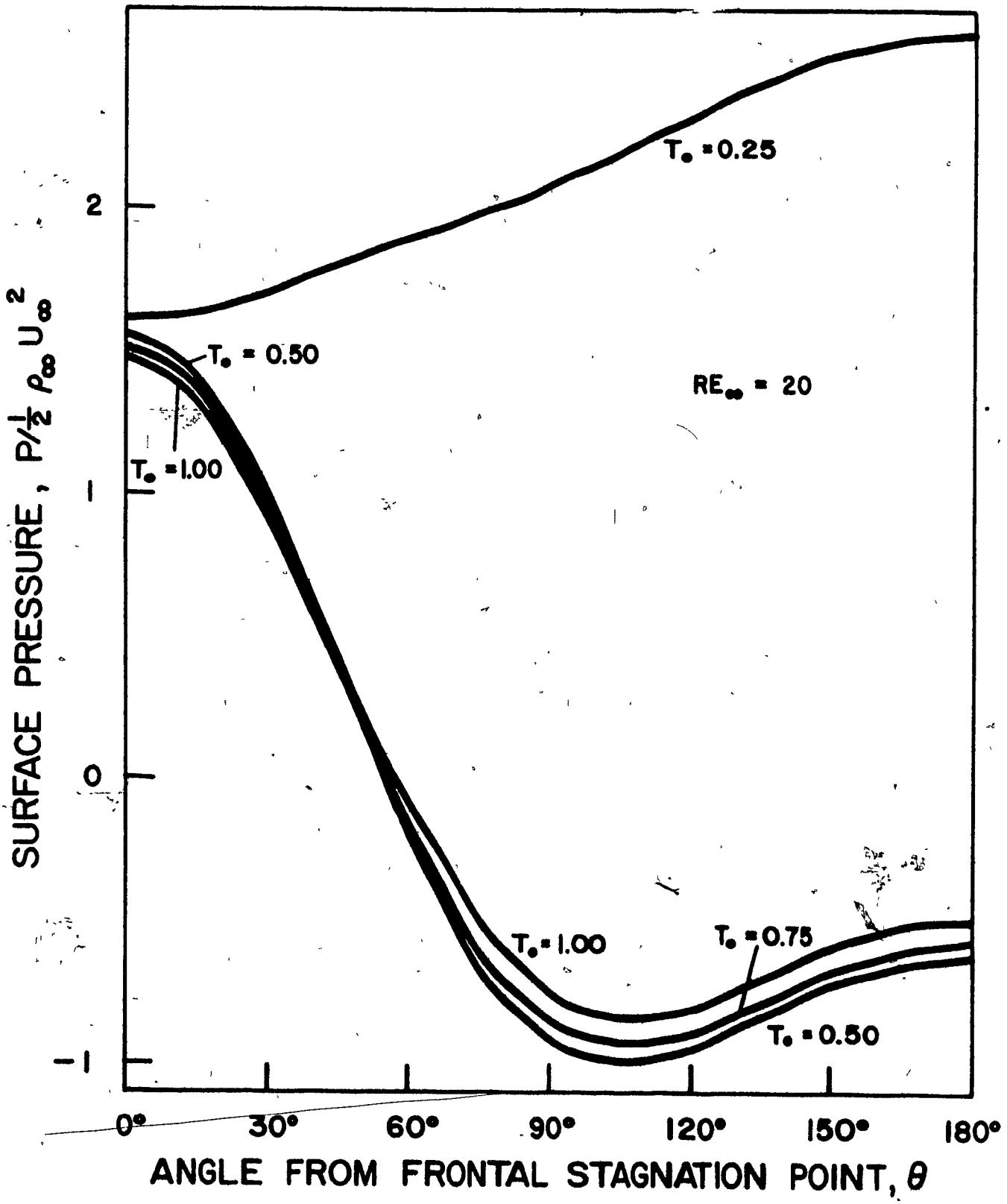
$T_\bullet = 0.25$
$T_\bullet = 0.50$
$T_\bullet = 1.00$
$RE_\infty = 20$
$T_\bullet = 1.00$
$T_\bullet = 0.75$
$T_\bullet = 0.50$
2
1
0
−1
SURFACE PRESSURE, $P/\frac{1}{2}\rho_\infty U_\infty^2$
0°
30°
60°
90°
120°
150°
180°
ANGLE FROM FRONTAL STAGNATION POINT, θ

FIGURE 29

EFFECT OF SURFACE TEMPERATURE

ON SURFACE PRESSURE DISTRIBUTION

RE = 30

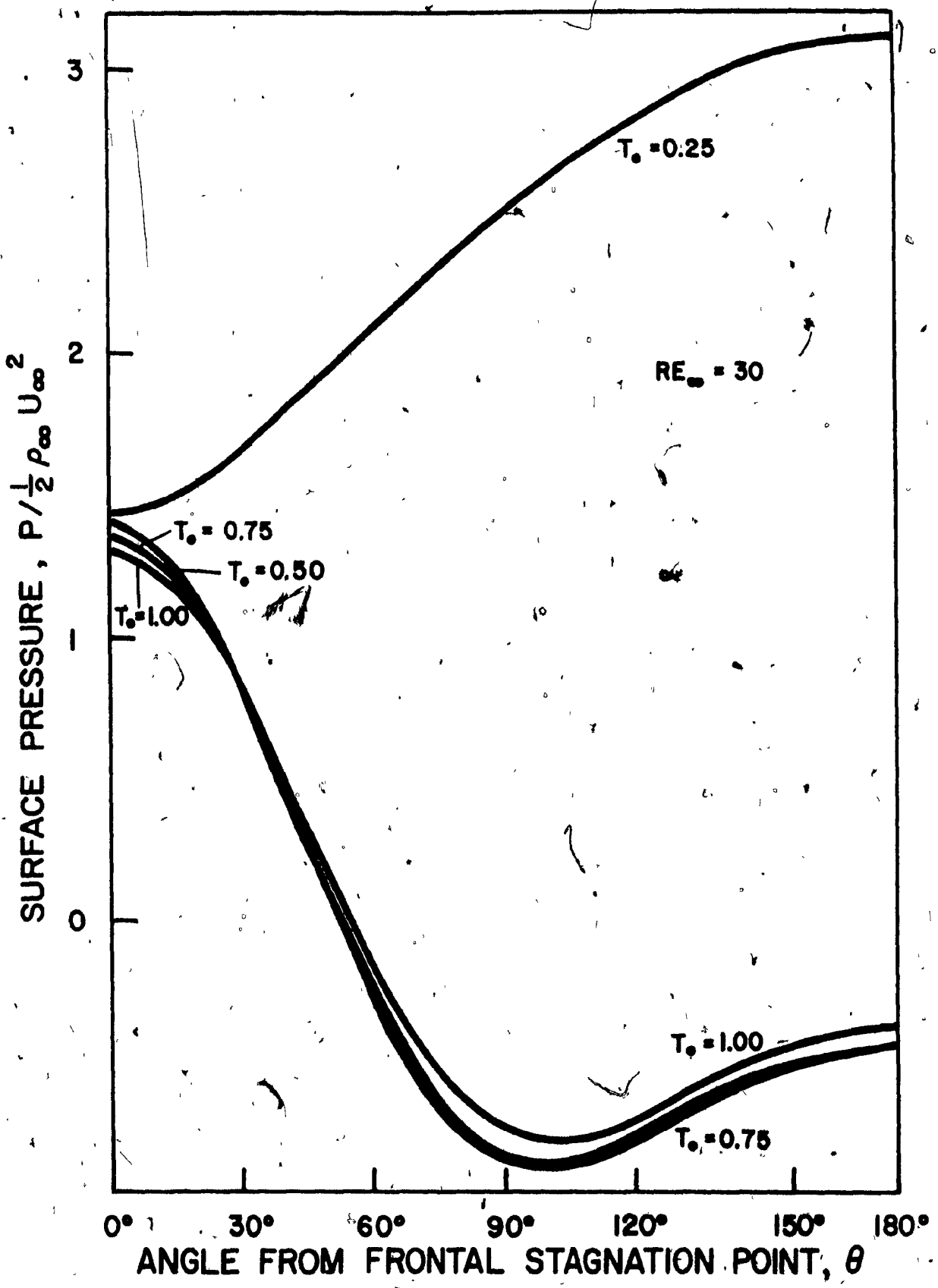
SURFACE PRESSURE, $P/\frac{1}{2}\rho_\infty U_\infty^2$
3
2
1
0
T_o = 0.25
RE_∞ = 30
T_o = 0.75
T_o = 0.50
T_o = 1.00
T_o = 1.00
T_o = 0.75
0°
30°
60°
90°
120°
150°
180°
ANGLE FROM FRONTAL STAGNATION POINT, θ

FIGURE 30

EFFECT OF SURFACE TEMPERATURE

ON SURFACE PRESURE DISTRIBUTION

RE = 50

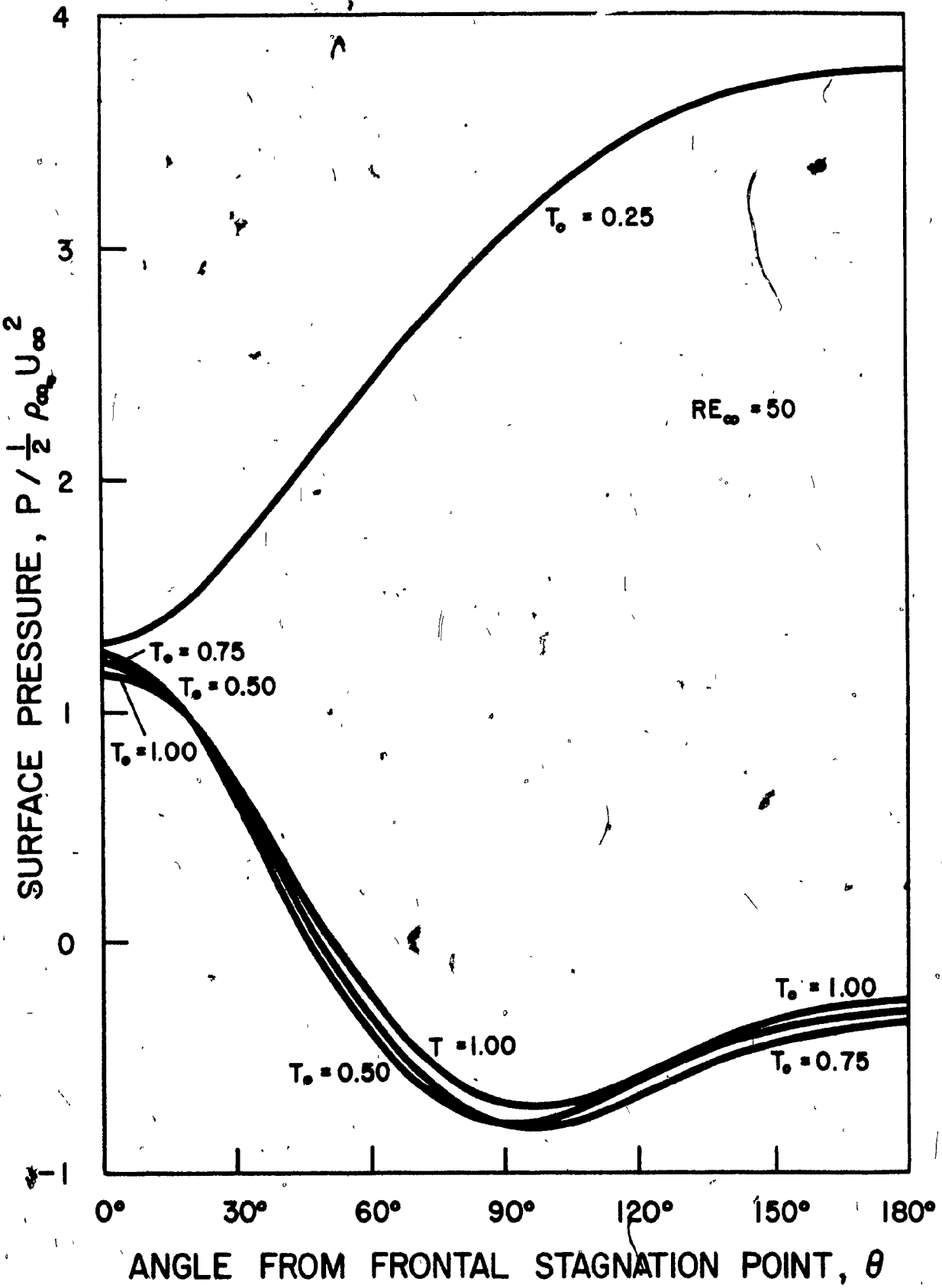
SURFACE PRESSURE, $P / \frac{1}{2} \rho_\infty U_\infty^2$
4
3
2
1
0
−1
$T_o = 0.25$
$RE_\infty = 50$
$T_o = 0.75$
$T_o = 0.50$
$T_o = 1.00$
$T_o = 1.00$
$T = 1.00$
$T_o = 0.50$
$T_o = 0.75$
0°
30°
60°
90°
120°
150°
180°
ANGLE FROM FRONTAL STAGNATION POINT, θ

FIGURE 31

VARIATION OF FRONT STAGNATION PRESSURE

WITH THE REYNOLDS NUMBER

FOR CONSTANT-PROPERTY FLOW

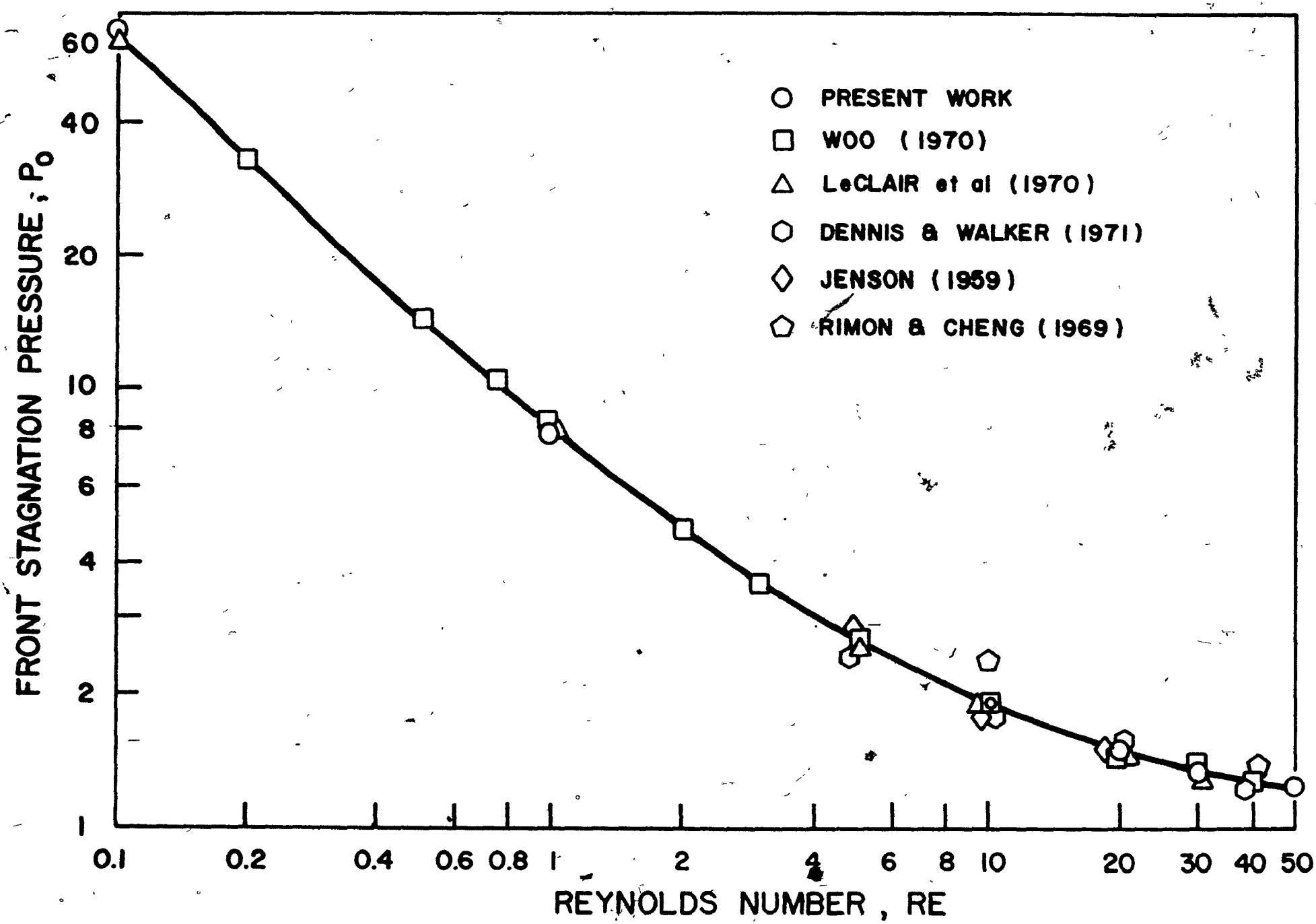
PRESENT WORK
WOO (1970)
LeCLAIR et al (1970)
DENNIS & WALKER (1971)
JENSON (1959)
RIMON & CHENG (1969)
FRONT STAGNATION PRESSURE , P_0
60
40
20
10
8
6
4
2
1
0.1
0.2
0.4
0.6
0.8
1
2
4
6
8
10
20
30
40
50
REYNOLDS NUMBER , RE

and $T_o > 0.5$ the effect of varying fluid properties on the surface pressure distribution was not very marked. However, at $T_o = 0.25$ the surface pressure gradient $\partial p/\partial \Theta$ became less steep and at $Re > 20$ its direction changed from negative to positive. Consequently, the surface pressure increased with Θ leading to $p(\pi) > p_o$. The explanation for this phenomenon can be deduced from the Navier-Stokes equation. At the sphere surface, the inertia forces are equal to zero because of the no-slip condition. Hence, the change in the momentum transfer by viscous forces is balanced by an equal change in the pressure force. The rate of momentum gain by viscous transfer in the Θ direction at the sphere surface is proportional to $\partial/\partial z(-\mu\zeta r)$. For constant property flow, the viscosity is constant and the change in momentum transfer is positive since $\partial\zeta r/\partial z$ is negative. Consequently, the change in the pressure force is negative. However, when the viscosity is also changing with radial position, the overall change in momentum transfer can be either negative or positive depending on the relative magnitude of the viscosity and velocity gradients.

From a purely physical point of view, it must be admitted that the behaviour at $T_o = 0.25$ is highly anomalous. The increase in surface pressure at $Re > 20$ predicted by the numerical analysis is extremely difficult to reconcile with the classical physical visualization of boundary layer flow. Flow without separation in the presence of such large positive pressure gradients could only be sustained if the boundary layer were turbulent; the transition

occurring in the frontal region of the sphere. A turbulent boundary layer would also account for the very low total drag coefficients, reported in the next section, under these conditions. It must be emphasized, however, that the numerical analysis was entirely based on laminar flow considerations. The solutions would, therefore, be invalid if turbulence were present. Nor can the analysis predict the onset of turbulence. The interpretation must, therefore, be strictly based on the momentum transfer considerations mentioned above.

Drag Coefficients

The values of the friction, pressure and total drag coefficients are listed in Tables V to VII. Since the friction drag is directly proportional to the viscosity and inversely proportional to the Reynolds number, it decreased monotonically with increasing Re and decreasing T_o. The pressure drag is a result of differences in the pressure over the sphere surface and is, therefore, directly related to the shape of the pressure distribution curve. As was discussed earlier, for $T_o > 0.5$ the effect of decreasing T_o on $p(\Theta)$ was small and consequently the variation of C_{DP} with T_o is also small. At $T_o = 0.25$, however, the shape of $p(\Theta)$ vs. Θ curves was drastically changed and hence the pressure drag coefficients were significantly reduced.

The constant-property drag coefficients obtained in this study are compared in Figure 32 with experimental and theoretical

TABLE V

FRICTION DRAG COEFFICIENTS

Re	$T_o = 1.0$	$T_o = 0.75$	$T_o = 0.50$	$T_o = 0.25$
0.1	168.4	148.1	129.2	103.8
1	18.45	16.56	14.63	12.42
10	2.96	2.69	2.46	2.19
20	1.07	1.65	1.52	1.37
30	1.35	1.26	1.16	1.04
50	0.96	0.90	0.84	0.77

TABLE VI

PRESSURE DRAG COEFFICIENTS

Re	$T_o = 1.0$	$T_o = 0.75$	$T_o = 0.50$	$T_o = 0.25$
0.1	82.3	87.7	85.0	38.0
1	9.04	9.90	9.70	2.90
10	1.63	1.77	1.89	0.33
20	1.79	1.18	1.21	-0.61
30	0.86	0.95	0.93	-1.04
50	0.67	0.72	0.66	-1.52

TABLE VII

TOTAL DRAG COEFFICIENTS

Re	T_o = 1.0	T_o = 0.75	T_o = 0.50	T_o = 0.25
0.1	250.6	235.8	214.1	146.2
1	27.49	26.46	24.33	15.32
10	4.59	4.46	4.36	2.52
20	2.86	2.83	2.73	0.76
30	2.21	2.21	2.10	0.007
50	1.62	1.62	1.50	-.075

FIGURE 32

VARIATION OF FRICTION, PRESSURE AND TOTAL DRAG COEFFICIENTS WITH THE REYNOLDS NUMBER FOR CONSTANT-PROPERTY FLOW

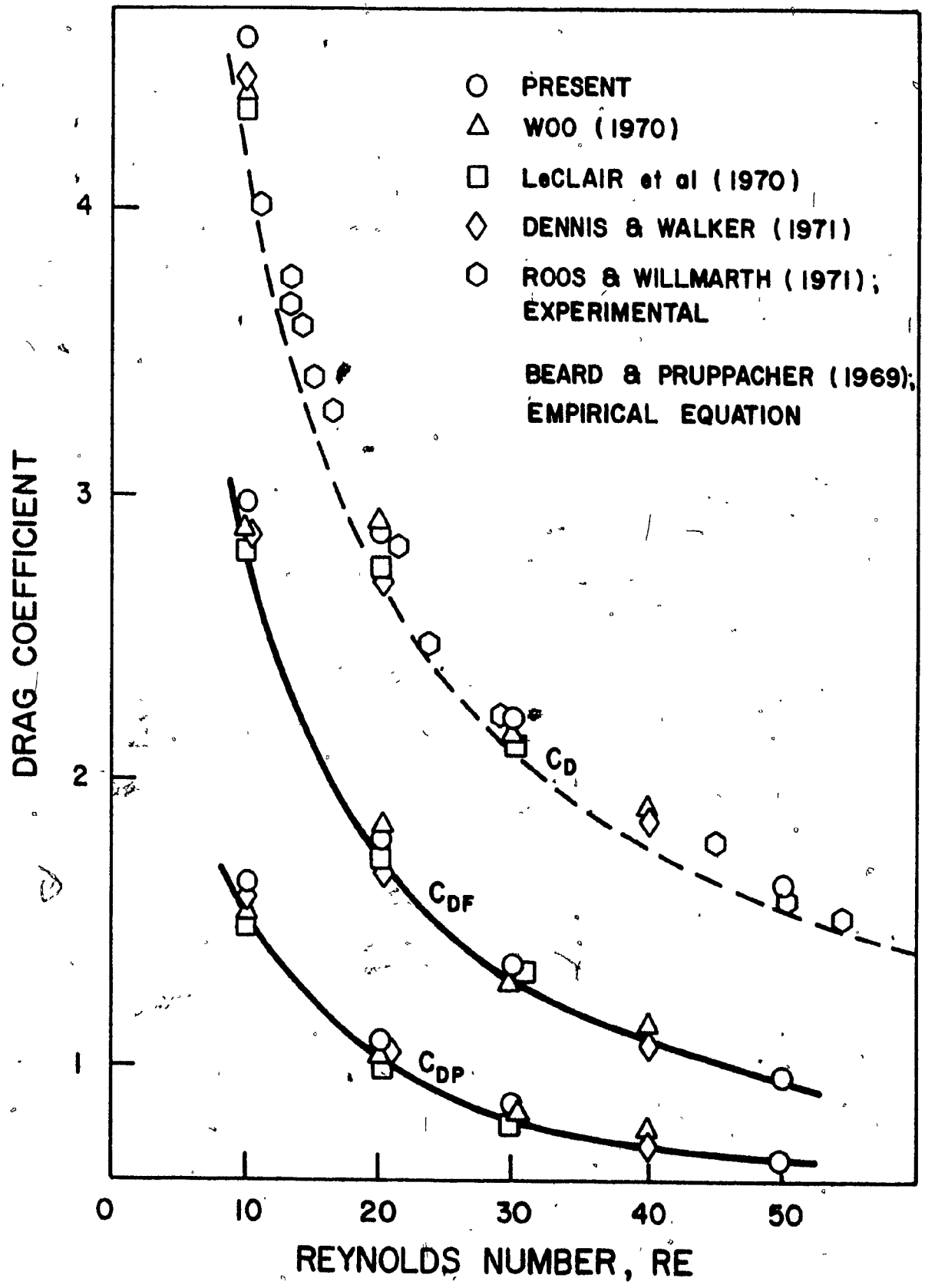
PRESENT
WOO (1970)
LeCLAIR et al (1970)
DENNIS & WALKER (1971)
ROOS & WILLMARTH (1971); EXPERIMENTAL
BEARD & PRUPPACHER (1969); EMPIRICAL EQUATION
C_D
C_{DF}
C_{DP}
DRAG COEFFICIENT
REYNOLDS NUMBER, RE
0
10
20
30
40
50
1
2
3
4

results of other workers. The present results are slightly higher than most of the rest. This discrepancy is possibly due to the closer outer boundaries selected for the present analysis ($r_\infty = 7.4$) as compared to $r_\infty = 90$ in LeClair's (1970) solution.

CORRELATION OF HEAT TRANSFER RESULTS

The values of the overall Nusselt number for all of the cases studied are listed in Table VIII. In the following analysis a correlation will be derived for constant-property flow which will then be modified to include the effect of variable properties.

Constant-Property Transfer

In Figure 33 the constant-property results of this study are compared with the theoretical results of Woo (1971) and Dennis et al. (1973) and to the experimental equations of Whitaker (1972), Beard and Pruppacher (1971) and Ranz and Marshall (1952). Woo solved the governing equations numerically by finite-difference methods, while Dennis et al. applied the series truncation method to both of the flow and energy equations. Beard and Pruppacher's equations for heat transfer are:

$$\text{Re} > 2 \quad : \quad 1/2\ \text{Nu} = 0.78 + 0.308\ \text{Pr}^{1/3}\ \text{Re}^{1/2} \tag{70}$$

$$\text{Re} < 2 \quad : \quad 1/2\ \text{Nu} = 1 + 0.108\ (\text{Pr}^{1/3}\ \text{Re}^{1/2})^2 \tag{71}$$

Whitaker's correlation for constant-property flow is:

$$\text{Nu} = 2 + (0.4\ \text{Re}^{1/2} + 0.06\ \text{Re}^{2/3})\ \text{Pr}^{0.4} \tag{72}$$

TABLE VIII

OVERALL NUSSELT NUMBER, hD/k_∞

Re UD/ν_∞	$T_o = 1.0$*	$T_o = 0.75$	$T_o = 0.50$	$T_o = 0.25$
0.1	2.021	1.918	1.687	1.370
1	2.232	2.123	1.879	1.526
10	3.323	3.161	2.924	2.537
20	4.022	3.872	3.614	3.136
30	4.560	4.425	4.143	3.584
50	5.411	5.281	4.979	4.313

* $T_o = 1.0$ refers to constant-property solution

FIGURE 33

VARIATION OF THE OVERALL NUSSELT NUMBER WITH THE REYNOLDS NUMBER FOR CONSTANT-PROPERTY FLOW

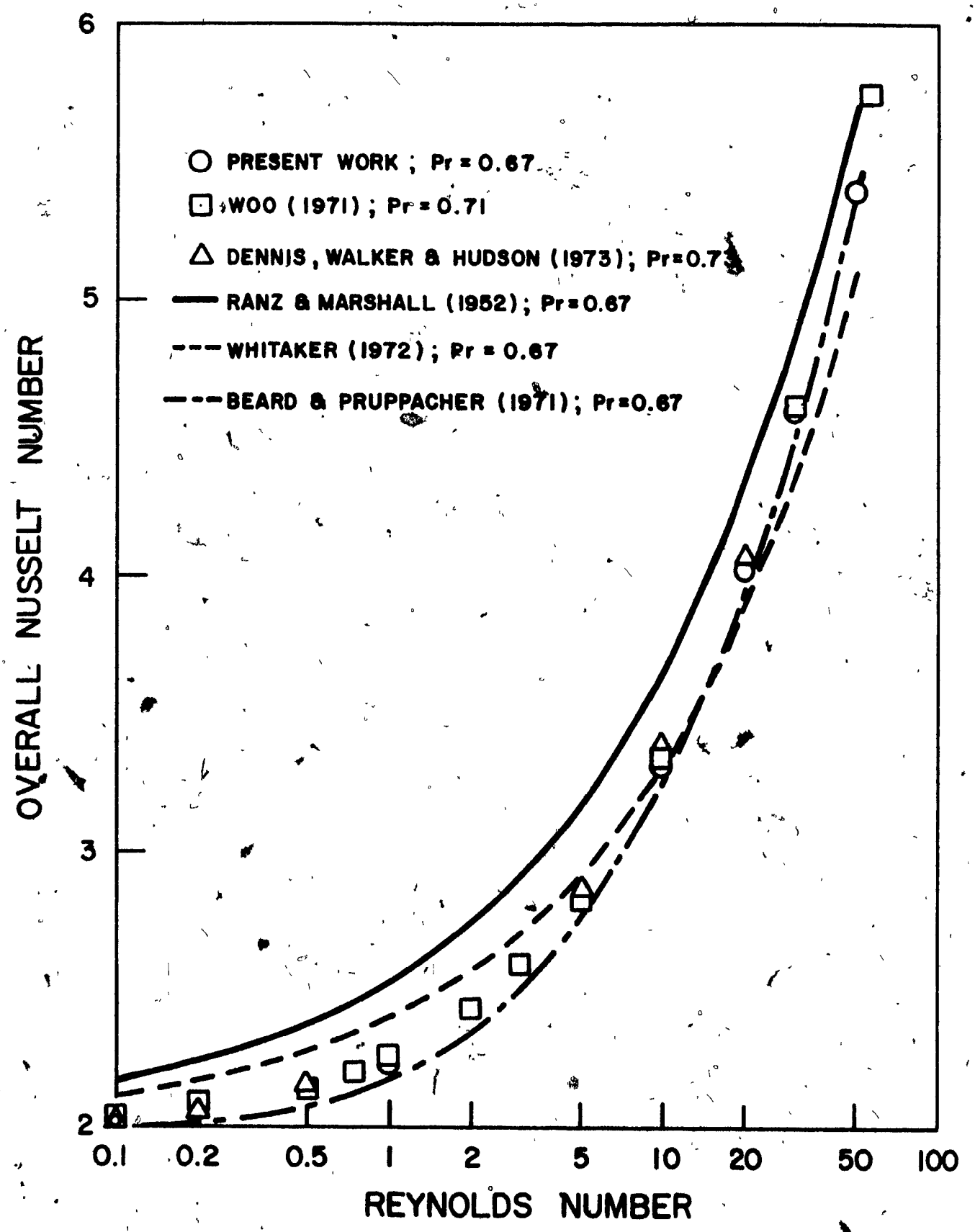
PRESENT WORK ; Pr = 0.67
WOO (1971) ; Pr = 0.71
DENNIS, WALKER & HUDSON (1973); Pr=0.7
RANZ & MARSHALL (1952); Pr=0.67
WHITAKER (1972); Pr = 0.67
BEARD & PRUPPACHER (1971); Pr=0.67
OVERALL NUSSELT NUMBER
REYNOLDS NUMBER
6
5
4
3
2
0.1
0.2
0.5
1
2
5
10
20
50
100

and Ranz and Marshall's is:

$$Nu = 2 + 0.6\ Pr^{1/3}\ Re^{1/2} \qquad (73)$$

Excellent agreement can be observed among the theoretical results, including those of the present study. The experimental correlations, however, are accurate for only very small ranges of the Reynolds number. A new correlation will, therefore, be proposed here to fit the numerical results. The general form of the equation will be assumed to be:

$$Nu = a + b\ Pr^{m}\ Re^{n} \qquad (74)$$

a is the limiting Nusselt number at Re = 0. For a sphere immersed in a constant-property fluid, a has the value of 2. The exponents m and n need not necessarily be constants.

In the present work, only one value of the Prandtl number was studied, namely, Pr = 0.67. Consequently, it was not possible to investigate the effect of the Prandtl number from the results. However, Hoffman and Ross (1972) solved the integral boundary-layer formulation of the energy equation numerically, and proposed the following equation for the exponent m:

$$m = 1/3 + 2/3 \exp\ (-0.85\ Re^{0.24}) \qquad (75)$$

This equation was derived for the Prandtl number between 0.7 and 10. Equation (75) reduces to the asymptotic values of unity at very small Reynolds numbers and of 1/3, predicted by the boundary layer theory,

at high Reynolds numbers.

Woo (1970) solved the energy equation for Re between 1 and 300 and $0.25<Pr<5$. Based on Equation (74), the exponent m in the range $0.5<Pr<2$ can be derived from Woo's results as:

$$m = 0.78\ Re^{-0.145} \tag{76}$$

for $0.2<Re<100$. For $Re<0.2$, m approaches the value of unity and at high Re (>100) a value of 0.435. Both of Equations (75) and (76) will be used to correlate the present results. Using Equation (75) the Nusselt number dependence on Re and Pr was found to be:

$$Nu = 2 + 0.461\ Pr^{m}\ Re^{0.552} \tag{77}$$

and when Equation (76) was used:

$$Nu = 2 + 0.473\ Pr^{m}\ Re^{0.552} \tag{78}$$

It should be noted here that the exponent n is constant and the same in both of the above equations. The Nusselt numbers obtained from these equations are compared to the results of the numerical solution in Table IX. Very good agreement is observed for $Re>1$. Since Woo's results were more accurate, Equation (78) will be the one used.

Variable-Property Transfer

For the limiting case of the Reynolds number approaching zero, the Nusselt number for a sphere submerged in an infinite constant-

TABLE IX

COMPARISON OF THEORETICAL AND EMPIRICAL

NUSSELT NUMBERS

CONSTANT-PROPERTY FLOW

Re	Nu Numerical Solution	Nu Equation (77)	Nu Equation (78)
0.1	2.021	2.096	2.089
1	2.232	2.361	2.347
10	3.323	3.355	3.350
20	4.022	4.015	4.022
30	4.560	4.539	4.559
50	5.411	5.395	5.438

property fluid approaches a value of 2, which represents conduction heat transfer. This value, however, deviates from 2 for variable-property fluids due to the variation of the gas conductivity with radial distance away from the sphere. The energy equation at zero Re reduces to:

$$(1/r^2)\ d/dr\ (r^2 q_r) = 0 \qquad (79)$$

or

$$r^2 k\ dT/dr = 0 \qquad (80)$$

where c is constant. Substituting the relation between k and T into the above equation and integrating between the limits of the sphere surface and infinity give in dimensional variables:

$$T^{i+x} = T_\infty^{i+x} - R/r\ (T_\infty^{i+x} - T_s^{i+x}) \qquad (81)$$

or in dimensionless variables:

$$T'^{(i+x)} = 1 - 1/r'\ (1 - T_0^{i+x}) \qquad (82)$$

For $T_0 = 0.25$, $T' = 0.5$ occurs at $r' = 1.50$ for the constant-property case ($x = 0$) and at $r' = 1.29$ for variable-property flow ($x = 0.8$). These distances are very similar to those shown in Figure 16 for the isotherms $T = 0.5$ at $Re = 0.1$. The expression for the temperature gradient at the surface at zero Re can be obtained from Equation (82), thus:

$$dT'/dr' = (1 - T_0^{i+x})/[(1 + x)T_0^x] \qquad (83)$$

This equation shows that as the thermal conductivity becomes

more dependent on the temperature (x increases), the temperature gradient at the sphere surface becomes steeper.

The overall Nusselt number based on properties evaluated at the surface temperature is given by:

$$Nu_o = hD/k_s = R/(T_\infty - T_s) \int_0^\pi dT/dr\Big|_{r=R} \sin\theta \, d\theta \qquad (84)$$

In dimensionless variables:

$$Nu_o = 1/(1 - T_o) \int_0^\pi dT'/dr'\Big|_{r'=1} \sin\theta \, d\theta \qquad (85)$$

Substituting Equation (83) and integrating gives, for Re = 0:

$$Nu_f = 2(1 - T_o^{1+x})/[(1 + x)(1 - T_o)\, T_o^x] \qquad (86)$$

When using a dimensionless reference temperature, T_f instead of T_o to evaluate the thermal conductivity, the above equation becomes:

$$Nu_f = hD/k_f = 2(1 - T_o^{1+x})/[(1 + x)(1 - T_o)\, T_f^x] \qquad (87)$$

since $k_f/k_s = (T_f/T_o)^x$

As x approaches zero, i.e., constant-property, the limiting Nusselt number approaches the value of 2. Equation (87) can be re-written as:

$$Nu_f = 2\, f_f \qquad (88)$$

where $f_f = (1 - T_o^{1+x})/[(1 + x)(1 - T_o)\, T_f^x] \qquad (89)$

Equation (78) for constant-property transfer can now be modified to include the effect of variable properties, thus:

$$Nu_{fk} = 2 f_{fk} + 0.473 Pr^{m} Re_{f\nu}^{0.552} \qquad (90)$$

In this equation the Nusselt number is evaluated at reference temperature T_{fk} and the Reynolds number at $T_{f\nu}$. Reference temperatures are used to account for changing physical properties in the flow field. Since the thermal conductivity and the kinematic viscosity do not change in the flow field in exactly the same manner, nor is their effect on the heat transfer process identical, there is no justification for presuming that the reference temperatures at which Re and Nu are evaluated are the same. Obviously, the function, f, should be evaluated at the same temperature as Nu.

From the numerical results it was found that Equation (90) gave the best fit when the Nusselt number was evaluated at surface temperature and the Reynolds number at $T_{0.19}$, where

$$T_{0.19} = T_s + 0.19 (T_\infty - T_s) \qquad (91)$$

The value 0.19 was mainly dependent on the value of the exponent of the Reynolds, n, used. Therefore, this reference temperature was equally applicable to Equation (77). The exponent of the Prandtl number in both of Equations (77) and (78) was calculated using $Re_{0.19}$. It should be mentioned here that it was not possible to correlate the result accurately by using a single reference temperature.

From Figures 17 and 18 it can be seen that the temperature gradients for variable-property flow are very steep near the surface due to the increased velocity in that region. In other words, most

of the heat transfer was taking place in the vicinity of the sphere. Consequently, surface conditions have a higher influence on the transfer process than the condition in the bulk of the flow. This explains why Nu and Re were evaluated at near surface conditions in Equation (90). As a matter of fact, at Re = 50 and T_o = 0.25, the reference temperature, $T_{o,1}$, in the front half, occurred at a distance of only 0.05R away from the sphere surface.

A common method for accounting for variable-property variations is to multiply the heat transfer equation by a property ratio raised to a certain power. This method was not used in the present analysis for two reasons: (a) the equation does not reduce to the variable-property limiting Nusselt number at Re = 0 and (b) there is no theoretical justification for this property ratio.

CONCLUSIONS

1. Numerical solutions have been obtained for the coupled momentum and energy equations for variable-property flow past a sphere. The constant-property solutions were generally in excellent agreement with numerical and experimental results reported in the literature. No such comparison was possible for the variable-property case, due to the unavailability of pertinent data.

2. Convergence became more difficult as the Reynolds number or the temperature difference was increased. Very low relaxation coefficient had to be used, thus increasing computation time signi-

ficantly. This limited the present analysis to Re of 50 and dimensionless surface temperature to 0.25.

3. In general, the effect of variable properties was to drastically increase the flow velocity, vorticity and temperature and vorticity gradients near the surface. The Nusselt number and the drag coefficients were decreased as a result of lower thermal conductivity and viscosity near the surface.

4. The flow separation and the size of the vortex were not markedly affected by the change in the surface temperature. However, as the surface temperature was decreased the surface pressure was drastically changed, leading in some instances to negative values of the pressure drag coefficient.

5. A general heat transfer correlation has been derived that applies equally to constant- and variable-property flows. The variations in the fluid properties were accounted for by choosing suitable reference temperatures for the kinematic viscosity and thermal conductivity, and by introducing the variable-property limiting Nusselt number. This equation can be written as:

$$Nu_o = 2 f_o + 0.473 \, Pr^m \, Re_{o.19}^{0.552}$$

where

$$m = 0.78 \, Re_{o.19}^{+0.145}$$

$$f_o = (1 - T_o^{1+x}) \, / \, [(1 + x)(1 - T_o) \, T_o^x]$$

$$Re_{o.19} = UD/\nu_{o.19}$$

The kinematic viscosity is evaluated at $T_{0.19}$, where:

$$T_{0.19} = T_s + 0.19 (T_\infty - T_s)$$

Use of the mean film temperature resulted in errors as high as 20%. The applicability of these reference temperatures for gases having values of $\underline{x}$ other than that of 0.8 was not, however, verified.

6. The change in the drag coefficient due to positive pressure gradient over the sphere surface cannot be predicted from the constant-property situation and, therefore, the use of average temperatures to correct for varying properties can lead to highly erroneous results.

NOMENCLATURE

A	-	Lattice spacing in z-direction
A	-	Characteristic area, Equation (52)
a	-	Constant, Equation (74)
B	-	Lattice spacing in θ-direction
b	-	Constant, Equation (74)
c	-	Constant, Equation (80)
C_D	-	Total drag coefficient
C_{DF}	-	Friction drag coefficient
C_{DP}	-	Pressure drag coefficient
c_v	-	Heat capacity at constant volume
c_p	-	Heat capacity at constant pressure
D	-	Diameter of sphere
E^2	-	Differential operator
E_k	-	Characteristic kinetic energy term, Equation (52)
F	-	Arbitrary function of vorticity, defined in Equation (31)
F_k	-	Total force acting on a sphere
F_n	-	Total pressure force acting on a sphere
F_s	-	Static pressure force on a sphere
F_t	-	Skin friction force acting on a sphere
f	-	Function defined in Equation (89)

G	-	Arbitrary function of vorticity defined in Equation (32)
h	-	Lattice spacing, general
$\bar{h}$	-	Heat transfer coefficient
$h(\Theta)$	-	Local heat transfer coefficient
I	-	Subscript defining mesh point in Θ-direction
J	-	Subscript defining mesh point in z-direction
L	-	vortex length, dimensional
M	-	Total number of divisions in grid, z-direction
m	-	Exponent of Prandtl number, Equation (74)
N	-	Total number of divisions in grid, Θ-direction
n	-	Exponent of Reynolds number, Equation (74)
Nu	-	Overall Nusselt number, $\bar{h}D/k$
P	-	Coefficient defined in Equation (40)
p	-	Pressure, dimensional
p_o	-	Front stagnation pressure, dimensionless
$p(\pi)$	-	Rear stagnation pressure, dimensionless
$p(\Theta)$	-	Surface pressure, dimensionless
Pe	-	Peclet number, Pr.Re
Pr	-	Prandtl number, $c_p\mu/k$
Q	-	Coefficient defined in Equation (40)
q	-	Heat flux
R	-	Radius of sphere
r	-	Radial distance
r_∞	-	Distance from sphere surface to outer boundary, dimensionless
Re	-	Reynolds number, UD/ν
Res	-	Residue from iteration step

T - Temperature

$T_{o.i.}$ - Reference temperature defined in Equation (91), dimensional

U - Free-stream velocity

$\bar{v}$ - Velocity vector

v - Velocity vector component

W - Relaxation coefficient

x - Transport property exponent

z - Dimensionless radial distance

Greek Letters

α - Dampening factor

Γ - Function defined in Equation (19)

Δ - Difference

ζ - Vorticity, ϕ-component

θ - Angle measured from front stagnation point

θ_s - Separation angle, measured from rear stagnation point

μ - Viscosity

ν - Kinematic viscosity

ρ - Density

Σ - Function defined in Equation (18).

τ_{rr}

$\tau_{r\theta}$

$\tau_{\theta\theta}$ - Components of stress tensor, defined in Equations (4) to (7)

$\tau_{\phi\phi}$

Φ - Arbitrary function

ϕ - Angle, in spherical coordinates

Ψ - Stream function

Ω - Components of vorticity vector

Subscripts

f - Evaluated at reference temperature

r - In r-direction

s - Evaluated at surface conditions, dimensional variables only

θ - In θ-direction

ϕ - In ϕ-direction

∞ - Evaluated at free-stream conditions

o - Evaluated at surface condition, dimensionless variables only

Superscript

' - Dimensionless variable

REFERENCES

Amdur, I. and Mason, A.E., "Properties of Gases at Very High Temperatures", Phys. Fluids 1, 370 (1958)

Beard, K.V. and Pruppacher, H.R., "A Determination of the Terminal Velocity and Drag of Small Water Drops by Means of a Wind Tunnel", J. Atmos. Sci. 26, 1066 (1969)

Beard, K.V. and Pruppacher, H.R., "A Wind Tunnel Investigation of the Rate of Evaporation of Small Water Drops Falling at Terminal Velocity in Air", J. Atmos. Sci. 28, 1455 (1971)

Bird, R.B., Stewart, W.E. and Lightfoot, E.N., Transport Phenomena, J. Wiley and Sons, Inc., New York (1960)

Cheng, S.I., "Numerical Integration of Navier-Stokes Equations", AIAA Journal 8 (2), 2115 (1970)

Dennis, S.C.R. and Walker, J.D.A., "Calculation of the Steady Flow Past a Sphere at Low and Moderate Reynolds Numbers", J. Fluid Mech. 48 (4), 771 (1971)

Dennis, S.C.R., Walker, J.D.A. and Hudson, J.D., "Heat Transfer from a Sphere at Low Reynolds Numbers", J. Fluid Mech. 60 (2), 273 (1973)

Drellishak, K.S., Knopp, C.F. and Cambel, A.B., "Partition Functions and Thermodynamic Properties of Argon Plasma", Arnold Engineering Development Centre, Report No. AEDC, TDR63-146 (1963)

Hamielec, A.E., Hoffman, T.W. and Ross, L.L., "Numerical Solution of the Navier-Stokes Equation for Flow Past Spheres", AIChE Journal 13 (2), 212 (1967)

Hoffman, T.W. and Ross, L.L., "A Theoretical Investigation of the Effect of Mass Transfer on Heat Transfer to an Evaporating Droplet", Int. J. Heat Mass Transfer 15, 559 (1972)

Jenson, V.G., "Viscous Flow Round a Sphere at Low Reynolds Numbers (<40)", Proc. Roy. Soc. (London) 249A, 346 (1959)

Lapidus, L., Digital Computation for Chemical Engineers, McGraw Hill (1962)

LeClair, B.P., Hamielec, A.E. and Pruppacher, H.R., "A Numerical Study of the Drag on a Sphere at Low and Intermediate Reynolds Numbers", J. Atmos. Sci. 27 (2), 308 (1970)

Ranz, W.E. and Marshall, W.R., "Evaporation from Drops - I and II", Chem. Eng. Prog. 48, 141 and 173 (1952)

Rimon, Y. and Cheng, S.I., "Numerical Solution of a Uniform Flow over a Sphere at Intermediate Reynolds Numbers", Phys. Fluids 12 (5), 949 (1969)

Roache, P.J., Computational Fluid Dynamics, Hermosa Publ., Albaquerque, N. Mexico (1972)

Roos, F.W. and Willmarth, W.W., "Some Experimental Results on Sphere and Disk Drag", AIAA Journal 9 (2), 285 (1971)

Taneda, S., "Experimental Investigation of the Wake Behind a Sphere at Low Reynolds Numbers", J. Phys. Soc. Japan 11, 1104 (1956)

Whitaker, S., "Forced Convection Heat Transfer Correlations for Flow in Pipes, Past Flat Plates, Single Cylinders, Single Spheres, and for Flow in Packed Beds and Tube Bundles", AIChE Journal 18 (21), 361 (1972)

Woo, S.E., "Simultaneous Free and Forced Convection around Submerged Cylinders and Spheres", Ph.D. Thesis, McMaster University, Hamilton (1970)

Woo, S.E. and Hamielec, A.E., "A Numerical Method of Determining the Rate of Evaporation of Small Water Drops Falling at Terminal Velocity in Air", J. Atmos. Sci. 28 (8) 1448 (1971)

Yuan, S.W., Foundations of Fluid Mechanics, Prentice Hall, New Jersey (1967)

EXPERIMENTAL MEASUREMENTS OF HEAT TRANSFER

TO A STATIONARY SPHERE IN A PLASMA JET

INTRODUCTION

In most solid-gas plasma processes the rate-controlling step appears to be the rate of heat transfer to the individual particles. An accurate knowledge of the heat transfer rate is, therefore, necessary for the reliable design of such devices. As was pointed out in the Literature Review chapter, most of the studies on heat transfer to spheres were carried out at relatively low temperatures (less than 1 000 K) where variations in the fluid properties were small and could be accounted for by choosing a reference mean film temperature. The applicability of the mean film temperature concept to large temperature difference has not yet been verified. Some workers on heat transfer to cylinders have introduced a temperature or property ratio correction factor to account for these variations in the physical properties. The form of the correction employed, however, had no sound theoretical basis and was chosen arbitrarily to merely correlate the experimental results.

The aim of the work presented in this chapter was to experimentally determine the rates of heat transfer to single stationary spheres under conditions where large variations in the physical properties existed between the sphere surface and the bulk of the fluid. The results of these experiments were then compared

with the predictions of the heat transfer equation derived in the numerical analysis presented in the previous chapter.

EXPERIMENTAL APPARATUS

The apparatus used in this study consisted of a plasma torch, a test chamber and a sphere support assembly (see Figure 1). The confinement of the plasma jet in a test chamber was necessary to avoid contamination of the plasma gas with entrained air from the surroundings. The presence of air inside the chamber would have led to rapid oxidation and tarnishing of the metal specimen and also would have caused changes in the physical properties of the fluid surrounding the sphere.

The Plasma Torch

The plasma was generated in a radio-frequency induction torch operating at 4.5 MHZ. The induction torch was preferred to a d.c. jet generator because of the lower velocities and larger volume plasma produced in the former. The plasma torch, manufactured by TAFA (Concord, N.H.), consisted of a copper heating coil wound three turns around a 40 mm-diameter quartz tube. Cold argon gas entered the torch from the top, through a gas distributor. The gas distributor allowed the introduction of the gas in three different directions: axial, radial and tangential directions. The tangential swirl stream served the purpose of stabilizing the flow and preventing the hot plasma fire-ball, formed near the axis, from reaching the inner walls of the quartz tube. The induction coil was kept cool by

FIGURE 1

SCHEMATIC DIAGRAM OF EXPERIMENTAL APPARATUS

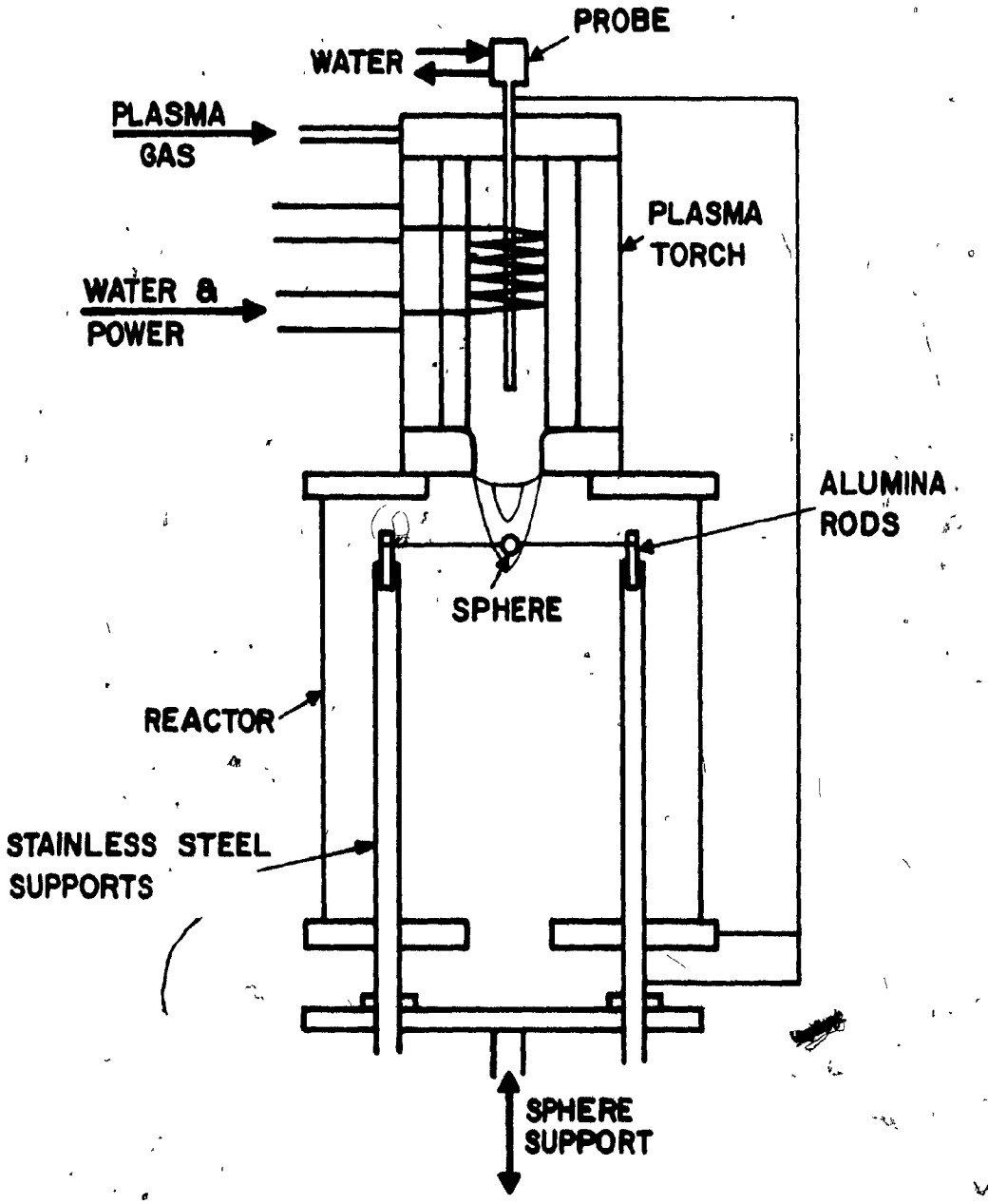
PROBE
WATER
PLASMA
GAS
PLASMA
TORCH
WATER &
POWER
ALUMINA
RODS
SPHERE
REACTOR
STAINLESS STEEL
SUPPORTS
SPHERE
SUPPORT

the flow of water in the annulus between the quartz tube and the outer Teflon jacket. The circulating water helped also in cooling the quartz tube, the gas distributor and the nozzle. The plasma gas, heated up and ionized in the coil section, left the torch as a low velocity jet through a constricting nozzle, 25 mm in diameter.

The operating variables of the plasma torch were the power input and the gas flow rate. Power input to the high-voltage power supply was of the order of 6 KVA. Only 30-40% of this power input did actually go in the plasma gas. The rest, lost in the transformer, oscillator and induction coil in the form of heat, was carried away by the cooling circuit in the power supply. Separate rotameters were used to monitor the three modes of gas flow in the torch. During operation, only the radial and tangential flows were kept open, while the axial stream was used in place of the radial stream during start-ups. The ratio of the radial to tangential gas flow rates was adjusted, at each power level, to give a stable, laminar and non-flickering tail-flame.

The Test Chamber

The test chamber was attached directly to the bottom of the plasma torch, and served the purpose of confining the issuing plasma jet. The chamber consisted of a Pyrex glass tube, 150 mm in diameter and 250 mm long. It was equipped at both ends with brass flanges, 20 mm thick. The orifice of the inlet flange was 77 mm in diameter, and that of the outlet flange 25 mm (the same as the torch nozzle

diameter). The diameter of the inlet orifice was made as wide as possible in order to reduce the interference of the flange with the jet to a minimum. The bottom outlet flange had two small openings, located diametrically opposite to each other and 125 mm apart, to accommodate the sphere support legs which passed through them.

The Sphere Assembly

The sphere assembly consisted of the metal sphere, two vertical support rods and a moving platform. Three different sphere sizes were used, 2.2, 3.3 and 5.6 mm in diameter, respectively. The spheres were accurately machined from high-purity molybdenum rods. Molybdenum was selected for several reasons: (a) high melting point (2 833 K); (b) ease of machining; (c) known emissivity (as a pure metal); and most importantly (d) the high volatility of its oxide.

Although great care was taken to avoid the contamination of argon with air during the operation of the torch, air still managed to diffuse inside the chamber once the torch was switched off. The presence of oxygen in the chamber while the sphere was still hot, naturally, led to oxidation and tarnishing of its surface. Purging with cold argon after shut-down reduced the degree of oxidation by forming a blanket of inert atmosphere around the sphere. It was not possible, however, to eliminate oxidation completely. Since maintaining a very clear surface was essential for the reproducibility of the measurements and for accurate estimation of the radiation losses, it was, therefore, necessary to use a metal that was able

to lose its oxide layer when heated up to high temperatures. The slight oxidation of the sphere at the end of one run and the subsequent evaporation of the oxide in a following run gave the sphere a highly polished surface and freed it of any roughness or scratches caused during machining. It was noticed that the spheres' temperature had to be raised to above 2 000 K before the surface was thoroughly clean.

The spheres were supported horizontally by means of a thin tungsten wire passing through the axis of the sphere. The diameter of the wire was 0.25 mm for the medium and large spheres and 0.125 mm for the small sphere. The size and the shape of the hole in the sphere depended on the method of temperature measurement. When the temperature was measured optically, the hole was simply a cylindrical bore 0.35 mm in diameter (0.22 mm for the small sphere). On the other hand, when thermocouples were used, the method of attachment was more complicated, as the sphere itself constituted the thermocouple junction. This will be discussed in more detail later on.

The sphere support wire was held in place by two vertical stainless steel tubes, 3 mm in diameter and over 100 mm apart. The wide spacing of the support tubes and their small size were necessary to reduce interference with the flow. The bottom ends of the tubes fitted snugly in holes drilled in a thin Plexiglass plate. This whole assembly was fixed on an adjustable manual jack. Plexiglass was used to isolate the metal supports, electrically, from the jack.

The sphere and support were introduced in the chamber through the bottom flange. Their level in the chamber was adjusted by raising or lowering the jack. Four hair-lines, painted 90° apart on the outside of the glass chamber, were used to align the spheres exactly on the jet axis.

MEASUREMENT TECHNIQUES

The three variables needed for calculating the heat transfer rates to the sphere were the gas temperature, gas velocity and the sphere temperature. A review of the experimental methods applicable to plasma conditions was presented in the first chapter. The actual measurement techniques used in this study are described below.

Gas Temperature Measurements

Thermocouples were first used to measure the gas temperature. Calorimetric probes were too bulky and elaborate and presented no real advantage over thermocouples. Spectroscopy was inaccurate at the temperature levels expected (below 5 000 K). Measurements were made by raising and lowering the thermocouple leads in the chamber while making sure that the thermocouple junction remained at the axis of the jet. This method, however, turned out to be highly susceptible to arcing, because of the large size of the thermocouple circuit. Arcing was found to take place between the plasma gas and any conducting object that was placed inside the chamber and that was large enough to act as a ground. As a result of this problem, the use of thermocouples had to be abandoned.

An alternative method was used for the gas temperature measurement. This method was based on the same principle as the one behind the thermocouple technique, namely, to estimate the gas temperature by measuring the temperature of a small object suspended in the flow. A thin tungsten wire, 0.25 mm in diameter, was held horizontally and perpendicular to the jet axis by the same method of support as that of the sphere. The temperature of the wire at its centre (at the jet axis) was determined with a high-resolution optical pyrometer. Heat losses from the wire by conduction and radiation cause a temperature difference between the wire and the gas. The magnitude of this difference depends largely on the wire diameter and emissivity, and increases with increasing wire diameter. Correction for these losses introduces an element of uncertainty in the determination of the gas temperature and it was therefore desirable to use a wire of as small a diameter as possible in order to reduce the relative effect of such possible errors. One problem was however encountered when a smaller wire (0.125 mm in diameter) was used, and that was the difficulty of focusing on the wire. To facilitate a good comparison between the pyrometer filament and the smaller wire, a lens of higher magnification (and narrower depth of field) was required. This reduction in the depth of field made focusing very difficult and sensitive to slight movement of the instrument. The inaccuracies caused by ill-focusing more than overshadowed the benefit gained by the use of the 0.125 mm wire and therefore measurements were limited to the 0.25 mm wire.

Since tungsten ages with the period it is kept hot (around 2 000 K), the surface characteristics and especially the emissivity of a new wire are not the same as that of a used one. For this reason the first few runs with a new wire always indicated higher temperatures on the wire. These runs were discarded since the emissivity values reported in the literature were obtained mostly with aged tungsten specimens. Wires had to be replaced regularly to avoid reduction in their diameter caused by slight oxidation losses at the end of the runs. Tungsten, like molybdenum, forms volatile oxides that leave the surface when the wire is brought up to the test temperatures.

Gas Velocity Measurements

The axial velocity of the jet was measured by means of total pressure and static pressure probes. The probes were not cooled so as to keep their size (and interference with the flow) down to a minimum. The probes, therefore, had to be made out of a high melting point material. The probes consisted of two parts, a 65 mm long molybdenum tip and a 400 mm long stainless steel stem. The lower portion of the tip fitted tightly inside the stainless steel tube. Molybdenum tubes were not available at the time. The probes were round-nosed, 3.2 mm in diameter with a 1.6 mm inside bore. This was the smallest practical size, as smaller probes tended to melt because of lower radiation and conduction losses from the tip. The taps on the static pressure probe consisted of four holes, 0.5 mm in diameter, bored 90° apart and normal to the wall of the probe. These taps were

located 26 mm down from the closed nose. The temperature of the nose was measured with an optical pyrometer. Total and static pressures were measured in separate runs by means of a capacitance-type differential pressure transducer. The transducer was able to indicate pressure differences as low as 10^{-3} mm Hg. One tap of the transducer was kept open to the atmosphere. The probes were introduced from the bottom of the chamber and were aligned vertically along the axis of the jet. The lower end of the probe was attached to a Plexiglass platform. The platform was moved up and down by means of the manual jack. A flexible plastic tubing connected the lower ends of the probes to the pressure transducer.

Sphere Temperature Measurement

The temperature of solid, in the range between 1 500 and 3 000 K, can be measured by two methods: thermocouples or optical pyrometry. Thermocouples cannot be used in the hot regions of a plasma generated by high voltage, because of arcing.

In optical pyrometry, the brightness temperature of an object, at a certain wavelength, is compared to that of a reference tungsten filament. The current passing through the tungsten filament gives a direct measure of the power input to the filament and, therefore, of its temperature. Special narrow-band filters are used to allow the comparison of the temperatures to be made at a single wavelength only. Auxiliary filters can also be used to attenuate the radiation coming from the object. These filters extend the

upper limit of the pyrometer without excessively over-heating the tungsten filament. To obtain an accurate comparison of brightness between the filament and the object surface, the object size must be several (approximately five) times larger than the filament diameter. To facilitate this, a high-resolution pyrometer (Pyro Micro-Optical Pyrometer, The Pyrometer Instrument Co. Inc., Northvale, N.J.) was used. The pyrometer was supplied with six interchangeable objective lenses that permitted measurements to be made at distances varying from 120 mm to infinity with object sizes as small as 0.1 mm.

The spheres' temperatures were measured by focusing the pyrometer filament on the equator portion of the spheres. It was noticed that the sphere temperature went through cyclic variation, mainly caused by cyclic changes in the flow conditions. The period of these fluctuations was of the order of 10 seconds. Larger objects tended to dampen this effect, which was very pronounced in the wire temperature measurements. In order to obtain an average value of the temperature, the filament current was so adjusted that the filament was darker and brighter than the sphere for equal lengths of time.

Thermocouple Arrangement

Bare thermocouples were used to measure the gas temperature. The thermocouple leads were held horizontally by two separate supports. The two wires formed a cross and the point of intersection was the thermocouple junction. This method of forming the junction was preferred over conventional arc welding for several reasons. The

only thermocouple materials that are able to withstand the high temperature of the plasma are tungsten and tungsten-rhenium alloys. These thermocouples are very brittle and readily-oxidizable at high temperatures. Consequently, it was very difficult to form a bead junction with a standard arc welded and if formed, the junction was very weak and did not last very long. Another important drawback of such a junction was the difficulty in characterizing the bead. The exact shape and size of the junction bead was not reproducible and was hard to measure. Furthermore, the emissivity was dependent on the degree of tarnishing of the surface inherent in the welding process. As a result of these uncertainties, it would have been difficult to calculate the radiation losses or to estimate the convective and conductive heat transfer rates to the junction.

In the thermocouple assembly, one end of each lead was attached to one leg of the support, via an electrically insulating mullite rod; the other end was passed through thin mullite tubes placed inside the stem of the stainless steel support. The mullite tubes were used to insulate the leads electrically from the supports. The thermocouple leads were connected to a battery-operated millivolt chart recorder. A high-frequency cut-off filter was placed in the circuit to prevent the radio-frequency noise, produced in the heating coil, from reaching the recorder.

To measure the temperature of the sphere, the two thermocouple leads were passed through the mullite insulating tubes inside of the support legs. The leads were then attached directly to the

sphere. In other words, the sphere itself formed the junction and was held in place by the thermocouple leads. A diagram of the cross-section of the sphere is shown in Figure 2. The wires passed through small grooves in the screw. Part of the screw was not threaded in order to lock the screw in place, flush with the sphere surface. Great care was taken to ensure that the two leads did not touch each other directly. The wires' temperature being higher than that of the sphere, this direct contact would have caused the thermocouple to indicate values that did not truly represent the actual temperature of the sphere. The screw arrangement gave a much better contact between the wires and the sphere, than by merely placing the junction inside a hole in the sphere.

Arcing

The high voltage used to generate the plasma causes the gas inside the torch to reach a fairly high electric potential, of the order of several kilovolts. This potential decays rapidly as the gas moves away from the torch exit. When this gas comes in contact with a grounded object, or with an object large enough to act as a ground, discharge between the gas and the object takes place. The higher the temperature of the gas, the easier it is to form a conductive path between the object and the high potential regions of the gas - in the plasma core. Arcing causes over-heating at the points of discharge, leading in some instances to etching of the surface. This is highly undesirable in a heat transfer study as heat is transferred to the object by an additional mechanism that

FIGURE 2

CROSS-SECTION OF THERMOCOUPLE SPHERE

DETAIL OF THERMOCOUPLE SPHERE

POLISHED MOLYBDENUM SPHERE

3-6 mm dia.

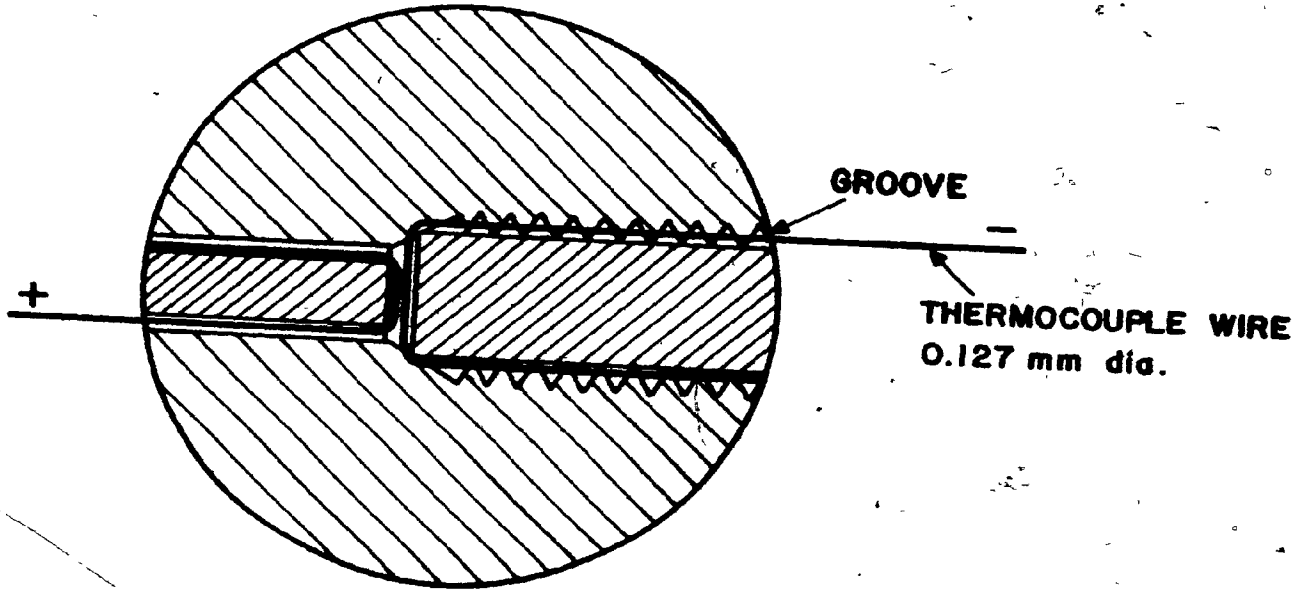

cannot be accounted for quantitavely. Also, the damage caused to the surface alters its radiative properties. Furthermore, if the solid constitutes a part of an electric circuit, for example when using a thermocouple, arcing causes electric interference and noise many times larger than the actual signal carried.

It should be noted, at this point, that the problem of arcing was not restricted to the thermocouple measurements only, but was also encountered when the temperatures were measured by optical pyrometry. This meant that even with the absence of the recorder, the system was still large enough to induce arcing.

One way of preventing arcing was to maintain the object at a potential level comparable to that of the gas. To bring up the sphere assembly to the plasma potential, a water-cooled probe, 6.3 mm in diameter, was introduced inside the plasma core, along the axis of the heating coil, as shown in Figure 3. Copper wire connected this probe, electrically, to all of the metallic objects that were to be brought in contact with the plasma gas. When thermocouples were used, grounding of the assembly was avoided by using a battery-operated chart recorder. The whole system was then floated at the probe potential by connecting the recorder chassis to the water-cooled probe. The support and the negative lead of the thermocouple were also connected to the probe.

The thermocouple measurements were successfully employed in the lower sections of the test chamber, as arcing was eliminated

FIGURE 3

DETAILS OF THERMOCOUPLE CIRCUIT

THERMOCOUPLE CIRCUIT

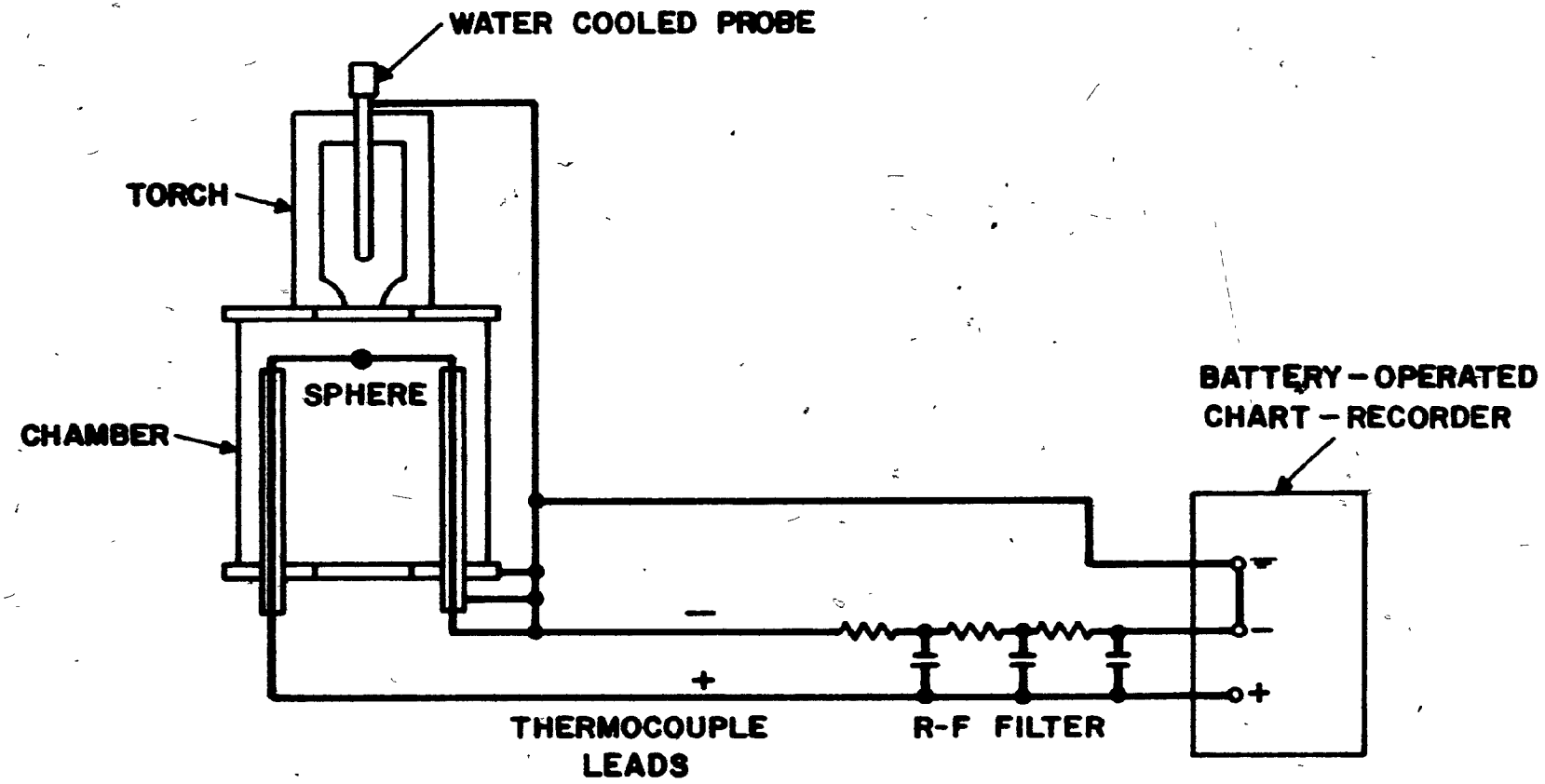

completely by the above-described method. However, it seemed that the potential attained by the probe was not exactly that of the gas. This difference in potentials manifested itself by sustained arcing in the upper sections of the chamber. An attempt was made to bring the thermocouple assembly to the gas potential by connecting it to the nozzle or the ground lead of the induction coil. These attemps, however, were even less successful in reducing arcing.

When the optical pyrometer was used, the probe method worked only when the object was several centimeters away from the nozzle. With closer objects, arcing persisted. The reason for this was the large size of the assembly. To overcome this problem, the sphere was isolated from the support by means of short mullite rods fixed to the top ends of the stainless steel tubes. The sphere and its support wire were, hence, allowed to float electrically in the plasma gas. As a result of the reduced object size, arcing did not take place. However, the sphere support and the bottom flange still had to be connected to the probe to avoid arcing.

Although only the sphere assembly was discussed above, the problems and the solutions were equally applicable to the case of the wire temperature measurements.

EXPERIMENTAL PROCEDURE

Four different conditions of plasma power and gas flow rates were studied. When selecting the plasma conditions, careful consideration was given to the stability and the laminar behaviour of

the jet. The presence of the confining chamber tended to cause a cyclic eccentric rotation of the jet. This instability was eliminated by adjusting the ratio of the swirl to radial components of the gas stream to the torch. The operating variables of the four plasma conditions are listed in Table I.

For each of the above conditions, the total and static pressures, wire temperature and the three spheres' temperatures were measured at points along the axis of the jet. Each of these measurements were repeated several times to ensure reproducibility. For temperature measurements, the sphere (or wire) was raised to the highest position in the chamber and then the temperatures were determined at discrete positions with the specimen moving downwards. This was done in order to remove the oxide layer at the highest temperature possible. Moreover, with the specimen moving downwards only, slight tarnishing of the surface that might have taken place at lower positions did not affect higher points' measurements. Before the end of each run, the specimens were raised to the highest position in the chamber and were purged with cold argon after shut-down to reduce the extent of oxidation. The reproducibility of different runs, under identical conditions, was very sensitive to the metal surface conditions.

EXPERIMENTAL RESULTS

Sphere and Wire Temperatures

Pyrometer ammeter readings are pre-calibrated with an NBS

TABLE I

PLASMA OPERATING CONDITIONS

CONDITION	PLATE CURRENT AMP	PLATE VOLTAGE KV	GAS FLOW, SWIRL, G/S	GAS FLOW, RADIAL, G/S
I	1.50	3.25	0.289	0.578
II	1.55	3.35	0.325	0.723
III	1.65	3.45	0.325	0.506
IV	1.70	3.55	0.289	0.434

standard light source to indicate the temperature of a black body that has the same brightness as the tungsten filament, when a specific d.c. current is passed through the latter. Calibration is carried out at a single wavelength, usually 0.65 micron. Radiation from real bodies and, consequently, their brightness temperature are both lower than those from a black body. When the temperature of a real body is measured with an optical pyrometer, the value indicated by the ammeter is, therefore, less than the actual surface temperature of the object.

The spectral radiance from a black body can be described by Planck Distribution Law [Branstetter (1966)]:

$$N_{\lambda,b} = 2 \pi c^2 h \lambda^{-5} / (e^{ch/\lambda KT} - 1) \qquad (1)$$

or simplified to:

$$N_{\lambda,b} = C_1 \lambda^{-5} / (e^{C_2/\lambda T} - 1) \qquad (2)$$

At short wavelengths and/or low temperatures, the Wien approximation can be used, thus,

$$N_{\lambda,b} = C_1 \lambda^{-5} e^{-C_2/\lambda T} \qquad (3)$$

At the wavelength of the pyrometer filter (0.65 micron) and surface temperatures of less than 3 500 K, the error incurred by this approximation is less than 1 K, for a constant radiance flux. The spectral emissivity of a real body is defined as:

$$\varepsilon_\lambda = N_\lambda / N_{\lambda,b} \qquad (4)$$

and, therefore, the spectral radiance from a real body can be written as:

$$N_\lambda = \varepsilon_\lambda C_1 \lambda^{-5} / (e^{C_2/\lambda T} - 1) \qquad (5)$$

and approximately:

$$N_\lambda = \varepsilon_\lambda C_1 \lambda^{-5} e^{-C_2/\lambda T} \qquad (6)$$

An optical pyrometer compares spectral radiance from a real surface to that from the filament and, hence, the temperature indicated by the meter is that of a black body having the same radiance as the object. In terms of Planck's equation:

$$N'_{\lambda,b} = C_1 \lambda^{-5} e^{-C_2/\lambda T_b} \qquad (7)$$

In this equation the value of $N'_{\lambda,b}$ is equal to the value of N_λ given by Equation (6). The substitution of Equation (6) into (7) gives:

$$1/T - 1/T_b = \lambda/C_2 \ \ell n \varepsilon_\lambda \qquad (8)$$

The value of C_2 is 14.38 mm K. Equation (8) can be used to correct for pyrometer readings. A knowledge of the variation of the spectral emissivity of the surface is necessary for the pyrometer correction.

The two metals used in this study, namely, molybdenum and tungsten, were of high purity and their surfaces were maintained clean and polished throughout the experiments. This meant that it was possible to use emissivity values reported in the literature

without introducing significant uncertainties in final corrected temperature. The spectral emissivity values for tungsten were taken from Kovalev (1970), Latyev (1969) and Sadykov (1965); for molybdenum, Makarenko's (1970) results were used. Correction plots were made, with the use of the spectral emissivity data, to transform Equation (8) into a direct relation between T and T_b. Figures 4 to 19 show the variation of the true wire and spheres' temperatures with axial position in the chamber, for the four plasma conditions investigated. It can be seen from these figures that the reproducibility of the plasma conditions was excellent, since the points shown in each of these figures represent data obtained from at least three separate runs.

Pressure Tube Analysis

The results of the static and total pressure measurements, for the four plasma conditions, are shown in Figures 20 to 23. To transform these measurements into actual gas velocities, a relation between the stagnation pressure and the free-stream velocity and physical properties is required.

For isothermal, high Reynolds number flows, the pitot tube equation, as derived from Bernoulli's equation, is:

$$U = \sqrt{2\,(P_t - P_\infty)\,/\,\rho} \qquad (9)$$

This equation is obtained by assuming potential flow, where the effect of viscosity is neglected. At low Reynolds numbers and/or non-iso-

FIGURE 4

VARIATION OF 0.25 mm WIRE TEMPERATURE

WITH DISTANCE FROM NOZZLE EXIT

(CONDITION I)

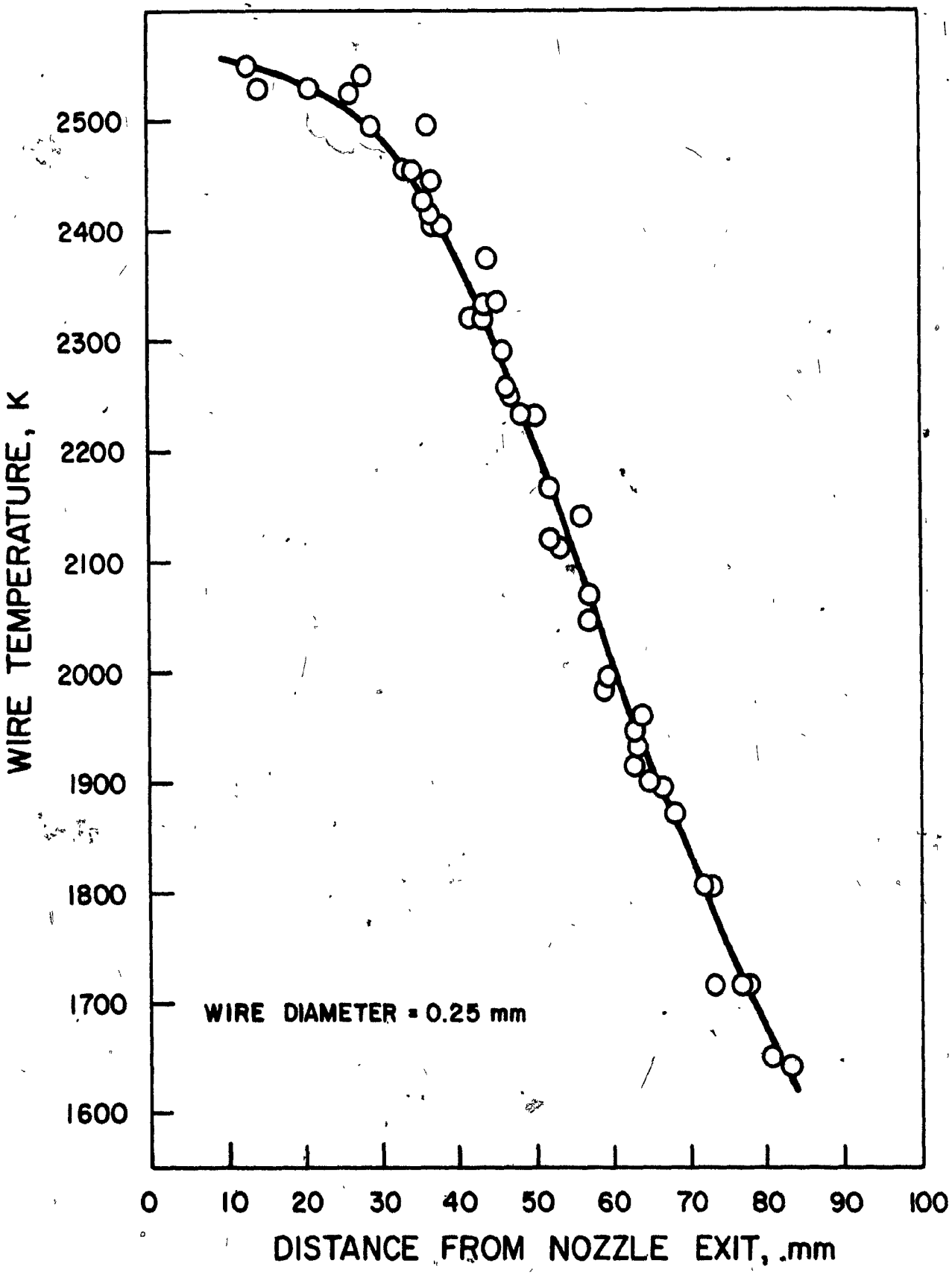
WIRE TEMPERATURE, K
2500
2400
2300
2200
2100
2000
1900
1800
1700
1600
WIRE DIAMETER = 0.25 mm
0
10
20
30
40
50
60
70
80
90
100
DISTANCE FROM NOZZLE EXIT, .mm

FIGURE 5

VARIATION OF 2.2 mm SPHERE TEMPERATURE

WITH DISTANCE FROM NOZZLE EXIT

(CONDITION I)

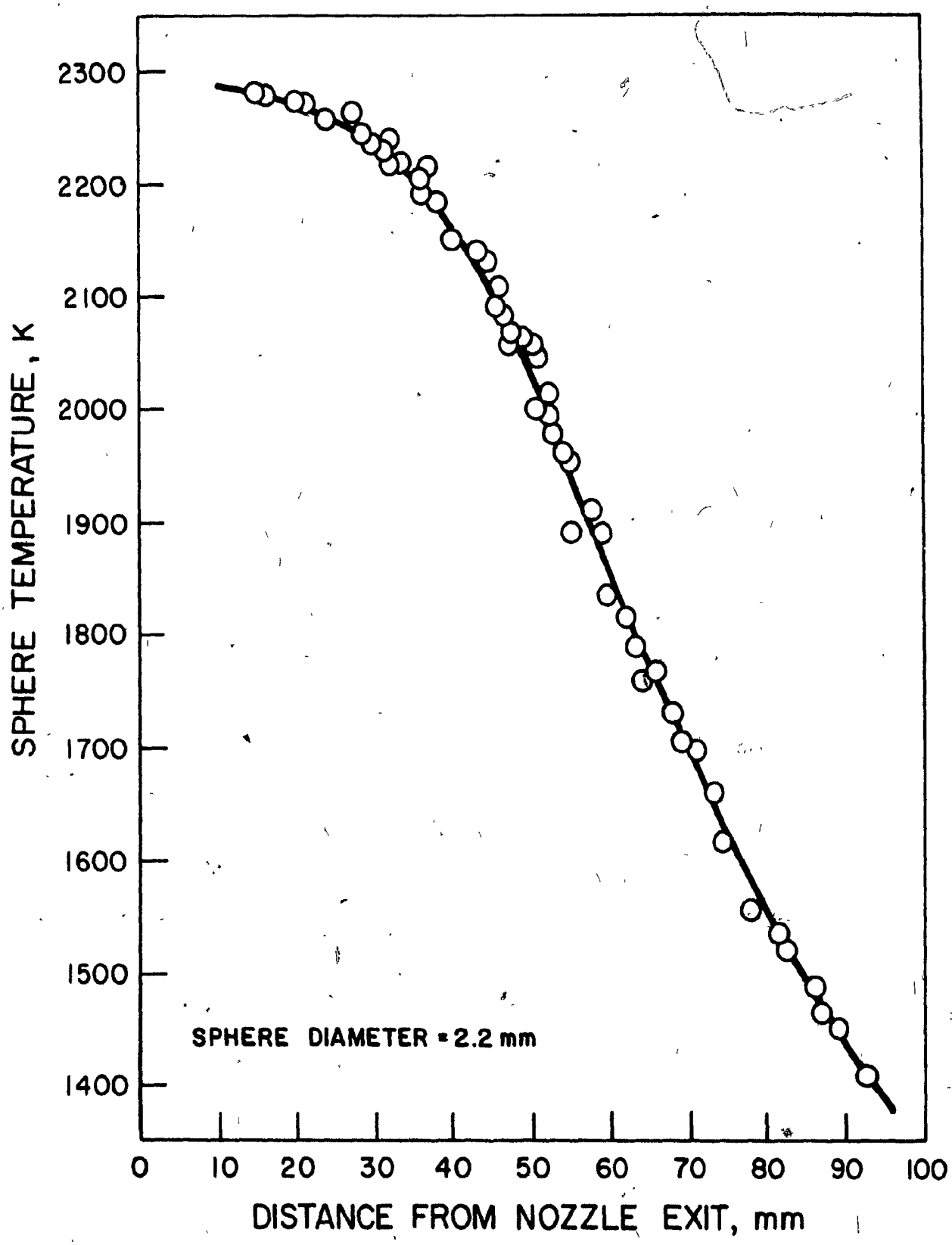
SPHERE TEMPERATURE, K
2300
2200
2100
2000
1900
1800
1700
1600
1500
1400
SPHERE DIAMETER = 2.2 mm
0
10
20
30
40
50
60
70
80
90
100
DISTANCE FROM NOZZLE EXIT, mm

FIGURE 6

VARIATION OF 3.3 mm SPHERE TEMPERATURE

WITH DISTANCE FROM NOZZLE EXIT

(CONDITION I)

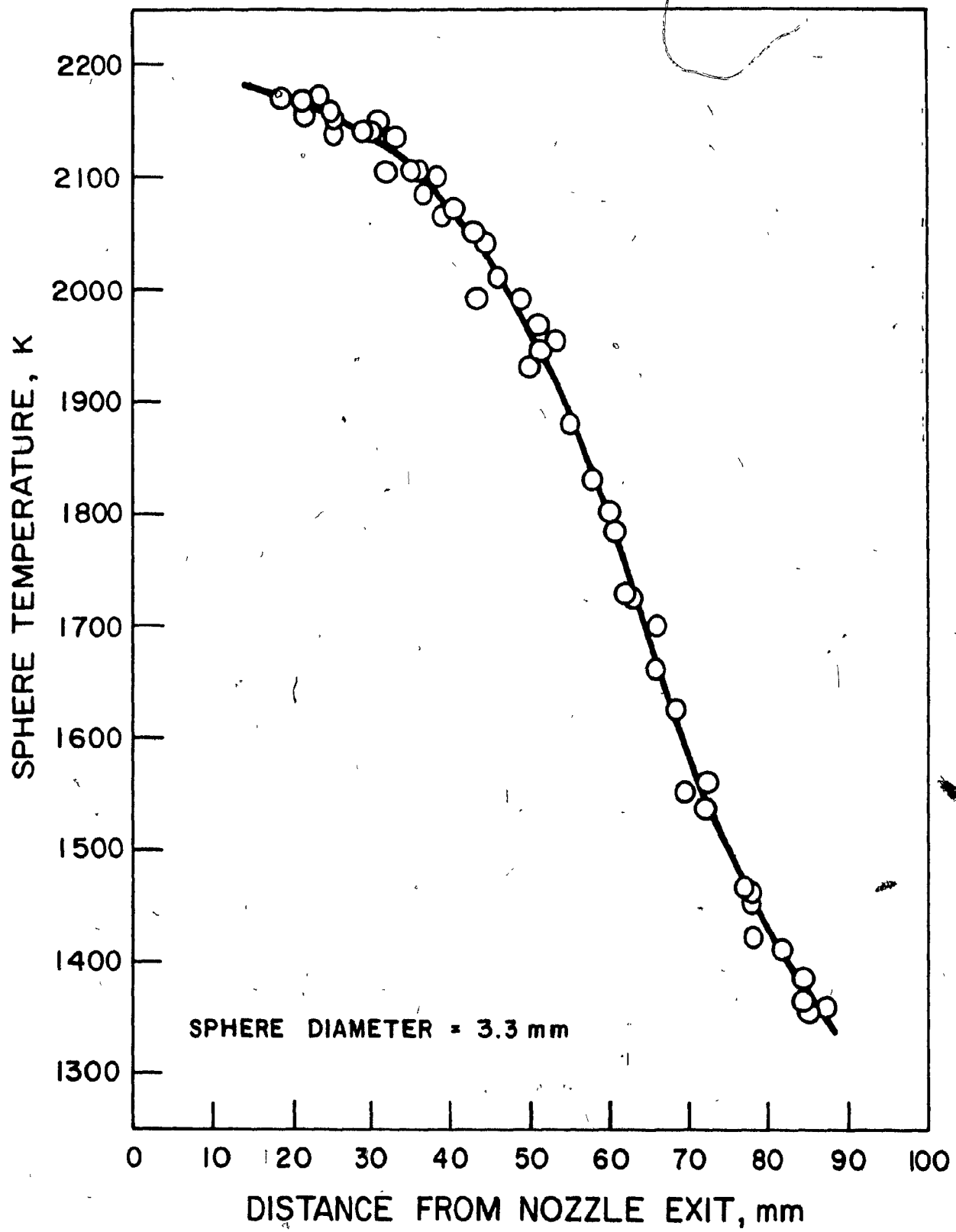
SPHERE TEMPERATURE, K
2200
2100
2000
1900
1800
1700
1600
1500
1400
1300
SPHERE DIAMETER = 3.3 mm
0
10
20
30
40
50
60
70
80
90
100
DISTANCE FROM NOZZLE EXIT, mm

FIGURE 7

VARIATION OF 5.6 mm SPHERE TEMPERATURE

WITH DISTANCE FROM NOZZLE EXIT

(CONDITION I)

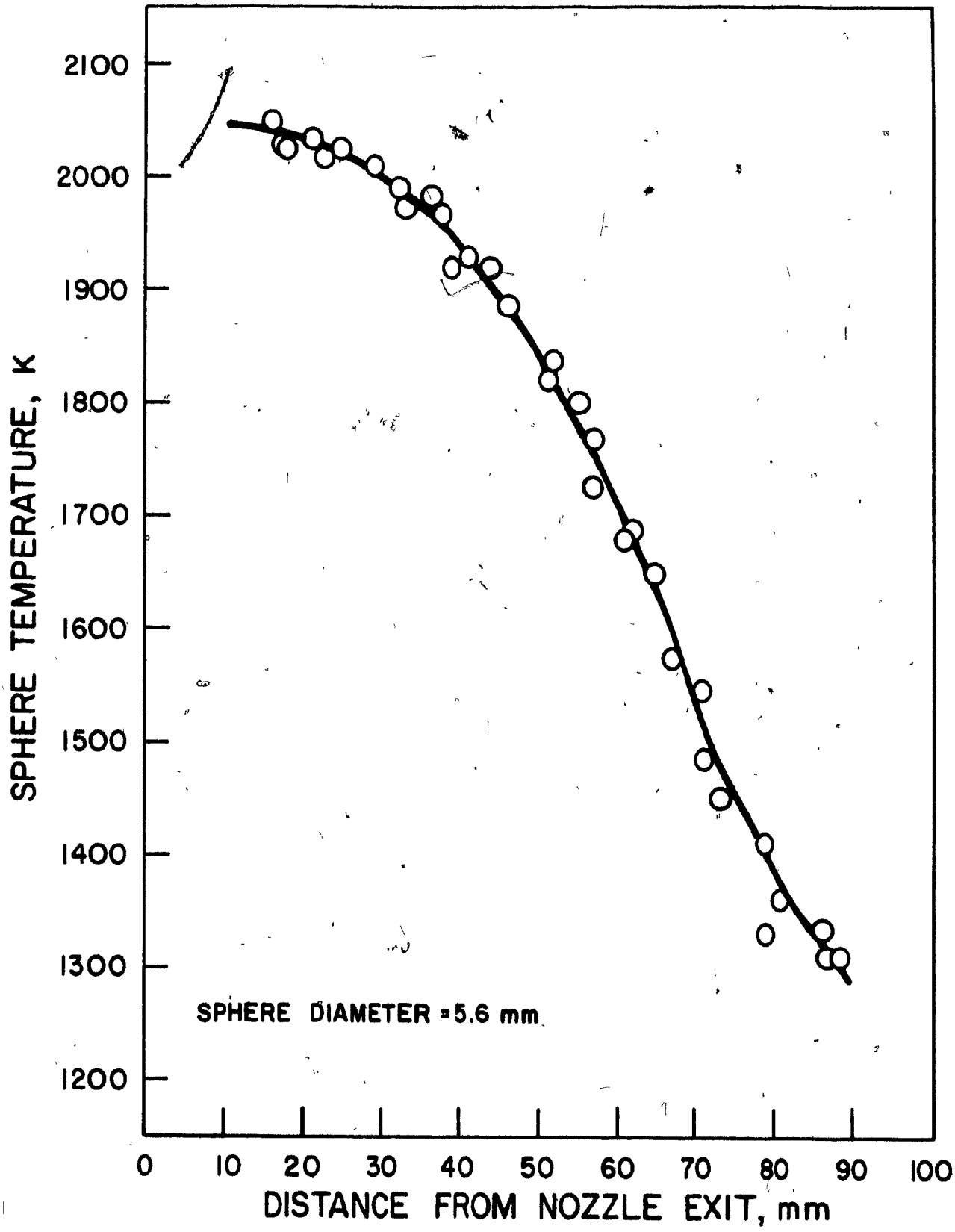
SPHERE TEMPERATURE, K
2100
2000
1900
1800
1700
1600
1500
1400
1300
1200
SPHERE DIAMETER = 5.6 mm
0
10
20
30
40
50
60
70
80
90
100
DISTANCE FROM NOZZLE EXIT, mm

FIGURE 8

VARIATION OF 0.25 mm WIRE TEMPERATURE

WITH DISTANCE FROM NOZZLE EXIT

(CONDITION II)

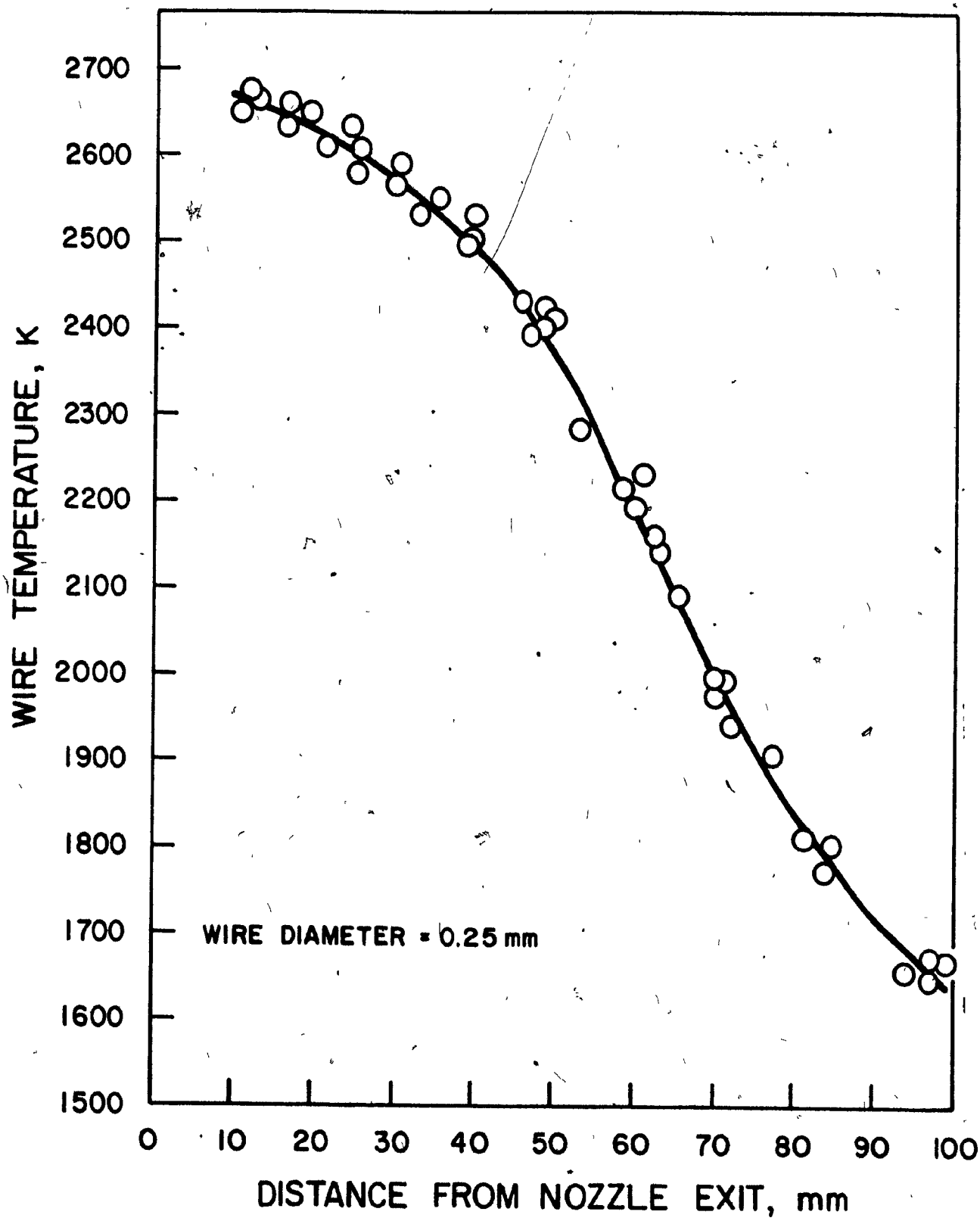
WIRE TEMPERATURE, K
2700
2600
2500
2400
2300
2200
2100
2000
1900
1800
1700
1600
1500
WIRE DIAMETER = 0.25 mm
0
10
20
30
40
50
60
70
80
90
100
DISTANCE FROM NOZZLE EXIT, mm

FIGURE 9

VARIATION OF 2.2 mm SPHERE TEMPERATURE

WITH DISTANCE FROM NOZZLE EXIT

(CONDITION II)

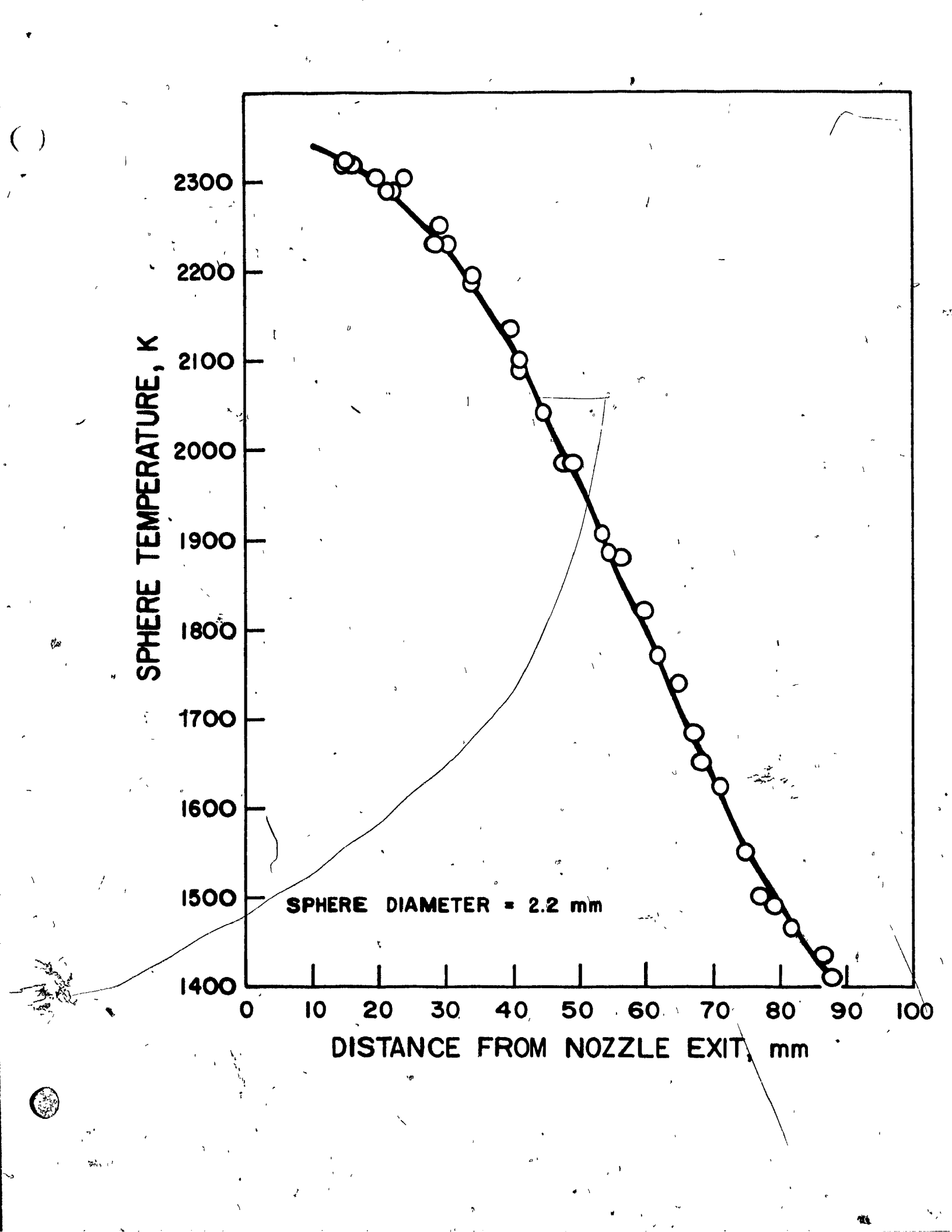
SPHERE TEMPERATURE, K
2300
2200
2100
2000
1900
1800
1700
1600
1500
1400
SPHERE DIAMETER = 2.2 mm
0
10
20
30
40
50
60
70
80
90
100
DISTANCE FROM NOZZLE EXIT, mm

FIGURE 10

VARIATION OF 3.3 mm SPHERE TEMPERATURE

WITH DISTANCE FROM NOZZLE EXIT

(CONDITION II)

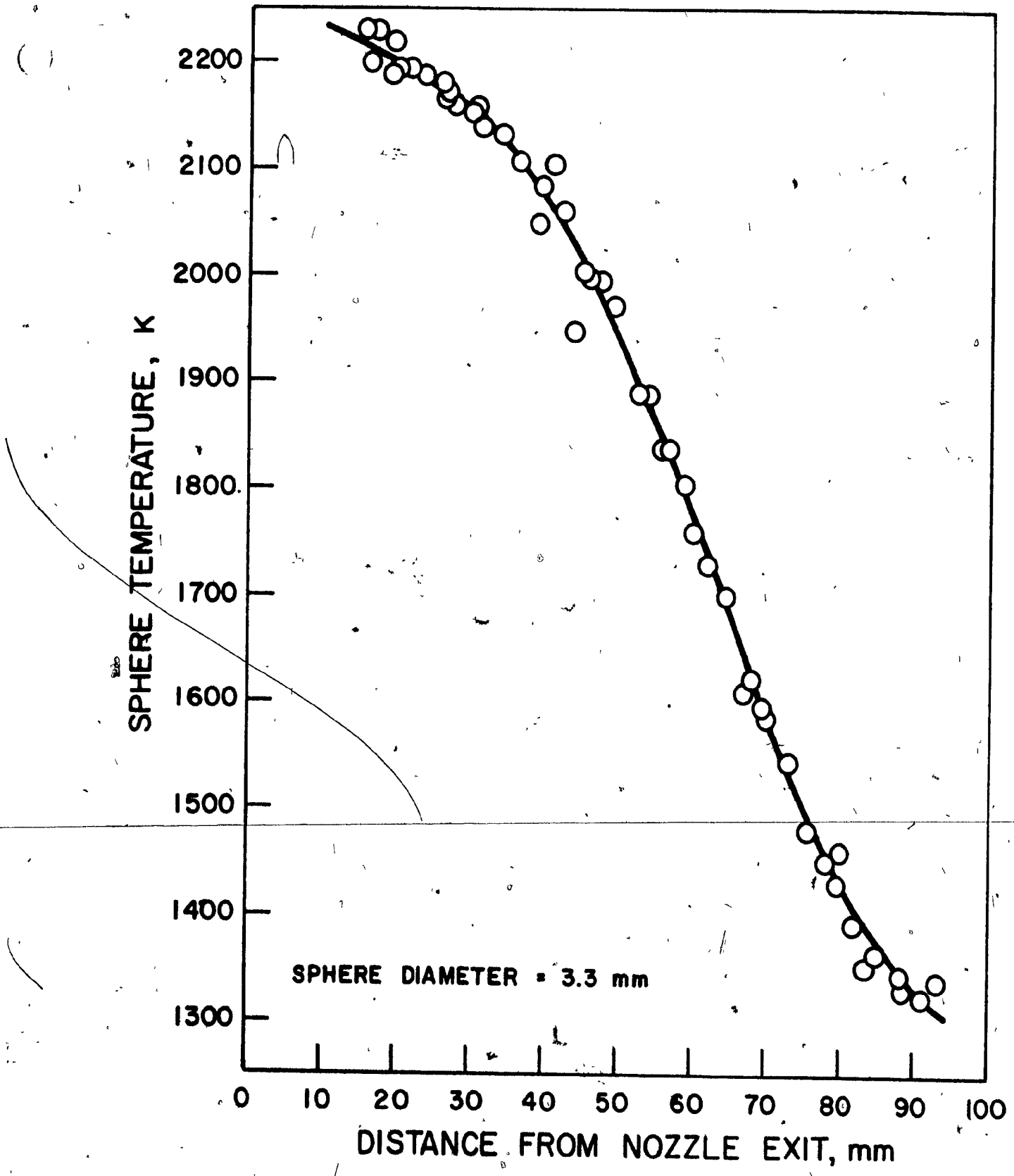
SPHERE TEMPERATURE, K
2200
2100
2000
1900
1800
1700
1600
1500
1400
1300
SPHERE DIAMETER = 3.3 mm
0
10
20
30
40
50
60
70
80
90
100
DISTANCE FROM NOZZLE EXIT, mm

FIGURE 11

VARIATION OF 5.6 mm SPHERE TEMPERATURE

WITH DISTANCE FROM NOZZLE EXIT

(CONDITION II)

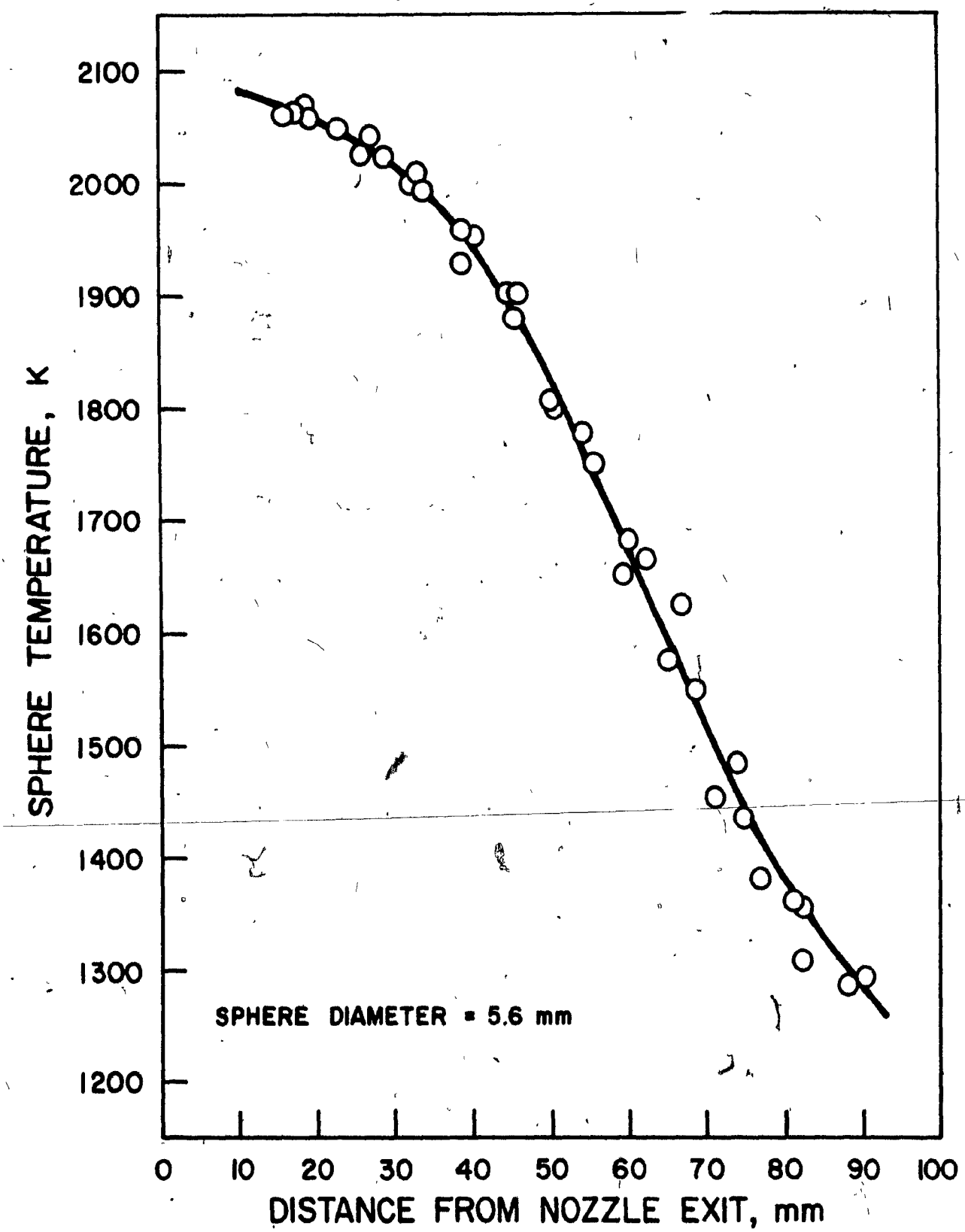
SPHERE TEMPERATURE, K
2100
2000
1900
1800
1700
1600
1500
1400
1300
1200
SPHERE DIAMETER = 5.6 mm
0
10
20
30
40
50
60
70
80
90
100
DISTANCE FROM NOZZLE EXIT, mm

FIGURE 12

VARIATION OF 0.25 mm WIRE TEMPERATURE

WITH DISTANCE FROM NOZZLE EXIT

(CONDITION III)

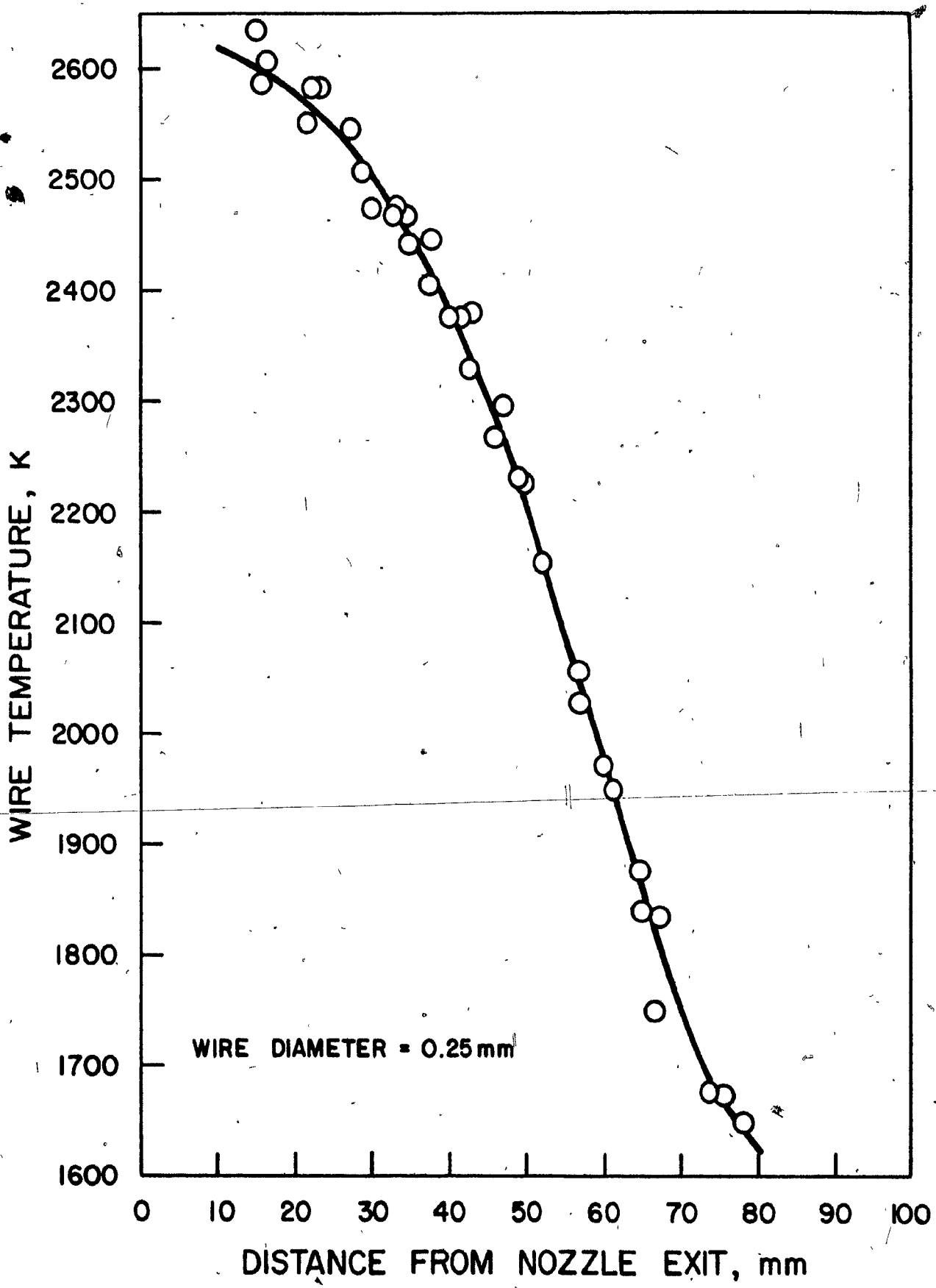
WIRE TEMPERATURE, K
2600
2500
2400
2300
2200
2100
2000
1900
1800
1700
1600
WIRE DIAMETER = 0.25 mm
0
10
20
30
40
50
60
70
80
90
100
DISTANCE FROM NOZZLE EXIT, mm

FIGURE 13

VARIATION OF 2.2 mm SPHERE TEMPERATURE

WITH DISTANCE FROM NOZZLE EXIT

(CONDITION III)

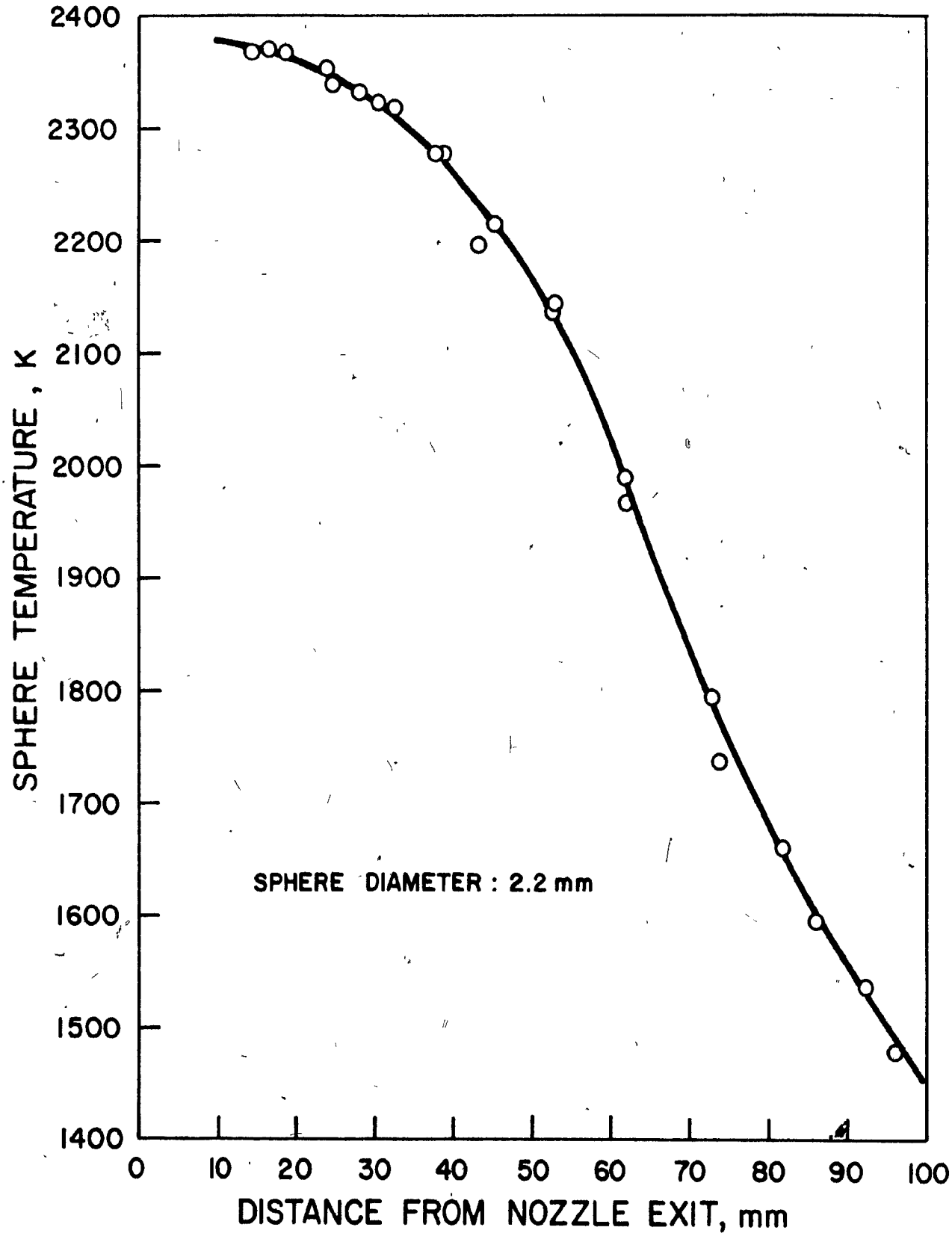
SPHERE TEMPERATURE , K
2400
2300
2200
2100
2000
1900
1800
1700
1600
1500
1400
SPHERE DIAMETER : 2.2 mm
0
10
20
30
40
50
60
70
80
90
100
DISTANCE FROM NOZZLE EXIT, mm

FIGURE 14

VARIATION OF 3.3 mm SPHERE TEMPERATURE

WITH DISTANCE FROM NOZZLE EXIT

(CONDITION III)

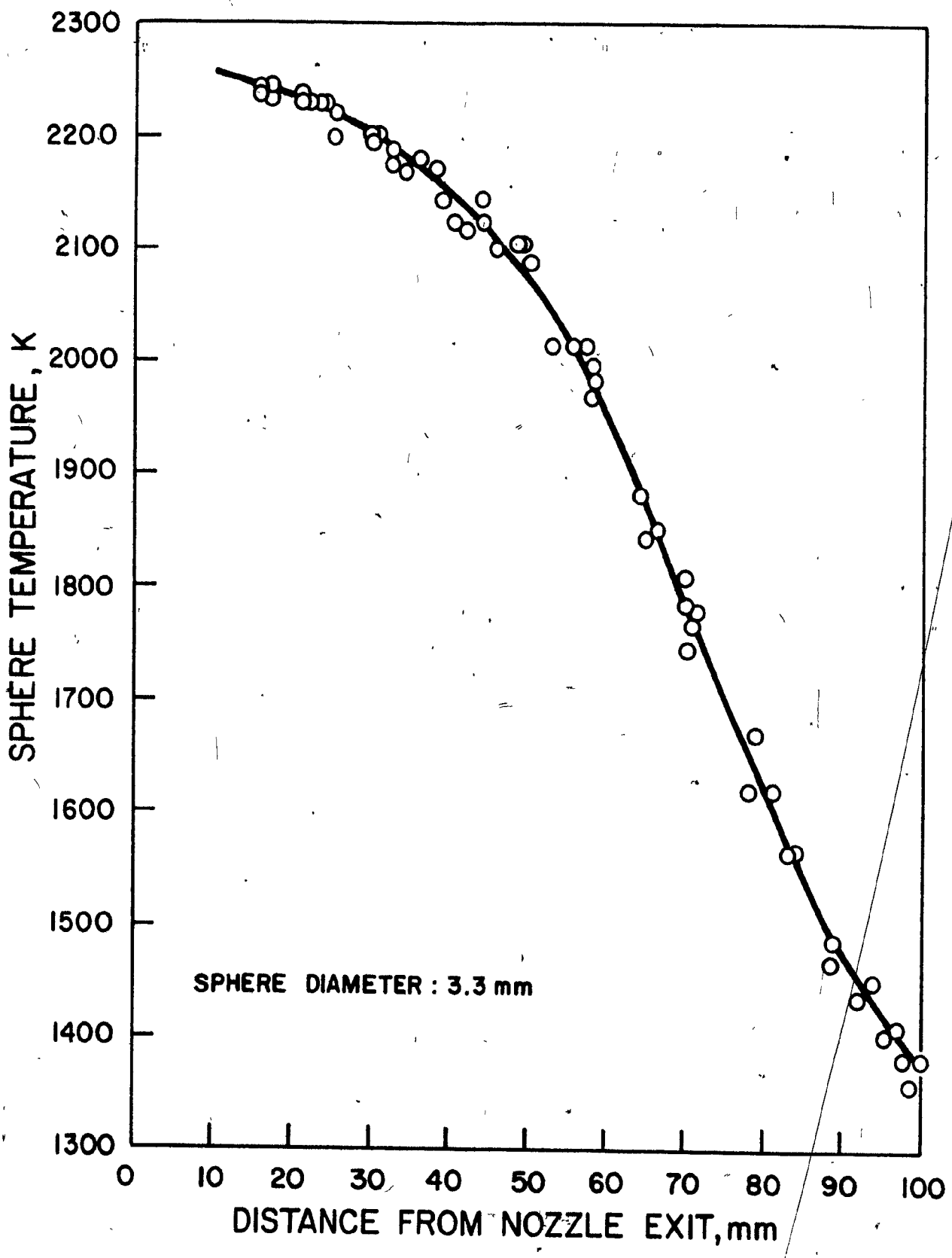
2300
2200
2100
2000
1900
1800
1700
1600
1500
1400
1300
SPHERE TEMPERATURE, K
SPHERE DIAMETER : 3.3 mm
0
10
20
30
40
50
60
70
80
90
100
DISTANCE FROM NOZZLE EXIT, mm

FIGURE 15

VARIATION OF 5.6 mm SPHERE TEMPERATURE

WITH DISTANCE FROM NOZZLE EXIT

(CONDITION III)

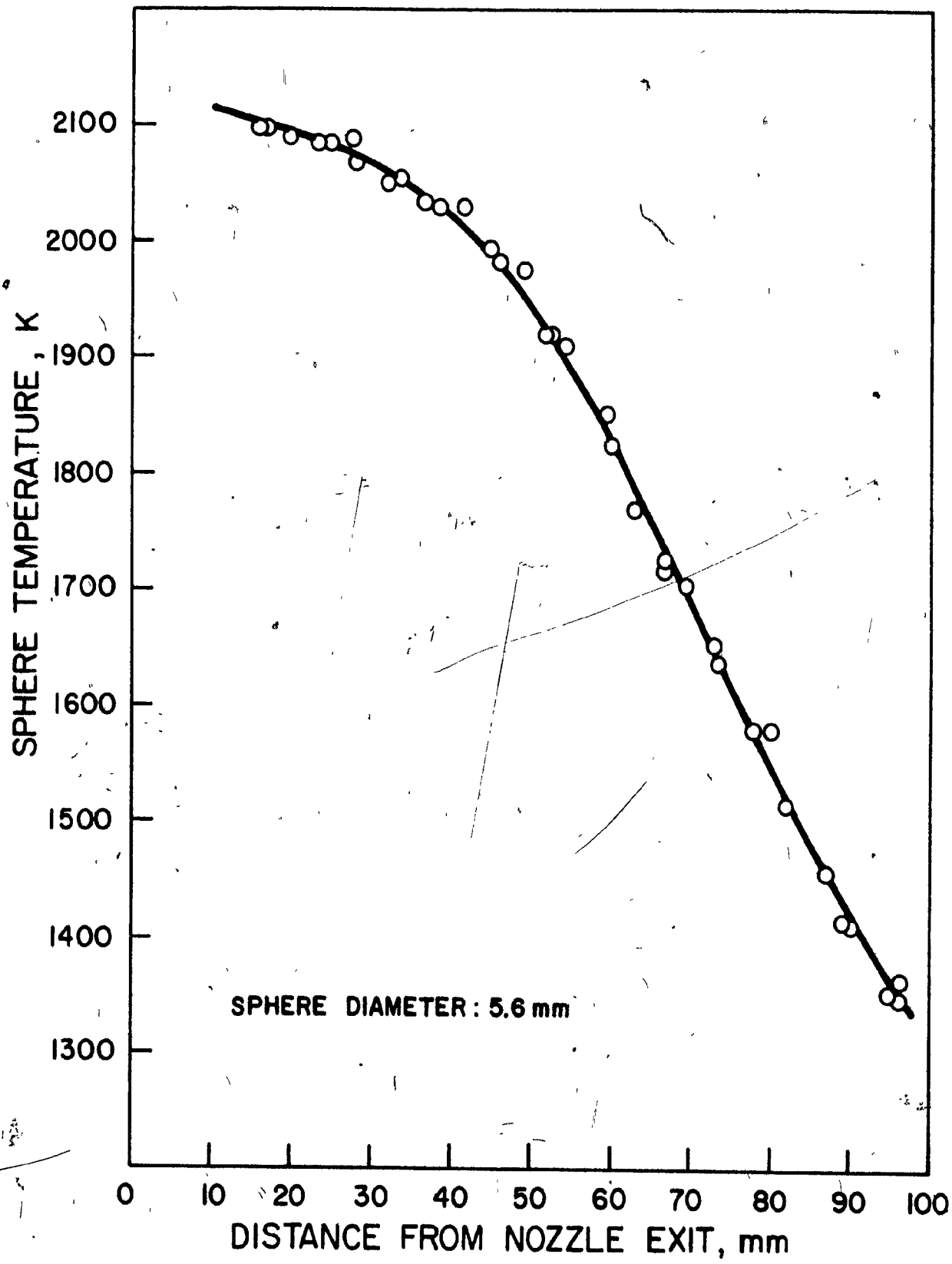
SPHERE TEMPERATURE, K
2100
2000
1900
1800
1700
1600
1500
1400
1300
SPHERE DIAMETER : 5.6 mm
0
10
20
30
40
50
60
70
80
90
100
DISTANCE FROM NOZZLE EXIT, mm

FIGURE 16

VARIATION OF 0.25 mm WIRE TEMPERATURE

WITH DISTANCE FROM NOZZLE EXIT

(CONDITION IV)

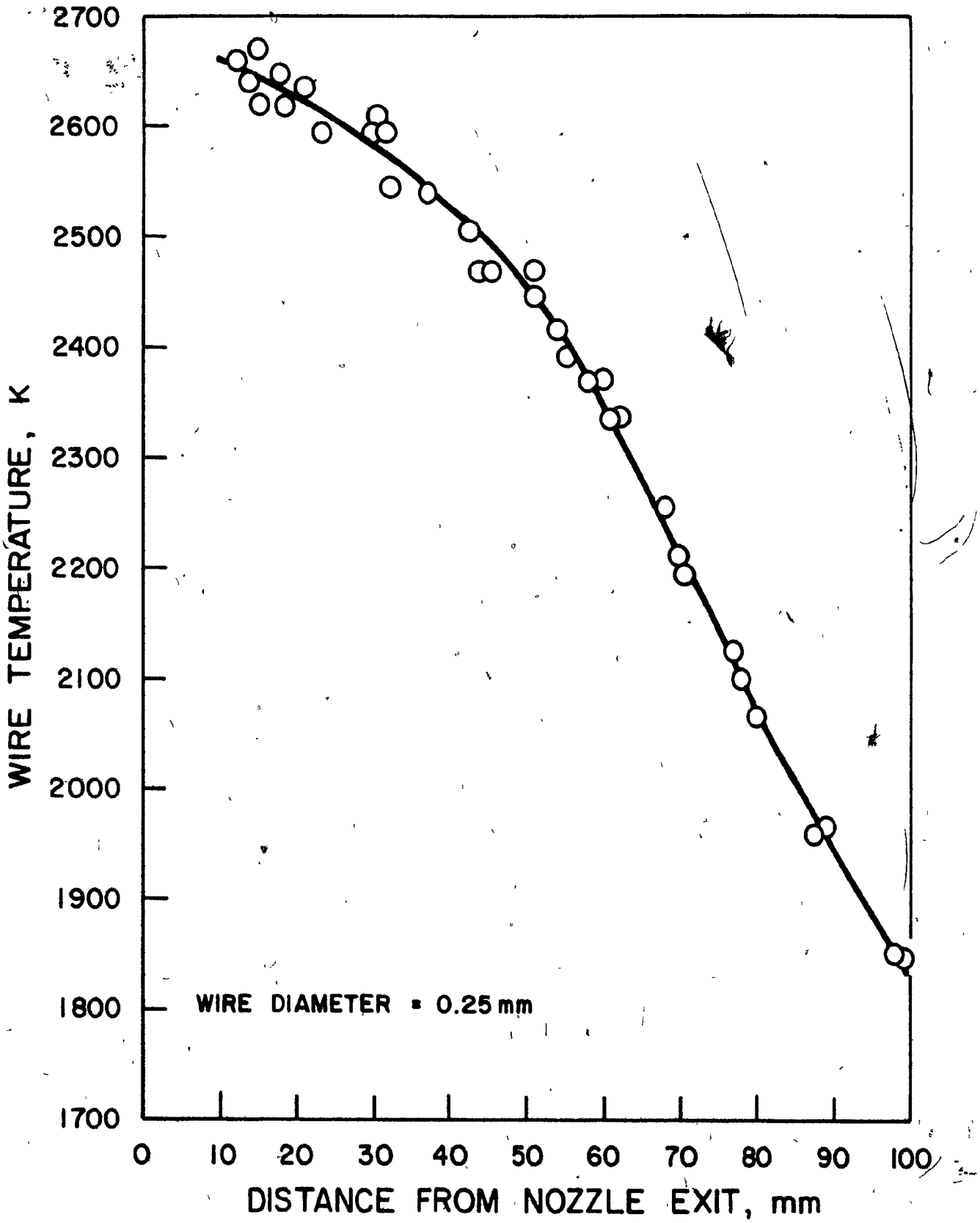
2700
2600
2500
2400
2300
2200
2100
2000
1900
1800
1700
WIRE TEMPERATURE, K
WIRE DIAMETER = 0.25 mm
0
10
20
30
40
50
60
70
80
90
100
DISTANCE FROM NOZZLE EXIT, mm

FIGURE 17

VARIATION OF 2.2 mm SPHERE TEMPERATURE

WITH DISTANCE FROM NOZZLE EXIT

(CONDITION IV)

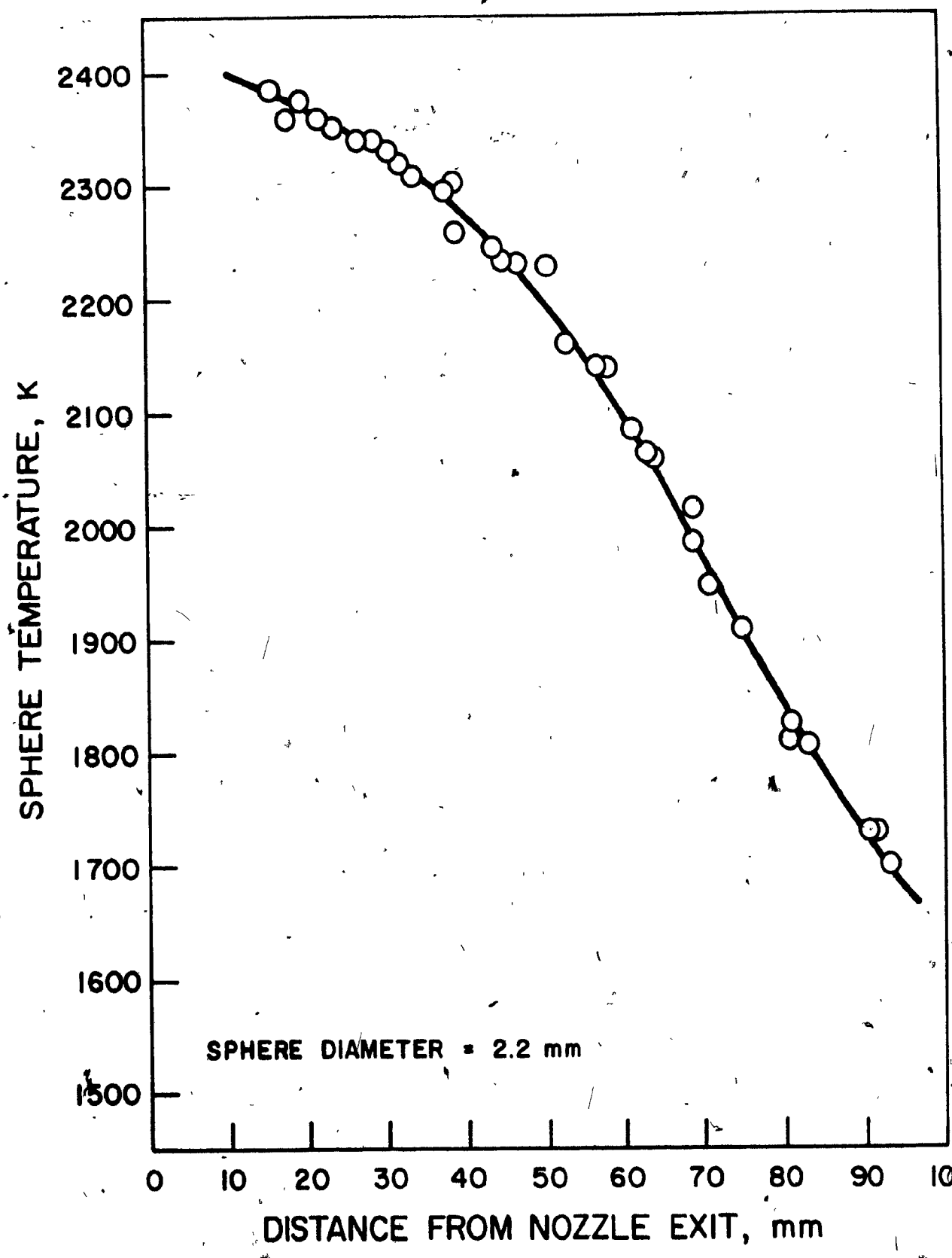
SPHERE TEMPERATURE, K
2400
2300
2200
2100
2000
1900
1800
1700
1600
1500
SPHERE DIAMETER = 2.2 mm
0
10
20
30
40
50
60
70
80
90
100
DISTANCE FROM NOZZLE EXIT, mm

FIGURE 18

VARIATION OF 3.3 mm SPHERE TEMPERATURE

WITH DISTANCE FROM NOZZLE EXIT

(CONDITION IV)

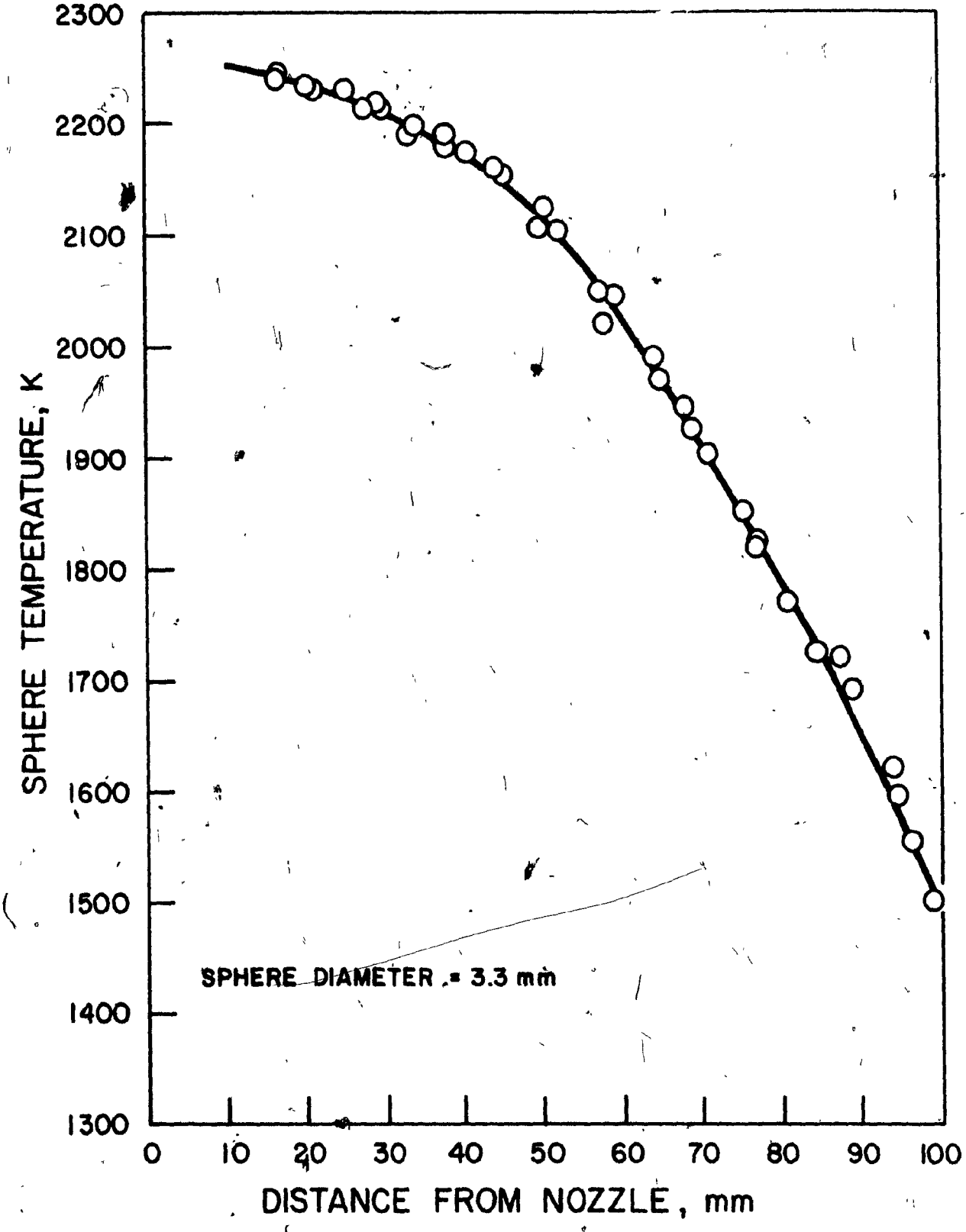
2300
2200
2100
2000
1900
1800
1700
1600
1500
1400
1300
SPHERE TEMPERATURE, K
SPHERE DIAMETER = 3.3 mm
0
10
20
30
40
50
60
70
80
90
100
DISTANCE FROM NOZZLE, mm

FIGURE 19

VARIATION OF 5.6 mm SPHERE TEMPERATURE

WITH DISTANCE FROM NOZZLE EXIT

(CONDITION IV)

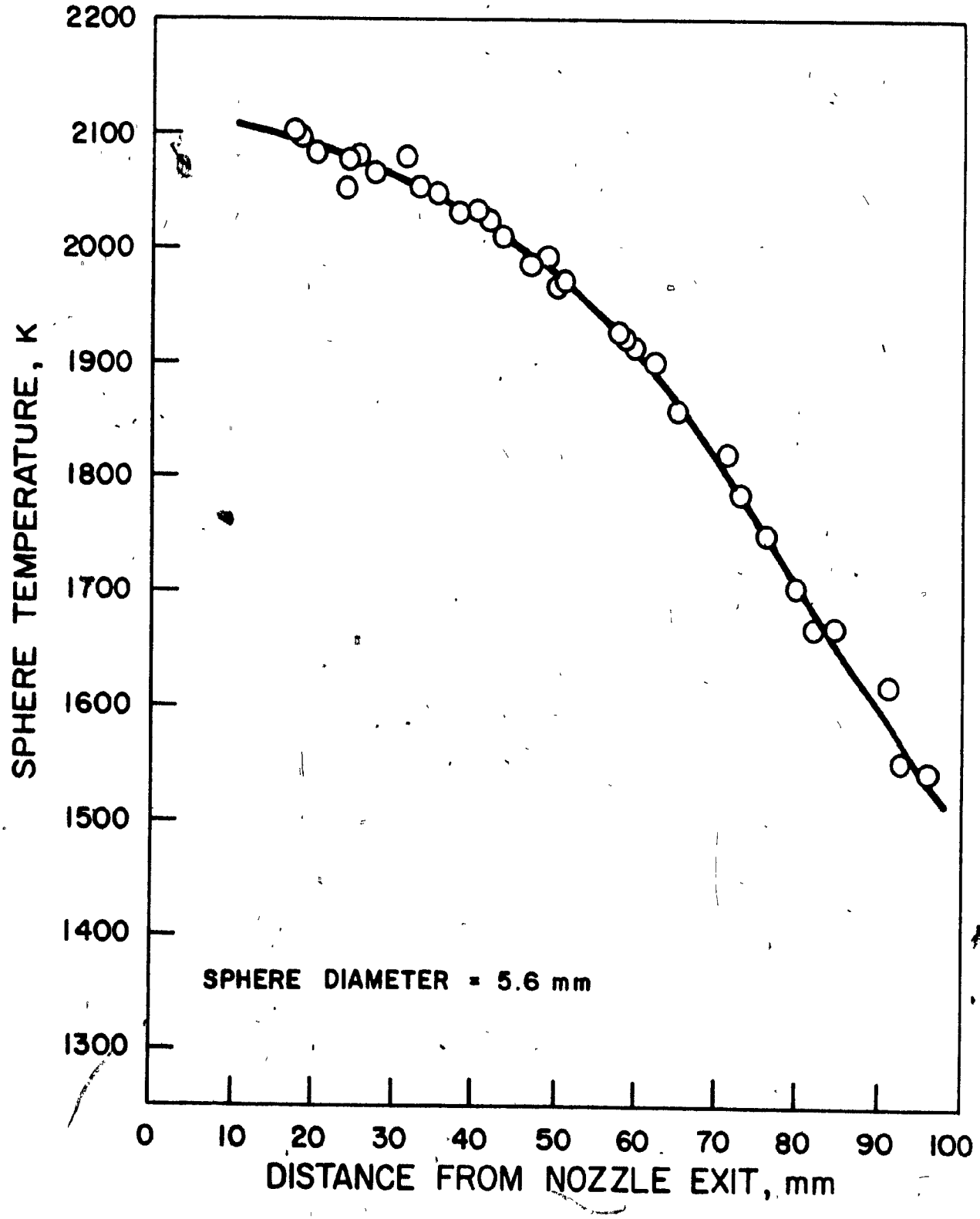
2200
2100
2000
1900
1800
1700
1600
1500
1400
1300
SPHERE TEMPERATURE, K
SPHERE DIAMETER = 5.6 mm
0
10
20
30
40
50
60
70
80
90
100
DISTANCE FROM NOZZLE EXIT, mm

FIGURE 20

VARIATION OF TOTAL AND STATIC PRESSURE

WITH DISTANCE FROM NOZZLE EXIT

(CONDITION I)

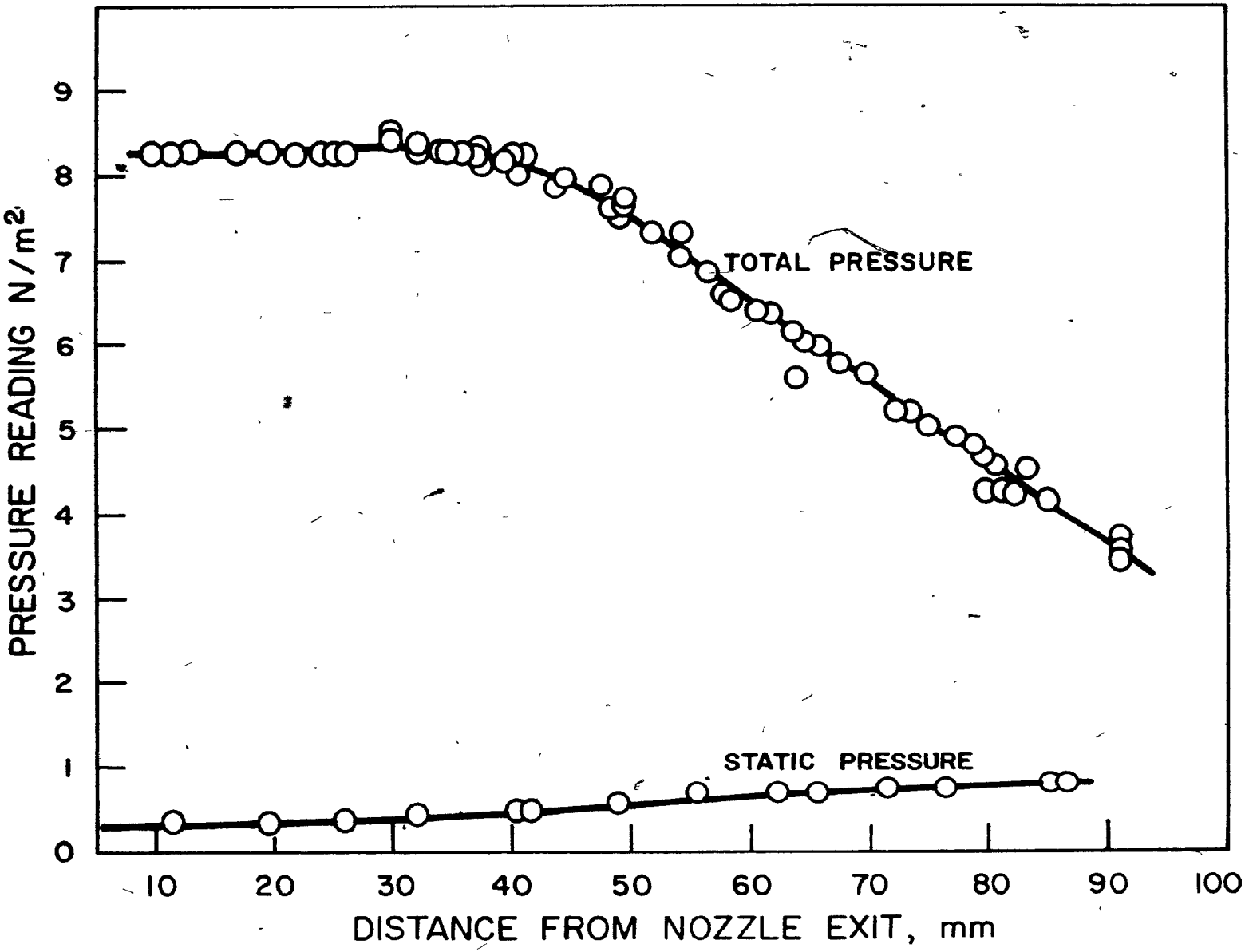
PRESSURE READING N/m²
0
1
2
3
4
5
6
7
8
9
TOTAL PRESSURE
STATIC PRESSURE
10
20
30
40
50
60
70
80
90
100
DISTANCE FROM NOZZLE EXIT, mm

FIGURE 21

VARIATION OF TOTAL AND STATIC PRESSURE

WITH DISTANCE FROM NOZZLE EXIT

(CONDITION II)

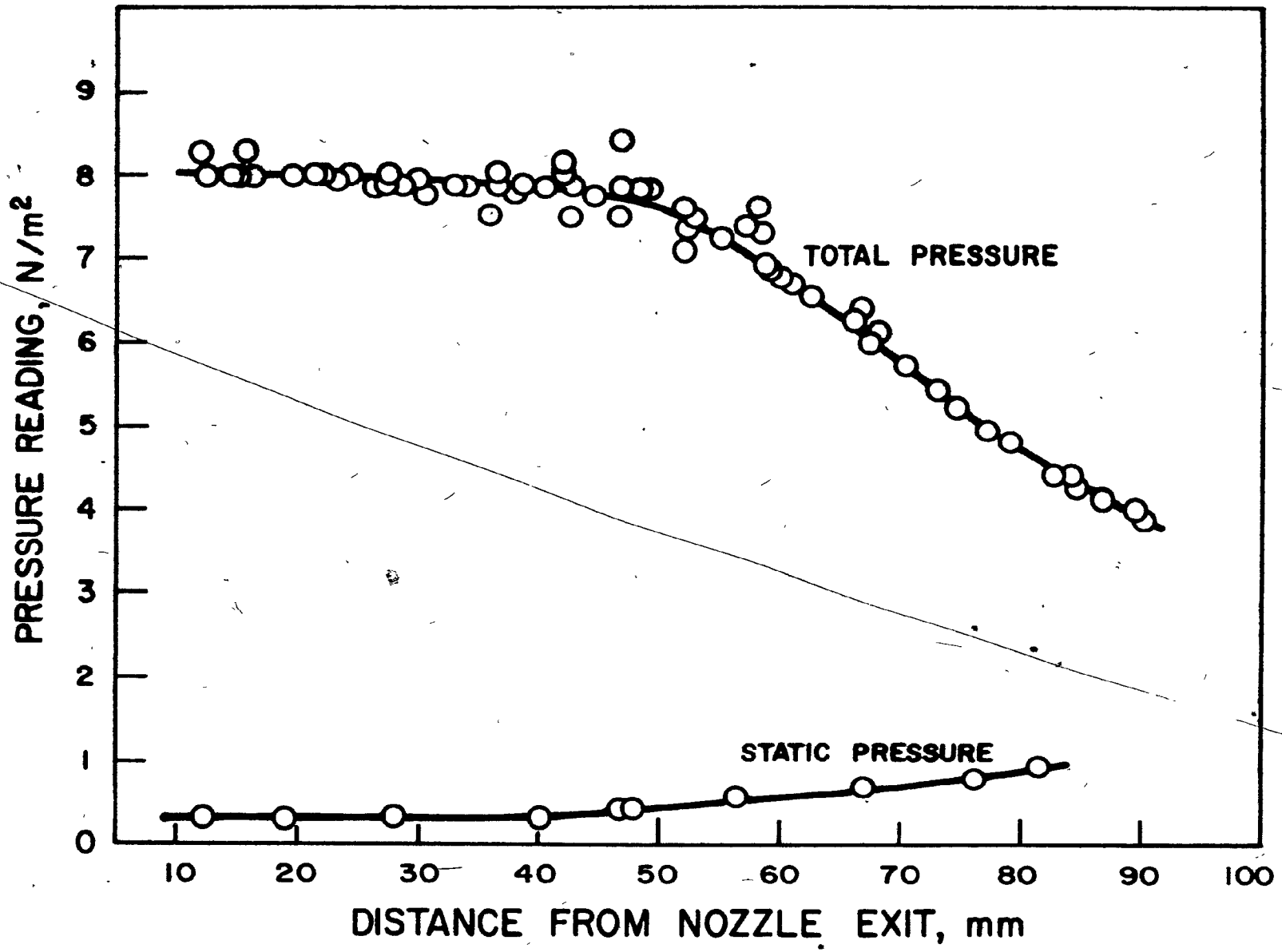
PRESSURE READING, N/m²
0
1
2
3
4
5
6
7
8
9
TOTAL PRESSURE
STATIC PRESSURE
10
20
30
40
50
60
70
80
90
100
DISTANCE FROM NOZZLE EXIT, mm

FIGURE 22

VARIATION OF TOTAL AND STATIC PRESSURE

WITH DISTANCE FROM NOZZLE EXIT

(CONDITION III)

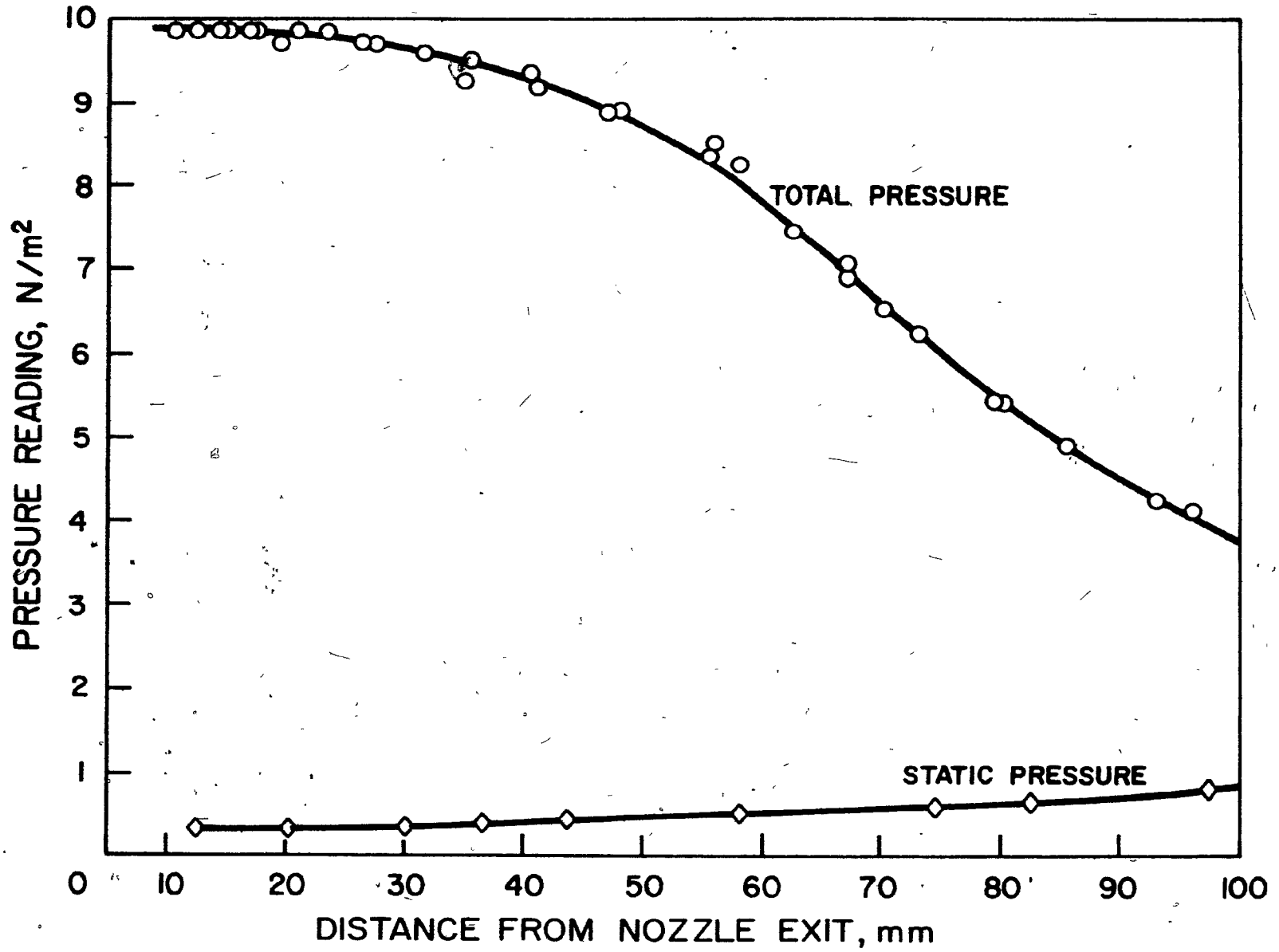
PRESSURE READING, N/m²
10
9
8
7
6
5
4
3
2
1
0
10
20
30
40
50
60
70
80
90
100
DISTANCE FROM NOZZLE EXIT, mm
TOTAL PRESSURE
STATIC PRESSURE

FIGURE 23

VARIATION OF TOTAL AND STATIC PRESSURE

WITH DISTANCE FROM NOZZLE EXIT

(CONDITION IV)

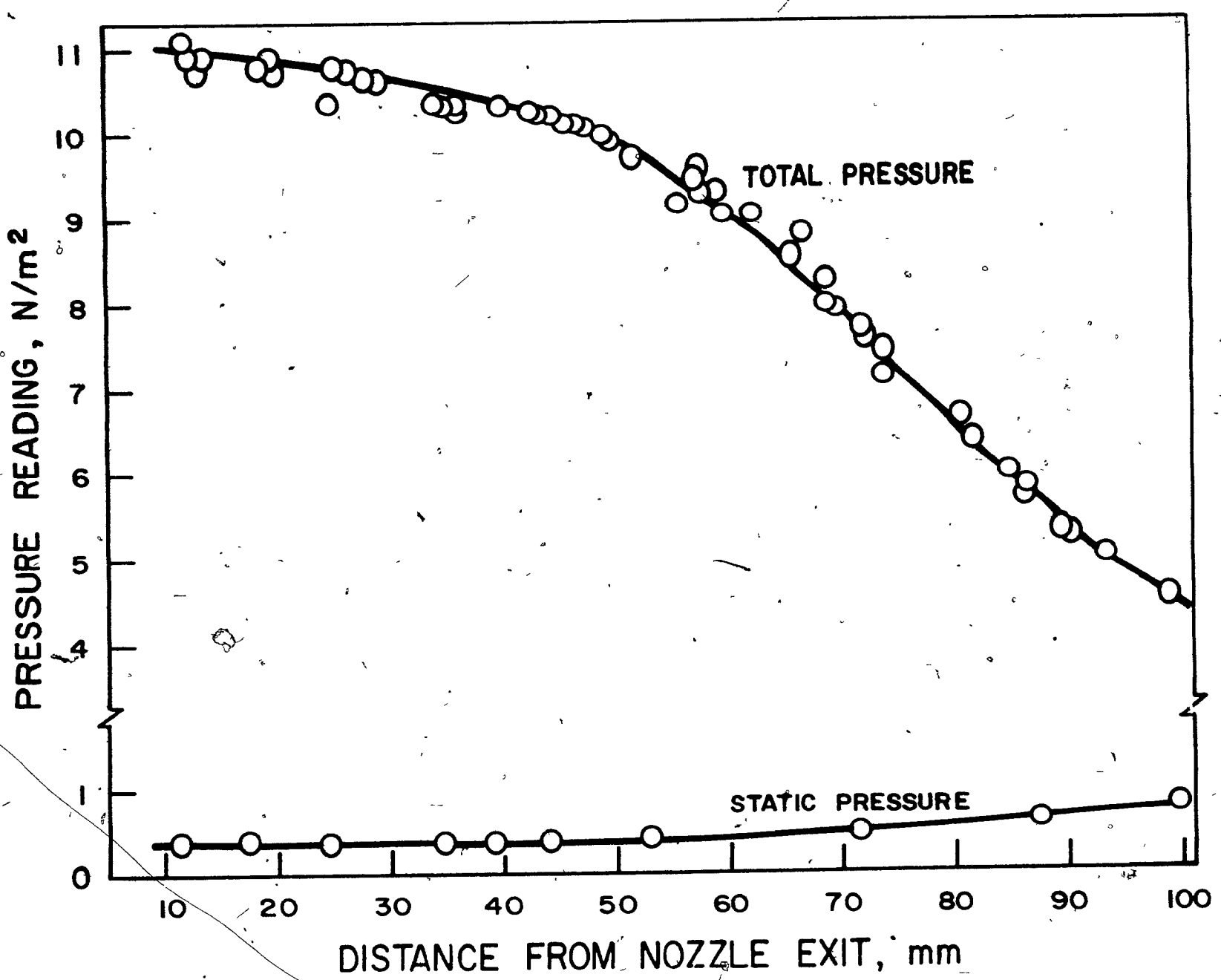
PRESSURE READING, N/m²
11
10
9
8
7
6
5
4
1
0
TOTAL PRESSURE
STATIC PRESSURE
10
20
30
40
50
60
70
80
90
100
DISTANCE FROM NOZZLE EXIT, mm

thermal condition, Equation (9) modifies to:

$$C_p = (P_t - P_\infty) / (\rho_\infty U_\infty^2/2) \qquad (10)$$

The value of C_p depends on the Reynolds number of the pressure probe and on the flow and temperature conditions upstream from the probe. Chue (1975) reviewed experimental calibrations and theoretical solutions for round- and square-nosed pitot tubes at low Reynolds numbers. He concluded that for the low Reynolds number range, corrections based on theoretical solutions were quite adequate for hemispherical-nose probes, irrespective of their orifice size, provided it lay in the range $0.2<d/D<0.74$.

The surface pressure distribution over a sphere at different Reynolds numbers and temperature conditions has been calculated by the author by solving the momentum and energy equations simultaneously. Details of these solutions were presented in the Numerical Analysis chapter of this thesis. For a hemispherical-nose probe, the pressure distribution at the nose is assumed to be the same as that around the leading half of a sphere, under similar thermal and dynamic conditions. It was at first thought that integration of this distribution over an area equivalent to the probe bore size would give the average stagnation pressure on the impact probe, for that particular flow condition, thus:

$$C_p = [\int_0^\Theta P(\theta) \sin\theta \, d\theta] / (1 - \cos\theta_1) \qquad (11)$$

If only the axial component of the pressure is taken, while

dropping out the radial component because it does not act on the column of gas inside the impact tube, Equation (11) modifies to:

$$C_p = \left[\int_0^{\Theta} P(\Theta) \sin\Theta \cos\Theta \, d\Theta \right] (1 - \cos\Theta_1) \qquad (12)$$

Results of the numerical integrations of Equations (11) and (12), using the Trapezoidal Rule, are listed in Table II. The pressure distributions were those obtained for constant-property flow. These results indicate that the value of C_p drops well below unity, at Reynolds numbers as low as 30. On the other hand, experimental calibrations of pitot tubes reported in the literature [Chue (1975)] give much higher values than the ones obtained by either Equation (11) or (12). They also show no tendency for C_p to go below unity. Some workers noted that C_p can be less than one, but the minimum value they gave was 0.98 and only at Re higher than 50. In conclusion, it can be said that the averaging procedure gives erroneous values of C_p.

Comparison of the pressure at the frontal stagnation point, for constant-property flow, with experimental C_p values from the literature shows reasonable agreement. This trend is not expected to be different for non-isothermal flows since the pressure distribution over the front half of the sphere, in a variable-property flow, is very similar to that for isothermal flow, provided that the sphere temperature is not much lower than one half the value of the gas temperature. In this work, therefore, the numerical results obtained for the frontal stagnation pressure will be used to evaluate

TABLE II

PITOT TUBE PRESSURE COEFFICIENTS

Reynolds Number UD/ν_∞	C_p Average		
	Equation (11) $T_o = 1.00$	Equation (12) $T_o = 1.00$	Equation (11) $T_o = 0.50$
10	1.589	1.486	1.643
20	1.199	1.123	1.245
30	1.058	0.993	1.092
50	0.936	0.877	0.950

C_p. This confirms Chue's findings that theoretical calibration of pitot tubes is independent of the orifice size. Figure 24 shows the variation of C_p with the temperature ratio, at several Reynolds numbers.

To determine the flow conditions around the probe, the temperature of the probe tip must be known. This was measured with the optical pyrometer. The variation of the tip temperature with axial distance from the nozzle, for the four plasma conditions, is shown in Figure 25. A knowledge of the gas temperature is also necessary. This is discussed in the following section.

Gas Temperature Correction

As stated earlier, the temperature of a wire finite size, immersed in a hot gas, is always lower than the actual temperature of the gas, owing to radiation and conduction losses. To evaluate the magnitude of this difference, a heat balance is made on the wire, thus:

$$Q_{conv.} + Q_{gas\ rad.} = Q_{rad.} + Q_{cond.} \qquad (13)$$

or $$(\pi Ddl)\, h_w\, (T_g - T_w) + (\pi Ddl/2)\, \varepsilon_{plasma} \alpha_w \sigma T^4_{plasma} =$$

$$\varepsilon_w \sigma (\pi Ddl)\, T_w^4 - (\pi D^2/4)\, [k_w dT/dl|_{l=l+dl} -$$

$$k_w dT/dl|_{l=l}] \qquad (14)$$

Equation (14) can be simplified to:

FIGURE 24

EFFECT OF REYNOLDS NUMBER AND TEMPERATURE RATIO ON

PITOT-TUBE PRESSURE COEFFICIENT

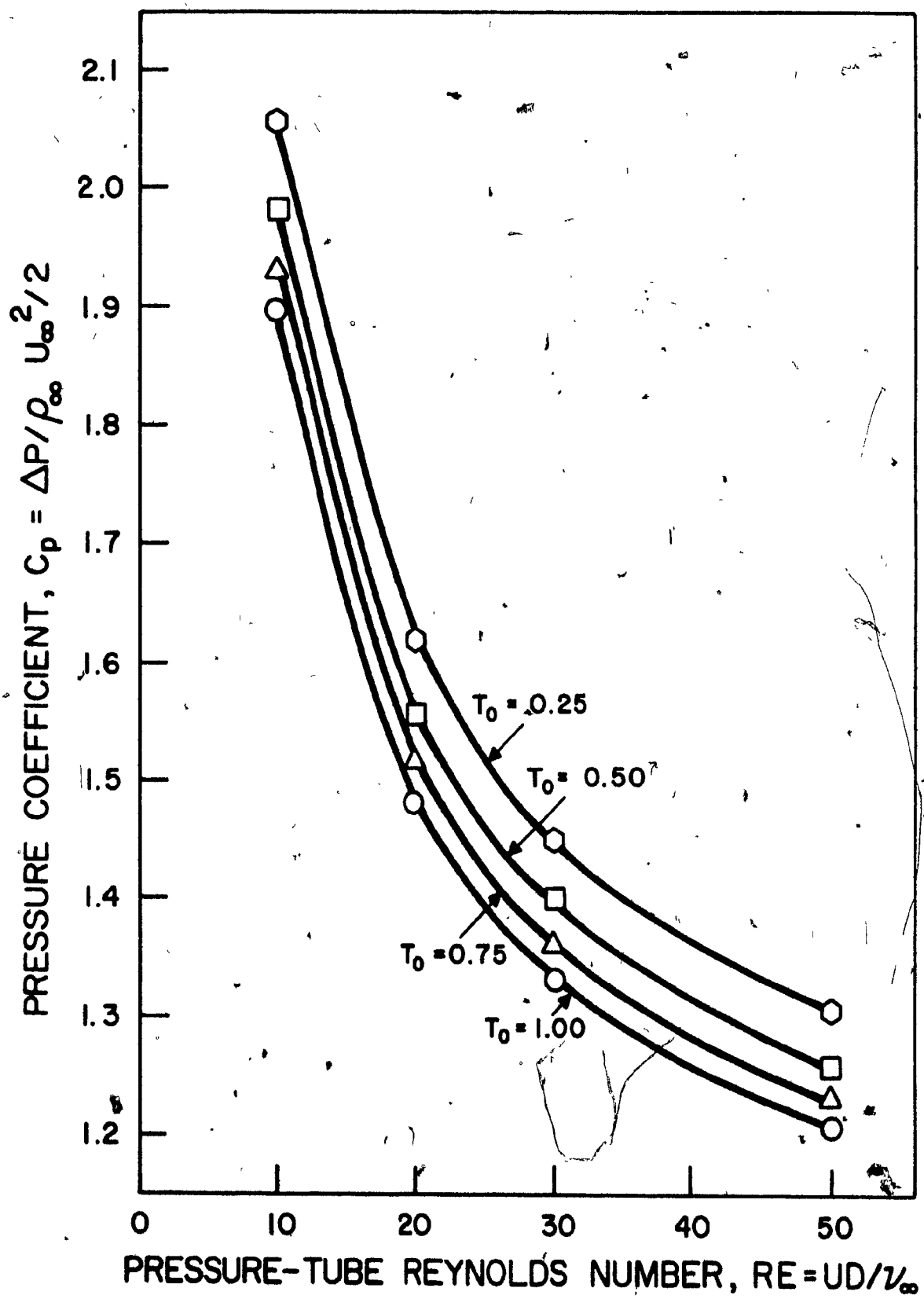
PRESSURE COEFFICIENT, $C_p = \Delta P/\rho_\infty U_\infty^2/2$
2.1
2.0
1.9
1.8
1.7
1.6
1.5
1.4
1.3
1.2
0
10
20
30
40
50
PRESSURE-TUBE REYNOLDS NUMBER, RE = UD/ν_∞
T_0 = 0.25
T_0 = 0.50
T_0 = 0.75
T_0 = 1.00

FIGURE 25

VARIATION OF PRESSURE PROBE TIP TEMPERATURE

WITH DISTANCE FROM NOZZLE EXIT

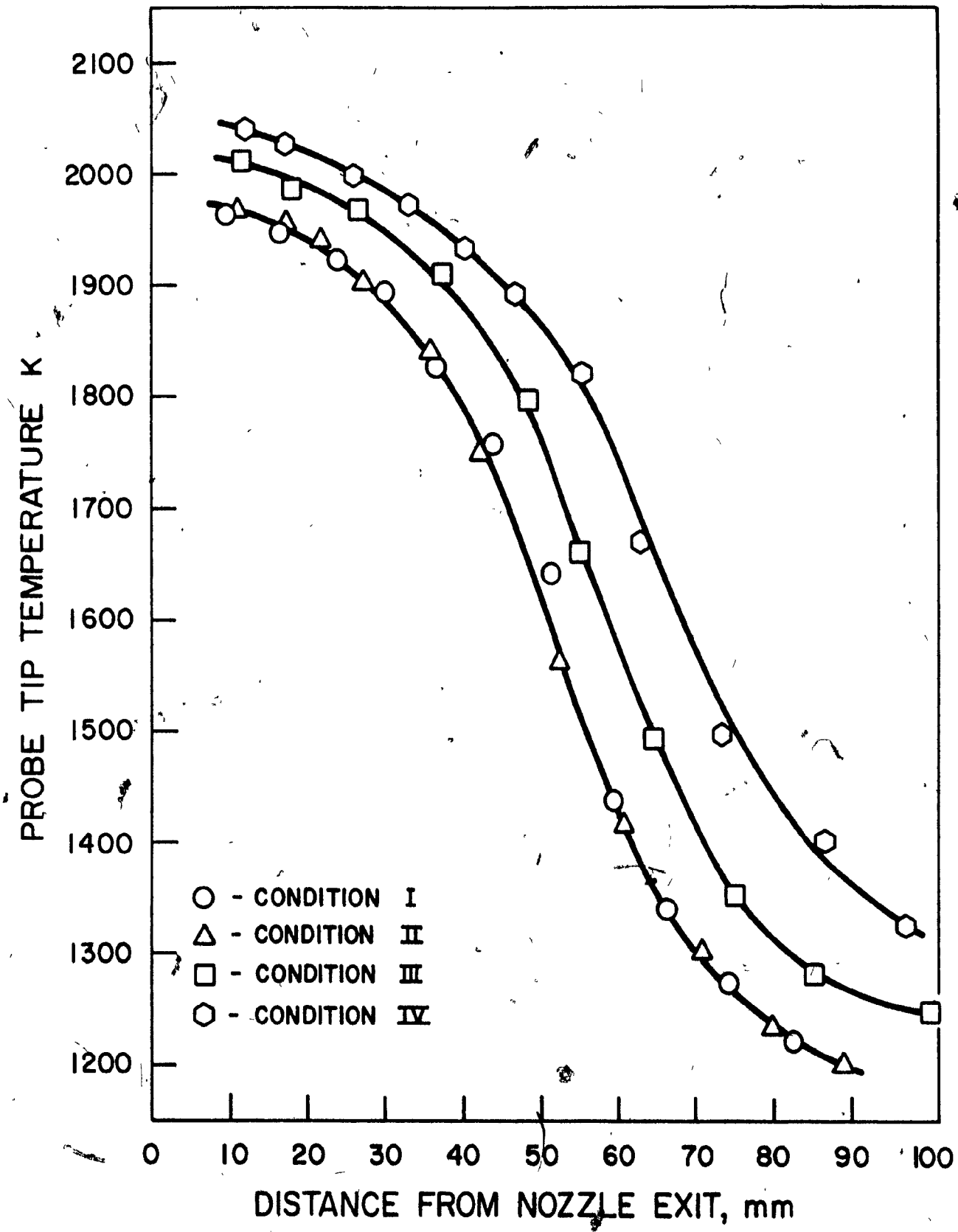
2100
2000
1900
1800
1700
1600
1500
1400
1300
1200
PROBE TIP TEMPERATURE K
O - CONDITION I
Δ - CONDITION II
□ - CONDITION III
⬡ - CONDITION IV
0
10
20
30
40
50
60
70
80
90
100
DISTANCE FROM NOZZLE EXIT, mm

average plasma gas temperature over a depth of 100 mm near the coil region, then the radiation received by the wire from the gas is less than 0.5% of the total convective transfer. No effect of viewing angle was included in this calculation. With the presence of the water-cooled probe along the axis of the torch, average plasma temperature is not expected to be over 6 000 K in that vicinity. Furthermore, the presence of the probe blocked the view for direct radiation to the wire at positions further down from the nozzle, and, therefore, the relative effect of radiation was still insignificant even though the convective transfer rates were lower at these points. Consequently, Equation (15) simplifies to:

$$T_g = \varepsilon_w \sigma T_w^4 / h_w + T_w \qquad (16)$$

To evaluate T_g, the convective heat transfer rates to thin wires must be known, for conditions where an appreciable temperature difference between the wire and the gas exists. Heat transfer to cylinders was discussed in the Literature Review chapter. Some of the more reliable results were those reported by Collis and Williams (1969). However, their experiments were carried out on heat transfer from a hot wire to a colder gas and the applicability of their results to the reverse situation has not been verified. On the other hand, Woo (1970) obtained numerical results for local and overall Nusselt numbers around infinite cylinders in the Reynolds number range of 2 to 175. His results will now be modified to include the effect of variable fluid properties. Woo's results for heat transfer in air in the range $2<Re<40$ can be correlated by the following

$$4/D\ h_w\ (T_g - T_w) + 2/D\ \varepsilon_{plasma}\alpha_w\sigma T^4_{plasma} =$$

$$4/D\ \varepsilon_w\sigma T^4_w - d/dl(k_w dT/dl) \qquad (15)$$

In Equation (14) only the top part of the wire was assumed to be subjected to plasma radiation. Curvature effects were not included.

The temperature gradient along the wire near its mid-section is proportional to the radial temperature gradient in the jet. If the jet temperature profile near the axis is flat then the temperature gradient in the wire will be very close to zero, and conduction losses from the wire at this point will be insignificant. On the other hand, neglecting conduction losses when the gas temperature gradient is appreciable, will lead to an underestimate of the axial gas temperature. This underestimate is directly proportional to the gas temperature gradient. Since spheres of finite sizes were used in this study, then the average temperature of the gas surrounding the sphere was not exactly the temperature at the axis but a slightly lower value, due to the radial temperature gradient in the jet. The difference between this average value and the axial temperature is also directly proportional to the temperature gradient. Consequently, errors introduced by neglecting conduction in the wire when a radial temperature gradient exists are balanced by the averaging effect of the finite sphere size.

Moskvin (1968) reported some emissivity values for argon in the temperature range between 6 000 and 12 000 K. Assuming an

equation:

$$Nu = 0.2496 + 0.5817\ Re^{0.455} \qquad (17)$$

Also for air, Collis and Williams' experimentally-derived equation can be written as:

$$Nu_m (T_m/T_\infty)^{-0.17} = 0.24 + 0.56\ Re_m^{0.45} \qquad (18)$$

It can be seen that the exponent on the Reynolds number is approximately the same in the two correlations.

In the numerical analysis presented in the preceding chapter, the constant-property heat transfer equation to a sphere was found to be of the following form:

$$Nu = A + B\ P_r^m\ Re^n \qquad (19)$$

This equation was later modified to include the effect of variable fluid properties, thus:

$$Nu_o = Af_o + B\ Pr^m\ Re_{o.19}^n \qquad (20)$$

where $$f_o = (1 - T_o^{1+x}) \ / \ [(1 + x)(1 - T_o)T_o^x] \qquad (21)$$

and the kinematic viscosity of the gas is evaluated at $T_{o.19}$ where

$$T_{o.19} = T_s + 0.19(T_g - T_s) \qquad (22)$$

Af_o is the limiting Nusselt number at Re = 0, for variable-property fluids. f_o gives the Nusselt number in terms of surface temperature

conditions.

For cylinders, the limiting Nusselt number is indeterminate. However, the ratio of the limiting Nusselt numbers for variable- to constant-property flow is still equal to f_o. Assuming the effect of variable property is similar for spheres and cylinders, then Equation (17), for variable-property fluids, becomes:

$$Nu_o = 0.2496\, f_o + 0.5817\, Re_{0.19}^{0.455} \tag{23}$$

The general form of heat transfer correlations for cylinders is:

$$Nu = (A + BRe^n)\, Pr^m \tag{24}$$

m is between 0.3 and 1/3. To convert a correlation obtained in air to one applicable for argon, the equation is multiplied by the Prandtl number ratio to the power m. For argon, Equations (18) and (23) become, respectively:

$$Nu_m\, (T_m/T_\infty)^{-0.17} = 0.235 + 0.47\, Re_m^{0.45} \tag{25}$$

$$Nu_o = 0.2417\, f_o + 0.5633\, Re_{0.19}^{0.455} \tag{26}$$

Both of these equations will be used to evaluate h, and the results will then be compared.

The total hemispherical emissivity of tungsten is also required for the evaluation of the gas temperature from Equation (16). Since the emissivity varies with the temperature, the value

of ε_w used must correspond to the actual wire temperature T_w. The values used in this work were those given by Logunov (1969) and Sadykov (1965), which agree very well with the values reported in the International Critical Tables (1926).

The velocity of the gas must be known in order to evaluate the heat transfer coefficient. Since the velocity, in turn, requires a knowledge of the temperature, then these must be found simultaneously by an interative method. The values of the wire temperature and the stagnation pressure were taken from the smoothed curves of the experimental results, at 5 mm-intervals along the axis, for the four plasma conditions. An empirical equation relating C_p to Re and T_o was derived based on the numerical results. Values of the velocity and temperature were assumed and then inserted in this empirical equation to give a first approximation of the gas velocity. This velocity was used in Equation (25) or (26) to find h, from which Tg was calculated with the aid of Equation (16). This procedure was repeated until the difference between two consecutive values of the velocity and temperature was less than 0.1% of the absolute value. It was found that at each point, this process required only three to four iterations.

Gas Velocity and Temperature Profiles

The gas velocity and temperature profiles calculated from the stagnation pressure and wire temperature are shown in Figures 26 to 29, for the four conditions of gas flow rate and power input. The

FIGURE 26

GAS VELOCITY CALCULATED FROM EXPERIMENTAL DATA,

AS A FUNCTION OF DISTANCE FROM NOZZLE EXIT

(CONDITIONS I & IV)

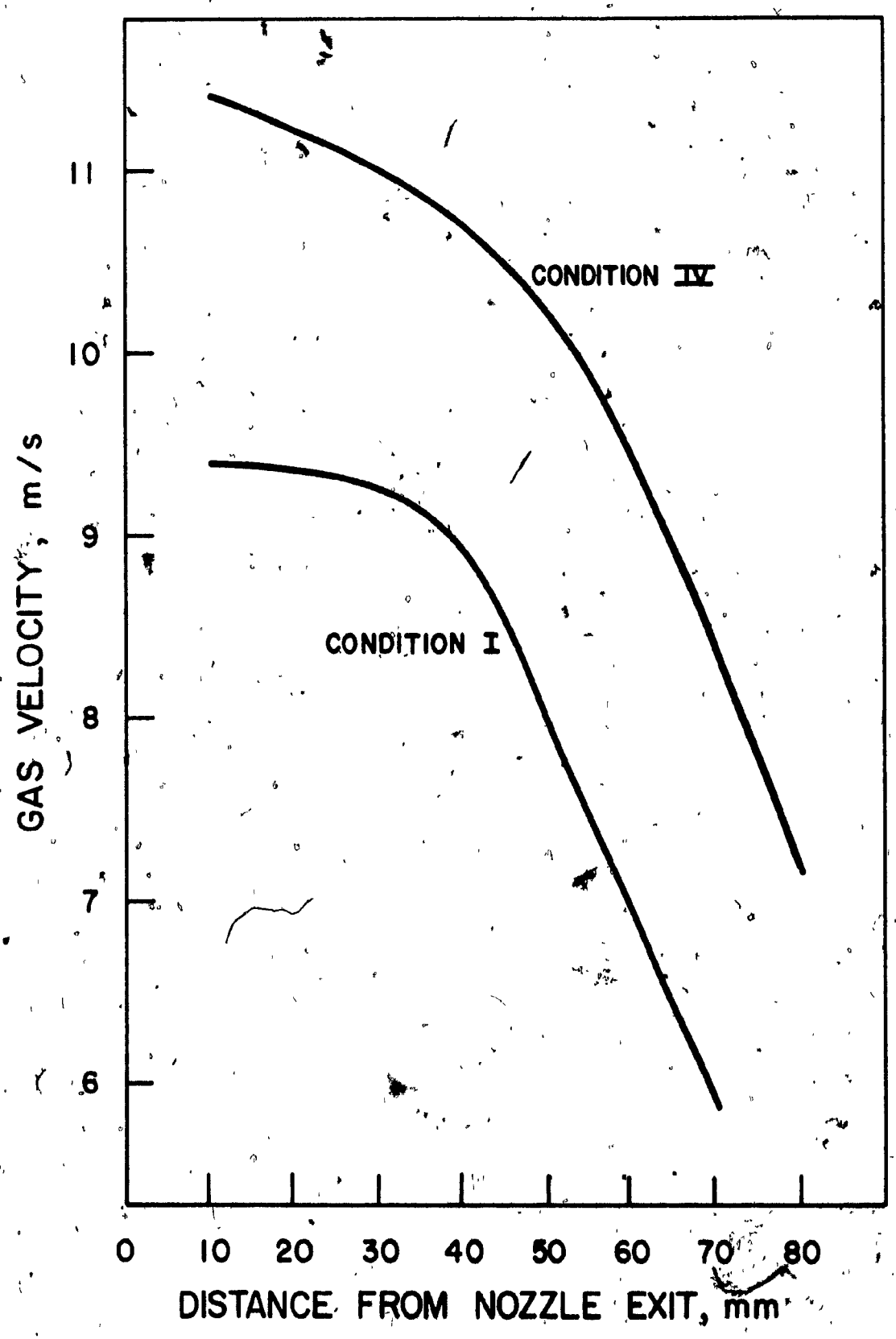
CONDITION IV
CONDITION I
GAS VELOCITY, m/s
11
10
9
8
7
6
0
10
20
30
40
50
60
70
80
DISTANCE FROM NOZZLE EXIT, mm

FIGURE 27

GAS VELOCITY CALCULATED FROM EXPERIMENTAL DATA,

AS A FUNCTION OF DISTANCE FROM NOZZLE EXIT

(CONDITIONS II & III)

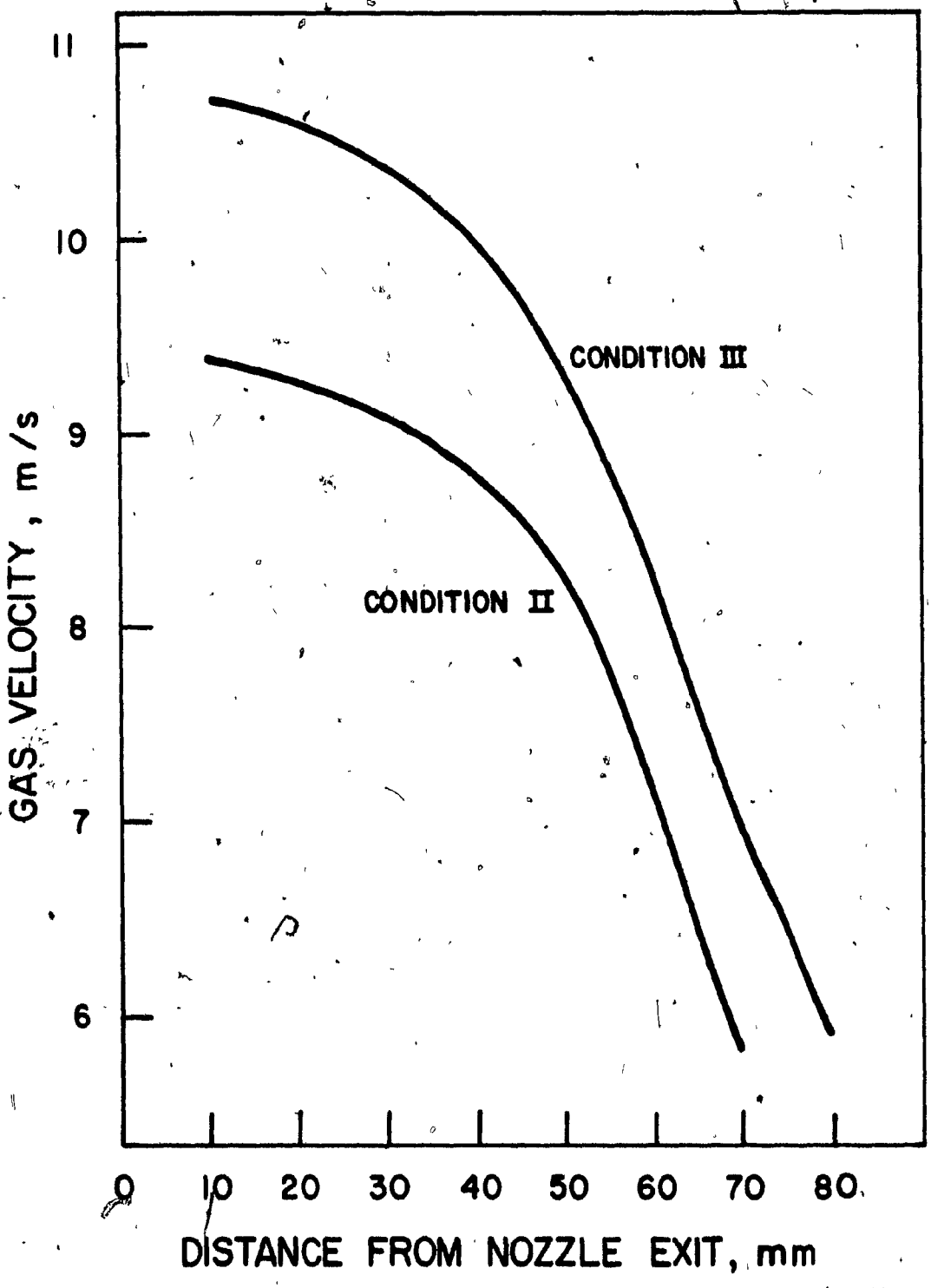
11
10
9
8
7
6
GAS VELOCITY, m/s
CONDITION III
CONDITION II
0
10
20
30
40
50
60
70
80
DISTANCE FROM NOZZLE EXIT, mm

FIGURE 28

GAS TEMPERATURE CALCULATED FROM EXPERIMENTAL DATA,

AS A FUNCTION OF DISTANCE FROM NOZZLE EXIT

(CONDITIONS I & IV)

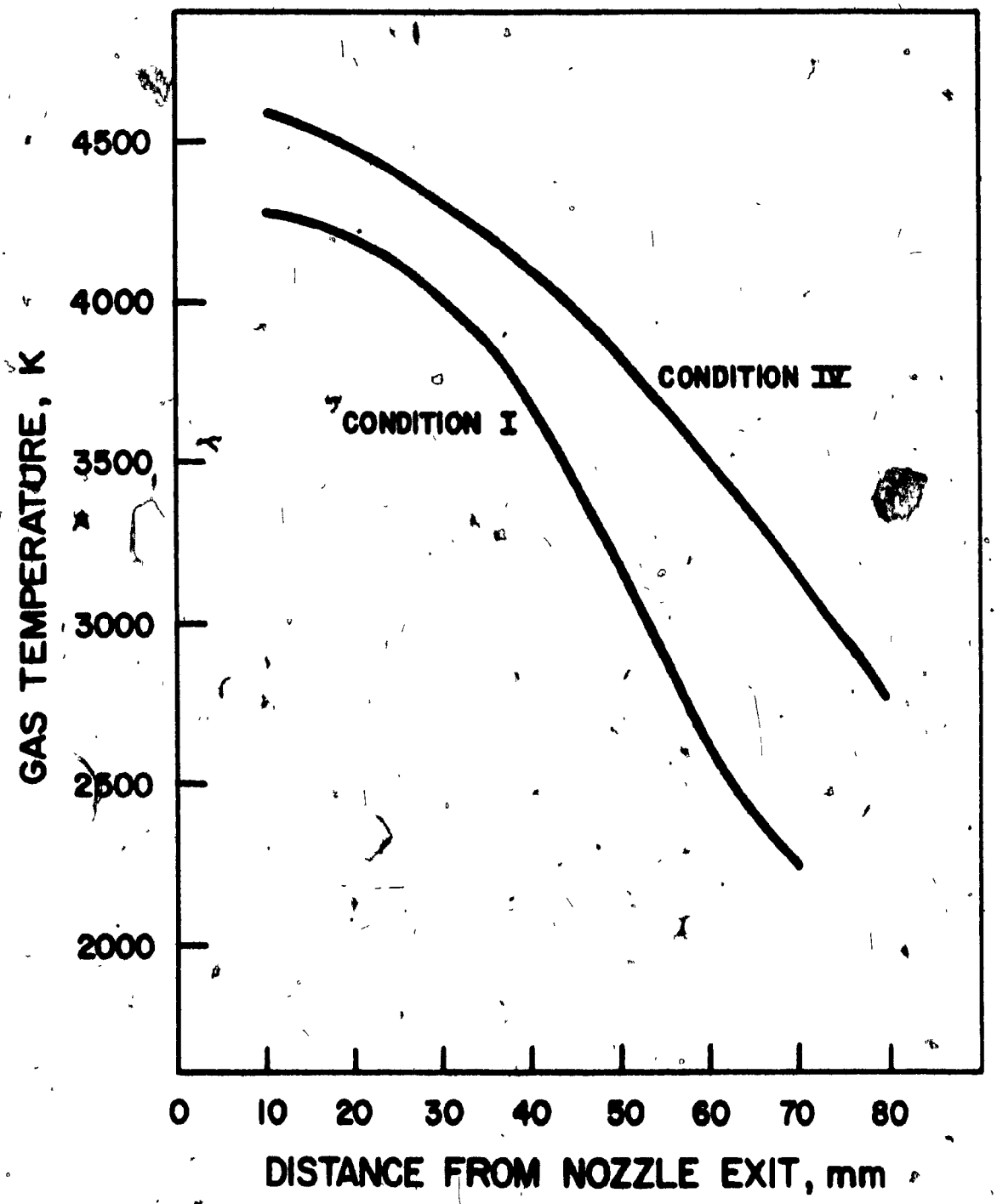
4500
4000
3500
3000
2500
2000
GAS TEMPERATURE, K
CONDITION IV
CONDITION I
0
10
20
30
40
50
60
70
80
DISTANCE FROM NOZZLE EXIT, mm

FIGURE 29

GAS TEMPERATURE CALCULATED FROM EXPERIMENTAL DATA,

AS A FUNCTION OF DISTANCE FROM NOZZLE EXIT

(CONDITIONS II & III)

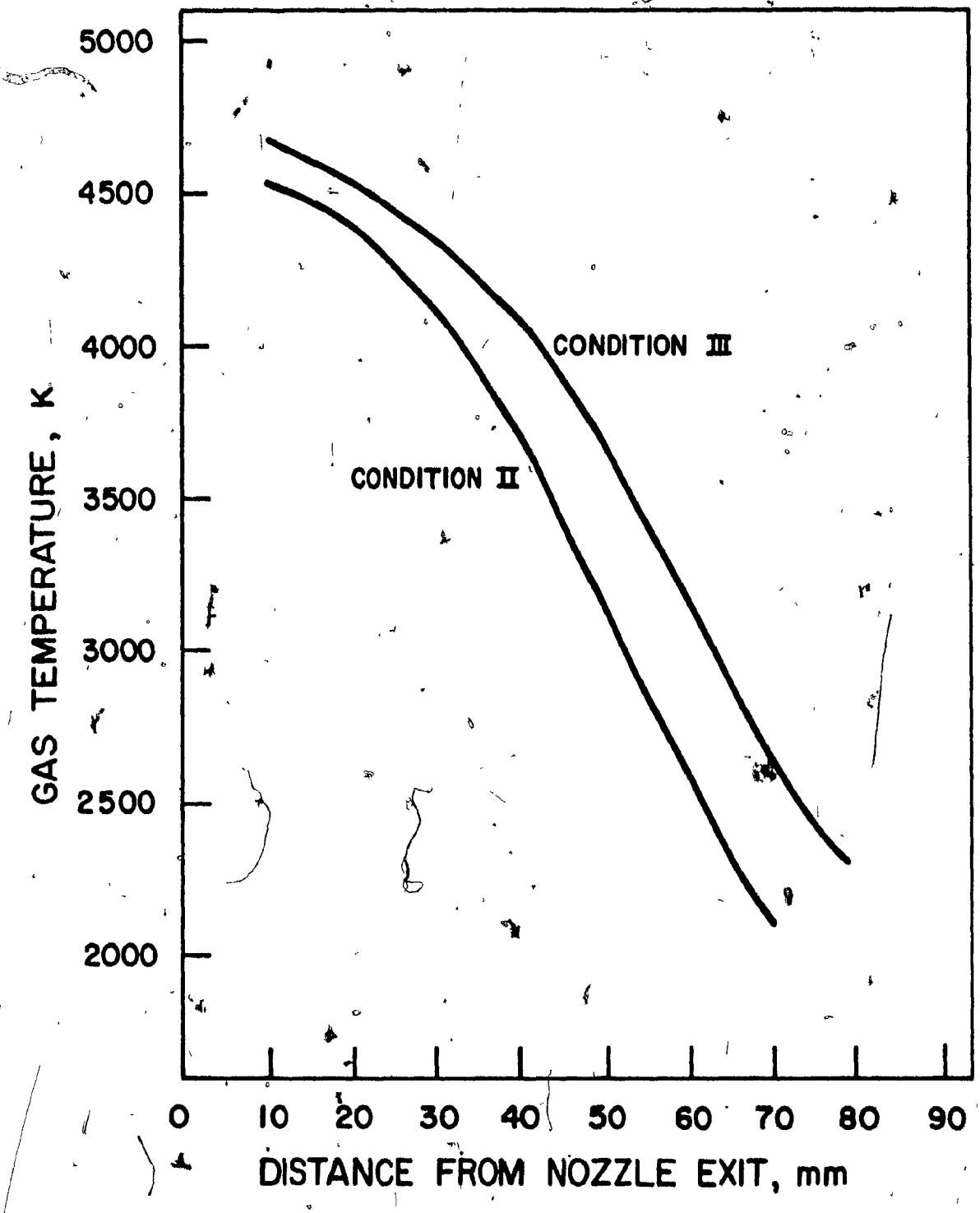
5000
4500
4000
3500
3000
2500
2000
GAS TEMPERATURE, K
CONDITION III
CONDITION II
0
10
20
30
40
50
60
70
80
90
DISTANCE FROM NOZZLE EXIT, mm

results obtained using Equations (25) and (26) were exactly the same for the gas velocity and within a fraction of a percent for the gas temperature. Tables III and IV list the temperatures and velocities calculated by the two equations, for two plasma operating conditions. This agreement reconfirms the concept of using variable-property limiting Nusselt number and the reference temperature $T_{o.19}$ for evaluating the Reynolds number.

HEAT TRANSFER CALCULATIONS

Heat Balance

A similar heat balance can be written around a sphere as that given for cylinders in Equations (13) and (14), namely:

$$h_s (\pi D^2) (T_g - T_s) + \varepsilon_{plasma} \alpha_s (\pi D^2/2) \sigma T^4_{plasma} = \varepsilon_s \sigma (\pi D^2) T_s^4 + Q_{cond.} \quad (27)$$

$Q_{cond.}$ cannot be written in an exact form since the wire was in contact with the sphere at only a few discrete points. The wire temperature was always higher than that of the sphere at the points of contact. However, due to the relatively small size of the wire and the small area of contact, heat transfer by conduction from the wire to the sphere was assumed to have insignificant influence on the overall heat transfer process.

Radiation from the plasma gas was discussed earlier. For an average gas temperature of 6 000 K over a depth of 100 mm in the hot

TABLE III

GAS VELOCITY AND TEMPERATURE PROFILES

Plasma Power = 1.5 A x 3.25 KV

Gas Flow Rate = 0.87 g/s

Distance mm	Equation (26) Temperature K	Equation (26) Velocity m/s	Equation (25) Temperature K	Equation (25) Velocity m/s
10	4277	9.41	4275	9.41
20	4218	9.38	4217	9.38
30	4032	9.24	4035	9.24
40	3705	8.90	3713	8.90
50	3170	8.04	3182	8.04
60	2632	6.92	2645	6.93
70	2263	5.86	2274	5.87

TABLE IV

GAS VELOCITY AND TEMPERATURE PROFILES

Plasma Power = 1.7 A x 3.55 KV

Gas Flow Rate = 0.72 g/s

Distance mm	Equation (26) Temperature K	Equation (26) Velocity m/s	Equation (25) Temperature K	Equation (25) Velocity m/s
10	4590	11.43	4581	11.42
20	4473	11.25	4467	11.24
30	4322	11.00	4320	11.00
40	4103	10.69	4105	10.69
50	3830	10.24	3837	10.25
60	3524	9.49	3534	9.50
70	3154	8.40	3167	8.40
80	2790	7.20	2803	7.20

core, radiation from the plasma amounted to less than 0.5% of the overall heat transfer rate. This simplifies Equation (27) to:

$$h_s = \varepsilon_s \sigma T_s^4 / (T_g - T_s) \quad (28)$$

This equation shows the direct influence of the total hemispherical emissivity on the value of the heat transfer coefficient calculated.

Assumptions in Experimental Model

1. Flow is uniform and unidirectional along the axis of the jet. Velocity and temperature gradients in the gas are not important.

2. Radiation from the plasma core is negligible.

3. No conduction losses through the support.

4. No turbulence effects on the heat transfer process. The jet is assumed to be laminar.

5. Natural convection is very small compared to forced convection.

6. Sphere temperature is uniform over the entire surface.

These assumptions will be discussed individually. Point (1): in an axisymmetric jet, the only velocity component at the axis is the axial component. Radial and angular components start to gain importance with increasing distance away from the axis. Radial tem-

perature and velocity gradients in a jet are not very steep near the axis, especially at points close to the nozzle exit plane. The disturbance caused by the presence of the sphere depends on the ratio of the sphere diameter to the nozzle diameter, or more specifically, on the ratio of their cross-sectional areas. In this study, the largest sphere size used was 5.6 mm and the nozzle diameter was 25.4 mm, which amounts to 5% maximum blockage near the nozzle, and much less as the jet expands. With the largest sphere diameter of 5.6 mm, the maximum distance the spheres extended to away from the axis was less than 3 mm. At this distance it was presumed that radial and angular components of the flow were still very small compared to the axial component.

Points (2) and (3) have already been discussed. Point (4): turbulence in a plasma jet was studied by Incropera and Leppert (1966). Turbulence was assumed to be a function of the jet noise. The Reynolds number of the jet was evaluated at bulk gas properties, thus:

$$Re = 4 \dot{m} / \pi D \mu_g \qquad (29)$$

The criteria set for flow transitions were the following:

Laminar	at	$Re < 110 - 250$
Transitional	at	$110 - 250 < Re < 300 - 800$
Turbulent	at	$Re > 300 - 800$

Transition from turbulent to transitional was at $300 < Re < 600$ and

from transitional to laminar at $210 < Re < 250$.

The maximum mass flow rate of argon used in the experiments of the present study was 0.9 g/sec. Assuming an average gas temperature of 4 000 K, which has a viscosity of 1.53×10^{-4} N s/m^2, then the bulk Reynolds number of the jet is:

$$Re = 4 \times 0.9/(\pi \times 1.53 \times 10^{-4} \times 25.4) = 295$$

This means that the jet was in the transitional regime. However, a surprising result was found by Incropera and Leppert when the Reynolds number was computed with the viscosity evaluated at the nozzle wall temperature. In all the cases studied, the Reynolds number for transition to a laminar jet was approximately 2 300. Assuming a conservative wall temperature of 300 K where argon viscosity is about 2×10^{-5} N sec/m^2, the surface Reynolds number of the plasma jet in the present work becomes:

$$Re_Q = 4 \times 0.9/(\pi \times 2.4 \times 10^{-5} \times 25.4) = 1880$$

This Reynolds number indicates positively that the jet was laminar. Moreover, Richardson (1965) stated that at low and moderate Reynolds number, free stream turbulence does not have a strong influence on the heat transfer to cylinders. It can be safety assumed that this observation applies equally to heat transfer to spheres. In conclusion, it can be said that the plasma jet was laminar and even if slight turbulence existed, its effect on the heat transfer rate could be neglected.

Point (5): Pei (1965) found that for free convection to be negligible, the ratio Gr/Re^2 must be less than 0.05. This ratio can be written as:

$$Gr/Re^2 = \frac{\beta g D^3 \Delta T/\nu^2}{U^2 D^2/\nu^2} = \beta g D \Delta T/U^2 \qquad (30)$$

For ideal gases $\beta = 1/T$. From the experimental results, the temperature difference, ΔT, was approximately equal to one half of the value of the gas temperature. Also,

$$D \sim 5 \text{ mm}$$

$$U \sim 10 \text{ m/sec}$$

then $$Gr/Re^2 = (1/T) \times g \times 5 \times (T/2)/(10{,}000)^2$$

$$Gr/Re^2 \sim 3 \times 10^{-4}$$

The value of Gr/Re^2 is therefore much less than the limit proposed by Pei.

Point (6): the condition for gradients to exist within the sphere is that its Biot number is higher than 0.2. The Biot number is defined as:

$$Bi = hR/k_{sphere} \qquad (31)$$

or $$Bi = Nuk_s/2k_{sphere}$$

Assuming a high value of 15 for the Nusselt number with a sphere temperature of 2 500 K, then the upper limit of the Biot number is:

$$Bi = 15 \times 1.57 \times 10^{-4}(2{,}500)^{0.8}/(2 \times 42)$$

$$Bi \sim 0.01$$

At lower Nusselt numbers and sphere temperatures the value of the Biot number will be even less than 0.01.

Results

Equation (28) was used to calculate the forced-convection heat transfer coefficients to the three spheres. The spheres' temperatures were read from the smoothed experimental curves. Values were taken at intervals of 5 mm, along the jet axis. The results of these calculations are given in Tables V to XVI for the four plasma conditions.

The values of the total hemispherical emissivity of molybdenum were taken from the works of Makarenko (1970), Peletskii and Druzhinin (1969) and of Sadykov (1965).

CORRELATION AND DISCUSSION OF RESULTS

The general form of the heat transfer equation can be expressed as:

$$Nu = A + B\ Pr^{m}\ Re^{n} \qquad (32)$$

In the numerical analysis chapter, the momentum and energy equations for flow past a sphere were solved numerically for constant-property flow and for cases involving large variations in the physical

TABLE V

POWER = 1.50 A X 3.25 KV
GAS FLOW RATE = 0.870 G/S
SPHERE DIAMETER = 2.2 MM

°Z	H	TO	RE_∞	NU_∞	RE_o	NU_o
1.0	183.9	0.526	14.3	3.168	45.3	5.292
1.5	184.3	0.529	14.5	3.192	45.4	5.312
2.0	181.9	0.530	14.6	3.166	45.7	5.261
2.5	181.5	0.536	15.0	3.204	46.0	5.276
3.0	182.1	0.546	15.6	3.285	46.3	5.333
3.5	182.9	0.560	16.4	3.405	46.7	5.415
4.0	180.5	0.574	17.4	3.478	47.3	5.421
4.5	184.9	0.605	19.2	3.789	47.5	5.668
5.0	177.3	0.628	20.7	3.858	47.8	5.596
5.5	172.2	0.660	22.8	4.031	48.3	5.621
6.0	161.8	0.687	24.7	4.062	48.5	5.486
6.5	144.3	0.706	26.2	3.853	49.0	5.090
7.0	130.9	0.723	27.1	3.687	48.7	4.779

TABLE VI

POWER = 1.50 A X 3.25 KV

GAS FLOW RATE = 0.870 G/S

SPHERE DIAMETER = 3.3 MM

Z	H	TO	RE_∞	NU_∞	RE_o	NU_o
1.0	136.9	0.501	21.4	3.537	74.3	6.146
1.5	137.0	0.504	21.7	3.560	74.5	6.162
2.0	135.0	0.505	21.9	3.526	75.0	6.095
2.5	136.2	0.511	22.5	3.606	75.2	6.168
3.0	134.1	0.519	23.4	3.628	76.1	6.133
3.5	135.7	0.533	24.6	3.787	76.4	6.262
4.0	132.6	0.546	26.1	3.833	77.6	6.217
4.5	137.9	0.577	28.8	4.239	77.5	6.578
5.0	138.8	0.605	31.1	4.529	76.7	6.769
5.5	132.1	0.635	34.3	4.640	77.7	6.676
6.0	122.8	0.661	37.0	4.624	77.9	6.439
6.5	102.6	0.674	39.3	4.109	79.9	5.632
7.0	75.6	0.672	40.7	3.196	83.3	4.393

TABLE VII

POWER = 1.50 A X 3.25 KV

GAS FLOW RATE = 0.870 G/S

SPHERE DIAMETER = 5.6 MM

Z	H	TO	RE_∞	NU_∞	RE_o	NU_o
1.0	94.0	0.470	37.7	4.268	146.5	7.806
1.5	93.9	0.472	38.1	4.290	146.9	7.816
2.0	92.4	0.473	38.5	4.240	148.0	7.717
2.5	92.0	0.478	39.5	4.284	148.8	7.727
3.0	92.2	0.487	41.1	4.384	149.8	7.794
3.5	92.5	0.500	43.3	4.539	150.6	7.898
4.0	90.8	0.513	46.0	4.614	152.6	7.866
4.5	94.3	0.543	50.6	5.094	152.0	8.302
5.0	94.6	0.570	54.6	5.425	150.3	8.509
5.5	93.2	0.602	60.2	5.751	149.9	8.626
6.0	87.5	0.630	65.1	5.790	149.5	8.381
6.5	76.0	0.646	69.1	5.348	151.5	7.581
7.0	63.0	0.655	71.6	4.675	153.3	6.559

TABLE VIII

POWER = 1.55 A X 3.35 KV

GAS FLOW RATE = 1.050 G/S

SPHERE DIAMETER = 2.2 MM

Z	H	TO	RE_∞	NU_∞	RE_o	NU_o
1.0	186.2	0.508	12.8	3.064	43.4	5.266
1.5	180.1	0.508	13.0	2.984	43.9	5.127
2.0	179.0	0.515	13.4	3.020	44.3	5.132
2.5	174.2	0.522	13.9	2.998	45.0	5.047
3.0	171.7	0.533	14.8	3.045	45.8	5.037
3.5	166.2	0.547	15.8	3.065	46.9	4.965
4.0	157.6	0.561	17.1	3.032	48.4	4.813
4.5	147.5	0.580	18.8	2.996	50.3	4.635
5.0	146.9	0.612	21.4	3.205	51.8	4.749
5.5	145.7	0.650	24.1	3.455	52.3	4.878
6.0	136.1	0.679	26.2	3.475	52.6	4.738
6.5	131.4	0.714	28.6	3.631	52.4	4.755
7.0	120.3	0.743	30.9	3.591	52.7	4.553

TABLE IX

POWER = 1.55 A X 3.35 KV

GAS FLOW RATE = 1.050 G/S

SPHERE DIAMETER = 3.3 MM

Z	H	TO	RE_∞	NU_∞	RE_0	NU_0
1.0	140.0	0.484	19.3	3.455	71.0	6.[illegible]0
1.5	138.7	0.486	19.5	3.447	71.3	6.134
2.0	139.2	0.494	20.2	3.523	71.7	6.192
2.5	136.7	0.501	20.9	3.530	72.6	6.138
3.0	137.8	0.514	22.1	3.666	73.3	6.242
3.5	136.2	0.530	23.8	3.769	74.6	6.266
4.0	130.1	0.544	25.7	3.754	76.8	6.110
4.5	128.3	0.567	28.3	3.909	78.5	6.156
5.0	126.7	0.598	32.1	4.144	81.0	6.254
5.5	126.2	0.636	36.1	4.489	81.5	6.447
6.0	120.6	0.668	39.3	4.619	81.3	6.382
6.5	110.0	0.697	42.9	4.558	82.0	6.082
7.0	101.1	0.727	46.4	4.529	82.3	5.844

TABLE X

POWER = 1.55 A X 3.35 KV
GAS FLOW RATE = 1.050 G/S
SPHERE DIAMETER = 5.6 MM

Z	H	TO	RE_∞	NU_∞	RE_0	NU_0
1.0	94.6	0.453	33.9	4.106	140.9	7.738
1.5	93.0	0.454	34.3	4.064	141.8	7.641
2.0	93.5	0.462	35.4	4.158	142.4	7.717
2.5	93.1	0.469	36.7	4.224	143.5	7.738
3.0	92.5	0.481	38.9	4.327	145.4	7.774
3.5	93.2	0.497	41.8	4.530	146.9	7.923
4.0	91.9	0.514	45.1	4.659	149.6	7.939
4.5	89.2	0.534	49.7	4.776	153.5	7.885
5.0	88.7	0.565	56.4	5.100	157.4	8.048
5.5	88.3	0.604	63.4	5.518	157.4	8.264
6.0	81.9	0.632	69.0	5.516	157.7	7.964
6.5	75.3	0.662	75.3	5.483	158.3	7.626
7.0	69.9	0.693	81.5	5.502	157.7	7.378

TABLE XI

POWER = 1.65 A X 3.45 KV
GAS FLOW RATE = 0.830 G/S
SPHERE DIAMETER = 2.2 MM

Z	H	TO	RE_∞	NU_∞	RE_D	NU_c
1.0	195.5	0.504	14.0	3.150	48.2	5.453
1.5	195.4	0.507	14.2	3.171	48.3	5.465
2.0	198.6	0.514	14.6	3.268	48.3	5.569
2.5	195.7	0.519	14.9	3.267	48.7	5.525
3.0	194.3	0.525	15.3	3.298	48.8	5.522
3.5	191.9	0.533	15.7	3.323	48.8	5.500
4.0	189.1	0.546	16.6	3.390	49.2	5.499
4.5	186.1	0.560	17.4	3.450	49.4	5.489
5.0	181.1	0.575	18.3	3.494	49.5	5.439
5.5	183.6	0.604	19.9	3.763	49.3	5.635
6.0	168.5	0.623	21.3	3.663	50.0	5.349
6.5	158.4	0.653	23.3	3.714	50.2	5.226
7.0	147.4	0.678	24.9	3.704	50.1	5.053
7.5	130.0	0.693	26.0	3.446	50.4	4.621
8.0	116.6	0.707	26.6	3.250	49.7	4.289

TABLE XII

POWER = 1.65 A X 3.45 KV

GAS FLOW RATE = 0.830 G/S

SPHERE DIAMETER = 3.3 MM

Z	H	TO	RE_∞	NU_∞	RE_o	NU_o
1.0	142.1	0.477	21.0	3.436	79.7	6.210
1.5	141.5	0.480	21.3	3.445	79.9	6.201
2.0	141.9	0.486	21.8	3.504	80.2	6.245
2.5	141.2	0.491	22.4	3.536	80.7	6.246
3.0	139.5	0.497	23.0	3.554	80.9	6.218
3.5	137.1	0.504	23.6	3.562	81.0	6.164
4.0	139.6	0.520	24.9	3.754	80.8	6.337
4.5	140.2	0.535	26.1	3.898	80.5	6.436
5.0	139.1	0.551	27.4	4.025	80.2	6.483
5.5	138.7	0.578	29.8	4.263	80.1	6.611
6.0	131.8	0.600	32.0	4.298	80.3	6.468
6.5	125.8	0.631	34.9	4.425	80.1	6.400
7.0	120.7	0.660	37.4	4.548	79.0	6.342
7.5	104.3	0.673	39.1	4.149	79.8	5.699
8.0	89.0	0.682	39.9	3.721	79.5	5.055

TABLE XIII

POWER = 1.65 A X 3.45 KV

GAS FLOW RATE = 0.330 G/S

SPHERE DIAMETER = 5.6 MM

Z	H	TO	RE_∞	NU_∞	RE_ϕ	NU_ϕ
1.0	98.0	0.448	37.0	4.164	157.2	7.921
1.5	96.9	0.449	37.4	4.144	157.8	7.860
2.0	97.3	0.455	38.4	4.224	158.3	7.928
2.5	97.0	0.460	39.4	4.270	159.1	7.941
3.0	97.6	0.468	40.4	4.369	158.6	8.025
3.5	96.7	0.475	41.4	4.416	158.4	8.013
4.0	96.3	0.488	43.7	4.552	158.8	8.077
4.5	95.8	0.502	45.8	4.684	158.6	8.132
5.0	92.5	0.515	48.2	4.705	159.0	7.996
5.5	89.8	0.539	52.4	4.850	159.7	7.957
6.0	86.3	0.562	56.3	4.950	158.9	7.853
6.5	83.6	0.593	61.4	5.167	157.0	7.844
7.0	80.9	0.623	65.7	5.358	154.0	7.823
7.5	72.6	0.639	68.6	5.076	153.7	7.263
8.0	63.4	0.650	70.2	4.657	152.2	6.571

TABLE XIV

POWER = 1.70 A X 3.55 KV

GAS FLOW RATE = 0.720 G/S

SPHERE DIAMETER = 2.2 MM

Z	H	TO	RE_∞	NU_∞	RE_o	NU_o
1.0	209.0	0.514	15.3	3.406	50.8	5.800
1.5	208.5	0.518	15.5	3.428	50.8	5.805
2.0	206.8	0.522	15.8	3.440	50.9	5.787
2.5	203.9	0.526	16.1	3.433	51.1	5.741
3.0	200.3	0.531	16.4	3.423	51.4	5.683
3.5	199.1	0.538	17.0	3.468	51.7	5.691
4.0	195.9	0.546	17.5	3.488	51.9	5.657
4.5	189.6	0.556	18.3	3.470	52.7	5.553
5.0	182.8	0.564	18.9	3.434	53.1	5.430
5.5	177.4	0.574	19.6	3.432	53.1	5.347
6.0	165.0	0.584	20.3	3.308	53.5	5.088
6.5	156.5	0.596	21.0	3.260	53.2	4.930
7.0	142.9	0.610	21.8	3.122	53.2	4.638
7.5	131.6	0.624	22.5	3.013	52.7	4.395
8.0	124.8	0.641	23.2	2.996	51.6	4.277

TABLE XV

POWER = 1.70 A X 3.55 KV

GAS FLOW RATE = 0.720 G/S

SPHERE DIAMETER = 3.3 MM

Z	H	TO	RE_∞	NU_∞	RE_o	NU_o
1.0	146.1	0.484	23.0	3.573	84.9	6.383
1.5	145.4	0.487	23.3	3.587	85.0	6.376
2.0	145.7	0.492	23.7	3.635	84.9	6.410
2.5	146.2	0.497	24.1	3.693	84.8	6.456
3.0	145.7	0.503	24.6	3.736	84.8	6.471
3.5	146.9	0.512	25.4	3.840	84.8	6.500
4.0	147.1	0.521	26.3	3.927	84.8	6.613
4.5	147.5	0.533	27.5	4.047	85.2	6.693
5.0	145.4	0.544	28.4	4.098	85.2	6.673
5.5	138.1	0.552	29.4	4.009	85.6	6.450
6.0	131.3	0.563	30.5	3.949	85.7	6.252
6.5	123.5	0.574	31.5	3.858	85.4	6.010
7.0	119.1	0.593	32.8	3.903	84.0	5.930
7.5	110.5	0.607	33.8	3.797	82.9	5.658
8.0	101.1	0.622	34.8	3.639	81.8	5.323

TABLE XVI

POWER = 1.70 A X 3.55 KV
GAS FLOW RATE = 0.720 G/S
SPHERE DIAMETER = 5.6 MM

Z	H	TO	RF_∞	NU_∞	RE_o	NU_o
1.0	100.6	0.454	40.4	4.323	167.4	8.131
1.5	99.9	0.457	40.9	4.331	167.7	8.104
2.0	99.8	0.461	41.6	4.376	167.6	8.126
2.5	98.5	0.465	42.4	4.371	168.2	8.065
3.0	97.7	0.470	43.3	4.404	168.4	8.053
3.5	98.1	0.478	44.7	4.504	168.6	8.126
4.0	96.1	0.485	46.1	4.512	169.5	8.044
4.5	97.0	0.497	48.3	4.679	169.7	8.181
5.0	94.8	0.506	50.0	4.694	170.0	8.091
5.5	93.8	0.518	51.6	4.783	168.7	8.099
6.0	91.7	0.531	53.6	4.847	167.4	8.042
6.5	89.4	0.545	55.3	4.907	164.9	7.971
7.0	86.0	0.563	57.6	4.953	161.8	7.839
7.5	80.9	0.580	59.4	4.882	158.5	7.553
8.0	77.2	0.597	61.1	4.887	154.5	7.380

properties of the fluid. Comparison of the constant-property solution with the results of Woo (1970) and Dennis et al. (1973) indicated excellent agreement in the values of the calculated Nusselt number. These constant-property results can be correlated by the following equation, with a maximum error in the Nusselt number of less than 1% in the range 10<Re<100:

$$Nu = 2 + 0.473\ Pr^{m}\ Re^{0.552} \tag{33}$$

The exponent of the Prandtl number, m, was determined from Woo's results. m was found to be a function of the Reynolds number. In the ranges 0.2<Re<100 and 0.25<Pr<2, m can be expressed as:

$$m = 0.78\ Re^{-0.145} \tag{34}$$

with a maximum error of a few percents. In the range of 0.5<Pr<1 the error is less than 1%.

Equation (33) was assumed to apply to the variable-property case provided appropriate reference temperatures are used. The constant, 2, in Equation (33) is the limiting value of the Nusselt number at Re = 0. This constant was modified to include the effect of the temperature on the thermal conductivity, by integrating the energy equation at zero flow. Details of the derivation were presented in the numerical analysis chapter. A for variable-property transfer, therefore, becomes:

$$A = 2\ f_f \tag{35}$$

where $f_f = (T_g^{1+x} - T_s^{1+x})/[(1 + x)(T_g - T_s)\, T_f^x]$ (36)

T_f is the reference temperature at which the Nusselt number is evaluated.

Using Equation (33) the values of the reference temperatures for the thermal conductivity and kinematic viscosity which gave the best representation of the numerical results were found for the variable-property fluid. The reference temperature for the thermal conductivity was the surface temperature and $T_{0.19}$ for the kinematic viscosity, where:

$$T_{0.19} = T_s + 0.19\,(T_g - T_s) \tag{37}$$

In the ranges $10<Re_\infty<50$ and $0.25<T_0<1$, the error in the estimated Nusselt number when these two reference temperatures were used was of the order of one percent. The corresponding range of $Re_{0.19}$ was between 10 and 265.

The applicability of Equation (33) to the experimental results was tested using four different reference temperatures. The standard deviation was calculated for all of the points and for the individual spheres. The reference temperatures were: (a) free-stream temperature, (b) sphere surface temperature, (c) arithmetic mean film temperature and (d) surface temperature for evaluating the thermal conductivity and $T_{0.19}$ for the kinematic viscosity. The results of these tests are presented in Table XVII.

It can be seen from Table XVII that the reference temperatures

TABLE XVII

EFFECT OF REFERENCE TEMPERATURE ON THE ACCURACY OF HEAT TRANSFER EQUATION

Reference Temperature	Standard Deviation (% of Nu)			
	Overall	Small Sphere	Medium Sphere	Large Sphere
T_s	10.98	10.40	9.29	12.91
T_m	6.56	7.63	5.15	6.55
T_g	5.06	6.70	4.36	3.48
$T_s/T_{o.1}$	4.99	6.76	4.31	3.10

$T_s - T_{0.19}$ gave only marginally better correlation than T_g. The use of the mean temperature resulted in less accurate results, while large errors were encountered when the surface temperature was used. The reason for this can be found by examining Table XVIII, where the effect of the different reference temperatures on the calculated Nusselt number [Equation (33)] is shown for selected values of T_s/T_g and Re_∞. The results indicate that the discrepancy among the three reference temperatures becomes apparent only at low surface temperatures. In the Reynolds number and temperature ratio ranges of the experimental study ($10<Re_\infty<80$, $0.4<T_s/T_g<0.8$), the variations in the calculated Nusselt number [Equation (33)] caused by using the different reference temperatures are within 5% of the absolute value. Variations of this magnitude were within the range of experimental uncertainty, and thus it was not possible to determine the 'best' reference temperature using the experimental results only. However, the applicability of $T_s - T_{0.19}$ reference temperatures was confirmed, for heat transfer to cylinders. The heat transfer equation derived from numerical results gave results very similar to those reported in the literature, when these reference temperatures were used in the former.

Because of the influence of the surface temperature on the limiting Nusselt number, a plot of Nu vs. Re does not give a good representation of the experimental data, even if the Nusselt and the Reynolds numbers are evaluated at their respective reference temperatures. In Figures 3a, 30b and Figure 31, the parameter Nu-2f

TABLE XVIII

EFFECT OF REFERENCE TEMPERATURE ON CALCULATED NUSSELT NUMBER

Reynolds Number UD/ν_∞	$T_0 = T_s/T_g$	Nusselt Number, hD/K_∞		
		$T_f = T_g$	$T_f = T_m$	$T_f = T_s/T_{0.19}$
10	0.75	3.147	3.193	3.156
80	0.75	6.305	6.449	6.323
10	0.50	2.934	3.035	2.920
80	0.50	6.093	6.407	6.012
10	0.25	2.710	2.877	2.543
80	0.25	5.868	6.392	5.263

FIGURE 30 a & b

VARIATION OF THE PARAMETER

$Nu_o - 2f_o$ WITH $Re_{o\cdot ie}$

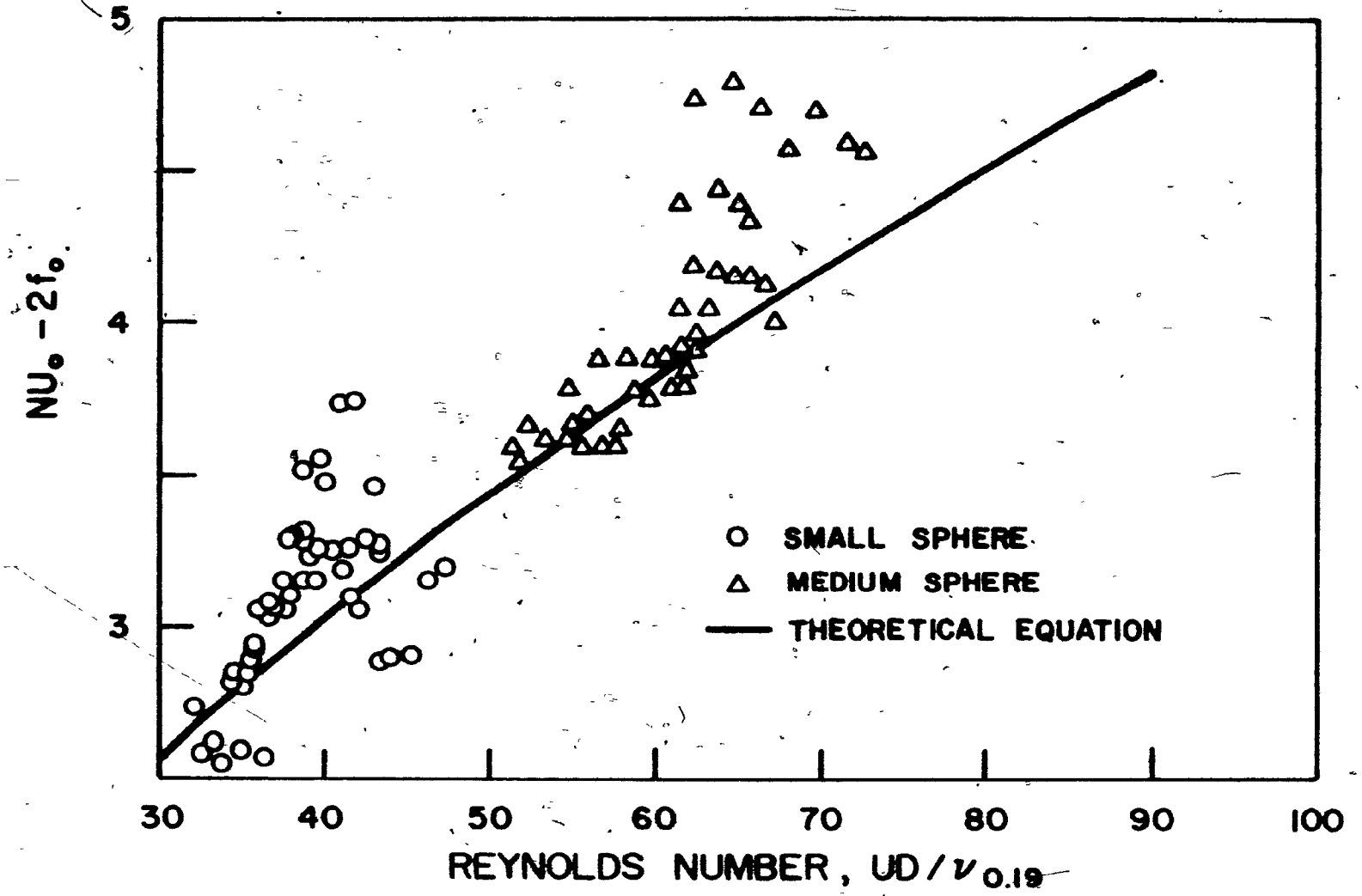
5
4
3
$Nu_o - 2f_o$
30
40
50
60
70
80
90
100
REYNOLDS NUMBER, $UD/\nu_{0.19}$
SMALL SPHERE
MEDIUM SPHERE
THEORETICAL EQUATION

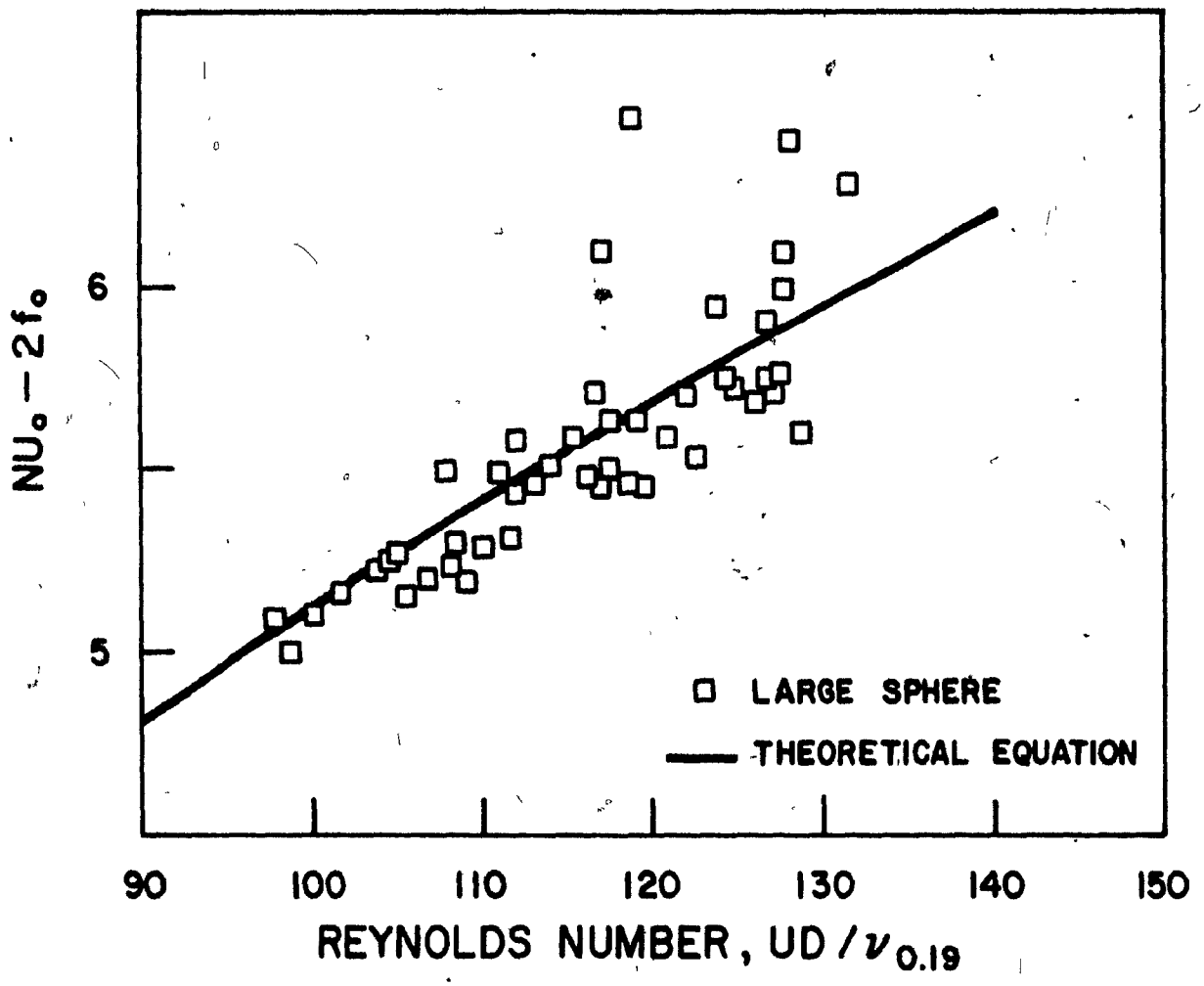
$NU_o - 2f_o$
6
5
LARGE SPHERE
THEORETICAL EQUATION
90
100
110
120
130
140
150
REYNOLDS NUMBER, $UD/\nu_{0.19}$

FIGURE 31

VARIATION OF THE PARAMETER

$Nu_\infty - 2f_\infty$ WITH Re_∞

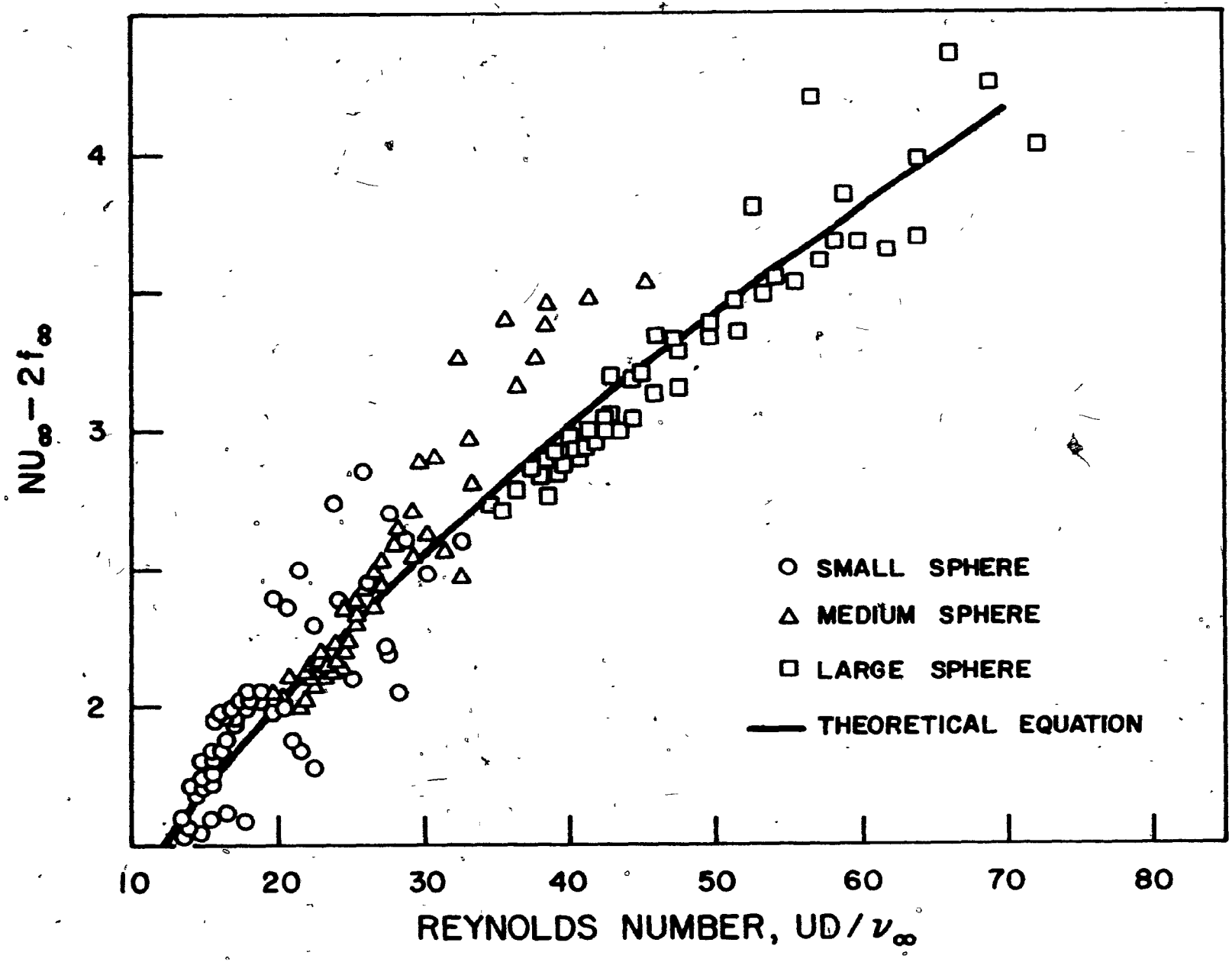
$NU_s - 2f_s$
4
3
2
10
20
30
40
50
60
70
80
REYNOLDS NUMBER, UD/ν_∞
SMALL SPHERE
MEDIUM SPHERE
LARGE SPHERE
THEORETICAL EQUATION

is plotted against the Reynolds number using the reference temperatures $T_s/T_{0.10}$ and T_g respectively. Figure 30 shows larger scatter of the data than Figure 31. The reason for this is that for the same flow conditions the ranges of Re_∞ and Nu_∞ are much smaller than of $Re_{0.10}$ and Nu_0, which tended to bring the points closer together in Figure 31.

In Figure 32 the values of the Nusselt number calculated from Equations (33) and (37), using experimental values of Re and T_0 are plotted against the experimental values of the Nusselt number. Nu_∞ was used in these plots for clarity as the values of Nu_0 were too close to each other. It can be seen that approximately 80% of the experimental points fall within ±5% of theoretical value.

Although it was not possible to determine from the experimental results which reference temperature gives the most accurate representation, the agreement of these results with the theoretical curve, as shown in Figure 32, confirms the accuracy of the other parameters in Equation (33), namely, A, B, m and n.

The scatter shown in Figures 30 and 31 could have been caused by two main factors: (a) errors introduced when interpreting the experimental measurements, and (b) errors caused by the presence of the sphere in the flow, thus changing the actual flow and temperature fields from those predicted. It should also be kept in mind that the experimental situation is rather difficult and that the stability of the induction-generated arc is not absolute.

FIGURE 32

COMPARISON OF EXPERIMENTAL

NUSSELT NUMBER WITH VALUES PREDICTED

BY EQUATIONS (33) AND (37)

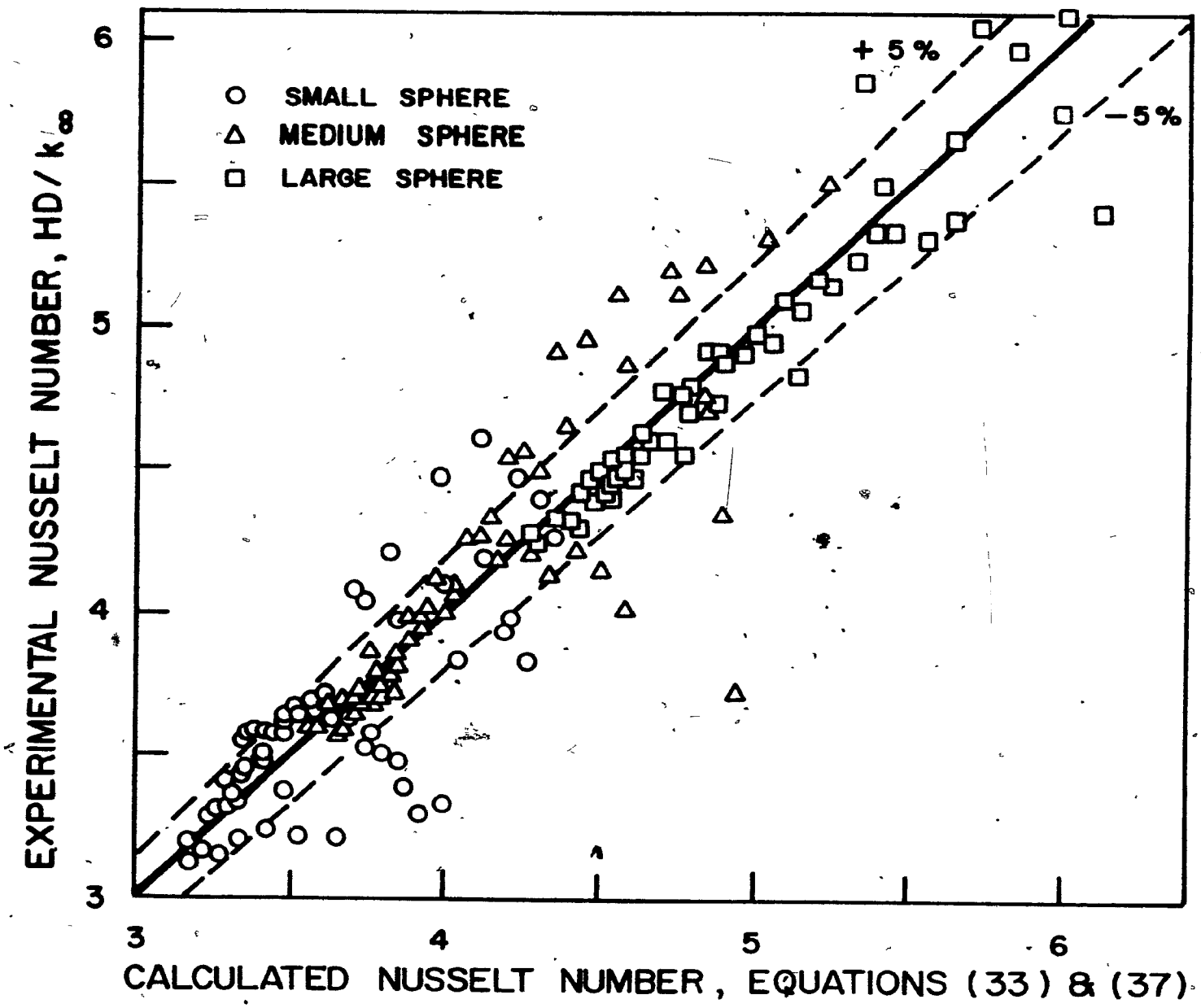
SMALL SPHERE
MEDIUM SPHERE
LARGE SPHERE
+5%
−5%
EXPERIMENTAL NUSSELT NUMBER, HD/k∞
CALCULATED NUSSELT NUMBER, EQUATIONS (33) & (37)
3
4
5
6

For the velocity measurements it was assumed that the effect of viscosity and temperature on C_p could be predicted from theoretical considerations. Errors introduced here due to uncertainties in C_p are small (within few percents). Since C_p was approximately 1.2 and U is proportional to the square root of C_p, the overall effect of C_p on the measured velocity is small. Another error may have been introduced in the velocity measurement, due to actual presence of the probe in the flow. This might have led to cooling down of the flow, thus changing its velocity. This effect was minimized by using the smallest practical size and by keeping the probe hot. Moreover, the disturbance of the flow by the probe was of a similar magnitude as that caused by the sphere.

Because of the finite size of the probe, the measured velocities were average velocities and not point velocities. This, however, was more desirable, since the spheres themselves were of a finite size.

The accuracy of the gas temperature determinations depended largely on two factors: the assumptions made in the heat balance and the values of h_w used. The assumptions have already been discussed in an earlier section. The values of the heat transfer coefficient were obtained from two correlations, one based on the work of Collis and Williams and the other derived from the numerical solution of heat transfer to cylinders. The latter was modified to include variable-property effects, by the use of reference temperatures. The

agreement between the two correlations was excellent. Consequently, it can be safely concluded that the values of h_w used were quite accurate.

One factor that might have led to scatter of the data in the lower sections of the chamber was the cooling effect of the sphere on the gas temperature, resulting in lower actual gas temperatures than those measured by the wire. In these sections, the temperature difference $(T_g - T_s)$ was small and very sensitive to slight changes in T_g, thus leading to appreciable errors in the values of h.

The surface emissivity influences radiation losses directly, and for the case when these are of the same magnitude as the convection transfer rates, errors in the emissivity values have large effect on the calculated heat transfer coefficients. In this study, data from several workers on the total hemispherical emissivity for both molybdenum and tungsten were examined and the reliable ones selected. These data were within a few percents of each other.

CONCLUSIONS

1. Heat transfer rates to stationary spheres were determined experimentally under high temperature conditions (5 000 K) and where temperature differences of the order of 2 000 K were present. The Reynolds number varied between 30 and 80.

2. The experimental results showed reasonable agreement with

the results of the numerical solution.

3. The effect of variable properties was accounted for by using a limiting Nusselt number that was a function of the temperature and by using reference temperatures for evaluating the fluid properties.

4. For argon, two sets of reference temperatures were found to correlate the results: (1) the gas temperature at free stream, and (2) T_s and $T_{0.19}$ to evaluate the thermal conductivity and kinematic viscosity, respectively. From the experimental results alone it was not possible to determine which of the two was more accurate. However, it was possible to obtain an excellent correlation for heat transfer to wires using the latter set. For design and engineering purposes, the use of T_s as the reference temperature is probably adequate, and offers the advantage of a somewhat easier computational approach.

NOMENCLATURE

A	-	Constant
B	-	Constant
Bi	-	Biot number
C_1	-	Constant, Equation (2)
C_2	-	Constant, Equation (2)
C_p	-	Pitot tube pressure coefficient, dimensionless
c	-	Speed of light
D	-	Diameter
dl	-	Increment of wire length
dT/dl	-	Temperature gradient along the wire
f	-	Effect of variable-properties on limiting Nusselt number defined in Equation (21)
g	-	Acceleration to the gravity
Gr	-	Grashoff number
h	-	Planck constant
h	-	Heat transfer coefficient, $J.m^{-2}.s^{-1}$
K	-	Boltzmann constant
k	-	Thermal conductivity of the fluid
k_{sphere}	-	Thermal conductivity of the sphere
k_w	-	Thermal conductivity of the wire

m	-	Exponent of Prandtl number
N_λ	-	Normal spectral radiance from a real body
$N_{\lambda,b}$	-	Normal spectral radiance from a black body
$N'_{\lambda,b}$	-	Normal spectral radiance from a black body equivalent to that from a real body
Nu	-	Nusselt number
n	-	Exponent on Reynolds number
P_t	-	Total pressure at stagnation point, dimensional
P_∞	-	Static pressure at stagnation point, dimensional
$P(\theta)$	-	Surface pressure distribution, dimensionless
$Q_{cond.}$	-	Conductive heat transfer rate
$Q_{cond.}$	-	Convective heat transfer rate
$Q_{gas.rad.}$	-	Rate of heat transfer by radiation from plasma
$Q_{rad.}$	-	Rate of heat transfer by radiation from plasma
R	-	Radius
Re	-	Reynolds number
T_b	-	Brightness temperature
T_{plasma}	-	Temperature of plasma core
U	-	Free-stream velocity
x	-	Property exponent

Greek Letters

α	-	Absorbitivity
β	-	Coefficient of volumetric expansion
Δ	-	Difference
ε	-	Total hemispherical emissivity

ϵ_λ - Spectral emissivity at wavelength, λ

Θ - Angle from front stagnation point

Θ_1° - Angle from front stagnation point that is subtended by the pressure probe bore

λ - Wavelength

μ - Viscosity

ν - Kinematic viscosity

ρ - Density

σ - Stephan-Boltzmann constant

Subscripts

f - Reference temperature condition

g - Bulk gas condition

m - Arithmetic mean film condition

s - Sphere surface condition

w - Wire surface condition

∞ - Free-stream condition

$_{0.19}$ - Reference condition at $T_{0.19}$

REFERENCE

Branstetter, J.R., "Some Practical Aspects of Surface Temperature Measurement by Optical Pyrometers", NASA TN-D3604, 1966

Chue, S.H., "Pressure Probes for Fluid Measurement", Prog.Aerospace Sci. 16 (2), 147 (1975)

Collis, D.C. and Williams, M.J., "Two-Dimensional Convection from Heated Wires at Low Reynolds Numbers", J. Fluid Mech. 6, 357 (1959)

Dennis, S.C.R., Walker, J.D.A. and Hudson, J.D., "Heat Transfer from a Sphere at Low Reynolds Numbers", J. Fluid Mech. 60 (2), 273 (1973)

Incropera, F.P. and Leppert, G., "Flow Transition Phenomena in a Subsonic Plasma Jet", AIAA Journal 4 (6), 1087 (1966)

International Critical Tables, Nat. Res. Council (U.S.A.), McGraw Hill, 1926

Kovalev, I.I. and Muchnik, G.F., "Normal Spectral Emissive Power of Tungsten, Niobium, Molybdenum and Tantalum ...", High Temp. 8 (5), 922 (1970)

Latyev, L.N., Chekhovskoi, V. Ya. and Shestakov, E.N., "Experimental Determination of Emissive Power of Tungsten in the Visible Region ...", High Temp. 7 (4), 610 (1969)

Logunov, A.V. and Kavolev, A.I., "Combined Determination of Thermal Conductivity, Electrical Resistance, and Emissivity on a Single Specimen at Temperatures of More Than 1 000°C", High Temp. 7 (4), 617 (1969)

Makarenko, I.N., Trukhanova, L.N. and Filippov, L.P., "Thermal Properties of Molybdenum at High Temperatures", High Temp. 8 (2), 416 (1970)

Moskvin, Yu. V., "Emissivity of Some Gases at High Temperatures of 6 000 - (2 000) - 12 000 K", High Temp. 6 (1), 1 (1968)

Pei, D.C.T., "Heat Transfer from Spheres Under Combined Forced and Natural Convection", C.E.P. Symp. Ser. 61 (59), 57 (1965)

Peletskii, V.E. and Druzhinin, V.P., "Experimental Determination of Integral Hemispherical Emissivity of Molybdenum at High Temperatures", High Temp. 7 (1), 60 (1969)

Richardson, P.D., "Convection from Heated Wires at Moderate and Low Reynolds Numbers", AIAA Journal 3 (3), 537 (1965)

Sadykov, B.S., "Temperature Dependence of the Radiating Power of Metals", High Temp. 3 (3), 352 (1965)

Woo, S.E., "Simultaneous Free and Forced Convection Around Submerged Cylinders and Spheres" Ph.D. Thesis, McMaster University, Hamilton, 1970

CONTRIBUTIONS TO KNOWLEDGE

1. The finite-difference technique was applied successfully to the solution of the coupled momentum and energy equations for flow past a sphere where large variations in the physical properties exist.

2. Flow and temperature fields, drag coefficients and the Nusselt number were calculated for surface temperatures to gas temperature ratios between 0.25 and unity and for Reynolds numbers between 0.1 and 50.

3. Experimental measurements of heat transfer to spheres confirmed the predictions of the numerical solution.

4. A correlation was derived for heat transfer to a single sphere which took into consideration the presence of large variations in the fluid properties.

SUGGESTION FOR FUTURE WORK

1. Devise new measurement techniques for determining gas velocities and temperatures more reliably in the temperature range between 2 000 and 5 000 K.

2. Study the effect of intense mass efflux from the surface of the sphere on the overall heat transfer rate. These results on the effects of superimposed mass transfer will find wide applicability in powder processing where evaporation or surface reaction accompanied by the evolution of a gaseous product is present.

3. Confirm experimentally the effects of large temperature gradients on the fluid flow phenomena past a sphere (principally, on the value of the overall drag coefficient) for comparison with those predicted theoretically in the present work.

APPENDIX A

FINITE-DIFFERENCE APPROXIMATIONS

DIFFERENCE FORMULAE

First Derivative

Central-difference :

$$dy_i/dx = (y_{i+1} - y_{i-1})/2h + 0(h^2) \qquad \text{(A-1)}$$

Forward-difference :

$$dy_i/dx = (-y_{i+2} + 4y_{i+1} - 3y_i)/2h + 0(h^2) \qquad \text{(A-2)}$$

Backward-difference :

$$dy_i/dx = (y_{i-2} - 4y_{i-1} + 3y_i)/2h + 0(h^2) \qquad \text{(A-3)}$$

Second Derivative

Central-difference :

$$d^2y_i/dx^2 = (y_{i+1} - 2y_i + y_{i-1})/h^2 + 0(h^2) \qquad \text{(A-4)}$$

$$\partial^2 y_i/\partial x \partial z = (y_{i+1,j+1} + y_{i-1,j-1} - y_{i-1,j+1} - y_{i+1,j-1})/4h_x h_z + 0(h^2) \qquad \text{(A-5)}$$

Forward-difference :

$$d^2y_i/dx^2 = (-y_{i+3} + 4y_{i+2} - 5y_{i+1} + 2y_i)/h^2 + 0(h^2) \qquad \text{(A-6)}$$

When $dy_i/dx = 0$:

$$d^2y_i/dx^2 = (8y_{i+1} - y_{i+2} - 7y_i)/2h^2 + 0(h^2) \qquad \text{(A-7)}$$

Backward-difference :

$$d^2y_i/dx = (y_{i-3} - 4y_{i-2} + 5y_{i-1} - 2y_i)/h^2 + 0(h^2) \qquad \text{(A-8)}$$

DIFFERENCE FORM OF FUNCTIONS Σ AND Γ

The velocity components are defined as:

$$v_r(I,J) = -T(I,J)[\Psi(I+1,J) - \Psi(I-1,J)]/(2Br^2 \sin\Theta) \quad (A-9)$$

$$v_\Theta(I,J) = T(I,J)[\Psi(I,J+1) - \Psi(I,J-1)]/(2Ar^2 \sin\Theta) \quad (A-10)$$

Also, $$\partial v_r(I,J)/\partial z = [v_r(I,J+1) - v_r(I,J-1)]/2A \quad (A-11)$$

$$\partial v_r(I,J)/ = [v_r(I+1,J) - v_r(I-1,J)]/2B \quad (A-12)$$

The derivatives of the functions $\underline{v}_\Theta$ and $\underline{T}$ can be written in a similar form to Equations (A-11) and (A-12). In a simplified form, the difference approximation of Σ is:

$$\Sigma(I,J) = 2x\, T(I,J)^{x-1}\{\partial T/\partial\Theta[v_r(I,J) \cdot \partial^2 v_r/\partial z^2 - \partial^2 v_\Theta/\partial z\partial\Theta - \cot\Theta(\partial v_\Theta/\partial z - v_\Theta(I,J))] + \partial T/\partial z\,[\partial v_r/\partial z\partial\Theta + \partial v_r/\partial\Theta + \partial^2 v_\Theta/\partial\Theta^2 - \partial v_\Theta/\partial z + \cot\Theta\,(\partial v_\Theta/\partial\Theta - \cot\Theta\, v_\Theta(I,J))] + (x-1)/T(I,J)\,[\partial^2 T/\partial z^2(\partial v_r/\partial\Theta - v_\Theta(I,J)) - \partial^2 T/\partial\Theta^2 \cdot \partial v_\Theta/\partial z + \partial^2 T/\partial z\partial\Theta(\partial v_\Theta/\partial\Theta + v_r(I,J) - \partial v_r/\partial z)]\} \quad (A-13)$$

and $$\Gamma(I,J) = -1/T(I,J)^2\,\{\partial T/\partial z[v_r(I,J)\cdot\partial v_r/\partial\Theta + v_\Theta(I,J)\partial v_\Theta/\partial\Theta] - \partial T/\partial\Theta[v_r(I,J)\partial v_r/\partial z + v_\Theta(I,J)\partial v_\Theta/\partial z]\} \quad (A-14)$$

BOUNDARY CONDITIONS

At z = 0:

$$\zeta = \partial v_\theta/\partial z = \partial/\partial z\ (1/\rho r^2 \sin\theta\ \partial\Psi/\partial z) \qquad \text{(A-15)}$$

$$\zeta = \partial\Psi/\partial z\ (\partial(1/\rho r^2 \sin\theta)/\partial z + 1/\rho r^2 \sin\theta\ \partial^2\Psi/\partial z^2$$

At the sphere surface $v_\theta = 0$ and consequently $\partial\Psi/\partial z$ is also zero. Therefore:

$$\zeta_o = 1/(\rho_o \sin\theta)\partial^2\Psi/\partial z^2 \qquad \text{(A-16)}$$

Substitution into Equation (A-7) gives:

$$\zeta(I,1) = T_o/\sin\theta.\,[8\Psi(I,2) - \Psi(I,3)]/2A^2 \qquad \text{(A-17)}$$

At $z = z_\infty$:

$$\partial T/\partial\theta = 0 \qquad \text{(A-18)}$$

From Equation (A-2):

$$\partial T(1,J)/\partial\theta = [-T(3,J) + 4T(2,J) - 3T(I,J)]/2B \qquad \text{(A-19)}$$

or
$$T(1,J) = [4T(2,J) - T(3,J)]/3 \qquad \text{(A-20)}$$

$$v_r(1,J) = -1/\rho r^2\ \partial^2\Psi/\partial\theta^2 \qquad \text{(A-21)}$$

Using central-difference approximation [Equation (A-4)],

$$\partial^2\Psi/\partial\theta^2 = [\Psi(2,J) - 2\Psi(1,J) + \Psi(0,J)]/B^2 \qquad \text{(A-22)}$$

From the condition of symmetry around the axis, $\Psi(0,J) = \Psi(2,J)$, and Equation (A-22) becomes:

$$\partial^2\Psi/\partial\Theta^2 = 2\Psi(2,J)/B^2 \qquad \text{(A-23)}$$

and $$v_r(1,J) = -2T(1,J)\ \Psi(2,J)/B^2r^2 \qquad \text{(A-24)}$$

Also $$F(1,J) = 1/r\ \partial\zeta/\partial\Theta \qquad \text{(A-25)}$$

$$\partial\zeta/\partial\Theta = [\zeta(2,J - \zeta(0,J)]/2B \qquad \text{(A-26)}$$

$$\zeta(0,J) = \zeta(2,J)$$

Therefore:

$$F(1,J) = 1/r\ \zeta(2,J)/B \qquad \text{(A-27)}$$

The boundary conditions at $\Theta=\pi$ can be derived in a similar manner.

APPENDIX B

DERIVATION OF DRAG COEFFICIENT EQUATIONS

STAGNATION PRESSURE

The r-component of the Navier-Stokes equation [Numerical Analysis, Equation (2)] can be written as:

$$\partial p/\partial r = \mu[4/3\partial\nabla.\bar{v}/\partial r - 1/r\ \partial\zeta/\partial\theta - \cot\theta\ \zeta/r] + \partial\mu/\partial\theta[1/r\ \partial v_\theta/\partial r - v_\theta/r^2 + 1/r^2\ \partial v_r/\partial\theta] + \partial\mu/\partial r[2\partial v_r/\partial r - 2/3\ \nabla.\bar{v}] - \rho[v_r\partial v_r/\partial r + v_\theta/r\ \partial v_r/\partial\theta - v^2{}_\theta/r] \quad (B\text{-}1)$$

Along $\theta = 0°$:

$$\zeta = 0 \qquad \partial T/\partial\theta = 0 \qquad v_\theta = 0$$

By taking limits $\zeta\cot\theta = \partial\zeta/\partial\theta$ and since μ = constant xT^x, then $\partial\mu/\partial\theta$ is also zero. Equation (B-1) thus simplifies to

$$dp/dr|_{\theta=0} = \mu[4/3\ \partial\nabla.\bar{v}/\partial r - 2/r\ \partial\zeta/\partial\theta] + \partial\mu/\partial r\ [2\partial v_r/\partial r - 2/3\ \nabla.\bar{v}] - \rho v_r\partial v_r/\partial r \quad (B\text{-}2)$$

From the continuity equation:

$$\rho\nabla.\bar{v} = -\bar{v}.\nabla\rho \quad (B\text{-}3)$$

or

$$\nabla.\bar{v} = -1/\rho(v_r\partial\rho/\partial r + v_\theta/r\ \partial\rho/\partial\theta) \quad (B\text{-}4)$$

At the axis, Equation (B-4) simplifies to:

$$\nabla.\bar{v} = -1/\rho\, v_r\, \partial\rho/\partial r \qquad \text{(B-5)}$$

Similarly,

$$\partial\nabla.\bar{v}/\partial r = \nabla.\bar{v}[\partial v_r/\partial r)/v_r + (\partial^2\rho/\partial r^2)/(\partial\rho/\partial r) - (\partial\rho/\partial r)/\rho] \qquad \text{(B-6)}$$

In dimensionless variables [$p' = (p - p_\infty)/(\rho_\infty U_\infty^2/2)$],

$$dp/dz = -8/Re\ \{\mu[\partial\zeta/\partial\Theta - 2/3\ \partial\nabla.\bar{v}/\partial z] + \partial\mu/\partial z[\nabla.\bar{v}/3 - 1/r\ \partial v_r/\partial z]\} - 2\rho v_r \partial v_r/\partial z \qquad \text{(B-7)}$$

where $$\nabla.\bar{v} = v_r/rT\ \partial T/\partial z \qquad \text{(B-8)}$$

and $$\partial\nabla.\bar{v}/\partial z = \nabla.\bar{v}[\partial v_r/\partial z)/v_r + (\partial^2 T/\ z^2)/(\partial T/\partial z) - (\partial T/\partial z)/T -)] \qquad \text{(B-9)}$$

$$\int_0^\infty (dp/dz)dz = p_\infty - p_o \qquad \text{(B-9)}$$

In dimensionless variables, $p_\infty = 0$. Therefore,

$$p_o = -\int_0^\infty (dp/dz)\, dz$$

or

$$p_o = 8/Re \int_0^{z_\infty} \{\mu[\partial\zeta/\partial\Theta - 2/3\ \partial\nabla.\bar{v}/\partial z] + \partial\mu/\partial z[\nabla.\bar{v}/3 - 1/r\partial v_r/\partial z]\}\, dz + 2\int_0^{z_\infty} [\rho v_r \partial v_r/\partial z]\, dz \qquad \text{(B-10)}$$

For constant properties, Equation (B-10) reduces to:

$$p_o = 8/Re \int_0^{z^\infty} (\partial\zeta/\partial\theta)\, dz + [v_r^2]_0^\infty$$

$$p_o = 8/Re \int_0^{z^\infty} (\partial\zeta/\partial\theta)\, dz + 1 \qquad \text{(B-11)}$$

SURFACE PRESSURE DISTRIBUTION

The θ-component of the Navier-Stokes equation [Numerical Analysis, Equation (3)] can be written as:

$$\partial p/\partial\theta = \mu[4/3\partial\nabla.\bar{v}/\partial\theta + r\,\partial\zeta/\partial r + \zeta] + \partial\mu/\partial r\,[\zeta r - 2v_\theta + 2\,\partial v_r/\partial\theta] + \partial\mu/\partial\theta\,[2/r\,\partial v_\theta/\partial\theta + 2v_r/r - 2/3\,\nabla.\bar{v}] - \rho r\,[v_r\,\partial v_\theta/\partial r + v_\theta/r\,\partial v_\theta/\partial\theta + v_r v_\theta/r] \qquad \text{(B-12)}$$

At the sphere surface the temperature is constant. Therefore $\partial\mu/\partial\theta = 0$. Also:

$$v_r = v_\theta = 0$$

$$\partial v_r/\partial\theta = \partial v_\theta/\partial\theta = 0$$

Equation (B-12) thus becomes:

$$dp/d\theta\big|_{r=R} = \mu\,[4/3\,\partial\nabla.\bar{v}/\partial\theta + r\partial\zeta/\partial r + \zeta] + \partial\mu/\partial r\,(\zeta r) \qquad \text{(B-13)}$$

$$\nabla.\bar{v} = -1/\rho v.\nabla\rho = -1/\rho\,(v_r\partial\rho/\partial r + v_\theta/r\,\partial\rho/\partial\theta)$$

$$\partial V.\bar{v}/\partial\theta = 1/\rho\ (\partial v_r/\partial\theta\partial\rho/\partial r + v_r\partial^2\rho/\partial r\partial\theta + 1/r\ \partial v_\theta/\partial\theta\ \partial\rho/\partial\theta + v_\theta/r\ \partial^2\rho/\partial\theta) + 1/\rho^2\partial\rho/\partial\theta\ (v_r\partial\rho/\partial r + v_\theta/r\ \partial\rho/\partial\theta) \quad \text{(B-14)}$$

All the terms in Equation (B-14) are equal to zero. In dimensionless variables Equation (13) can be written as:

$$dp/d\theta = 4T_o^x/Re\ [\partial\zeta/\partial z + \zeta + \zeta\ x/T\ \partial T/\partial z] \quad \text{(B-15)}$$

and

$$p(\theta) = p_o + 4T_o^x/Re \int_0^\theta [\partial\zeta/\partial z + \zeta\ (1 + x/T\ \partial T/\partial z)\ d\theta \quad \text{(B-16)}$$

For constant properties:

$$p(\theta) = p_o + 4/Re \int_0^\theta (\partial\zeta/\partial z + \zeta)\ d\theta \quad \text{(B-17)}$$

DRAC COEFFICIENT

The components of the drag force on a sphere are defined as [Numerical Analysis, Equations (53) and (54)]:

$$C_{Dp} = (F_n - F_s)/[\pi R^2\rho_\infty U_\infty^2/2] \quad \text{(B-18)}$$

$$C_{DF} = F_t/[\pi R^2\rho_\infty U_\infty^2/2] \quad \text{(B-19)}$$

where

$$F_n = \int_0^{2\pi}\int_0^\pi [p|_{r=R}\cos\theta]\ R^2\sin\theta\ \partial\theta\ \partial\phi \quad \text{(B-20)}$$

$$F_s = \int_0^{2\pi}\int_0^\pi [p_\infty|_{r=R}\cos\theta]\ R^2\sin\theta\ \partial\theta\ \partial\phi \quad \text{(B-21)}$$

$$F_t = \int_0^{2\pi}\int_0^\pi \{\mu[r\partial/\partial r(v_\theta/r) + 1/r\partial v_r/\partial\theta]|_{r=R}\sin\theta\}\sin\theta\ \partial\theta\ \partial\phi \quad \text{(B-22)}$$

For axisymmetric flow:

$$F_n - F_s = \pi R^2 \int_0^{\pi} (p - p_\infty) \sin 2\theta \, \partial\theta \qquad \text{(B-23)}$$

and

$$F_t = 2\pi R^2 \int_0^{\pi} \mu \, [\partial v_\theta / \partial r] \sin^2\theta \, \partial\theta \qquad \text{(B-24)}$$

From Equation (14) (Numerical Analysis):

$$\zeta = \partial v_\theta / \partial r + v_\theta / r - 1/r \, \partial v_r / \partial\theta \qquad \text{(B-25)}$$

At the surface, Equation (B-25) becomes:

$$\zeta = \partial v_\theta / \partial r \qquad \text{(B-26)}$$

and (B-24) reduces to:

$$F_t = 2\pi R^2 \int_0^{\pi} \mu\zeta \sin^2\theta \, \partial\theta \qquad \text{(B-27)}$$

Substitution into Equations (B-18) and (B-19) gives:

$$C_{DP} = \int_0^{\pi} (p - p_\infty)/(\rho_\infty U_\infty^2/2) \sin 2\theta \, \partial\theta \qquad \text{(B-28)}$$

$$C_{DF} = 4\mu/\rho_\infty U_\infty^2 \int_0^{\pi} \sin^2\theta \, \partial\theta \qquad \text{(B-29)}$$

In dimensionless variables:

$$C_{DP} = \int_0^{\pi} p(\theta) \sin 2\theta \, \partial\theta \qquad \text{(B-30)}$$

$$C_{DF} = 8/Re \, \mu_o \int_0^{\pi} \zeta_o \sin^2\theta \, \partial\theta \qquad \text{(B-31)}$$

APPENDIX C

PROPERTIES OF ARGON

Temperature K	Density kg. m^{-3}	Viscosity $N.s.m^{-2} \times 10^4$	Thermal Conductivity $J.m^{-1},s.^{-1} \times 10^2$
1000	0.487	0.541	4.23
1500	0.324	0.708	5.52
2000	0.243	0.886	6.90
2500	0.195	1.05	8.20
3000	0.162	1.21	9.46
3500	0.139	1.37	10.71
4000	0.122	1.53	11.92
4500	0.108	1.68	13.10
5000	0.0973	1.83	14.29
5500	0.0885	1.97	15.36

APPENDIX D

LISTING OF COMPUTER PROGRAMMES

VARIABLE-PROPERTY FLOW

Pages D- 2 to D- 9

CONSTANT-PROPERTY FLOW

Pages D-10 to D-16

```
      DIMENSION SF(32,42),VOR(32,42),T(32,42),WV(32,42),WT(32,42)
      DIMENSION  F(32,42),G(32,42),VR(32,42),VT(32,42)
      DIMENSION P(42),P2(42),TH(32),ANG(32),SN(32),CS(32)
      DIMENSION CO(32),BP2(32),BM2(32)
      DIMENSION ALPHA(32),BETA(42),OMEGA(42),P(32),ANU(32)
      READ(5,50) RE,TO,A,N,M
      READ(5,51) KKC,ACCL
      TOL=0.00001
      X=0.8
      XYZ=0.7
      PE=RE*0.672
      B=180./N
      WRITE(6,52) RE,PE,TO,X
      WRITE(6,56) A,B,N,M,TOL
      M1=M+1
      N1=N+1
      MI=M-1
      NI=N-1
      ANG(1)=0.
      DO 45 I=1,N
      ANG(I+1)=ANG(I)+B
   45 CONTINUE
      B=B/57.2957795
      A2=A*A
      B2=B*B
      AH=A*2.
      BH=B*2.
      TOX=TO**X
      AP2=(2.+A)/A2/2.
      AM2=(2.-A)/A2/2.
      COE=2./A2+2./B2
      A4B=4.*A*B
      A2B=A4B/2.
      BET=4.*TOX/RE
C
C
      DO 2 J=1,M1
      P(J)=EXP((J-1.)*A)
      P2(J)=P(J)*P(J)
    2 CONTINUE
C
      TH(1)=0.
      TH(2)=B
      DO 1 I=2,N
      TH(I+1)=TH(I)+B
      SN(I)=SIN(TH(I))
      CS(I)=COS(TH(I))
      CO(I)=CS(I)/SN(I)
      BP2(I)=(2.+CO(I)*B)/B2/2.
      BM2(I)=(2.-CO(I)*B)/B2/2.
    1 CONTINUE
      SN(1)=0.
      SN(N1)=0.
      CS(1)=1.
```

```
      CS(N1)=-1.
C
C
      READ(5,53)  (( SF(I,J),I=1,N1),J=1,M1)
      READ(5,53)  ((VOR(I,J),I=1,N1),J=1,M1)
      READ(5,53)  ((  T(I,J),I=1,N1),J=1,M1)
      DO 44 I=2,N
      DO 44 J=2,M
      G(I,J)=R(J)*SN(I)*VOR(I,J)*T(I,J)**X
      F(I,J)=VOR(I,J)/R(J)/SN(I)
   44 CONTINUE
C
C     BOUNDARY CONDITIONS
C
      DO 4 I=1,N1
      SF(I,M1)=0.5*(R(M1)*SN(I))**2
      SF(I,1)=0.
      VOR(I,M1)=0.
      T(I,1)=TO
      T(I,M1)=1.
      F(I,M1)=0.
      G(I,M1)=0.
      VR(I,1)=0.
      VR(I,M1)=-CS(I)
      VT(I,1)=0.
      VT(I,M1)=SN(I)
    4 CONTINUE
C
      DO 5 J=1,M1
      SF(1,J)=0.
      SF(N1,J)=0.
      VOR(1,J)=0.
      VOR(N1,J)=0.
      G(1,J)=0.
      G(N1,J)=0.
      VT(1,J)=0.
      VT(N1,J)=0.
    5 CONTINUE
C
C     CALCULATION OF RELAXATION COEFF.
C
      DO 6 I=2,N
      DO 6 J=2,M
      DSR=(SF(I,J+1)-SF(I,J-1))/AH
      DST=(SF(I+1,J)-SF(I-1,J))/BH
      SQ=SQRT(2.*(DSR*DSR+DST*DST))
      RES=ABS(RE/R(J)/SN(I)/4.)
      WV(I,J)=1./(1.+RES*SQ)
      PES=RES*0.672
      WT(I,J)=1./(1.+PES*SQ)
      VR(I,J)=-DST*T(I,J)/R2(J)/SN(I)
      VT(I,J)= DSR*T(I,J)/R2(J)/SN(I)
    6 CONTINUE
      WS=1./(1.+3.1416/N1)
```

```
C
CC      BOUNDARY CONDITIONS FOR VORTICITY AT THE SURFACE
C
        DO 9 I=2,N
        VOR(I,1)=(8.*SF(I,2)-SF(I,3))/(2.*A2*SN(I))*TQ
        G(I,1)=VOR(I,1)*SN(I)*TOX
        F(I,1)=VOR(I,1)/SN(I)
    9 CONTINUE
      WRITE(6,54) (VOR(I,1),I=1,N1,3)
C
CC      CALCULATING B.C.'S ALONG THE SYMMETRY AXIS
C
        DO 28 J=2,M
        T(1,J)=(4.*T(2,J)-T(3,J))/3.
        T(N1,J)=(4.*T(N,J)-T(NI,J))/3.
        F(1,J)=VOR(2,J)/R(J)/B
        F(N1,J)=-VOR(N,J)/R(J)/B
        VR(1,J)=-2.*T(1,J)*SF(2,J)/B2/R2(J)
        VR(N1,J)=2.*T(N1,J)*SF(N,J)/B2/R2(J)
   28 CONTINUE
C
CC      RELAXATION STARTS HERE
C
        I1=0
        I2=0
        JJ=0
        KK=0
        ACC=1.
    7 CONTINUE
        ERR=0.
        JJ=JJ+1
        KK=KK+1
        IF(KK.NE.KKC) GO TO 8
        KK=0
        ACC=ACCL
    8 CONTINUE
C
CC      CALC OF GRID POINTS STARTS HERE
C
        DO 25 I=2,N
        IF(I1.EQ.1) GO TO 12
        I1=1
        J1=1
        GO TO 11
   12 CONTINUE
        I1=0
        J1=0
   11 CONTINUE
        DO 25 J=2,M
        IF(J1.EQ.0) GO TO 13
        J1=0
        GO TO 14
   13 J1=1
        GO TO 25
```

```
 14 CONTINUE
    TEX=T(I,J)**X
    TI=1./T(I,J)
    RS=R(J)*SN(I)
    RERS=RE*RS/4.
    PERS=0.5*PE/RS
    DSR=(SF(I,J+1)-SF(I,J-1))/AH
    DST=(SF(I+1,J)-SF(I-1,J))/BH
    DTR=( T(I,J+1)- T(I,J-1))/AH
    DTT=( T(I+1,J)- T(I-1,J))/BH
    VRZ=(VR(I,J+1)-VR(I,J-1))/AH
    VTZ=(VT(I,J+1)-VT(I,J-1))/AH
    VRT=(VR(I+1,J)-VR(I-1,J))/BH
    VTT=(VT(I+1,J)-VT(I-1,J))/BH
    VR2Z=(VR(I,J+1)-2.*VR(I,J)+VR(I,J-1))/A2
    DT2Z=( T(I,J+1)-2.* T(I,J)+ T(I,J-1))/A2
    VT2T=(VT(I+1,J)-2.*VT(I,J)+VT(I-1,J))/B2
    DT2T=( T(I+1,J)-2.* T(I,J)+ T(I-1,J))/B2
    VRZT=(VR(I+1,J+1)+VR(I-1,J-1)-VR(I-1,J+1)-VR(I+1,J-1))/A4B
    VTZT=(VT(I+1,J+1)+VT(I-1,J-1)-VT(I-1,J+1)-VT(I+1,J-1))/A4B
    DTZT=( T(I+1,J+1)+ T(I-1,J-1)- T(I-1,J+1)- T(I+1,J-1))/A4B
    SIG=X*TEX*TI*(DTT*(VR(I,J)-VR2Z-VTZT-CO(I)*(VTZ-VT(I,J)))+
   1               DTR*(VRZT+VRT+VT2T-VTZ+CO(I)*(VTT-VT(I,J)*CO(I)))
   2              +(X-1.)*TI*(DT2Z*(VRT-VT(I,J))-DT2T*VTZ
   3              +DTZT*(VTT+VR(I,J)-VRZ)))
    GAMMA=-TI*TI*(DTR*(VR(I,J)*VRT+VT(I,J)*VTT)
   1             -DTT*(VR(I,J)*VRZ+VT(I,J)*VTZ))
    W=2.*(SIG*SN(I)-RERS*GAMMA)
    AV=G(I,J+1)*AM2+G(I,J-1)*AP2+G(I+1,J)*BM2(I)+G(I-1,J)*BP2(I)
   1          -COF*G(I,J)+RERS*(DST*(F(I,J+1)-F(I,J-1))/A-
   2                            DSR*(F(I+1,J)-F(I-1,J))/B)+W
    AV=AV/COF
    AS=SF(I,J+1)*AM2+SF(I,J-1)*AP2+SF(I+1,J)*BM2(I)+SF(I-1,J)*BP2(I)
   1     -COF*SF(I,J)-(G(I,J)*R2(J)/TEX-DTR*DSR-DTT*DST)*TI
    AS=AS/COF
    AT=T(I,J+1)*AP2+T(I,J-1)*AM2+T(I+1,J)*BP2(I)+T(I-1,J)*BM2(I)
   1          -COF*T(I,J)+X*TI*(DTR*DTR+DTT*DTT)
   2          +PERS/TEX*(DST*DTR-DSR*DTT)
    AT=AT/COF
    IF(AV.LT.ERR) GO TO 29
    ERR=AV
 29 IF(AT.LT.ERR) GO TO 10
    ERR=AT
 10 CONTINUE
    IF(I2.EQ.1) GO TO 15
    SF(I,J)=SF(I,J)+ACC*WS*AS
    G(I,J)=G(I,J)+ACC*WV(I,J)*AV*XYZ
    T(I,J)=T(I,J)+ACC*WT(I,J)*AT
    VOR(I,J)=G(I,J)/RS/TEX
    F(I,J)=VOR(I,J)/RS
    GO TO 25
 15 CONTINUE
    SF(I,J)=SF(I,J)+AS
    G(I,J)=G(I,J)+AV*XYZ
```

```
      T(I,J)=T(I,J)+AT
      VOR(I,J)=G(I,J)/RS/TEX
      F(I,J)=VOR(I,J)/RS
   25 CONTINUE
      IF(I2.EQ.0) GO TO 15
      I1=0
      I2=0
      GO TO 17
   16 I1=1
      I2=1
      GO TO 8
   17 CONTINUE
C
      DO 23 I=2,N
      DO 23 J=2,M
      DSR=(SF(I,J+1)-SF(I,J-1))/AH
      DST=(SF(I+1,J)-SF(I-1,J))/BH
      VP(I,J)=-DST*T(I,J)/R2(J)/SN(I)
      VT(I,J)= DSR*T(I,J)/R2(J)/SN(I)
   23 CONTINUE
C
C     BOUNDARY CONDITION FOR VORTICITY AT THE SURFACE
C
      DO 27 I=2,N
      VOR(I,1)=(8.*SF(I,2)-SF(I,3))/(2.*A2*SN(I))*TO
      G(I,1)=VOR(I,1)*SN(I)*TOX
      F(I,1)=VOR(I,1)/SN(I)
   27 CONTINUE
      WRITE(6,54) (VOR(I,1),I=1,N1,3),ERR
C
C     CALCULATING B.C.'S ALONG THE SYMMETRY AXIS
C
      DO 26 J=2,M
      T(1,J)=(4.*T(2,J)-T(3,J))/3.
      T(N1,J)=(4.*T(N,J)-T(N1,J))/3.
      F(1,J)=VOR(2,J)/R(J)/B
      F(N1,J)=-VOR(N,J)/R(J)/B
      VP(1,J)=-2.*T(1,J)*SF(2,J)/B2/R2(J)
      VR(N1,J)=2.*T(N1,J)*SF(N,J)/B2/R2(J)
   26 CONTINUE
      ACC=1.
      IF((KK+1).EQ.KKC) GO TO 18
   19 CONTINUE
      IF(ERR.LT.TOL) GO TO 100
      IF(JJ.EQ.500) GO TO 109
      IF(ERR.GT.1.) GO TO 101
      GO TO 7
   18 CONTINUE
C
C     CALCULATION OF RELAXATION COEFF.
C
      DO 21 I=2,N
      DO 21 J=2,M
      DST=(SF(I+1,J)-SF(I-1,J))/BH
```

```
      DSR=(SF(I,J+1)-SF(I,J-1))/AH
      SQ=SQRT(2.*(DSR*DSR+DST*DST))
      RES=ABS(RE/R(J)/SN(I)/4.)
      WV(I,J)=1./(1.+RES*SQ)
      PES=RES*0.672
      WT(I,J)=1./(1.+PES*SQ)
   21 CONTINUE
  100 CONTINUE
C
C     CALC. OF THE DRAG COEF.
C
      DO 31 J=2,M
      VRZ=(VR(1,J+1)-VR(1,J-1))/AH
      DTR=(T(1,J+1)-T(1,J-1))/AH
      DT2Z=(T(1,J+1)-2.*T(1,J)+T(1,J-1))/A2
      VR2Z=(VR(1,J+1)-2.*VR(1,J)+VR(1,J-1))/A2
      OMEGA(J)=VR(1,J)*VRZ/T(1,J)
      GRAD=VR(1,J)*DTR/R(J)/T(1,J)
      DGRAD=GRAD*(VRZ/VR(1,J)+DT2Z/DTR-DTR/T(1,J)-1.)
      BETA(J)=T(1,J)**X*(VOR(2,J)/B-2.*DGRAD/3.
     1                   +X/T(1,J)*DTR*(GRAD/3.-VRZ/R(J)))
   31 CONTINUE
C
C     CALC BETA AT THE STAGNATION POINT
C
      VRZ=(-VR(1,3)+4.*VR(1,2))/AH
      DTR=(-T(1,3)+4.*T(1,2)-3.*TO)/AH
      BETA(1)=TOX*(VOR(2,1)/B-DTR*VRZ/TO*(2./3.+X))
      VRZ=(-1.-4.*VR(1,M))/AH
      BETA(M1)=-X*(T(1,M1)-4.*T(1,M)+3.)/AH*VRZ/R(M1)
C
C     EVALUATION OF STAGNATION PRESSURE. INTEGRATION BY SIMPSON'S RULE
C
      SUM=8./RE*(BETA(1)+BETA(M1))
      AA=32./RE
      DO 32 J=2,M,2
      SUM=SUM+8.*OMEGA(J)+AA*BETA(J)
   32 CONTINUE
      AA=0.5*AA
      DO 33 J=3,M1,2
      SUM=SUM+4.*OMEGA(J)+AA*BETA(J)
   33 CONTINUE
      P(1)=A*SUM/3.
C
C     CALC ALPHA ALONG THE SURFACE
C
      DO 34 I=2,N
      VORZ=(-VOR(1,3)+4.*VOR(I,2)-3.*VOR(I,1))/AH
      DTZ=(-T(I,3)+4.*T(I,2)-3.*TO)/AH
      ALPHA(I)=VORZ+VOR(I,1)*(1.+X/TO*DTZ)
   34 CONTINUE
      ALPHA(1)=0.
      ALPHA(N1)=0.
C
```

```
C       CALC OF PRESSURE AT THE SURFACE. INTEGRATION BY TRAPEZOIDAL
C
        FACT=R*RET/2.
        DO 35 I=2,N1
        P(I)=P(I-1)+FACT*(ALPHA(I)+ALPHA(I-1))
     35 CONTINUE
C
C       CALC OF THE DRAG COEFF'S. INTEGRATION BY SIMPSON'S RULE
C
        CDP=0.
        CDF=0.
        DO 36 I=2,N,2
        CDP=CDP+8.*P(I)*SN(I)*CS(I)+4.*P(I+1)*SN(I+1)*CS(I+1)
        CDF=CDF+VOR(I,1)*SN(I)*SN(I)+0.5*VOR(I+1,1)*SN(I+1)*SN(I+1)
     36 CONTINUE
        CDP=CDP*B/3.
        CDF=CDF*B*RET*8./3.
        CD=CDF+CDP
        WRITE(6,57) CDP,CDF,CD
C
C       CALC. OF THE NUSSELT NUMBER
C
        DO 41 I=1,N1
        ANU(I)=(-T(I,3)+4.*T(I,2)-3.*T0)/A/(1.-T0)
     41 CONTINUE
        AVNU=0.
        DO 42 I=2,N,2
        AVNU=AVNU+2.*ANU(I)*SN(I)+ANU(I+1)*SN(I+1)
     42 CONTINUE
        AVNU=AVNU*B/3.
        WRITE(6,55) AVNU
        IF(JJ.EQ.500) GO TO 20
        IF(ERR.LT.TOL) GO TO 20
        GO TO 19
     20 CONTINUE
        WRITE(7,53) (( SF(I,J),I=1,N1),J=1,M1)
        WRITE(7,53) ((VOR(I,J),I=1,N1),J=1,M1)
        WRITE(7,53) ((  T(I,J),I=1,N1),J=1,M1)
    101 CONTINUE
        WRITE(6,62)
        WRITE(6,68)
        WRITE(6,58) (ANG(I),I=1,16)
        WRITE(6,59) (R(J),( SF(I,J),I=1,16),J=1,M1)
        WRITE(6,62)
        WRITE(6,68)
        WRITE(6,61) (ANG(I),I=17,N1)
        WRITE(6,60) (R(J),( SF(I,J),I=17,N1),J=1,M1)
        WRITE(6,63)
        WRITE(6,68)
        WRITE(6,58) (ANG(I),I=1,16)
        WRITE(6,59) (R(J),(VOR(I,J),I=1,16),J=1,M1)
        WRITE(6,63)
        WRITE(6,68)
        WRITE(6,61) (ANG(I),I=17,N1)
```

```
      WRITE(6,60) (R(J),(VOR(I,J),I=17,N1),J=1,M1)
      WRITE(6,64)
      WRITE(6,68)
      WRITE(6,58) (ANG(I),I=1,16)
      WRITE(6,59) (R(J),(  T(I,J),I=1,16),J=1,M1)
      WRITE(6,64)
      WRITE(6,68)
      WRITE(6,61) (ANG(I),I=17,N1)
      WRITE(6,60) (R(J),(  T(I,J),I=17,N1),J=1,M1)
      WRITE(6,65)
      WRITE(6,66) (P(I),I=1,N1)
      WRITE(6,67)
      WRITE(6,66) (ANU(I),I=1,N1)
   50 FORMAT(3E10.3,2I5)
   51 FORMAT(I10,F10.2)
   52 FORMAT(' ',10X,'RE=',F7.3,5X,'PE=',F10.6,5X,'TO=',F7.3,
     1       5X,'X=',F7.3)
   53 FORMAT(10Z8)
   54 FORMAT(' ',5X,11F10.6,F10.4)
   55 FORMAT(' ',15X,'NU=',F14.6)
   56 FORMAT(' ',10X,'A=',F8.6,5X,'B=',F9.5,5X,'N=',I6,5X,
     1       'M=',I6,5X,'TOL=',F8.6)
   57 FORMAT(' ',10X,'CDP=',F14.6,5X,'CDF=',F14.6,5X,'CD=',F14.6)
   58 FORMAT('0',11X,16F7.2/)
   59 FORMAT(' ',F7.2,5X,16F7.4)
   60 FORMAT(' ',F7.2,5X,15F7.4)
   61 FORMAT('0',11X,15F7.2/)
   62 FORMAT('1'///' ',50X,'STREAM  FUNCTION')
   63 FORMAT('1'///' ',50X,'VORTICITY')
   64 FORMAT('1'///' ',50X,'TEMPERATURE')
   65 FORMAT('1'////' ',15X,'SURFACE PRESSURE DISTRIBUTION'/)
   66 FORMAT(1H0,10X,8F15.6)
   67 FORMAT(' '////,15X,'LOCAL NUSSELT NUMBER'/)
   68 FORMAT('0',2X,'**R**',43X,'**ANGLE**')
      STOP
      END
```

```
      DIMENSION SF(32,42),VOR(32,42),T(32,42),WV(32,42),WT(32,42)
      DIMENSION F(32,42),G(32,42)
      DIMENSION R(42),R2(42),TH(32),ANG(32),SN(32),CS(32)
      DIMENSION CO(32),BP2(32),BM2(32)
      DIMENSION ALPHA(31), P(31),ANU(32)
      READ(5,50) RE,TO,A,N,M
      READ(5,51) KKC,ACCL,NSTART
      TOL=0.00001
      X=0.
      PE=0.672*RE
      B=180./N
      WRITE(6,52) RE,PE,TO,X
      WRITE(6,56) A,B,N,M,TOL
      N1=N+1
      M1=M+1
      MI=M-1
      NI=N-1
      ANG(1)=0.
      DO 45 I=1,N
      ANG(I+1)=ANG(I)+B
   45 CONTINUE
      P=B/57.2957795
      A2=A*A
      B2=B*B
      AH=A*2.
      BH=B*2.
      AP2=(2.+A)/A2/2.
      AM2=(2.-A)/A2/2.
      COF=2./A2+2./B2
      CONS=32./PP
      DO 2 J=1,M1
      R(J)=EXP((J-1.)*A)
      R2(J)=R(J)*R(J)
    2 CONTINUE
      TH(1)=0.
      TH(2)=B
      DO 1 I=2,N
      TH(I+1)=TH(I)+B
      SN(I)=SIN(TH(I))
      CS(I)=COS(TH(I))
      CO(I)=CS(I)/SN(I)
      BP2(I)=(2.+CO(I)*B)/B2/2.
      BM2(I)=(2.-CO(I)*B)/B2/2.
    1 CONTINUE
      SN(1)=0.
      SN(N1)=0.
      CS(1)=1.
      CS(N1)=-1.
      IF(NSTART.EQ.1) GO TO 46
      DO 3 I=1,N1
      DO 3 J=1,M1
      T(I,J)=1.-(1.-TO)/R(J)
      SF(I,J)=0.5*SN(I)*SN(I)*(R2(J)-1.5*R(J)+.5/R(J))
      VOR(I,J)=1.5*SN(I)/R2(J)
```

```
    3 CONTINUE
      GO TO 47
   46 CONTINUE
      READ(5,53)  (( SF(I,J),I=1,N1),J=1,M1)
      READ(5,53)  ((VOR(I,J),I=1,N1),J=1,M1)
      READ(5,53)  ((  T(I,J),I=1,N1),J=1,M1)
   47 CONTINUE
C
CC    BOUNDARY CONDITIONS
C
      DO 4 I=1,N1
      SF(I,M1)=.5*(R(M1)*SN(I))**2
      SF(I,1)=0.
      VOR(I,M1)=0.
      T(I,1)=T0
      T(I,M1)=1.
    4 CONTINUE
      DO 5 J=1,M1
      SF(1,J)=0.
      SF(N1,J)=0.
      VOR(1,J)=0.
      VOR(N1,J)=0.
    5 CONTINUE
C
CC    FLOW FIELD IS CALC. FIRST
CCCCC
CC    CALCULATION OF RELAXATION COEFF.
C
      DO 6 I=2,N
      DO 6 J=2,M
      AP=(SF(I,J+1)-SF(I,J-1))/A
      BP=(SF(I+1,J)-SF(I-1,J))/B
      SQ=SQRT(0.5*(AP*AP+BP*BP))
      RES=ABS(RE/R(J)/SN(I)/4.)
      WV(I,J)=1./(1.+RES*SQ)
    6 CONTINUE
      WS=1./(1.+3.1416/N1)
      WRITE(6,54)(VOR(I,1),I=1,N1,3)
C
CC    RELAXATION STARTS HERE
C
      JJ=0
      KK=0
      I1=0
      I2=0
      ACC=1.
    7 CONTINUE
      ERR=0.
      JJ=JJ+1
      KK=KK+1
      IF(KK.NE.KKC) GO TO 8
      KK=0
      ACC=ACCL
```

```
    8 CONTINUE
C
C     CALC OF GRID POINTS STARTS HERE
C
      DO 25 I=2,N
      IF(I1.EQ.1) GO TO 12
      I1=1
      J1=1
      GO TO 11
   12 CONTINUE
      I1=0
      J1=0
   11 CONTINUE
      DO 25 J=2,M
      IF(J1.EQ.0) GO TO 13
      J1=0
      GO TO 14
   13 J1=1
      GO TO 25
   14 CONTINUE
      PERS=RE/(8.*A**3*R(J)*SN(I))
      U=(SF(I+1,J)-SF(I-1,J))*PERS
      V=(SF(I,J+1)-SF(I,J-1))*PERS
      W=AH*U+1./SN(I)/SN(I)+COF-BH*CO(I)*V
      AV=VOR(I,J+1)*(AP2+U)+VOR(I,J-1)*(AM2-U)+VOR(I+1,J)*(BP2(I)-V)
     1   +VOR(I-1,J)*(BM2(I)+V)-VOR(I,J)*W
      AV=AV/W
      AS=SF(I,J+1)*AM2+SF(I,J-1)*AP2+SF(I+1,J)*BM2(I)+SF(I-1,J)*BP2(I)
     1    -COF*SF(I,J)-VOR(I,J)*R(J)*SN(I)*R2(J)
      AS=AS/COF
      IF(AV.LT.ERR) GO TO 29
      ERR=AV
      II=I
      JI=J
   29 CONTINUE
      IF(I2.EQ.1) GO TO 15
      SF(I,J)=SF(I,J)+ ACC*WS*AS
      VOR(I,J)=VOR(I,J)+ ACC*WV(I,J)*AV
      GO TO 25
   15 CONTINUE
      SF(I,J)=SF(I,J)+AS
      VOR(I,J)=VOR(I,J)+AV
   25 CONTINUE
      IF(I2.EQ.0) GO TO 16
      I1=0
      I2=0
      GO TO 17
   16 I1=1
      I2=1
      GO TO 8
   17 CONTINUE
C
C     BOUNDARY CONDITION FOR VORTICITY AT THE SURFACE
C
```

```
      DO 9 I=2,N
      VOR(I,1)=(8.*SF(I,2)-SF(I,3))/(2.*A2*SN(I))
    9 CONTINUE
      WRITE(6,54) (VOR(I,1),I=1,N1,3),ERR
      ACC=1.
      IF((KK+1).EQ.KKC) GO TO 18
   19 CONTINUE
      IF(ERR.LT.TOL) GO TO 200
      IF(JJ.EQ.300) GO TO 200
      GO TO 7
   18 CONTINUE
C
C     CALCULATION OF RELAXATION COEFF.
C
      DO 21 I=2,N
      DO 21 J=2,M
      AP=(SF(I,J+1)-SF(I,J-1))/A
      BP=(SF(I+1,J)-SF(I-1,J))/B
      SQ=SQRT(0.5*(AP*AP+BP*BP))
      RES=ABS(RE/R(J)/SN(I)/4.)
      WV(I,J)=1./(1.+RES*SQ)
   21 CONTINUE
  200 CONTINUE
C
C     CALC. OF THE DRAG COEF.
C
      SUM=VOR(2,1)+VOR(2,M1)
      DO 22 J=2,M,2
      SUM=SUM+4.*VOR(2,J)+2.*VOR(2,J+1)
   22 CONTINUE
      P(1)=1.+8.*A*SUM/3./B/RE
      DO 23 I=1,N1
      ALPHA(I)=(4.*VOR(I,2)-VOR(I,3)-3.*VOR(I,1))/(2.*A)+VOR(I,1)
   23 CONTINUE
      FACT=2.*B/RE
      DO 24 I=2,N1
      P(I)=P(I-1)+FACT*(ALPHA(I)+ALPHA(I-1))
   24 CONTINUE
      CDP=0.
      CDF=0.
      DO 26 I=2,N,2
      CDP=CDP+8.*P(I)*SN(I)*CS(I)+4.*P(I+1)*SN(I+1)*CS(I+1)
      CDF=CDF+VOR(I,1)*SN(I)*SN(I)+0.5*VOR(I+1,1)*SN(I+1)*SN(I+1)
   26 CONTINUE
      CDP=CDP*B/3.
      CDF=CDF*B*CONS/3.
      CD=CDF+CDP
      WRITE(6,57) CDP,CDF,CD
      IF(ERR.LT.TOL) GO TO 20
      IF(JJ.EQ.300) GO TO 20
      GO TO 19
   20 CONTINUE
      WRITE(7,53) (( SF(I,J),I=1,N1),J=1,M1)
      WRITE(7,53) ((VOR(I,J),I=1,N1),J=1,M1)
```

```
C
C       TEMPERATURE FIELD CALCULATION
C
C
C       CALC. OF RELAXATION COEFF.
C
        DO 106 I=2,N
        DO 106 J=2,M
        PES=PE/R(J)/SN(I)/2.
        AP=(SF(I,J+1)-SF(I,J-1))/AH*PES
        BP=(SF(I+1,J)-SF(I-1,J))/BH*PES
        SQ=SQRT(0.5*(AP*AP+BP*BP))
        WT(I,J)=1./(1.+SQ)
        F(I,J)=AP/BH
        G(I,J)=BP/AH
  106 CONTINUE
C
C       RELAXATION STARTS HERE
C
        JJ=0
        KK=0
        I1=0
        I2=0
        ACC=1.
  107 CONTINUE
        ERR=0.
        JJ=JJ+1
        KK=KK+1
        IF(KK.NE.KKC) GO TO 108
        KK=0
        ACC=ACCL
  108 CONTINUE
C
C       CALC. OF GRID POINTS
C
        DO 125 I=2,N
        IF(I1.EQ.1) GO TO 112
        I1=1
        J1=1
        GO TO 111
  112 CONTINUE
        I1=0
        J1=0
  111 CONTINUE
        DO 125 J=2,M
        IF(J1.EQ.0) GO TO 113
        J1=0
        GO TO 114
  113 J1=1
        GO TO 125
  114 CONTINUE
        AT=T(I,J+1)*(AP2+G(I,J1)+T(I,J-1)*(AM2-G(I,J))-COF*T(I,J)
     1     +T(I+1,J)*(BP2(I)-F(I,J))+T(I-1,J)*(BM2(I)+F(I,J))
        AT=AT/COF
```

```
      IF(AT.LT.ERR) GO TO 129
      ERR=AT
      II=I
      JI=J
  129 CONTINUE
      IF(I2.EQ.1) GO TO 115
      T(I,J)=T(I,J)+ACC*WT(I,J)*AT
      GO TO 125
  115 CONTINUE
      T(I,J)=T(I,J)+AT
  125 CONTINUE
      IF(I2.EQ.0) GO TO 116
      I1=0
      I2=0
      GO TO 117
  116 I1=1
      I2=1
      GO TO 108
  117 CONTINUE
C
C     CALCULATING B.C.'S ALONG THE SYMMETRY AXIS
C
      DO 109 J=2,M
      T(1,J)=(4.*T(2,J)-T(3,J))/3.
      T(N1,J)=(4.*T(N,J)-T(N-1,J))/3.
  109 CONTINUE
      ACC=1.
      IF((KK+1).EQ.KKC) GO TO 118
  119 CONTINUE
      IF(ERR.LT.TOL) GO TO 118
      IF(JJ.EQ.300) GO TO 118
      IF(ERR.LT.TOL) GO TO 120
      GO TO 107
C
C     CALC. OF THE NUSSELT NUMBER
C
  118 CONTINUE
      DO 41 I=1,N1
      ANU(I)=(-T(I,3)+4.*T(I,2)-3.*T0)/A/(1.-T0)
   41 CONTINUE
      AVNU=0.
      DO 42 I=2,N,2
      AVNU=AVNU+2.*ANU(I)*SN(I)+ANU(I+1)*SN(I+1)
   42 CONTINUE
      AVNU=AVNU*B/3.
      WRITE(6,55) AVNU
      IF(JJ.EQ.300) GO TO 120
      GO TO 119
  120 CONTINUE
      WRITE(7,53) ((  T(I,J),I=1,N1),J=1,M1)
      WRITE(6,62)
      WRITE(6,68)
      WRITE(6,58) (ANG(I),I=1,16)
      WRITE(6,59) (R(J),( SF(I,J),I=1,16),J=1,M1)
```

```
      WRITE(6,62)
      WRITE(6,68)
      WRITE(6,61) (ANG(I),I=17,N1)
      WRITE(6,60) (R(J),( SF(I,J),I=17,N1),J=1,M1)
      WRITE(6,63)
      WRITE(6,68)
      WRITE(6,58) (ANG(I),I=1,16)
      WRITE(6,59) (R(J),(VOR(I,J),I=1,16),J=1,M1)
      WRITE(6,63)
      WRITE(6,68)
      WRITE(6,61) (ANG(I),I=17,N1)
      WRITE(6,60) (R(J),(VOR(I,J),I=17,N1),J=1,M1)
      WRITE(6,64)
      WRITE(6,68)
      WRITE(6,58) (ANG(I),I=1,16)
      WRITE(6,59) (R(J),(  T(I,J),I=1,16),J=1,M1)
      WRITE(6,64)
      WRITE(6,68)
      WRITE(6,61) (ANG(I),I=17,N1)
      WRITE(6,60) (R(J),(  T(I,J),I=17,N1),J=1,M1)
      WRITE(6,65)
      WRITE(6,66) (P(I),I=1,N1)
      WRITE(6,67)
      WRITE(6,66) (ANU(I),I=1,N1)
   50 FORMAT(3E10.3,2I5)
   51 FORMAT(I10,F10.2,I10)
   52 FORMAT(' ',10X,'RE=',F7.3,5X,'PE=',F10.6,5X,'TO=',F7.3,
     1       5X,'X=',F7.3)
   53 FORMAT(10Z8)
   54 FORMAT(' ',11F10.6,F8.6)
   55 FORMAT(' ',15X,'NU=',F14.6)
   56 FORMAT(' ',10X,'A=',F8.6,5X,'B=',F9.5,5X,'N=',I6,5X,
     1       'M=',I6,5X,'TOL=',F8.6)
   57 FORMAT(' ',10X,'CDP=',F14.6,5X,'CDF=',F14.6,5X,'CD=',F14.6)
   58 FORMAT('0',11X,16F7.2/)
   59 FORMAT(' ',F7.2,5X,16F7.4)
   60 FORMAT(' ',F7.2,5X,15F7.4)
   61 FORMAT('0',11X,15F7.2/)
   62 FORMAT('1'///' ',50X,'STREAM  FUNCTION')
   63 FORMAT('1'///' ',50X,'VORTICITY')
   64 FORMAT('1'///' ',50X,'TEMPERATURE')
   65 FORMAT('1'////' ',15X,'SURFACE PRESSURE DISTRIBUTION')
   66 FORMAT(1H0,10X,8F15.6)
   67 FORMAT(' '////,15X,'LOCAL NUSSELT NUMBER')
   68 FORMAT('0',2X,'**R**',43X,'**ANGLE**')
      STOP
      END
```